(4)

The University of Texas at Dallas
Center for Quantum Electronics
The Gamma-Ray Laser Project
Annual Report FY-1987

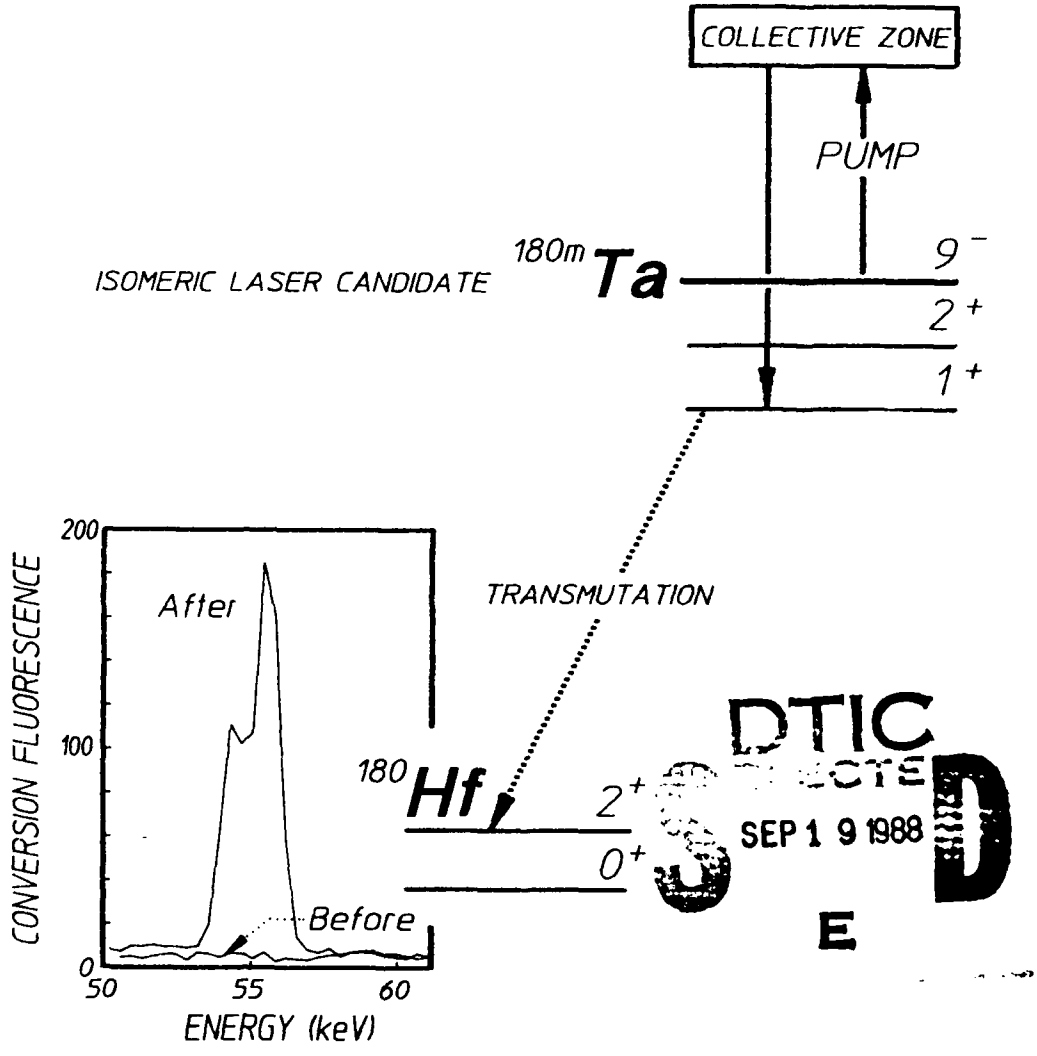

Report GRL/8705

PROOF OF THE FEASIBILITY OF COHERENT AND INCOHERENT SCHEMES FOR PUMPING A GAMMA-RAY LASER

Principal Investigator: Carl B. Collins
The University of Texas at Dallas
Center for Quantum Electronics
P.O. Box 830688
Richardson, Texas 75083-0688

June 1988

Annual Technical Progress Report
1 June 1987 through 31 May 1988
Contract Number N00014-86-C-2488

Prepared for
INNOVATIVE SCIENCE AND TECHNOLOGY DIRECTORATE
OF STRATEGIC DEFENSE INITIATIVE ORGANIZATION

Contracting Officer's Technical Representative
Dr. Paul Kepple, Code 4720
Naval Research Laboratory
4555 Overlook Avenue, SW
Washington, DC 20375-5000

SECURITY CLASSIFICATION OF THIS PAGE (When Data Entered)

REPORT DOCUMENTATION PAGE

READ INSTRUCTIONS BEFORE COMPLETING FORM

1. REPORT NUMBER: GRL/8705

2. GOVT ACCESSION NO.:

3. RECIPIENT'S CATALOG NUMBER:

4. TITLE (and Subtitle): PROOF OF THE FEASIBILITY OF COHERENT AND INCOHERENT SCHEMES FOR PUMPING A GAMMA-RAY LASER

5. TYPE OF REPORT & PERIOD COVERED: Annual Technical Progress 6/1/87 - 5/31/88

6. PERFORMING ORG. REPORT NUMBER:

7. AUTHOR(s): Carl B. Collins

8. CONTRACT OR GRANT NUMBER(s): N00014-86-C-2488

9. PERFORMING ORGANIZATION NAME AND ADDRESS:
University of Texas at Dallas
Center for Quantum Electronics
P. O. Box 830688
Richardson, TX 75083-0688

10. PROGRAM ELEMENT, PROJECT, TASK AREA & WORK UNIT NUMBERS:

11. CONTROLLING OFFICE NAME AND ADDRESS:
INNOVATIVE SCIENCE AND TECHNOLOGY DIRECTORATE
OF STRATEGIC DEFENSE INITIATIVE ORGANIZATION

12. REPORT DATE: June 1988

13. NUMBER OF PAGES: 184

14. MONITORING AGENCY NAME & ADDRESS (if different from Controlling Office):
Dr. Paul Kepple, Code 4720
Naval Research Laboratory
4555 Overlook Avenue, SW
Washington, DC 20375-5000

15. SECURITY CLASS. (of this report): Unclassified

15a. DECLASSIFICATION/DOWNGRADING SCHEDULE:

16. DISTRIBUTION STATEMENT (of this Report):
This document has been approved for public release and sale; its distribution is unlimited.

17. DISTRIBUTION STATEMENT (of the abstract entered in Block 20, if different from Report):

18. SUPPLEMENTARY NOTES:

19. KEY WORDS (Continue on reverse side if necessary and identify by block number):

20. ABSTRACT (Continue on reverse side if necessary and identify by block number):
Recent approaches to the problem of the gamma-ray laser have focused upon upconversion techniques in which metastable nuclei are pumped with long wavelength radiation. At the nuclear level the storage of energy can approach tera-Joules (10^{12}J) per liter for thousands of years. However, any plan to use such a resource for a gamma-ray laser poses problems of a broad interdisciplinary nature requiring the fusion of concepts taken from

(continued on next page)

DD FORM 1 JAN 73 1473 EDITION OF 1 NOV 65 IS OBSOLETE

SECURITY CLASSIFICATION OF THIS PAGE (When Data Entered)

20. Abstract (continued)

relatively unrelated fields of physics. Our research group has described several means through which this energy might be coupled to the radiation fields with cross sections for stimulated emission that could reach 10^{-17} cm^2. Such a stimulated release could lead to output powers as great as 3×10^{21} Watts/liter. Since 1978 we have pursued an approach for the upconversion of longer wavelength radiation incident upon isomeric nuclear populations that can avoid many of the difficulties encountered with traditional concepts of single photon pumping. Recent experiments have confirmed the general feasibility and have indicated that a gamma-ray laser is feasible if the right combination of energy levels and branching ratios exists in some real material. Of the 1886 distinguishable nuclear materials, the present state-of-the-art has been adequate to identify 29 first-class candidates, but further evaluation cannot proceed without remeasurements of nuclear properties with higher precision. A laser-grade database of nuclear properties does not yet exist, but the techniques for constructing one are currently being developed. Resolution of the question of the feasibility of a gamma-ray laser now rests upon the determination of: 1) the identity of the best candidate, 2) the threshold level of laser output, and 3) the upconversion driver for that material.

This second year's report continues to focus upon our approach that is the nuclear analog to the ruby laser. It embodies the simplest concepts for a gamma-ray laser and not surprisingly, the greatest rate of achievement in the quest for a subAngstrom laser continues in that direction. For ruby the identification and exploitation of a bandwidth funnel were the critical keys in the development of the first laser. There was a broad absorption band linked through efficient cascading to the narrow laser level.

During this reporting period we discovered that comparable structure exists at the nuclear level. Giant resonances were found in the first two of the 29 candidate isomers that could be tested. When pumped with flash x-rays they funneled across drastic changes of angular momentum the populations pumped with 10^4 to 10^6 more efficiency than theory predicted. In a major milestone experiment populations of $^{180}Ta^m$, were dumped with peak x-ray powers of only $4W/cm^2$. This report focuses upon the details of that achievement, the implications and the spin-off technology realized this year.

TABLE OF CONTENTS

PREFACE

Presented here is the second annual report describing progress in the demonstration of the feasibility of a gamma-ray laser. The contexts of our work, both historical and conceptual, have been reviewed in the literature and it suffices here to repeat only the consequences of the theoretical renaissance we began in the late 70's. So great is the promise of these new upconversion techniques, that *a gamma-ray laser is definitely feasible if a sufficiently ideal isotope exists in reality*. This is the single most critical issue to the development of a gamma-ray laser--the identity of the most nearly ideal candidate for upconversion.

Despite the many applications of beautiful and involved techniques of nuclear spectroscopy, the current data base is inadequate in both coverage and resolution either to answer the question of whether an acceptable isotope exists or to guide in the selection of a possible candidate medium for a gamma-ray laser. Problems posed by the evaluation of candidate materials are of a broad interdisciplinary nature requiring the fusion of concepts and methodologies from previously unrelated fields of physics.

Of the several possible approaches, it is the nuclear analog of the ruby laser that embodies the simplest concepts for a gamma-ray laser. Not surprisingly, the greatest rate of achievement in the quest for a subAngstrom laser continues in that direction. This annual report focuses upon the second and third major milestones achieved along this path of research. Last year the first had shown that bandwidth funneling works at the nuclear level, just as it did for ruby on the molecular scale. Experiments pumping ^{77}Se and ^{79}Br produced eleven orders of magnitude increase in fluorescence intensity over what could have been obtained by direct excitation.

This year, the second milestone demonstrated great success in optically pumping the first of the 29 actual candidates for a gamma-ray laser, $^{180}Ta^{m}$. Not a particularly attractive candidate, <u>a priori</u>, $^{180}Ta^{m}$ had been the only one for which a macroscopic sample was available. The need to span a formidably large $\Delta J = 8$ between isomer and fluorescence level supported little initial enthusiasm for this nucleus. However, when actually pumped, it showed the largest integrated cross section ever reported for interband transfer in any material, 4×10^{-22} cm^2 eV. This corresponded to a partial width for absorption from $^{180}Ta^{m}$ isomer to fluorescence that was measured to be about 0.5 eV, *a value far*

exceeding the 1 μeV usually offered as a rule of thumb that would limit the interband transfer of nuclear population.

Achieved most recently in FY-87, the third major milestone demonstrated that the successes with $^{180}Ta^{m}$ could be extended to another of the 29 candidate isomers. While milligram-sized samples are not available for any of the remaining 28 candidates, one admits an alternative procedure for testing. Instead of dumping the isomer it can be produced by pumping it up from the ground state with flashes of x-rays. The candidate $^{123}Te^{m}$ is one of the few which has both a radioactive signature sufficiently distinctive to permit the unequivocal detection of such a long-lived isomer and a stable ground state from which to fabricate a target. Reviewed in this report is the excitation of ^{123}Te to the candidate isomer $^{123}Te^{m}$ with flash x-rays through a partial width of 0.05 eV, another enormous value. The inverse could easily approach the 0.5 eV measured for the dumping of $^{180}Ta^{m}$ since pumping down in energy should be more favorable than pumping up.

These results with seemingly unattractive candidates indicate the probabilities should be raised for the full success of one of the other 27 materials. Two out of two candidates examined to date have narrowly missed being acceptable. They performed 10^3 to 10^4 times better than would have been expected theoretically. Perhaps, as suggested last year, collective oscillations which break the symmetries of the nuclei provide this major windfall making it easier to dump isomers by mixing single particle states needed in the transfer process. Much more experimentation will be needed to identify whether this is the actual mechanism responsible and to understand if the lessons taught by these first two materials are generally applicable in the pool of candidate isomers.

This report focuses upon the details of these major milestone achievements, their implications and the spin-off technology they motivated. At this time it is a pleasure to have the opportunity to thank the 30 faculty, students and staff of the Center for Quantum Electronics for their splendid efforts in support of our program this past year.

- C. B. Collins
- Director
- Center for Quantum Electronics

MAJOR MILESTONE REPORT

Affecting the Feasibility of Coherent and Incoherent Schemes
for Pumping a Gamma-Ray Laser
October 16, 1987

C. B. Collins, Center for Quantum Electronics, University of Texas at Dallas

Achievement

X-ray pulses have been used to pump very large amounts of nuclear fluorescence from hundred-microgram quantities of the first of the 29 candidate isomers to be tested for a gamma-ray laser.

Technical Background

The nuclear analog of the ruby laser embodies the simplest concepts for a gamma-ray laser. Not surprisingly, the greatest rate of achievement in the quest for a subAngstrom laser has developed in that direction.

For ruby the identification and exploitation of a bandwidth funnel were the critical keys in the development of the first laser. There was a broad absorption band linked through efficient cascading to the narrow laser level.

Nuclei to be used in the analog of the ruby laser can start in either ground or isomeric states. However, with the latter, most of the output power can be derived from the energy stored in the isomeric state at its creation. Then in addition to the obvious need to transfer energy in order to reach a fluorescence level to be populated for lasing, there must also be a substantial transfer of angular momentum. Major milestones we reported previously proved that bandwidth funneling worked for nuclei of simulated candidates but the change in angular momenta did not need to be very large in those materials. It was found that nuclear fluorescence could be pumped by flash x-rays through integrated cross-sections as large as 30 in the usual units ($\times 10^{-29}$ cm^2 keV). However, many of the 29 actual candidate isomers have angular momenta which are very different from the laser levels to which they are supposed to be dumped. The concern has lingered that actual candidates would have pumping cross-sections of only a minute fraction of a unit, if not actually zero, and so would be entirely useless.

Reported here is an experimental breakthrough which answers this concern. *A population of candidate isomer ^{180m}Ta has been dumped through an integrated cross-section of 80,000 units.*

Report

Most of the nuclear data bases do not yet record the recent discovery that nature's rarest element, tantalum-180, is actually an isomer lying 80 keV above a ground state which is unstable against transmutation to tungsten and hafnium. Having a very high spin of 9^-, the isomer ^{180m}Ta has a cosmic lifetime and traces remain on earth mixed with the normal commercial tantalum, ^{181}Ta. Because of a curious importance to the cosmic nucleosynthesis of the heavier elements, astrophysicists have studied the energetics of the lower levels of the ^{180}Ta system as shown in Fig. 1, except for the broad level near 2000 keV which has been added here as a result of our work.

In this major milestone experiment about 500 μg of naturally occuring isomeric ^{180m}Ta diluted in 4.75 g of ^{181}Ta were irradiated with the bremsstrahlung from a 6 MeV linac. The accumulated dose at 2 MeV near the peak of the spectrum was 3.8×10^{10} photons/cm^2/keV. The excitation energy of the gateway state shown in Fig. 1 was assumed to be 2000 keV in order to obtain a minimum value for the cross section, since smaller fluxes were available at even higher energies.

The spectrum of the radioactive debris shown in Fig. 2 demonstrates that isomeric ^{180m}Ta nuclei were pumped through a broad level cascading finally to the unstable ground state of ^{180}Ta. The amount of debris determines the cross section for the process to be about 80,000 of the usual units ($\times 10^{-29}$ cm^2 keV).

Significance

There is a threefold significance to this demonstration of the efficiency for pumping isomers with x-rays.

1) The first real isomer to be tested for a gamma-ray laser was successfully pumped down with an astonishingly large cross section of 80,000 on a scale where 10 describes a fully allowed process.

2) The nuclear analog to the ruby laser is a fully viable scheme for a gamma-ray laser, and ^{180m}Ta narrowly misses being an acceptable candidate. It performed about 10^4 times better than would have been expected theoretically.

3) These results with a seemingly unattractive candidate indicate the probabilities should be raised for full success of one of the other 28 materials.

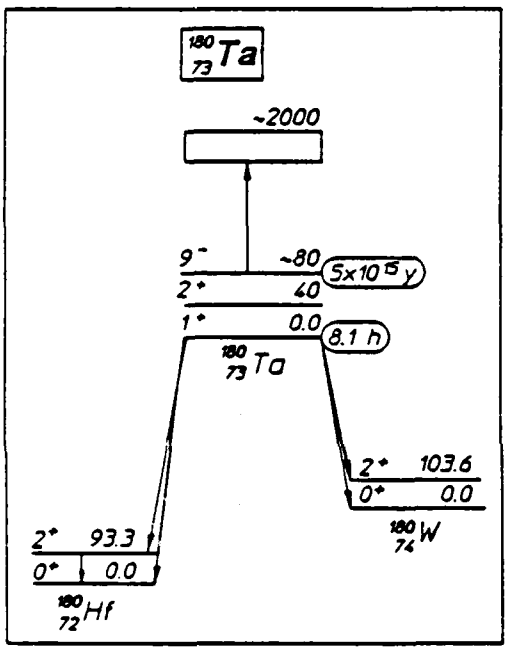

Figure 1: Schematic energy level diagram of ^{180}Ta and its daughters. Half-lives are shown in ovals to the right of the ground and isomeric levels. Energies are in keV. The pump band is shown by the arrow pointing upward to the broad state represented by the rectangle. Cascade through the potential laser levels of ^{180}Ta is not known, but leads finally to the ground state. Electron capture to the left and beta decay to the right are indicated by the diagonal downward arrows. The final debris from pumping down the isomer is found in the fluorescence from the 93.3 keV transition of ^{180}Hf characterized by the 8.1 hour lifetime of its ^{180}Ta parent.

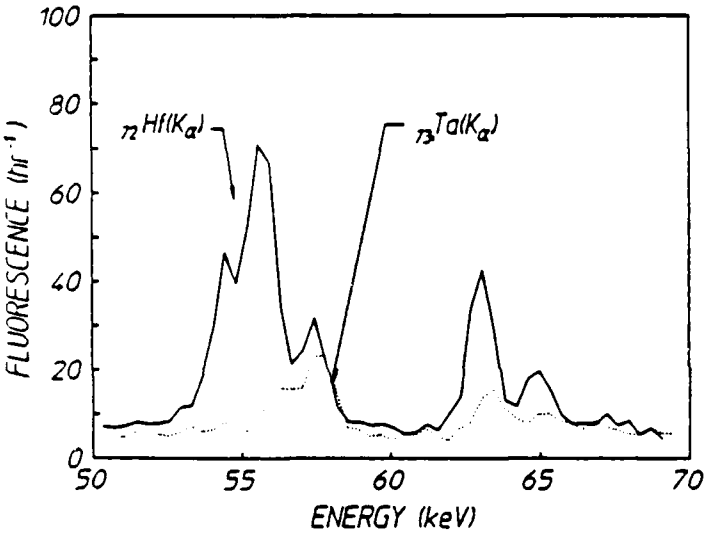

Figure 2: Dotted and solid curves show, respectively, the spectra obtained before and after dumping some of the 500 μg of isomeric ^{180m}Ta. An HPGe detector was used to obtain the dotted spectrum excited in the 4.75 g of diluent ^{181}Ta by the traces of natural activity in the counting shield. The solid curve shows activity resulting from the transmutation of the pumped ^{180}Ta measured in the same sample and counting system after irradiation. The prominent addition is the K_α pair from hafnium excited by the internal conversion of the 93 keV transition shown in Fig. 1.

MAJOR MILESTONE REPORT

Strengthening the Feasibility of a Gamma-Ray Laser

February 8, 1988

C. B. Collins, Center for Quantum Electronics, University of Texas at Dallas

Achievement

Discovered in the first of the 29 candidate isomers to be tested for a gamma-ray laser was a critical nuclear structure enabling performance to approach the ideal. Now a similar arrangement has been found in the second of the 29 candidates.

Technical Background

The nuclear analog of the ruby laser embodies the simplest concepts for a gamma-ray laser. Not surprisingly, the greatest rate of achievement in the quest for a subAngstrom laser continues in that direction. For ruby the identification and exploitation of a bandwidth funnel were the critical keys in the development of the first laser. There was a broad absorption band linked through efficient cascading to the narrow laser level.

Recently we reported a major milestone which showed that comparable structure existed at the nuclear scale in the first of the 29 candidate isomers available for testing, $^{180}Ta^{m}$. Populations of the isomer were successfully pumped down with flashes of x-rays absorbed through an astonishingly large cross section of 40,000 on the usual scale ($\times 10^{-29}$ cm^2 keV) where 10 describes a fully allowed process. This corresponded to a partial width for useful absorption of 0.5 eV, even better than what had been assumed for idealized nuclei. Such extremely favorable attributes allowed us to perform those experiments with as little as one milligram of $^{180}Ta^{m}$.

Milligram sized samples are not available for any of the remaining 28 candidates. However, one admits an alternative procedure for testing. Instead of dumping them, the isomers can be produced by pumping them up from the ground state with flashes of x-rays. The candidate $^{123}Te^{m}$ is one of the few which has both a radioactive signature sufficiently distinctive to permit the unequivocal detection of such a long-lived isomer and a stable ground state from which to fabricate a target. In this case the ^{123}Te is a rare, but naturally occurring isotope with 0.91% abundance.

Reported here is the excitation of ^{123}Te to the candidate isomer $^{123}Te^{m}$ with flash x-rays through an integrated cross section of 10,000 units.

Report

The excitation of $^{123}Te^{m}$ can be detected by the 159 keV photon emitted with 84% efficiency as part of the decay scheme of this isomer, as shown in Fig. 1. After pumping, the intensity of this spectral line should decay with the characteristic 119.7 day half-life of the isomer. In this major milestone experiment, 171 milligrams of the ground state ^{123}Te diluted in 32.4 grams of natural tellurium were irradiated with the bremsstrahlung from a 6 MeV linac. The accumulated dose at 2 MeV near the peak of the spectrum was 5.6×10^{10} photons/cm^2/keV delivered in a sequence of pulses each having a peak intensity of about 4 W/cm^2 at the sample.

The excitation energy of the gateway state was assumed to be 2000 keV in order to obtain a <u>minimum</u> value for the cross section, since smaller fluxes were available at even higher energies. Data shown in Figs. 2 and 3 determined the integrated cross section for the process to be about 10,200 of the usual units ($\times 10^{-29}$ cm^2 keV). This is an enormous value exceeded only by the cross section for the inverse process of dumping the only other laser candidate tested to date.

Significance

There is a threefold significance to this demonstration of the efficiency for producing populations of the second laser candidate to be considered.

1) The first and second real isomers to be tested for a gamma-ray laser were successfully destroyed and created, respectively, by optical pumping with astonishingly large cross sections. The partial width for creating the $^{123}Te^{m}$ isomer corresponds to 0.05 eV, an enormous value, and the inverse could easily approach the 0.5 eV measured for the dumping of $^{180}Ta^{m}$, since pumping down in energy should be more favorable than pumping up.

2) The nuclear analog to the ruby laser is a fully viable scheme for a gamma-ray laser, and both $^{180}Ta^{m}$ and $^{123}Te^{m}$ narrowly missed being acceptable candidates. They performed about 10^{4} and at least 10^{3} times better than would have been expected theoretically.

3) These results with seemingly unattractive candidates indicate the probabilities should be raised for full success of one of the other 27 materials.

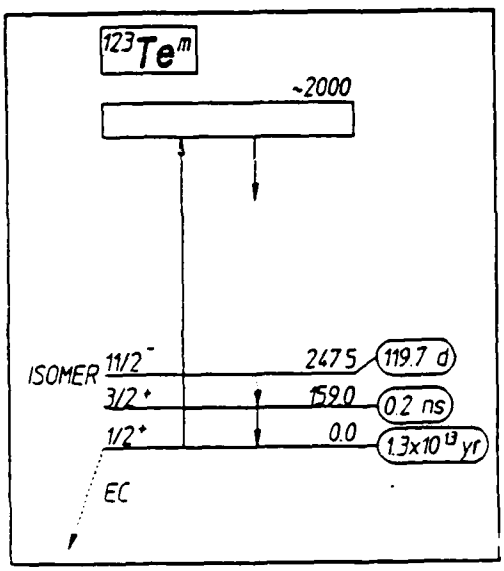

Figure 1: Schematic energy level diagram of ^{123}Te. Half-lives are shown in ovals to the right of the levels, and energies are in keV. The pump band is shown by the arrow pointing upward to the broad state represented by the rectangle. Cascade from this gateway is not known, but leads finally to the isomeric state. The resulting population of the laser candidate $^{123}Te^{m}$ is detected by the 159 keV fluorescence with a 119.7 day half-life.

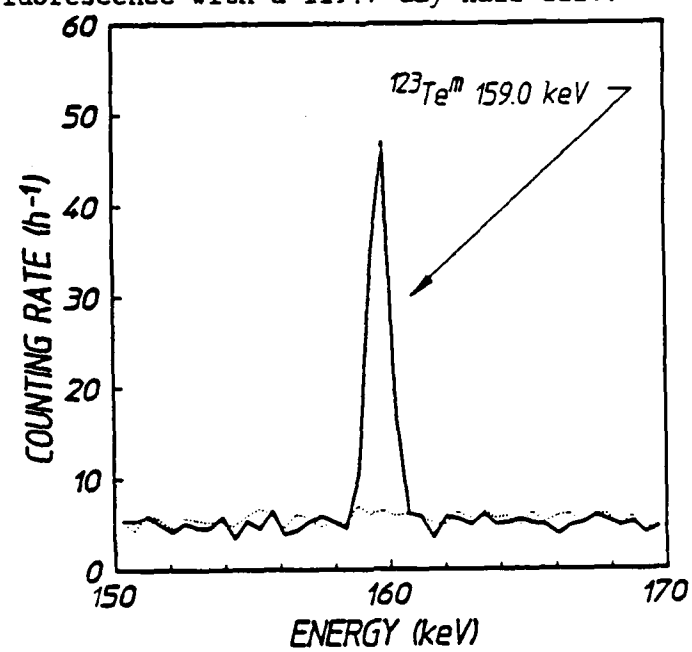

Figure 2 (top, right): Dotted and solid curves show, respectively, the spectra obtained before and after pumping some of the 171 mg of ^{123}Te to the isomeric $^{123}Te^{m}$.

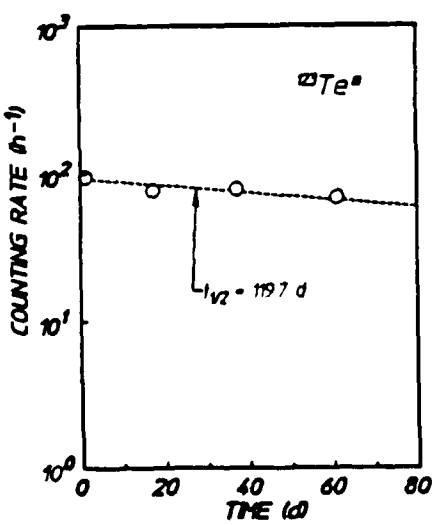

Figure 3 (bottom, left): Plot of the time decay of the activity of the $^{123}Te^{m}$ pumped into the target by the irradiation with the x-rays. The size of the plotted points represents 1 σ deviation, and the slope corresponds to the expected 119.7 day half-life.

INTRODUCTION

Efforts to demonstrate the feasibility of a gamma-ray laser scored major advances in 1987. Culminating with the successes in optically pumping the first of the 29 actual candidate isomers, priority issues were brought into better focus by the lessons learned from a wealth of new results. Perceptions were advanced so greatly that it has become necessary to reassess the critical issues remaining for 1988. However, the bottom line remains the same. *A gamma-ray laser is feasible if the right combination of energy levels occurs in some real material.* The likelihood of this favorable arrangement has been markedly increased by the experimental results of 1987.

From the inception of the gamma-ray laser program, it had been realized that levels of nuclear excitation which might be efficiently stimulated in a gamma-ray laser would be very difficult to pump directly. To have sharply-peaked cross sections for stimulated emission, such levels must have very narrow widths for interaction with the radiation field. This is a fundamental attribute that had led to the facile criticism that "absorption widths in nuclei are too narrow to permit effective pumping with x-rays."

The same concerns had been voiced in atomic physics before Maiman's great discovery, and it has proven very useful to pursue this analogy between ruby and gamma-ray lasers. The identification and exploitation of a bandwidth funnel in ruby were the critical keys in the development of the first laser. There was a broad absorption band exciting a state of Cr^{3+} which quickly decayed by cascading its population into levels of lower energy. A reasonably favorable pattern of branching insured that much of the cascading populated the narrow level. At the core of our simplest proposal[1] for pumping a gamma-ray laser is the use of the analog of this effect at the nuclear level as shown in Fig. 1. A detailed analysis of this mechanism was reviewed as early[2] as 1982 and has been emphasized in more recent reports[3,4] together with the breakthrough actually demonstrating the great utility of bandwidth funneling at the nuclear level. Yields of gamma-ray fluorescence in ^{77}Se and ^{79}Br were enhanced by eleven orders of magnitude by this effect.[5]

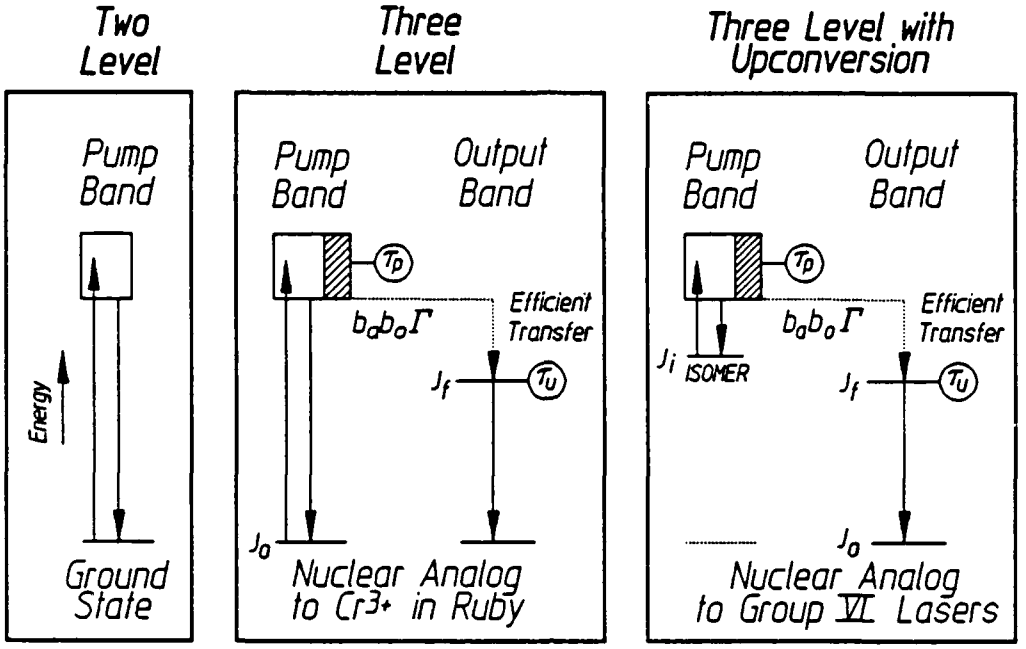

Figure 1: Schematic representation of the energetics of the priority schemes for pumping a gamma-ray laser with flash x-rays. The large width of the level defining the pump band is implied by the height of the rectangle representing the level and the shaded portion indicates that fraction, b_o, which is attributed to the transition to the upper laser level. Angular momenta of the ground, isomeric, and fluorescent levels are denoted by J_o, J_i, and J_f, respectively.
(a) Traditional two-level approach.
(b) Three-level analog of the ruby laser serving to illustrate the important concept of bandwidth funneling.
(c) Refinement of the three-level scheme which incorporates upconversion in order to lessen the energy per photon which must be supplied in the pumping step.

Also shown in Fig. 1 is a further refinement of the incoherent pumping scheme benefiting from upconversion. As has been often discussed,[2,6] upconversion as shown in Fig. 1c has many advantages. Most prior reports have emphasized those tending to enhance performance and efficiencies; however, upconversion also makes threshold itself much more accessible. Higher energy isomers need less pump energy to reach the broad states that would optimize bandwidth funneling, and the required pump energies can fall in the range where strong x-ray lines may be found to concentrate the spectral intensity.

Whether or not the initial state being pumped is isomeric, the principal figure of merit for bandwidth funneling is the partial width for the transfer, $b_a b_o \Gamma$. Contributing parameters are identified in Fig. 2 where it can be seen that the branching ratios b_a and b_o specify the probabilities that a population pumped by absorption into the i-th broad level will decay back into the initial or fluorescent levels, respectively. It is not often that the sum of branching ratios is unity, as channels of decay to other levels are likely. However, the maximum value of partial width for a particular level i occurs when $b_a = b_o = 0.5$.

In 1986 one of the strongest tenets of theoretical dogma insisted that for processes of optical pumping involving long-lived isomers,

$$b_a b_o \Gamma \leq 1.0 \ \mu eV \quad , \tag{1}$$

so that the efficacy of bandwidth funneling would be seriously limited in all important cases. The first major milestone[5,7,8] of 1987 demonstrated partial widths of 39, 5, and 94 μeV for the excitation with bremsstrahlung of isomers of ^{77}Se, ^{79}Br, and ^{115}In, respectively, from ground state populations. While providing a "moral victory" by breaking the absolute limits of Eq. (1), these results still left an aura of credibility to the rule-of-thumb that partial widths for isomers would be limited to the order of magnitude of μeV.

The actual measurement of partial widths involves the correlation of fluorescence yields excited by a pulse of continuous x-rays in the scheme of Fig. 2 with those expected from the expression,[4-9]

$$N_f = N_o \sum_i \xi_i \frac{\varphi_i}{A} \quad , \tag{2a}$$

where N_o and N_f are the numbers of initial and fluorescent nuclei respectively, (φ_i/A) is the spectral intensity of the bremsstrahlung in keV/keV/cm^2 at the energy E_i of the i-th pump band, and the summation is taken over all of the possible pump bands capable of cascading to the same fluorescence level of interest. The ξ_i is a combination of nuclear parameters including the partial width $b_a b_o \Gamma$ in keV,

$$\xi_i = \frac{(\pi b_a b_o \Gamma \sigma_o/2)_i}{E_i} \quad , \tag{2b}$$

where σ_o is the peak of the Breit-Wigner cross section for the absorption step. The combination of parameters in the numerator of Eq. (2b) is termed the integrated cross section for the transfer of population according to the scheme of Fig. 2.

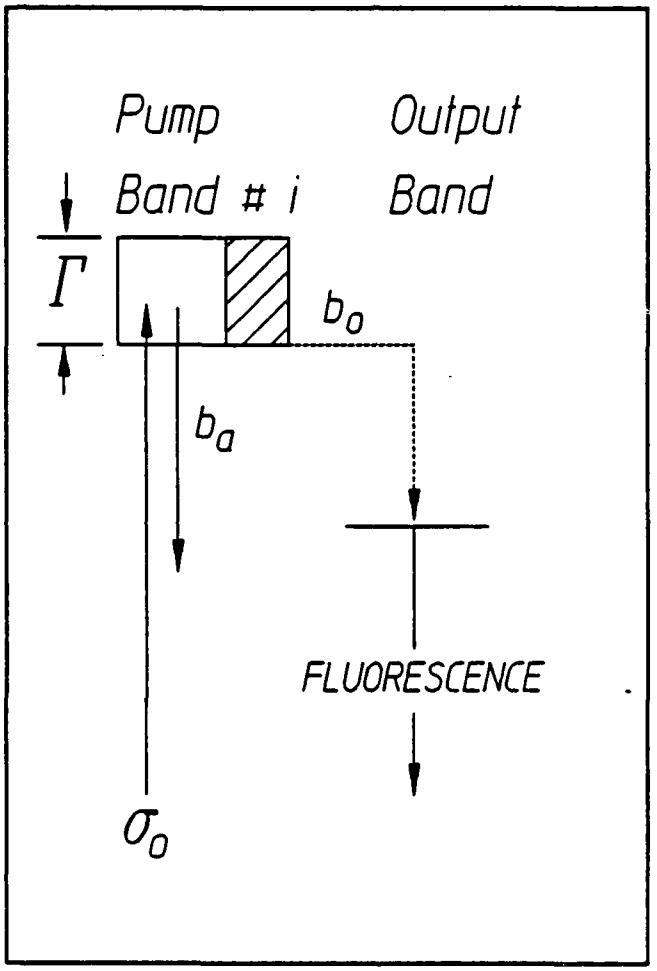

Figure 2: Schematic representation of the decay modes of a gateway state of width Γ sufficiently large to promote bandwidth funneling. The initial state from which population is excited with an absorption cross section σ_o can be either ground or isomeric.

Of the many potential systems for a test of the formulations of Eq.(2a) and (2b), the literature[10] supports the calculation of integrated cross sections for very few. Table I summarized those which are known with sufficient accuracy to serve as standards. In the convenient units of 10^{-29} cm^2 keV, values range from the order of unity to a few tens for bandwidth funnels that are sufficient for demonstrations of nuclear fluorescence from reasonable amounts of material at readily accessible levels of input. The largest integrated cross section ever inferred[11] for transfer to an isomer was 380 ($\times 10^{-29}$ cm^2 keV) for a pump band in ^{87}Sr at 2.66 MeV. Being of singular size, it was not considered as a proof of the fallibility of the rule of Eq. (1), established some years after that report.

Table I

Summary of nuclides, pump lines, and integrated cross sections for the excitation of delayed fluorescence suitable for use as calibration standards.

	PUMP LINE keV	$\pi b_a b_o \Gamma \sigma_o/2$ 10^{-29} cm^2 keV
^{79}Br	761	6.2
^{77}Se	250	0.20
	480	0.87
	818	0.7
	1005	30
^{115}In	1078	20

In a series of experiments[8,12] we conducted in 1987 that were designed to confirm the optical pumping model of Eqs.(2a) and (2b), samples of the standard nuclei of Table I were pumped with intense pulses of bremsstrahlung from the DNA nuclear simulator, PITHON. The clear signal-to-noise ratios that typified subsequent measurements of nuclear fluorescence excited through the pump bands of Table I are shown in Fig. 3. The quality of such data enabled us to "invert" Eqs. (2a) and (2b) so that the spectral intensities of the pump could be obtained at three energies from the measured values of fluorescence excited from a single pulse. Figure 4 shows a typical result[8] in comparison with a

calculation of the bremsstrahlung spectrum from that particular source on that particular shot. Both measurement and calculation are absolutes with no free parameters to adjust. Such a direct measurement of the spectrum from an intense pulse of x-ray continua had not been previously reported, and the agreement with expectations was gratifying. Moreover, it confirmed that this type of nuclear analog of the optical double resonance measurements at the atomic level can be performed with a reasonable level of accuracy as detailed in the following chapter.

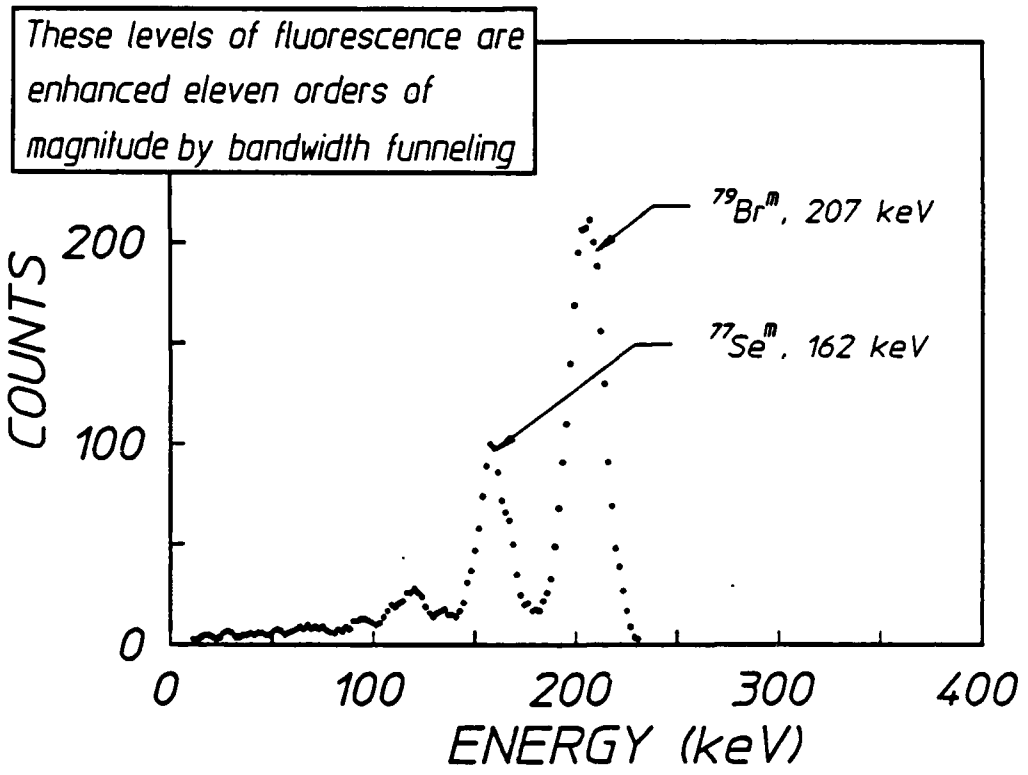

Figure 3: Fluorescence spectrum from a target containing 1.25 g LiBr and 1.20 g of elemental Se, both in natural abundances, excited with a single irradiation by the bremsstrahlung produced by the DNA/PITHON electron beam device. Acquisition time of this data was 80 s. Prominent lines are contributed by the isomeric transitions indicated.

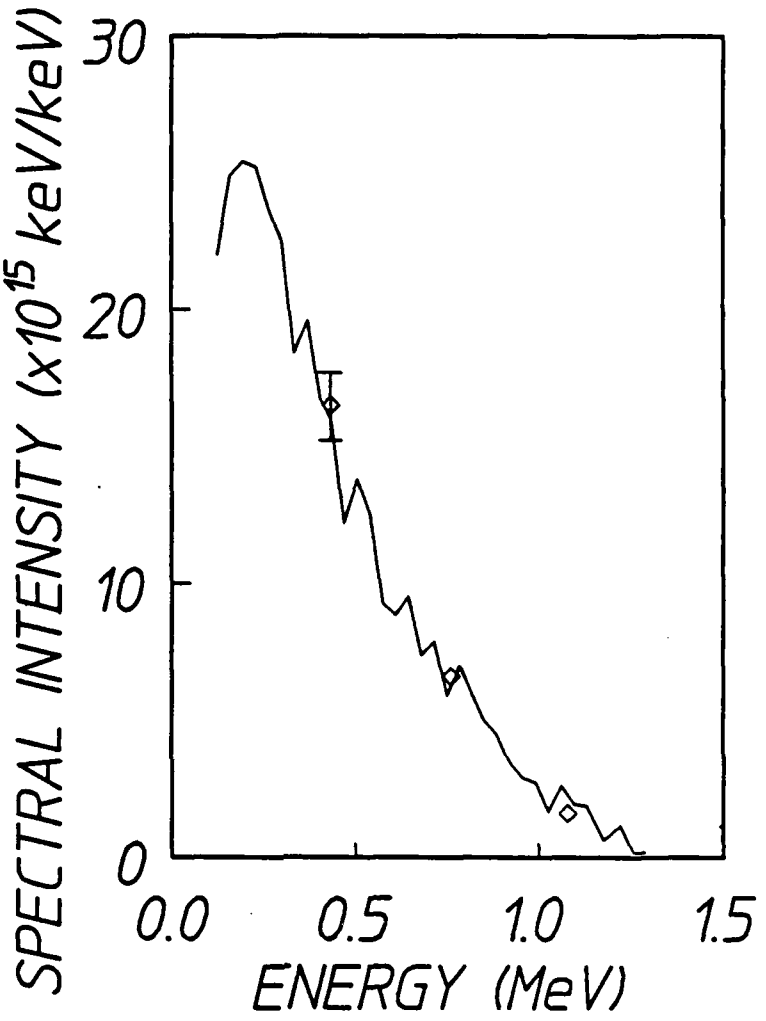

Figure 4: Data points plot the spectral intensities measured directly with our nuclear activation technique using the parameters of Table I in comparison to the spectrum computed with a coupled electron, photon transport code for a typical PITHON shot. Vertical bars show uncertainty in the measurement at the one point for which that uncertainty was larger than the plotted size of the symbol.

Tempering expectations that these successes might be readily extended to the pumping of actual isomeric candidates for a gamma-ray laser was a concern for the conservation of various projections of the angular momenta of the nuclei. Many of the interesting isomers belong to the class of nuclei deformed from the normally spherical shape. For those systems there is a quantum number of dominant importance, K, which is the projection of individual nucleonic angular momenta upon the axis of elongation. To this is added the collective rotation of the nucleus to obtain the total angular momentum J. The resulting system of energy levels resembles those of a diatomic molecule for which

$$E_x(K,J) = E_x(K) + B_xJ(J + 1) \quad , \qquad (3)$$

where $J \geq K \geq 0$ and J takes values $|K|$, $|K| + 1$, $|K| + 2, \ldots$. In this expression B_x is a rotational constant and $E_x(K)$ is the lowest value for any level in the resulting "band" of energies identified by other quantum numbers x. In such systems the selection rules for electromagnetic transitions require both $|\Delta J| \leq M$ and $|\Delta K| \leq M$, where M is the multipolarity of the transition.

In most cases of interest, the lifetime of the isomeric state is large because it has a value of K differing considerably from those of lower levels to which it would, otherwise, be radiatively connected. As a consequence, bandwidth funneling processes such as shown in Fig. 1c must span substantial changes in ΔK and component transitions have been expected to have large, and hence unlikely, multipolarities.

Attempts to confirm these rather negative expectations in an actual experiment have been confounded by the rarity of the 29 candidate isomers of interest for a gamma-ray laser. Experiments[9] in which the simpler cycle of Fig. 1b was pumped through a change of $\Delta J = 4$ or 5 with a pulsed source of continua, at first confirmed these reservations, showing an integrated cross section of only 10^{-25} cm^2 eV. Such values implied that one of the constituent transitions was significantly hindered as was expected for nuclei in which K and J remain good quantum numbers at all energies of relevance. The corresponding partial width was only 37 μeV, again tending to confirm the order of magnitude for the rule-of-thumb, Eq. (1). Dogma would insist that partial widths decrease further as the values of ΔK needed for transfer would be increased.

From this perspective the candidate isomer $^{180}Ta^m$ is the one of the 29 that is the most initially unattractive as it has the largest change

of angular momentum between isomer and ground state, 8h. However, because it was the only isomer for which a macroscopic sample was readily available, $^{180}Ta^{m}$ became the first isomeric material to be optically pumped to a fluorescent level.

This particular one of the 29 candidates for a gamma-ray laser, $^{180}Ta^{m}$, carries a dual distinction. It is the rarest stable isotope occurring in nature[13] and it the only naturally occurring isomer.[14] The actual ground state of ^{180}Ta is 1^{+} with a half-life of 8.1 hours while the tantalum nucleus of mass 180 occurring with 0.012% natural abundance is the 9^{-} isomer, $^{180}Ta^{m}$. It has an adopted excitation energy of 75.3 keV and half-life in excess of 1.2×10^{15} years.[14] Deexcitation of the isomer is most readily affirmed by the detection of the x-rays from the $_{72}Hf$ daughter resulting from decay of the ^{180}Ta ground state with an 8.1 hour half-life.

The target used in these experiments[15] conducted at the end of 1987 was enriched to contain 1.2 mg of $^{180}Ta^{m}$ in 30 mg of ^{181}Ta. Deposited as a dusting of oxide near the center of the surface of a 5 cm disk of Al and overcoated with a 0.25 mm layer of Kapton, this sample was believed free from self-absorption of the x-rays from the daughter Hf.

Figure 5 shows the spectra of the enriched target before and after 4 hours' irradiation with the bremsstrahlung from a LINAC having a 6 MeV end point energy. Figure 6 shows the dependence upon time of the counting rate observed in the Hf(K_{α}) peaks after irradiation. Data points are plotted at the particular times at which the instantaneous counting rate equals the average counting rate measured over the finite time interval shown. The figure shows the close agreement of the measured rates to the decay expected for a half-life assumed to be 8.1 hours.

From these data and the calibrated dose from the pump shown in Fig. 7, the integrated cross section for the deexcitation of the isomer can be readily calculated if the reaction is assumed to occur through a gateway state narrow in comparison to the range of energies spanned by the irradiation. A <u>minimum value</u> of $\sigma\Gamma = 4.8 \times 10^{-22}$ cm^2 eV is obtained for the integrated cross section if the gateway energy is assumed to be near 2.0 MeV. Even larger cross sections would result from the assumption that the gateway lies at higher energies where the pumping flux is decreased. This is an enormous value exceeding anything reported for

any interband transfer by two orders of magnitude. In fact, it is 10,000 times larger than the values measured for nuclei usually studied in our work. Moreover, the relatively straightforward analysis shown schematically in Fig. 8 leads to rather astonishing conclusions.

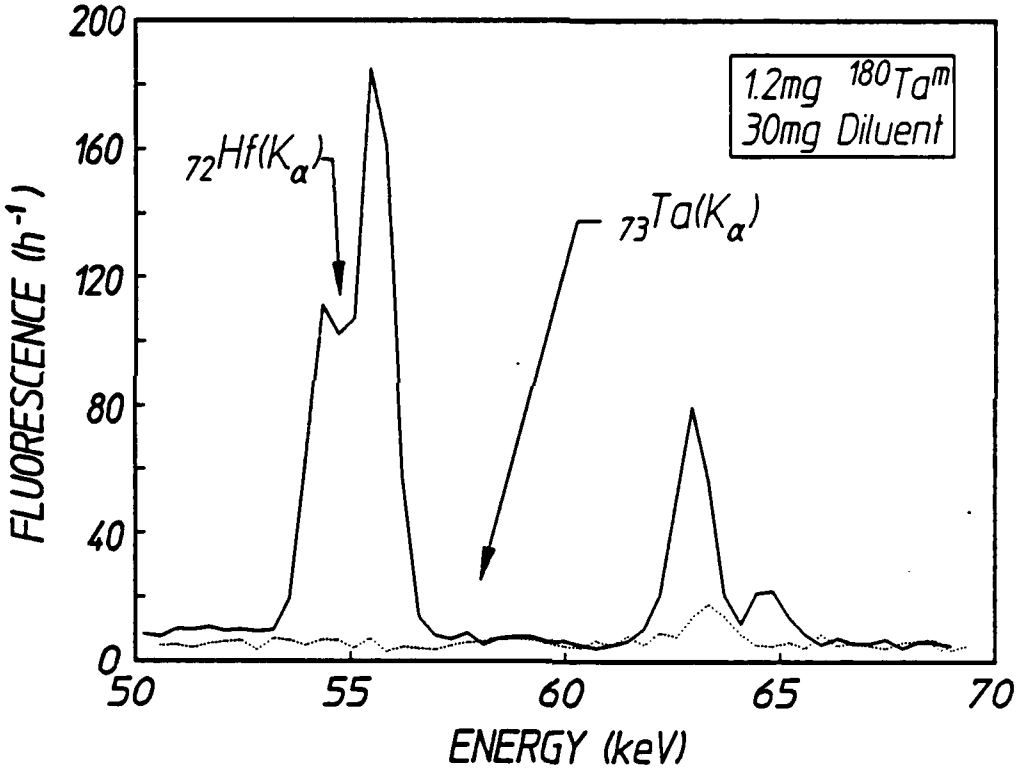

Figure 5: Dotted and solid curves show, respectively, the spectra obtained before and after dumping some of the isomeric $^{180}Ta^{m}$ contained in a target sample enriched to 5%. An HPGe detector was used to obtain the dotted spectrum before irradiation. The feature at 63 keV is from traces of natural activity in the counting shield. The solid curve shows activity resulting from the transmutation of the pumped ^{180}Ta measured in the same sample and counting system after irradiation. The prominent additions are the K_α and K_β hafnium x-ray lines resulting from electron capture in the ^{180}Ta.

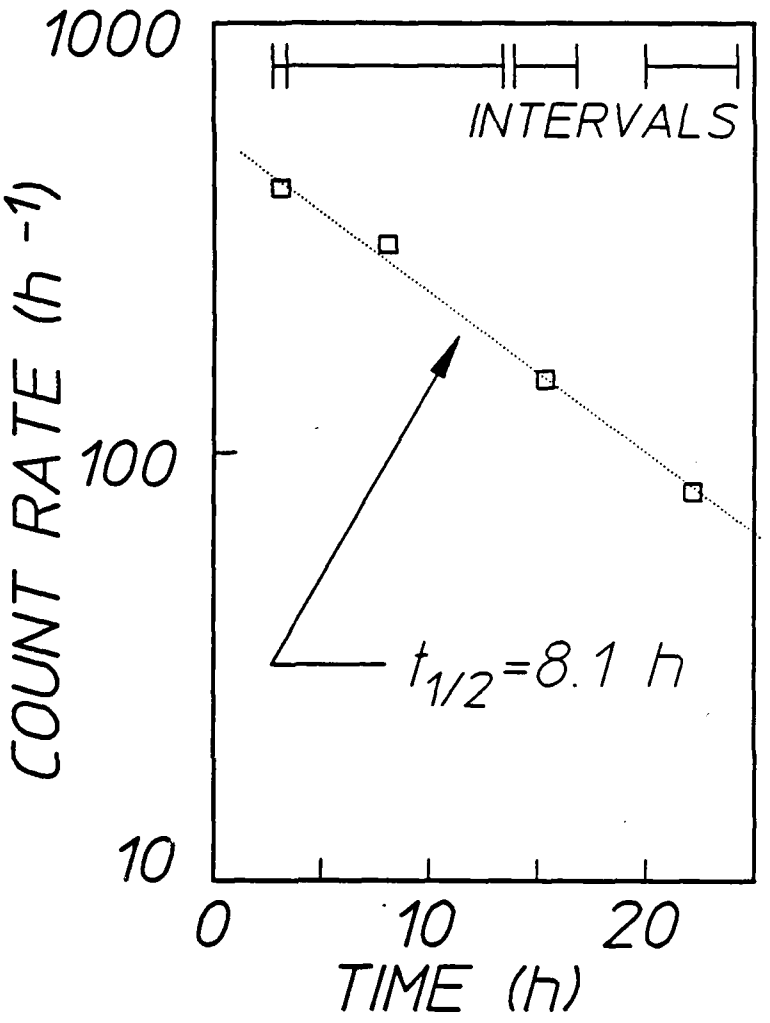

Figure 6: Plot of the counting rates measured for the Hf(K_α) fluorescence from the target as functions of the time elapsed from the end of the irradiation. The vertical dimensions of the data points are consistent with 1σ deviations of the measured number of counts accumulated during the finite counting intervals shown at the top of the graph. The dotted line shows the rate expected for a half-life of 8.1 hours.

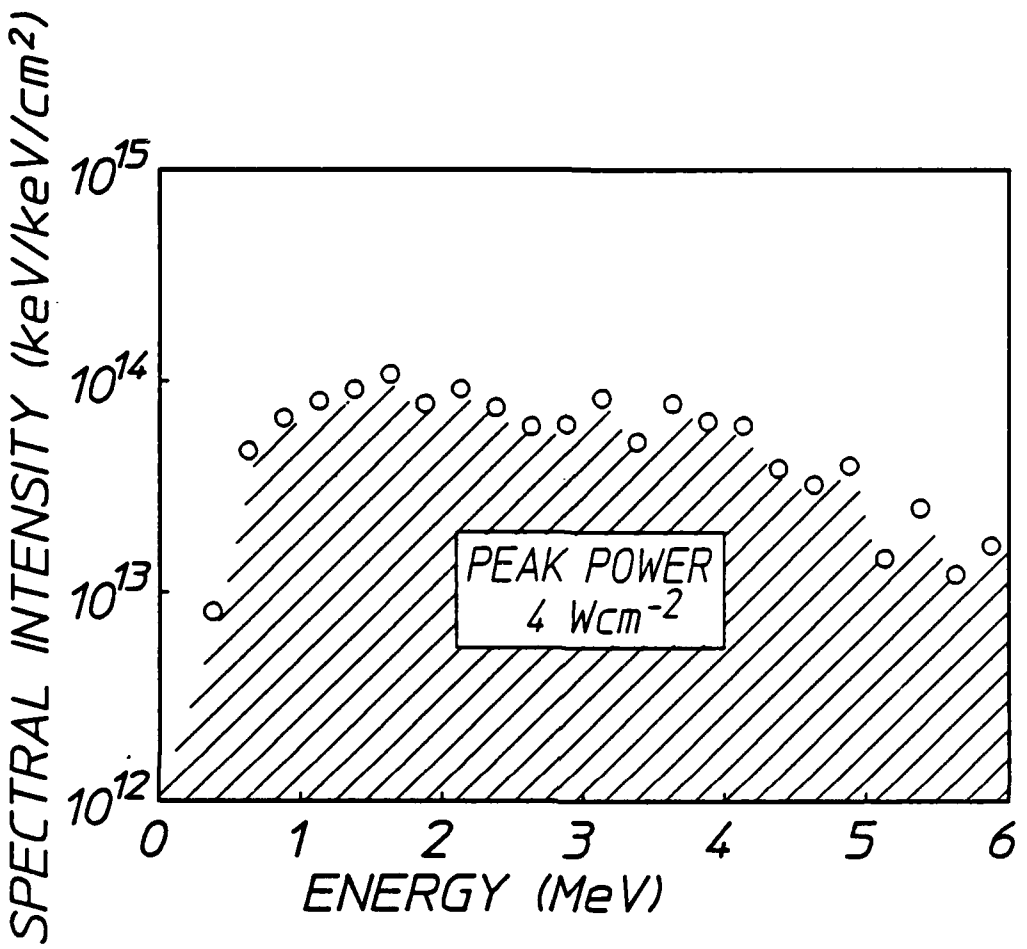

Figure 7: Spectral intensity of the bremsstrahlung used for irradiating the tantalum targets. Obtained as the total fluence from a number of successive pulses, the integral over all wavelengths of illumination corresponds to a peak power in any single pulse of only 4 W/cm².

Along the path of analyses of Fig. 8, assumptions are shown in ovals and derived results in rectangles. The most conservative results continue to be obtained by supposing the energy of the gateway band to which absorption first occurs to lie around 2 MeV. As shown in Fig. 8, this assumption together with the measured number of decays of ^{180}Ta gives the value being reported for the integrated cross section, $(\pi b_a b_o \Gamma \sigma_o/2)$.

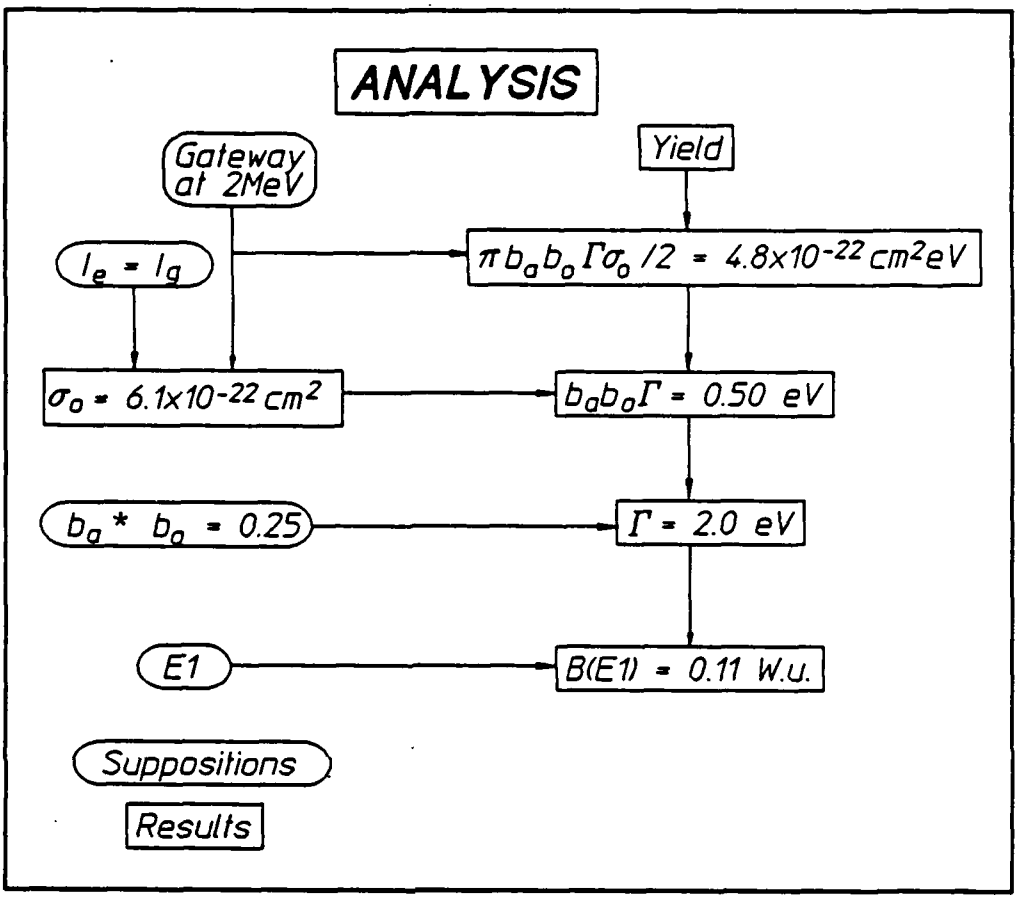

Figure 8: Flow chart showing the interrelation of assumptions and conclusions reached in the analysis of the tantalum data.

To obtain the partial width in the third row of Fig. 8 requires the Breit-Wigner cross section which peaks at

$$\sigma_o = \frac{\lambda^2}{2\pi} \frac{2I_e+1}{2I_g+1} \frac{1}{\alpha_p+1} \quad , \qquad (4)$$

where λ is the wavelength in cm of the gamma ray at the resonant energy, E_i; I_e and I_g are the nuclear spins of the excited and ground states, respectively; and α_p is the total internal conversion coefficient for the two-level system shown in Fig. 1a. The value of α_p is essentially zero for a 2 MeV transition which is highly allowed; and even were it not, σ_o would be reduced further and the partial width would become even larger. Nothing is known about the spin of the gateway state, but it is most reasonable to expect it to lie between that for the initial and

final states. In that case $I_e < I_g$, since the process is starting on the 9^- state. From Eq.(4) it can be seen that the assumption $I_e = I_g$ results in a probable overestimation of σ_o and again, in an underestimation of partial width. Even underestimated in this way, the partial width for pumping the isomer down to the ground state is an astonishing,

$$b_a b_o \Gamma = 0.5 \text{ eV} \quad . \tag{5}$$

With this result of Eq.(5) the guideline of Eq.(1) is completely destroyed as a meaningful rule. *The tenet of faith limiting to 1 μeV the partial widths for pumping isomers to radiating states has been proven to be nearly a million times too pessimistic.* An extraordinary result in itself, it implies yet another unexpected feature. If analyzed further as describing the width of a single state coupled to the isomer and <u>toward</u> the ground as shown in Fig. 1c, it must be concluded that the width of the gateway state is at least 2.0 eV, as shown in Fig. 8. From the uncertainty principle,

$$\Gamma = h/\tau_i \quad , \tag{6}$$

where τ_i is the lifetime of the funneling state, it is found,

$$t_{1/2}(\text{gateway}) = 0.22 \text{ fs} \quad . \tag{7}$$

To be consistent with the assumption $b_a = b_o = 0.25$ it must be concluded that the total width of 2.0 eV for the funneling level is contributed equally by two transitions, each of 1 eV width. As shown in Fig. 2, one must connect to the isomer and one to some other level with angular momentum more nearly comparable to that of the ground. Transition strengths are often measured in Weisskopf units (W.u.) since 1.0 W.u. is the maximum possible for the transition of a single nucleon for a given multipolarity.[16] Converted into those units the transition probability B(M) for one of the component steps of 1 eV width would become,

$$B(E1) = 0.058 \text{ W.u.} \quad , \tag{8a}$$

and

$$B(M1) = 6.0 \text{ W.u.} \quad , \tag{8b}$$

respectively, depending upon whether the multipolarity M were E1 or M1.

Again, these are enormous strengths, being almost without precedent. The expected[17] value for an electric dipole transition lies in the range 5×10^{-7} to 6×10^{-5} W.u. for heavy nuclei and fewer than ten are known[17,18] to approach 0.1 W.u. at these energies. For those exceptional cases, the width of the upper level is entirely due to the contribution from a single transition. Prior to the results being reported here there were no cases known where two transitions of such strength added comparable components of width to the same upper state.

The situation is little changed if the transitions are assumed to be mediated by the magnetic dipole, M1 operator. Generally, not as hindered as E1 transitions,[17] M1 strengths approach 0.1 W.u. in many cases. However, the scale of the W.u. for an M1 transition is smaller in physical units of width; so our measured widths correspond to a much larger number of W.u., thus presenting the equivalent problem. Fewer than ten M1 transitions are known[17] to have B(M1) > 1.0 W.u. and none are paired to share a common level.

While the width of the transfer process is difficult to interpret in the context of a single funneling state in a single particle model, a puzzle of comparable complexity is found in the efficiency with which ΔK is transferred. We have not yet been able to conceive of a cascade in the framework of pure single particle states from the funneling level to the ground state of $^{180}Ta^{m}$ which neither: 1) provides a "short circuit" of the flow of population between successive levels back to the initial isomeric state, nor 2) depends upon a transition away from the funneling state that would span a smaller change of energy and thus would require an even greater strength in W.u., nor 3) shortens the lifetime of the isomer by requiring the existence of a level having energy below that of the isomer and a value of J little different from 9. The width could be reduced by assuming the pumping proceeded through 1000 funneling states of comparable energy, but then the problem would remain that each had to support the transfer of a value of ΔJ which is difficult to accept even as a unique accident.

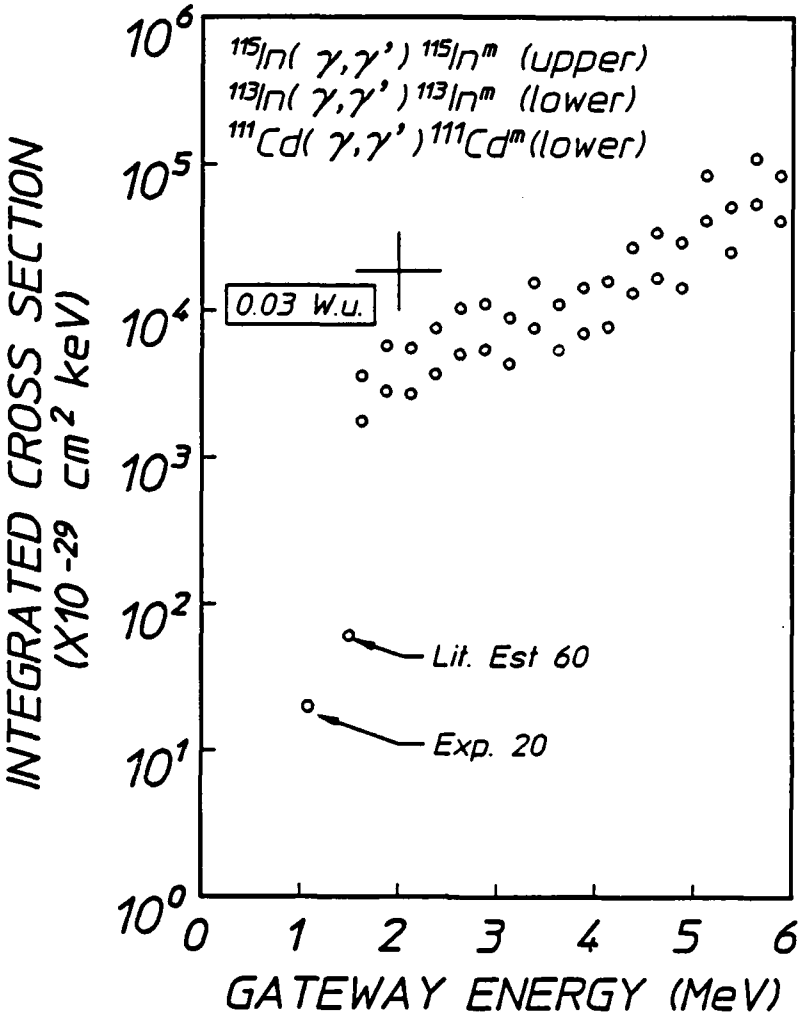

Figure 9: The integrated cross sections measured for the photoactivation of selected nuclei through individual, unknown gateway states as functions of the energies at which they could be assumed to lie. The lower family of points approximated the results obtained for the activation of both ^{111}Cd and ^{113}In to within the plotted sizes of the data. Shown at the successively lower energies are the two points taken from Refs. 11 and 7, respectively. Shown for comparison is the value corresponding to the excitation of a gateway coupled by two equal E1 transitions of the strength shown.

It is an interesting speculation that at certain energies of excitation collective oscillations of the core nucleons could break some of the symmetries upon which rest the identification of the pure single particle states. If single particle states of differing K were mixed in this way, the possibility for transferring larger amounts of ΔK with greater partial widths might be enhanced.

If the breadth of the partial cross section for interband transfer were dependent upon a collective property, a very large integrated cross section for pumping isomers from ground state nuclei might be found to be only slightly dependent upon the detailed single particle assignments of neighboring nuclei. Just such an effect was reported[20] in our group. Integrated cross sections of the order of 10,000 in units of 10^{-29} cm^2 keV were found for the excitation of isomers of ^{111}Cd, ^{113}In, and ^{115}In through resonant gateways pumped by bremsstrahlung from a linear accelerator producing most of its intensity near 2 MeV.

Figure 9 shows the resulting values of integrated cross sections as functions of the energy E_i at which the dominant funneling state may lie. The trend in the data reflects the fact that the accelerator produced fewer photons at the higher energies, reaching zero at 6 MeV. From Fig. 9 it can be seen that integrated cross sections for the excitation of isomers of indium and cadmium reach 10^{-22} cm^2 eV for pumping through channels open to the bremsstrahlung from a 6 MeV linear accelerator. This is three orders of magnitude greater than values characteristic of excitation with photons of energy below 1.4 MeV. Shown for scale is the value of cross section which would correspond to the excitation of a gateway coupled by two equal E1 transitions of the strength shown. The similarity of results for nuclei with both similar and dissimilar single particle structures does seem to support the identification of this strong channel for optically pumping isomers with some type of core property varying only slowly among neighboring nuclei.

In a most recent effort detailed in subsequent chapters, more nuclei were found to support the pumping of isomers through these enormous integrated cross sections approaching or exceeding 10^{-22} cm^2 eV. As will be seen, the partial widths nearly anticorrelate with the change in ΔJ. The largest remains $^{180}Ta^m$ with a change of $\Delta J = 8$, but the next is ^{195}Pt with about a quarter of the cross section for $\Delta J = 6$. Somewhat smaller bandwidth funnels were found for nuclei for which $\Delta J = 4$.

Whatever the mechanisms, the experimental fact remains that inter-band transfer processes reaching isomeric levels can be pumped through enormous partial widths reaching 0.5 eV, even when the transfer of angular momentum must be as great as $\Delta J = 8$. Elucidation of the process, together with identification of the gateways, has been propelled into a place of importance for 1988. The most available of the isomeric candidates for a gamma-ray laser, $^{180}Ta^{m}$, was shown to benefit greatly from this facility for bandwidth funneling. Successfully pumped with bremsstrahlung pulses having peak intensity of only $4W/cm^2$, the great width for the transfer in $^{180}Ta^{m}$ provided for adequate fluorescence signals from a milligram of isomer. This fixes a pragmatic scale for the evaluation of the other 28 candidates whenever samples become available in milligram quantities.

CALIBRATION OF PULSED X-RAY PUMP SPECTRA

From the traditional perspective of nuclear physics, the analogs of flash-lamp pumping are known as (γ,γ') reactions. While particle reactions are routinely used for the precise measurement of nuclear parameters, the same levels of accuracy have not been reached in the applications of (γ,γ') reactions. Although examples have been known for over 50 years,[21,22] only a few tens of papers can be found in the literature[23] and results reported for the same reactions show extreme variance. To the nonspecialist this would seem surprising because the analogous optical double resonance techniques are among the most powerful investigative tools at the molecular level.

In the past, the principal impediment to the quantitative study of (γ,γ') reactions seems to have arisen from the difficulties in calibrating the sources. Both accelerators and radioactive decay schemes have been traditionally used to provide electromagnetic excitation to reaction sequences such as shown in Fig. 1 in the previous chapter. Unfortunately, the combination of high flux and high photon energy in the excitation step has not permitted the use of standard spectroscopic techniques, and thus the target has had to be cycled between the irradiation device and the counting facility. In practice this has meant that studies were limited to the excitation of isomers with τ_u lifetimes of seconds to hours.

The difficulties in conducting (γ,γ') reactions are probably typified best by the excitation of the 269 minute isomer of ^{115}In at 336 keV. The principal gateway state that is radiatively connected to both the initial and the final isomeric level lies at 1078 keV and can be conveniently excited by resonant absorption of the Compton continuum from a ^{60}Co source mounted in close proximity. Nevertheless, an experiment reported[24] in 1981 produced such an excess of isomeric population that it was necessary to postulate a new mechanism in the ^{115}In for nonresonant absorption of the undegraded lines from the ^{60}Co source. Theory has not yet provided a process of the needed magnitude, and the most recent repetition of this work[25] has suggested that the excessive yield resulted not from dominance of an unknown process but rather from

In that latest, 1986 experiment, excess production was not observed.[25] Such a chaotic level of contradiction between theory and experiment and among the experiments themselves is typical in the literature and attests to the need for a better means for the calibration of intense sources of continuum radiation at energies above 200 keV.

Because of the absence of dispersive materials for such energies and because of the similarity of the absorptive properties contributed by the electrons of the various elements above 200 keV, the absolute calibration of pulsed electromagnetic continua has been virtually impossible. All large-scale sources have been "calibrated" by fitting a standard theoretical form for the intensity of bremsstrahlung continua as a function of energy to the end point energy and to the total dose.

Unfortunately, dosimeters are not uniform in their response to ionizing radiation. They are much more sensitive to the lower energy photons and thus weight by a large factor the area under the portion of the spectrum most likely to be distorted by effects of self-absorption which, themselves, have a complex dependence upon geometry. The consequence is that such "calibrations" are very sensitive to the particular structure of the spectrum at the low energies and so, in turn, are strongly affected by the accuracy of the parameterization of the individual converter being employed. It is not surprising that discrepancies as great as those affecting the ^{115}In experiments with ^{60}Co sources result from even the most careful efforts with accelerators.

A more direct means of calibration is offered by our approach to the nuclear analog of optical pumping.[5,8,26] There are a few nuclei which are known to have absorption resonances which are broad enough to channel large populations to readily detected states but which remain narrow on the scale of spectral structure of available sources. These few nuclei have been characterized by other types of nuclear studies and can be used to sample narrow slices of the intensity of a continuum. Last year we demonstrated[5] the efficacy of this technique by activating targets of ^{79}Br and ^{77}Se for the characterization of a pulsed source of bremsstrahlung continua at spectral intensities of the order of 10^{12} keV/keV. Excitation was provided by an in-house pulsed electron beam generator having a nominal end point energy of 1 MeV. Accuracy was dependent upon the precision assumed for the tabulated values[27] of nuclear parameters.

Reported this year was an extension of this technique to the larger range of photon energies, 0.2 to 1.5 MeV, and for intensities to 10^{16} keV/keV using the same target nuclei, ^{79}Br and ^{77}Se. In this work the self-consistency of the nuclear parameters was directly determined. Important changes and additions were found to be necessary and these were described. The resulting tabluation of the essential nuclear parameters is now self-consistent and capable of supporting the characterization of pulsed x-ray fluence over the larger range of energies and intensities.

Experimental Method

A schematic drawing of the apparatus used to calibrate the PITHON nuclear simulator at Physics International is shown in Fig. 10. Although only two counting systems are shown for the purposes of illustration, up to three samples could be irradiated during the x-ray pulse and then automatically transferred to the counters. The target-to-counter transit times for the pneumatic shuttles were measured for each shot, and averaged about 1.0 second.

For the work described here, a single sample which incorporated a mixture of LiBr and elemental selenium was used. Figure 11 shows the construction of the sample and lists the important parameters relating to it. After arrival at the counting station, the sample was analyzed for 80 seconds, which represented about four half-lives of the 17.4 second ^{77m}Se and 16 half-lives of the 4.8 second ^{79m}Br. Two NaI(Tl) spectrometers and one HPGe system were employed in the experimental series, but the data presented here was obtained exclusively with one of the 3" × 3" NaI(Tl) detectors. Samples with longer half-lives (e.g. 4.49 hour ^{115m}In) were manually inserted in the spectrometers after the short-lived materials were counted.

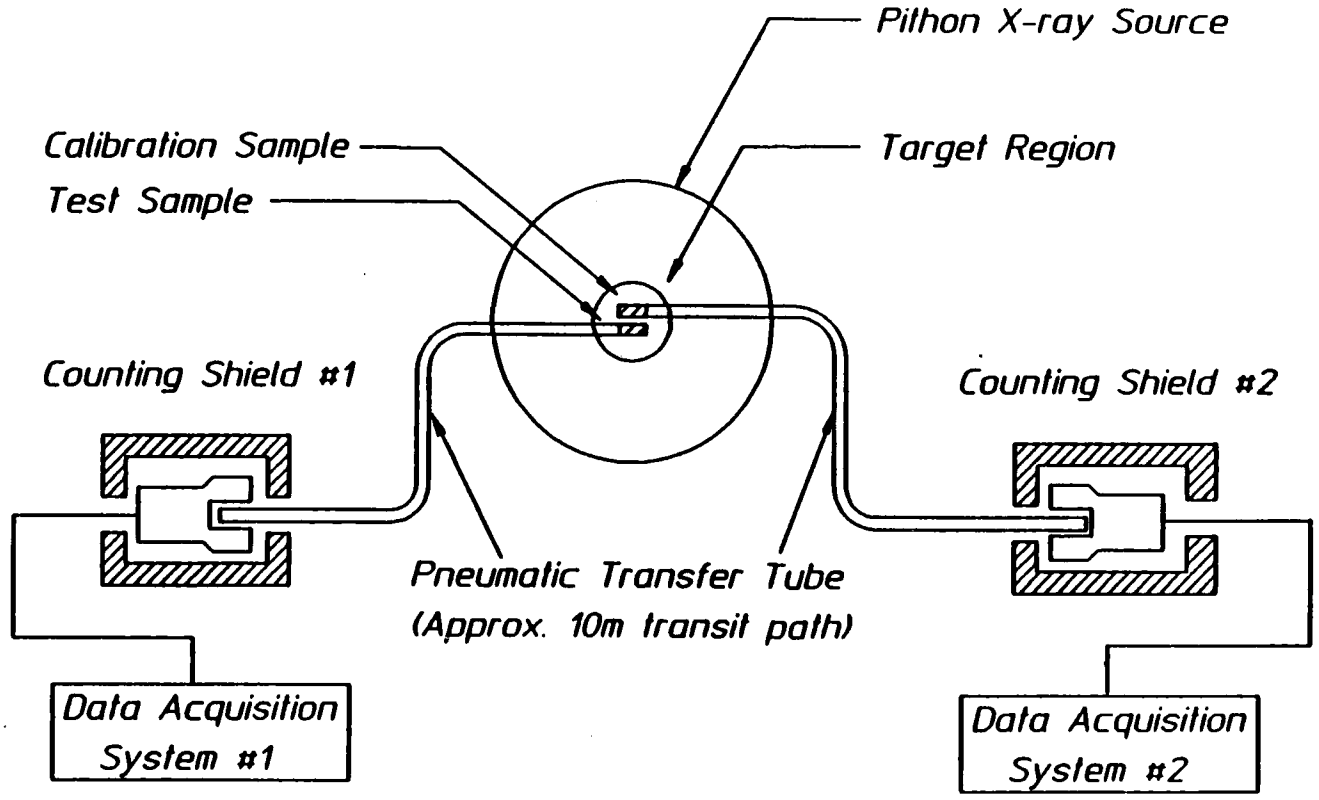

Figure 10: Apparatus for nuclear fluorescence measurements with the PITHON bremsstrahlung machine. Most of the x-ray energy was emitted in a 20 cm pattern in which the samples were centered. The PITHON sequence timer was used to trigger the automatic transfer of samples from the irradiation volume to the counters.

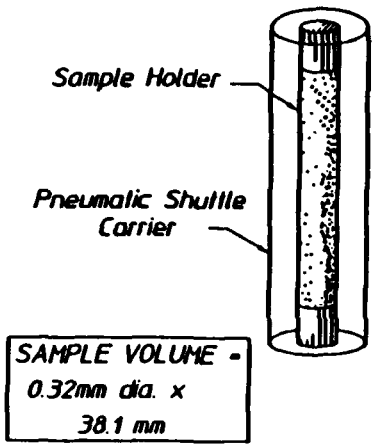

NUCLIDE	FORM	MASS (g)	COUNT TIME (sec)	TRANSIT TIME (sec)
^{79}Br	LiBr	1.250	80.0	1.02 ± 0.03*
^{77}Se	Elemental Se	1.196		

* INDIVIDUAL TRAVEL TIMES WERE USED TO CORRECT EACH TRIAL.

Figure 11: Sample holder for mixed LiBr/Se target. The sample itself was in a 0.64 cm diameter tube capped with plastic plugs. This tube was centered in a polyethylene "rabbit" running in a 1.9 cm diameter transfer tube.

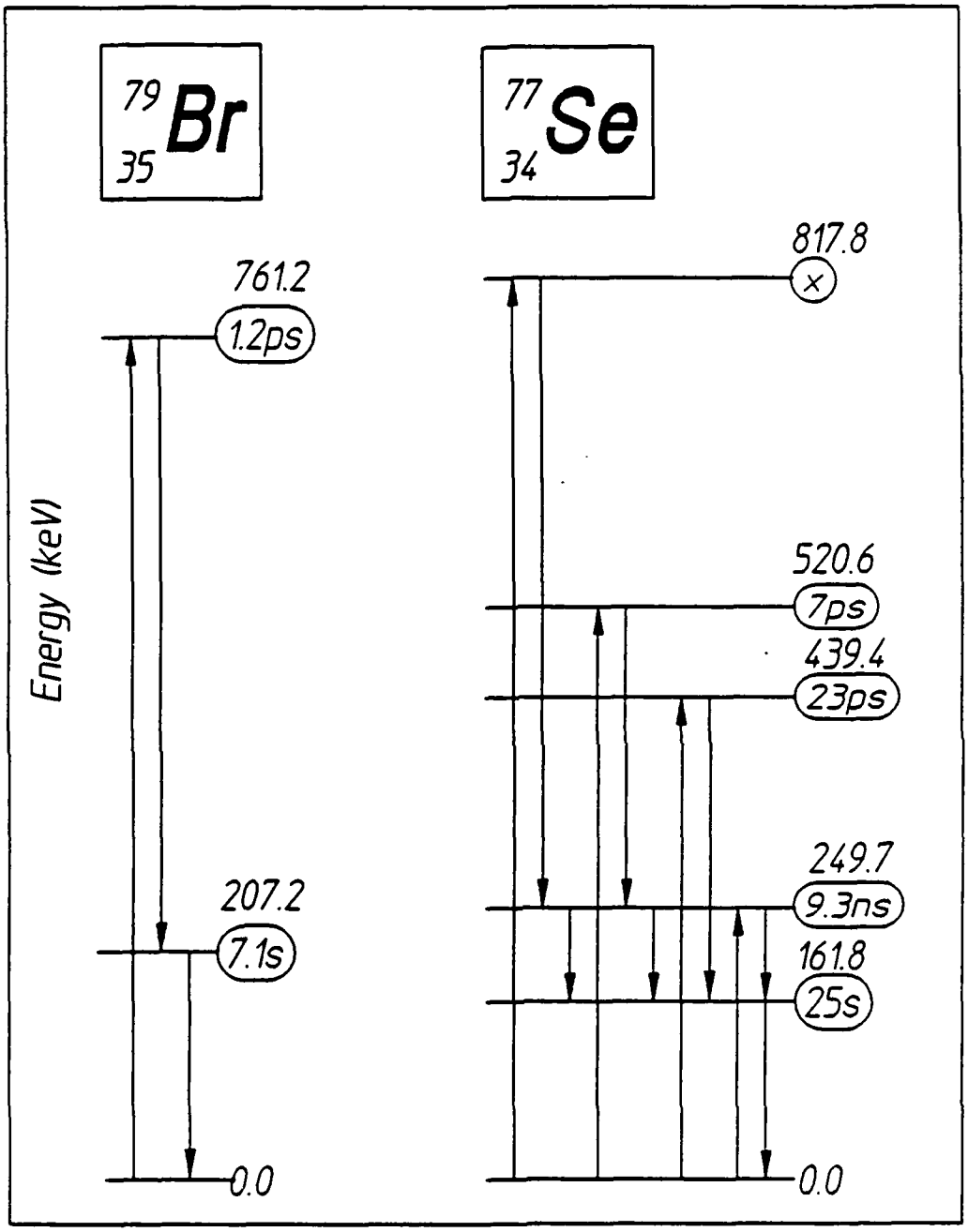

Figure 12: Energy level diagram of the excited states of ^{79}Br and ^{77}Se important in the production of populations of their respective isomers. Half-lives of the states are shown in the ovals to the right of each and sequences of transitions corresponding to the (γ,γ') reactions leading to the isomers are shown by the arrows. Downward γ' transitions also include effects of cascading through levels other than those shown.

Results and Analyses

During the period of these experiments, 23 shots were successfully instrumented with the calibration target and pneumatic shuttles. The nominal variation of 20% in source performance was augmented by the deliberate programming of firing parameters. As a result, shots were obtained for end point energies ranging from 0.9 to 1.5 MeV. A spectrum of the fluorescence obtained from a typical irradiation was shown in Fig. 3 of the previous chapter.

Of paramount concern in the examination of that type of data is whether the relative yields from ^{79}Br and ^{77}Se are in agreement with the accepted values for the nuclear parameters appearing in the most recent tabulations.[10] The first step in the resolution of such a question is the extraction of the relative numbers of excited nuclei actually produced in the sample. This requires correction for the finite duration of the sampling period over which the fluorescence is counted, the efficiency of the detector, the probabilities for internal conversion rather than radiation of the fluorescence, and the fraction of fluorescence reabsorbed in the sample. While the first three corrections are readily obtained from tables or by calibration, the last is dependent upon geometry in a more complex fashion. To minimize the importance of that particular correction, small samples were used for which the effects on the ^{79}Br and ^{77}Se data differed[28] by about 3%.

The number of excited nuclei produced in the course of an irradiation of the type shown in Fig. 2 was given by Eqs. (2a) and (2b). In Eq. (2a) the first term in the summation is composed of the nuclear parameters, while the second ratio describes the intensities of the pump x-rays which are assumed to be continuous, at least without structure on the fine scale of the nuclear absorption. In particular, the combination $\phi(E_i)/A$ is the spectral fluence at the energy E_i in units of keV/keV/cm^2. Tacitly, it has been assumed that the duration of the pump source is less than the fluorescence lifetime, τ_u.

The nucleus ^{79}Br is unique in its utility to efforts at calibration. According to latest data,[10] it has but a single broad level connecting to both ground and fluorescent states in the energy range 0 - 1.8 MeV. The relevant part of its scheme of energy levels is shown in Fig. 12. On the other hand, the ^{77}Se nucleus is more complex having at least four levels funneling to the same fluorescent transition at 161.8 keV, as shown in Fig. 12. The highest at 818 keV is insufficiently characterized, and the Γ_i parameter appearing in Eq. (2b) must be estimated. This was done and reported previously.[5] The "best" values[29] of the parameters of Eq. (2b) are listed in Table II for convenience, together with sources of the basic data and the values confirmed by this experiment.

Table II

Summary of nuclear fluorescence parameters reconciled by this work.

NUCLIDE	E_{in} (keV)	$\pi b_a b_o \Gamma \sigma_o/2$ (10^{-29} cm^2 keV)		E_{out} (keV)
		Ref.5	This work	
^{79}Br	761	6.2	6.2	207
^{77}Se	250	0.20	0.20	162
	480[a]	1.50	0.87	
	818	0.7	0.7	
	1005		30	
^{115}In	1078		20[b]	337

[a]The effects of the 440 keV and 521 keV transitions have been combined.
[b]From Ref. 7.

An additional difficulty encountered in the use of Eq. (2b) to model the performance of targets pumped with the device used in these experiments accrued from the geometry of the diode producing the bremsstrahlung x-rays. Since it was configured as a pinched diode, electrons did not arrive at the converter foil with normal incidence. In such cases the linear, Kulenkampff approximation to the spectrum used previously[5] is expected to become markedly concave.[30]

Of the 23 shots instrumented in this experimental series, five benefited from additional diagnostics. From records of the time dependent voltage and current, the spectral fluence was calculated with the one-dimensional coupled electron/photon Monte Carlo transport code, TIGER, an established procedure in the e-beam community.[31] Results are shown in Fig. 13 for a selection of those five shots. If plotted on a linear scale, those spectra would be considerably more concave than the idealized approximation[5] used for normal incidence. However, the ratio of fluence at a particular energy to that at some standard can be readily parameterized from curves such as shown in Fig. 13. In doing this, the energy of the single absorption line of ^{79}Br at 761 keV was chosen as a standard. Shown in Fig. 14 are the resulting curves for the empirical estimation of the relative spectral intensity, $\zeta(E_i)$,

$$\zeta(E_i) = \phi(E_i)/\phi(761\ \text{keV}) \quad , \tag{9}$$

plotted as functions of the end point energy, V_o, for four different E_i, 250, 480, 818, and 1005 keV. Data points record the values supplied by the TIGER code, and the curves were obtained by a smoothing procedure.

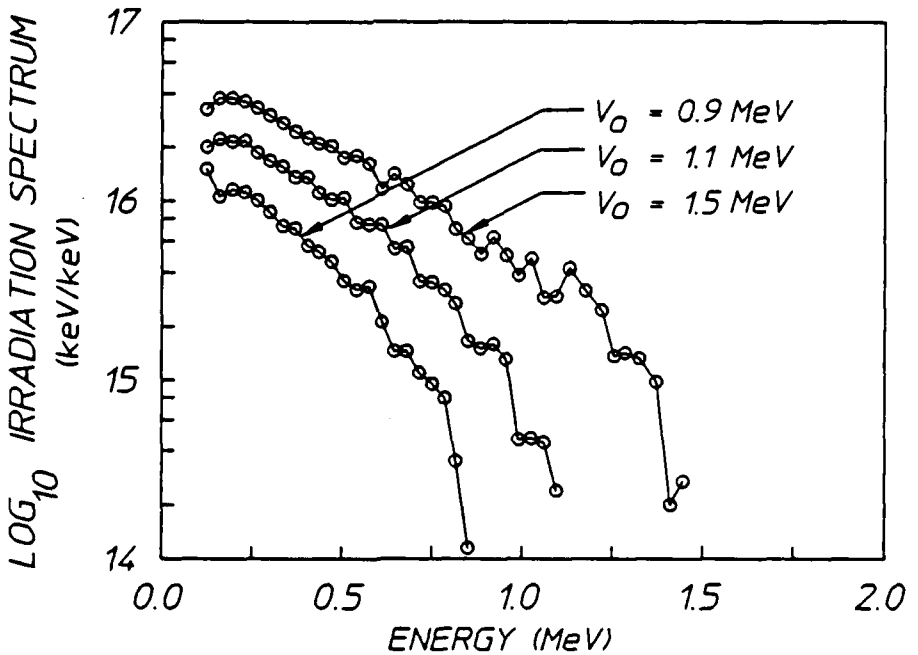

Figure 13: Plot of three bremsstrahlung spectra computed with the TIGER code for the particular characteristics of three electron beam discharges from the PITHON having end point energies V_o, as indicated.

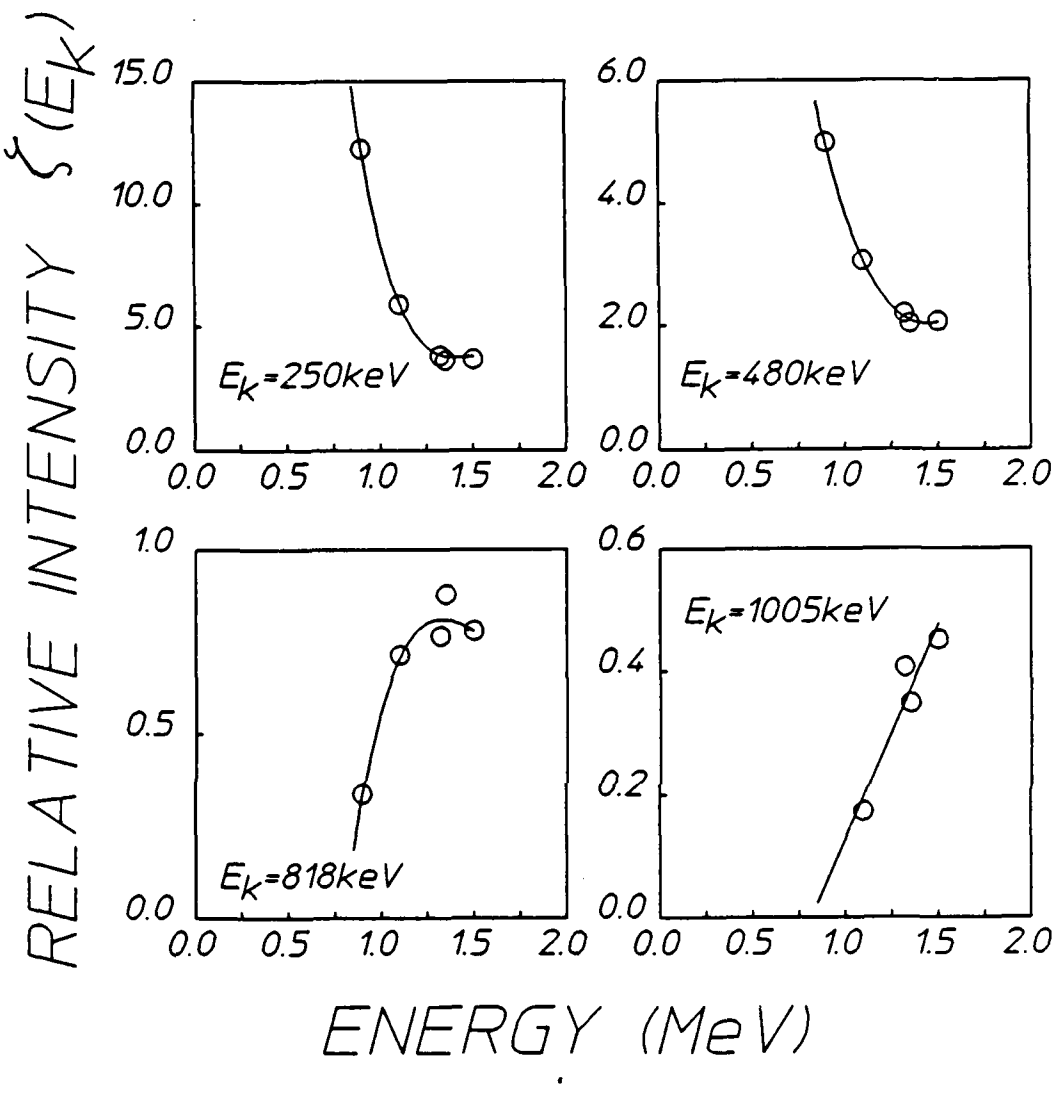

Figure 14: Graphs of the relative spectral intensities $\zeta(E_i)$ at the photon energy, E_i, plotted as functions of the end point energy of the electron beam producing the bremsstrahlung. Curves were obtained by smoothing and interpolating between the data points representing the results of TIGER code computations, three of which are shown in Fig. 13. Intensities are normalized to the spectral intensity at the reference energy, E = 761 keV.

From data such as presented in Fig. 14 the fluorescent yield expected from ^{77}Se can be readily computed in terms of that actually observed from ^{79}Br. The degree to which the calculated yield agrees with the measured fluorescence is a direct indication of the level of consistency between the values compiled for the nuclear parameters in Table II. This can be appreciated by writing Eq. (2a) for the irradiation of a sample of ^{79}Br,

$$S(Br) = N(Br)\xi_{761}(Br)\frac{\phi(761)}{A} \quad , \tag{10}$$

where

$$\xi_i = \frac{(\pi b_a b_o \sigma_o \Gamma/2)_i}{E_i} \quad , \tag{11}$$

from Eq. (2b), and $\phi(761)$ is the spectral intensity *at the target*. The corresponding expression for the ^{77}Se is,

$$S(Se) = N(Se)\left[\xi_{250}(Se)\frac{\phi(250)}{A} + \xi_{480}(Se)\frac{\phi(480)}{A} + \xi_{818}(Se)\frac{\phi(818)}{A} + \xi_k(Se)\frac{\phi(E_k)}{A}\right] \quad , \tag{12}$$

where the possibility of an extra contribution from an unexpected band at E_k has been included.

Dividing Eq. (12) by Eq. (10) and substituting from Eq. (9) and (11) yields after some rearrangement,

$$\frac{S(Se)}{S(Br)} - \frac{N(Se)}{N(Br)}\left[\frac{\xi_{250}(Se)}{\xi_{761}(Br)}\zeta(250) + \frac{\xi_{480}(Se)}{\xi_{761}(Br)}\zeta(480) + \frac{\xi_{818}(Se)}{\xi_{761}(Br)}\zeta(818)\right] = \frac{N(Se)}{N(Br)}\frac{\xi_k(Se)}{\xi_{761}(Br)}\zeta(E_k) \quad . \tag{13}$$

while formidable in appearance, Eq. (13) has a very straightforward interpretation, namely,

$$R(\text{exp}) - R(\text{model}) = \frac{N(Se)}{N(Br)} \frac{\xi_k(Se)}{\xi_{761}(Br)} \zeta(E_k) \quad , \qquad (14)$$

where R is the ratio of the numbers of excited nuclei produced in ^{77}Se and ^{79}Br.

Several points warrant comment. While $\phi(E_i)$ in Eq. (10) depends upon the poorly-characterized geometric efficiency through which the fluences of Fig. 13 are actually coupled to the target, the relative fluence, $\zeta(E_i)$ does not. Neither does it depend upon the entrance aperture of the target, A, another uncertain quantity in real configurations.

In actual experiments, the residues between experimental data and the results of the model appearing on the left of Eq. (14) should be scattered about zero, regardless of the end point energy of the irradiation--*provided the model is complete*. If an unknown channel is contributing, or if one of the $\xi_i(Se)$ is incorrect, then the residue should have a dependence upon experimental variables as shown to the right of Eq. (14). Since the $\zeta(E_k)$ of Fig. 14 have considerably different functional dependences upon V_o, it should be possible to identify the particular E_k contributing the residue, provided enough variation of V_o can be introduced into the experiment.

For the 23 data points of this experiment, the residues computed from Eq. (14) do <u>not</u> scatter about zero. Figure 15 shows a plot of the resulting residues as functions of end point energies. The functional dependence is striking and fits a line intercepting the horizontal axis near 1 MeV. Inspection of the right side of Eq. (14) suggests that this would be consistent with the contribution from an additional transition with a threshold energy for excitation near 1 MeV.

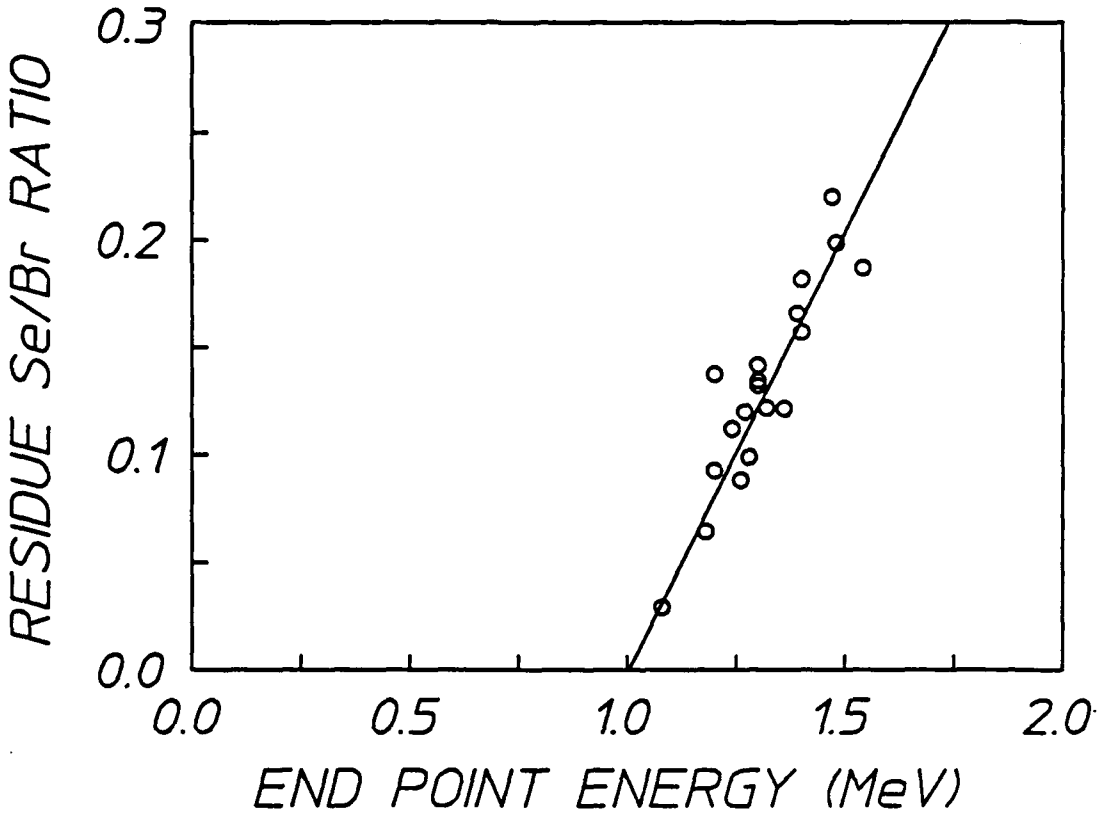

Figure 15: Plot of the residues obtained from the application of Eq. (9) to the data for a model containing the three lowest energy gateway levels of ^{77}Se plotted as a function of the end point energies of the electron beam discharges producing the bremsstrahlung.

The complete set of nuclear parameters appearing in Eq. (11) is not known for any of the transitions of ^{77}Se lying above 818 keV. However, the branching ratios are available for many of them. While optimal branching ratios could be offset by poor lifetimes, in principle, it is most reasonable to expect a significant new channel of excitation to correspond to a level for which branching ratios were, at least, favorable. Table III records the product $b_a b_o$ for levels of ^{77}Se above 818 keV, and the close correlation between the large value seen at 1005 keV and the intercept of Fig. 15 is extremely persuasive.

Table III

Compilation from Ref. 10 of the products of the branching ratios, $b_a b_o$, a, appearing in Eq. 11 for the transitions of ^{77}Se lying above 818 keV. Corresponding values of Γ have not been reported in the literature.

Level (keV)	$b_a b_o$
818	0.0063
825	0.00025
911	0.017
1005	0.031
1128	0.0012
1186	0.047
1230	0.0024

Once the excitation energy of the "new" channel was determined from Fig. 15 and Table III, the functional dependence of $\zeta(1005)$ upon end point energy could be determined. This was done, and the result is shown in Fig. 14. Again there is a striking similarity between the functional dependences upon V_o of the residues and of the $\zeta(1005)$, as would be required by Eq. (14).

Once the level missing from the model is identified as corresponding to E_k = 1005 keV, all of the terms of Eq. (14) are known except $\xi_{1005}(Se)$. In Fig. 16 the model residues are plotted as functions of $\zeta(1005)$ for the 19 shots of this experiment having end point energies above 1 MeV. From Eq. (14) it can be seen that the slope of such a plot should correspond[32] to $\xi_{1005}(Se)N(Se)/\xi_{761}(Br)N(Br)$. The least-squares fit to the data including the origin is shown by the heavy line in Fig. 16, together with the lighter lines bounding acceptable alternatives. These lead to a value

$$\xi_{1005}(Se) = (30 \pm 7.5) \times 10^{-32} \text{ cm}^2 \quad , \qquad (15a)$$

which from Eq. (11) gives,

$$\pi b_a b_o \sigma_o \Gamma/2 = (30 \pm 7.5) \times 10^{-29} \text{ cm}^2 \text{ keV} \quad , \qquad (15b)$$

in turn yielding,

$$t_{½}(1005) = 0.36 \text{ psec} \quad . \qquad (15c)$$

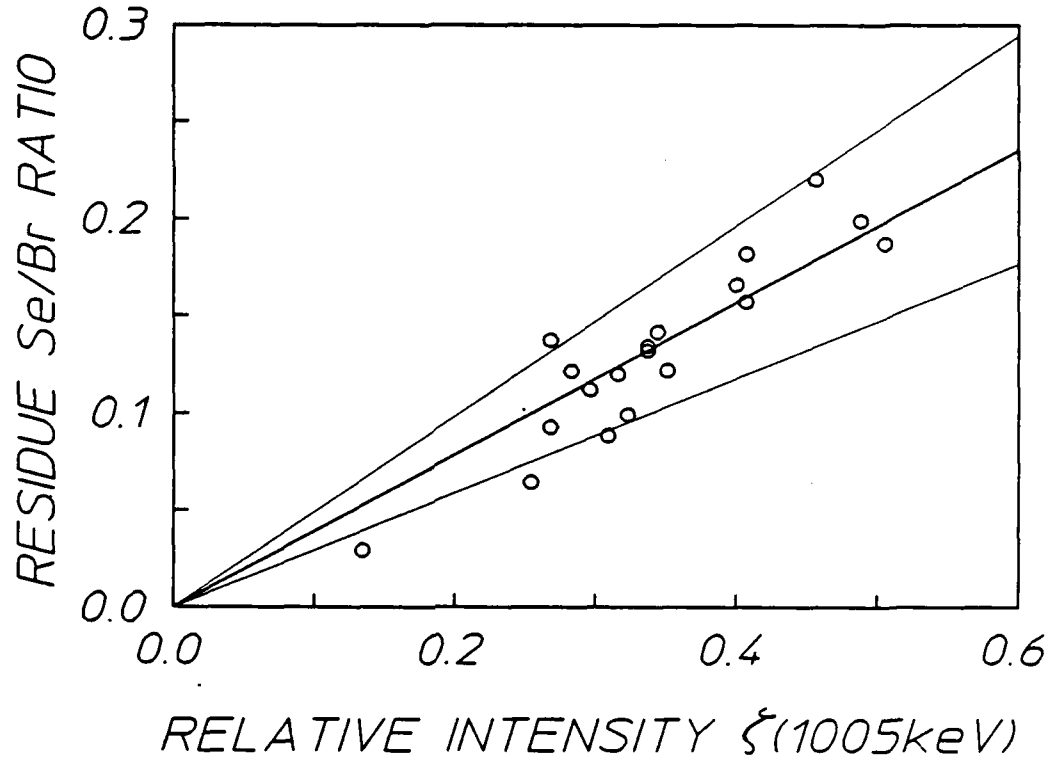

Figure 16: Plot of the residues of Fig. 15 as functions of the relative intensity of irradiation of 1005 keV.

As a final step of analysis, the residues of Eq. (14) were recomputed, including the term of Eq. (15a) into the model estimate, R(model), on the left of Eq. (14). Figure 17 shows the resulting residues as functions of the end point energies. This time the data appear[33] to scatter around the V_0 axis indicating that the model now contains a sufficient number of terms to predict the fluorescent yields up to an end point energy of 1.5 MeV to an accuracy of better than 10%.

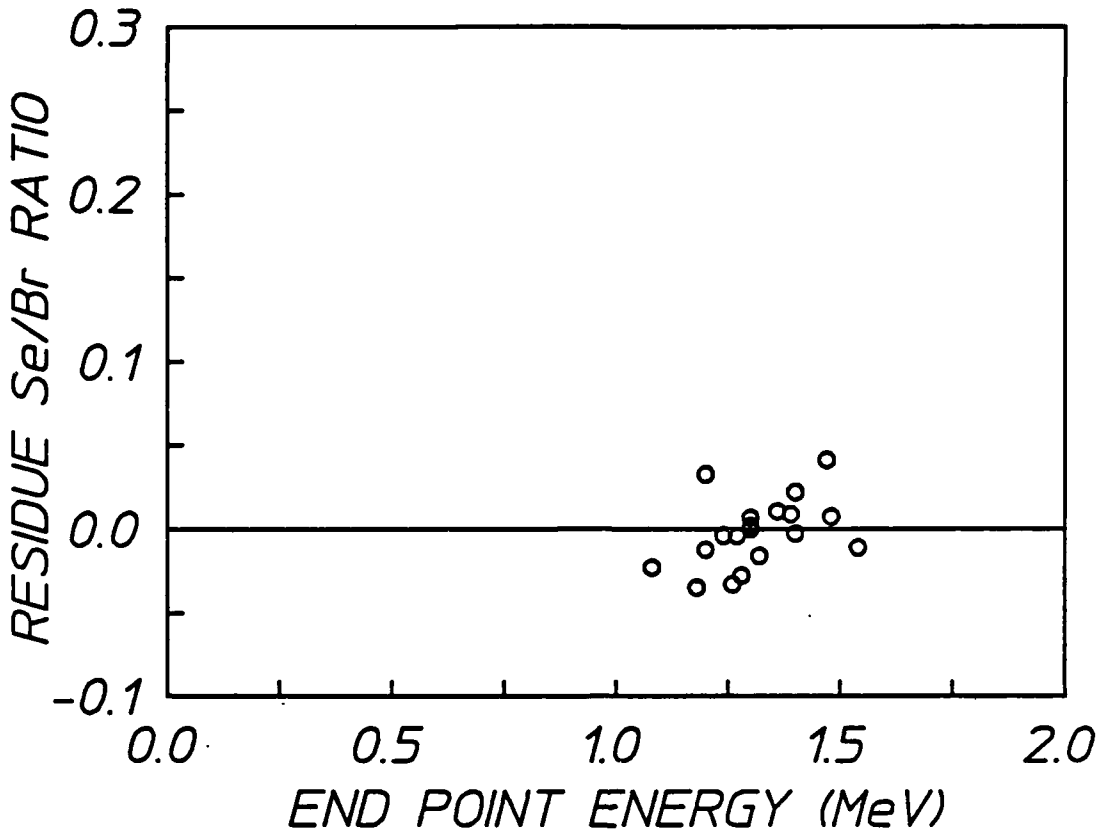

Figure 17: Plot of the residues obtained from the application of Eq. (14) to the data for a model containing the three lowest energy gateway levels of ^{77}Se together with the new level at 1005 keV, plotted as a function of the end point energies of the electron beam discharges producing the bremsstrahlung.

Discussion

The principal conclusion of this work is that the 1986 version[10] of the nuclear parameters for 77Se and 79Br is completely consistent. Provided no significant component of the x-ray flux lies above 1 MeV, those data are sufficient to predict the fluorescent yields from ^{79}Br and ^{77}Se. However, for the irradiation of samples with bremsstrahlung produced by electrons with end point energies above 1 MeV, the more complete set of parameters of Table II must be used. In such cases it is appropriate for all end point energies below 1.5 MeV.

The difference between the 1986 data and Table II lies in the inclusion of the pump channel in ^{77}Se at 1005 keV found in the course of this work. Corresponding to the considerable transition strength of 0.011 Weisskopf units for an M1 transition in the absorption channel, it is well-connected to both initial and fluorescent levels. As can be seen from Table II it will rapidly become the dominant channel for funneling population into the fluorescence level as the number of pump photons above 1 MeV increases in a source.

The striking consistency between the results from ^{79}Br and those from ^{77}Se argues favorably for the utility of this technique of selective nuclear excitation over a wider field of experimental variables than originally described.[5] It does not require an initial computer model. A measurement of the activation of ^{79}Br would determine the fluence at 761 keV at the position of the sample. Activation of ^{77}Se is more complex but tractable, once the ^{79}Br results are known. Assuming $\zeta(818) - \zeta(761)$ the contribution to ^{77}Se from the small 818 channel can be easily removed. The immediate residue is a weighted sample of the low energy portion of the irradiating spectrum and of the energies near 1 MeV. To separate these effects in cases where the end point energy lies above 1 MeV, recourse must be made to a third nuclei sampling only high energies. An ideal candidate is ^{115}In which is the subject of a forthcoming article as described in the subsequent chapter.[7] This isotope samples only the fluence at 1078 keV and the consistent value[7] for the corresponding reaction has also been included in Table II for convenience. From the activation of an ^{115}In component of the sample,

the contribution to ^{77m}Se population from the new 1005 keV channel can be removed. From the resulting second residue, the average fluence in the range 250 - 480 keV can be isolated.

As a demonstration of the efficacy of nuclear activation, such a procedure was performed on the activation of a composite target irradiated with a typical shot (4379) from PITHON. As expected, absolute measurements of the flux at the target could be obtained for three energies,[34] 433, 761 and 1078 keV. Then by multiplying those values of flux by the area of the forward (2π) hemisphere upon which the target was conceived to rest during irradiation, the absolute spectral intensity emitted by the source was determined. Results were plotted in Fig. 4 together with the predictions of the TIGER code calculations for that shot. Agreement is perhaps better than is warranted by the inherent level of mechanical inaccuracy in target positioning.

Uncertainty in the direct measurement of spectral intensity at the target arises from two sources, statistical error in the number of fluorescent counts and unknown error in the nuclear data of Table II. Results of the former are plotted in Fig. 4, but appear larger than the plotted symbol only at the lower energy point arising as a result of so many differences of data. Uncertainty due to residual inconsistency in the data of Table II is of unknown magnitude but should be less than the error introduced by the statistical uncertainty in the counts as a result of these efforts in determining consistency of the entries of Table II.

The results of this work indicate that (γ,γ') reactions can be studied with a high level of precision if the sources are carefully characterized. The existing data for the transitions of ^{79}Br and ^{77}Se, together with others to be discussed, clearly offer a convenient means of sampling the spectra of intense pulsed sources.

ACTIVATION OF ^{115m}In BY SINGLE PULSES OF INTENSE BREMSSTRAHLUNG

For the study of (γ,γ') reactions that produce isomeric products, ^{115}In has a particularly favorable combination of characteristic properties. Having only a few channels for reaction at energies below 1.4 MeV, it nevertheless displays a large integrated cross section for excitation of the 269 minute isomer at 336 keV. For these pragmatic reasons ^{115}In has served as the archetype material for the study of this type of reaction, and a number of efforts have been reported[8,10,11,21-24,35-41] in the past 48 years.

The relevant part of the energy level diagram[10] of ^{115}In is shown in Fig. 18, indicating only three levels through which a (γ,γ') reaction of multipolarity E1, M1, M2, or E2 could proceed to populate the isomeric state for photons below 1.4 MeV. The importance of the lowest dipole gateway level at 941 keV is negligible because it has a particularly small integrated cross section[42] for excitation in comparison to that of the nearby 1078 keV level, and the 934 keV $7/2^+$ level has a yet smaller cross section because of its longer lifetime.

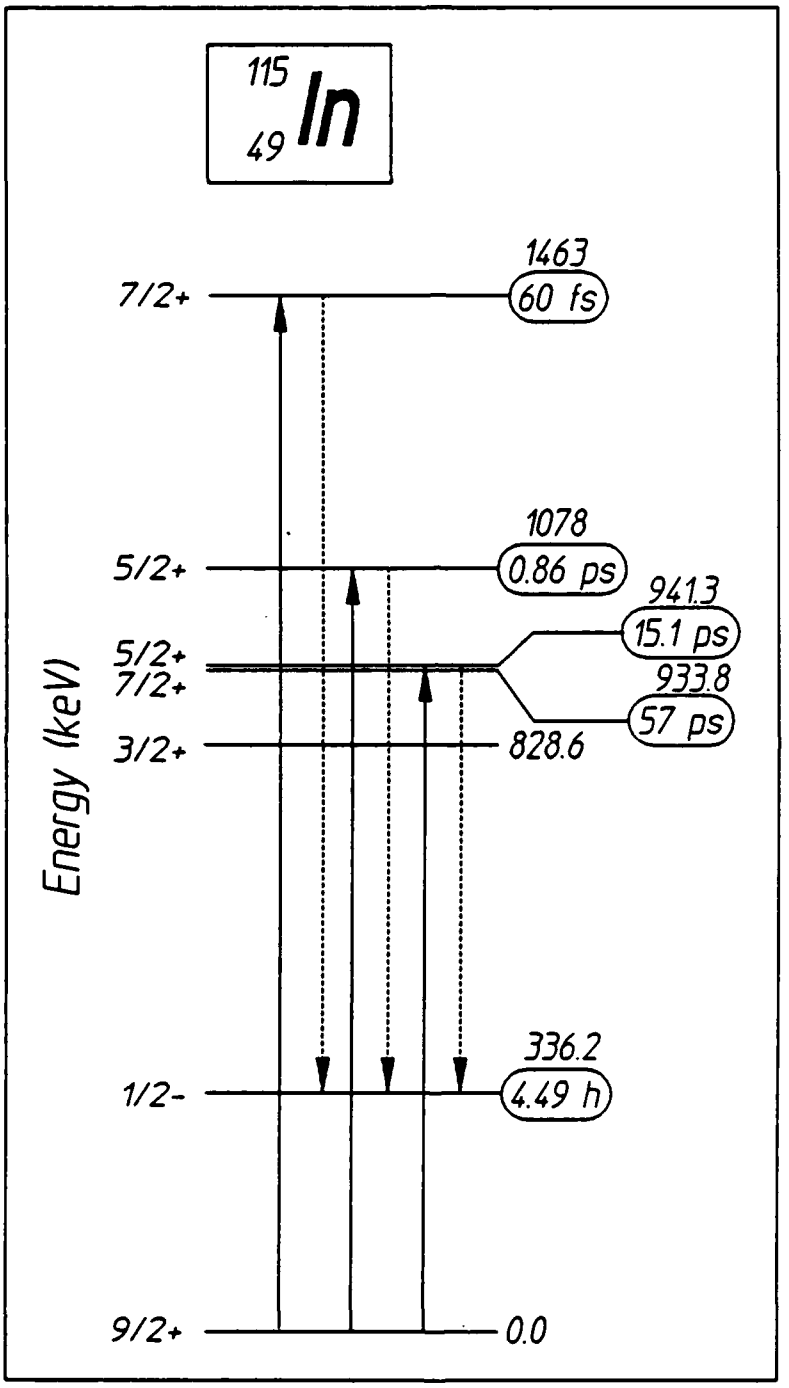

Figure 18: Energy level diagram of the excited states of the ^{115}In important in the production of popuations of the isomer.[10] Half-lives of the states are shown to the right of each, and sequences of (γ,γ') reactions leading to the isomer are shown by the arrows. Dashed γ' transitions occur by cascading through levels not shown.

Table IV

Summary of integrated cross sections reported for the reaction $^{115}In(\gamma,\gamma')^{115m}In$ through the 1078 keV $J^{\pi} = 5/2^{+}$ level.

Cross Section $\pi b_a b_o \sigma_o \Gamma/2$ ($\times 10^{-29}$ cm^2 keV)	Reference
23 ± 4	Ikeda and Yoshihara (Ref. 36)
20 ± 4	Veres (Ref. 37)
7.1 ± 2.3	Chertok and Booth (Ref. 38)
11.5 ± 4.0	Booth and Brownson (Ref. 11)
30 (+40,-20)	Boivin, Cauchois, and Heno (Ref. 39)
10.5 ± 2.7	Lakosi, Csuros, and Veres (Ref. 40)
19 ± 1	Watanabe and Mukoyama (Ref. 41)
5.39 ± 0.64	Ljubicic, Pisk, and Logan (Ref. 24)
18.1 ± 1.5	Yoshihara et. al. (Ref. 25)
18.7 ± 2.7	This work

In practical cases in which ^{115}In samples are excited either with gamma rays from a source or by bremsstrahlung from an accelerator operating below 1.4 MeV, the absorption spectrum for (γ,γ') reactions producing isomers is essentially monochromatic at 1078 keV. Nevertheless, quantitative measurements of the integrated cross section have shown a chaotic level of contradiction between theory and experiment and among the experiments themselves. Table IV presents a summary of values reported in the literature together with the results of this measurement, in terms of the integrated cross section as discussed in the first chapter.

We have recently argued[5] that the principal cause of such a large degree of variance among previous measurements of the ^{115}In excitation has been the generally inadequate level of characterization of the spectrum of the pump source. In the preceding chapter we showed that the spectrum from a pulsed source of intense bremsstrahlung could be

determined to a level of accuracy sufficient for the quantitative description of the reactions $^{77}Se(\gamma,\gamma')^{77m}Se$ and $^{79}Br(\gamma,\gamma')^{79m}Br$. In doing so, an important new channel for the excitation of ^{77m}Se was found through the 1005 keV $J^{\pi} = 3/2^-$ level.

It was the purpose of the work reviewed in this chapter to reexamine the reaction $^{115}In(\gamma,\gamma')^{115m}In$ with the same pulsed bremsstrahlung source used for the reconciliation of the absorption cross sections to ^{79m}Br and ^{77m}Se. Results for ^{115}In were found in this work to be consistent with that reconciliation. Moreover, the quantitative value for the integrated cross section we report can be seen to be in good agreement with the other value reported most recently as the result of excitation with a radioactive source.[23]

Methods and Apparatus

In our previous report[5,8] it was shown that the uncertainty in the absolute value of the geometric coefficient coupling the source of pump radiation to the absorbing target could be eliminated by normalizing both the pump fluence and the fluorescence counts to some standard material having a monochromatic excitation spectrum. The reaction $^{79}Br(\gamma,\gamma')^{79m}Br$ was found to be an ideal standard, having an integrated cross section of 6.2×10^{-29} cm^2 keV and a convenient radioactivity in the isomer. Following the formalism developed in the preceding chapter, the number of ^{115m}In nuclei, S(In), which could be excited by a flash of intense bremsstrahlung can be conveniently expressed as a ratio,

$$\frac{S(In)}{S(Br)} = \frac{N(In)}{N(Br)} \frac{\xi_{1078}(In)}{\xi_{761}(Br)} \zeta(1078) \quad , \qquad (16)$$

where S(x) and N(x) are the number of nuclei produced and the number of target nuclei of material x, respectively; $\zeta(1078)$ is the ratio of pumping intensity at 1078 keV to the intensity at 761 keV; and the $\xi_E(x)$ is the combinations of nuclear parameters involved in the excitation of the gateway level at energy E, described in Eq. (2b), namely,

$$\xi_E(x) = \frac{(\pi b_a b_o \sigma_o \Gamma/2)_E}{E} \quad . \qquad (17)$$

The collection of terms in parentheses in Eq.. (17) comprises the integrated cross section for excitation as usually reported; and the calibration value for ^{79}Br is $\xi_{761}(Br) = 8.2 \times 10^{-32}$ cm^2.

The source of excitation in these experiments[8] was the bremsstrahlung produced by the DNA/PITHON nuclear simulator at Physics International. The usual end point energy of the electrons producing the bremsstrahlung was 1.3 MeV with small shot-to-shot variance. For these particular experiments, the nominal firing parameters were deliberately perturbed so that successive irradiations could be obtained with end point energies varying from 0.9 to 1.5 MeV.

Intensities at the target were determined by measuring the nuclear activation of the ^{79}Br component of a sample of LiBr containing isotopes in natural abundance. This calibrating target was run in a pneumatic transfer system which enabled the population of ^{79m}Br produced by a single irradiation to be subsequently counted at a quiet location 30 m removed from the source. Activation lost during the 1.0 s transit time could be readily corrected during analysis.

The ^{115}In sample under study was in the form of a thin foil taped to a fiduciary mark near the pneumatic system. Since the ^{115m}In had a substantially longer half-life, it could be manually detached after exposure and transferred to the spectrometer, which consisted of a 3" × 3" NaI(Tl) detector with associated electronics. In typical cases, a counting time of one hour gave better than 2% statistical accuracy in the ^{115m}In peak after removal of background. In the course of this experimental series, twelve shots were obtained for sufficiently high end point energies to yield statistically significant numbers of fluorescent isomeric activity.

To confirm that the fluorescence being detected resulted only from decay of the ^{115m}In activity, additional foils were irradiated and then examined with an intrinsic Ge spectrometer, carefully shielded. In Fig. 19 we show spectra from an In foil irradiated by bremsstrahlung with an end point of 1.3 MeV. The fluorescence peak is at 336.2 keV, with a half-life seen to be consistent with a tabulated value of 4.49 hours.

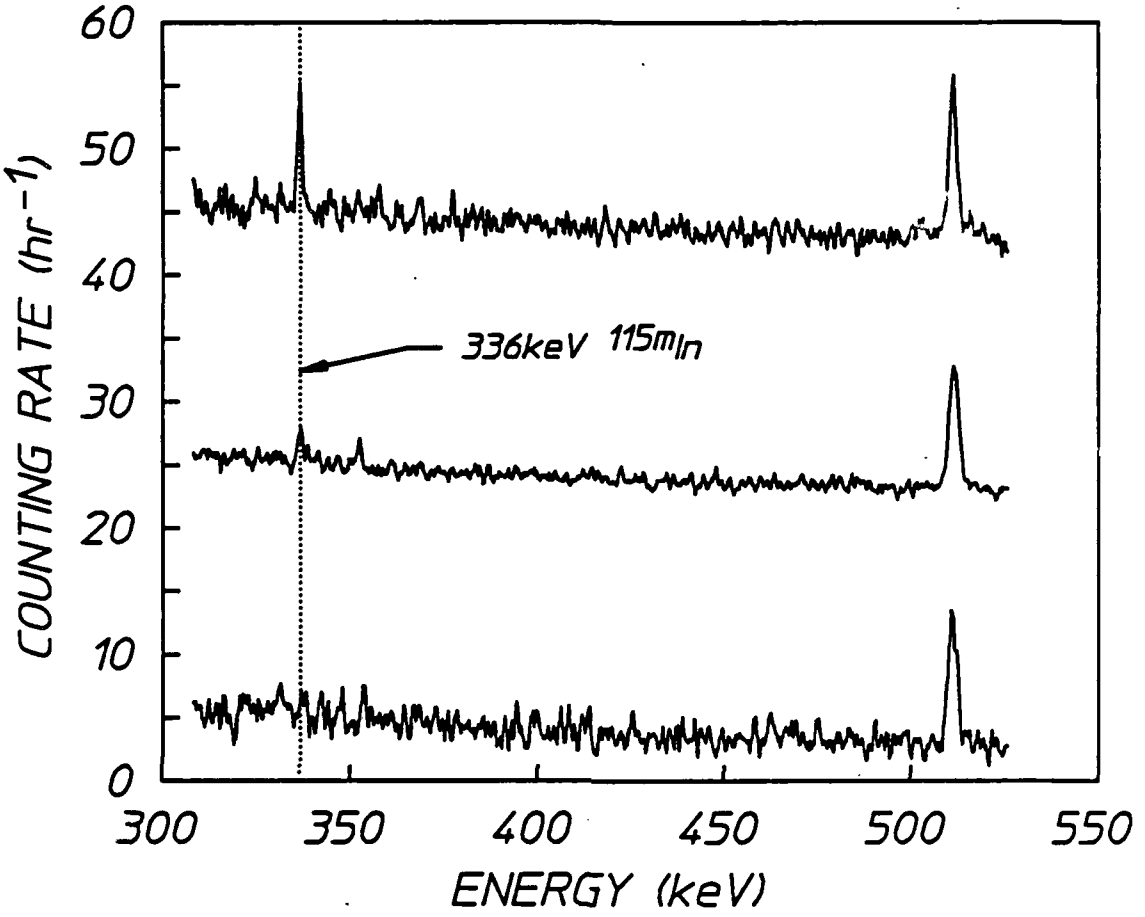

Figure 19: Three sequential spectra from an intrinsic Ge detector begun at times 6.5, 9.2, and 19.0 hours after the irradiation with a flash of bremsstrahlung with a 1.3 MeV end point. Data have been offset by 40, 20, and 0 counts/h, respectively. The 336.2 keV peak is seen to decay with the appropriate half-life of 4.49 hours for ^{115m}In. The other structure is the annihilation peak at 511 keV.

The relative bremsstrahlung intensity emitted at 1078 keV was a strong function of the end point energy of the accelerator as shown in Fig. 20. These data were obtained by numerically fitting theoretical computations of bremsstrahlung spectra. As reported in the preceding chapter, confidence was established by examining quantitatively the number of fluorescent nuclei produced by successive irradiations of samples of ^{79}Br and ^{77}Se at a variety of end point energies.

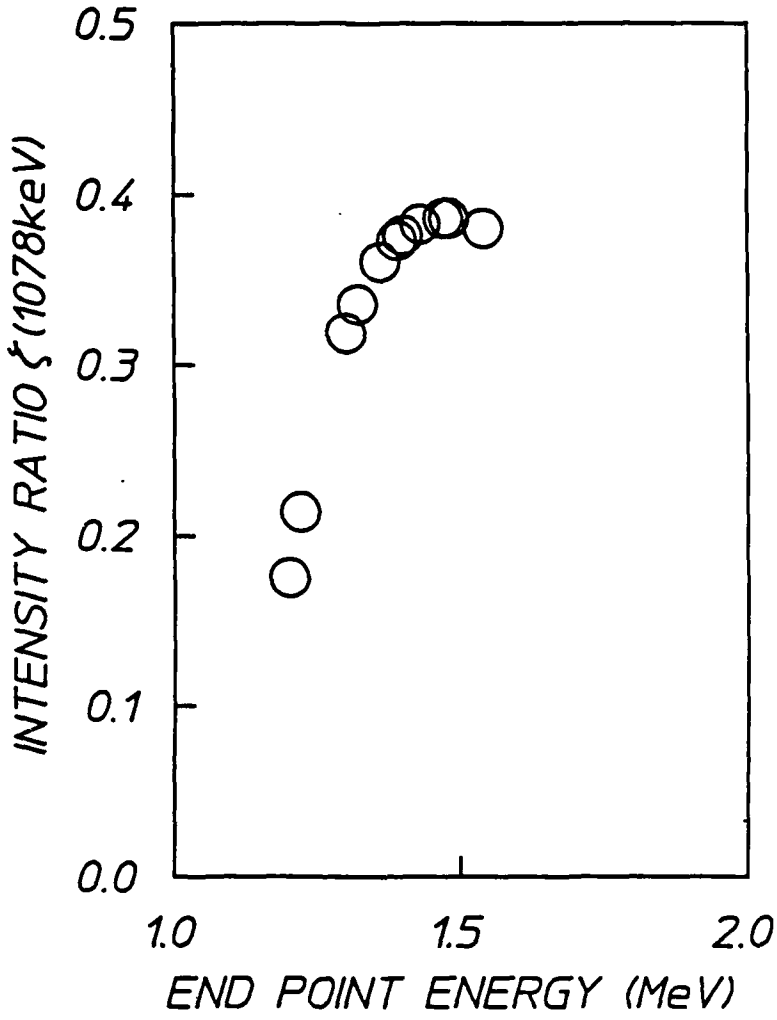

Figure 20: Plot of the ratio of intensities of the bremsstrahlung spectrum at 1078 keV to that at 761 keV as a function of the end point energy of the electron beam producing the photons.

Results

Because of a small physical displacement of the ^{115}In sample from the mixed ^{79}Br/^{77}Se target providing calibration, the actual number of fluorescent photons counted from the former had to be corrected for the extra path length from the source point to the absorber. This was done by mounting thermoluminescent diodes (TLD's) at both positions and then comparing the total dose recorded at the different points for each shot. The number of photons from ^{115m}In was scaled by the value of relative dose received at the ^{115}In and at the calibrating positions.

The indium sample was optically thin at the 336 keV energy of the fluorescence from the ^{115m}In, thus obviating corrections for self-absorption. Data were corrected for fluorescence and detector efficiencies. The resulting values of S(In)/S(Br) are obtained from Fig. 21 by multiplying the ratios of fluorescent counts shown there by 0.75, the ratio of correction factors for these effects.

The linear form of the dependence of the relative yield of fluorescence from the indium isomers seen in Fig. 21 between 1.0 and 1.45 MeV is a strong indication of the dominance of a single channel of excitation through a gateway level lying at an energy given by the value of intercept. From the data of Fig. 21, it is seen that the intercept lies between 1000 and 1200 keV in agreement with the known state at 1078 keV. Also shown in Fig. 21 is the energy of the next higher gateway state, $7/2^+$ at 1.463 MeV. It is interesting to observe that for end point energies above this value there may be a tendency of the data to depart from the simple linear fit because of the availability of this additional gateway. A greater number of measurements at successively higher end point energies would be needed to confirm this indication.

Once most of the data are established as being consistent with the model of excitation through a single level at 1078 keV, Eq. (16) provides a means of determining the absolute cross section for the excitation. In Fig. 22, data for the measured values on the left side of Eq. (16) are plotted as functions of the relative intensities ζ(1078) appearing on the right.[43] As can be seen from Eq. (16), the best slope around which the data of Fig. 22 scatter would represent our experimental determination of the product of the first two terms on the right of Eq. (16).

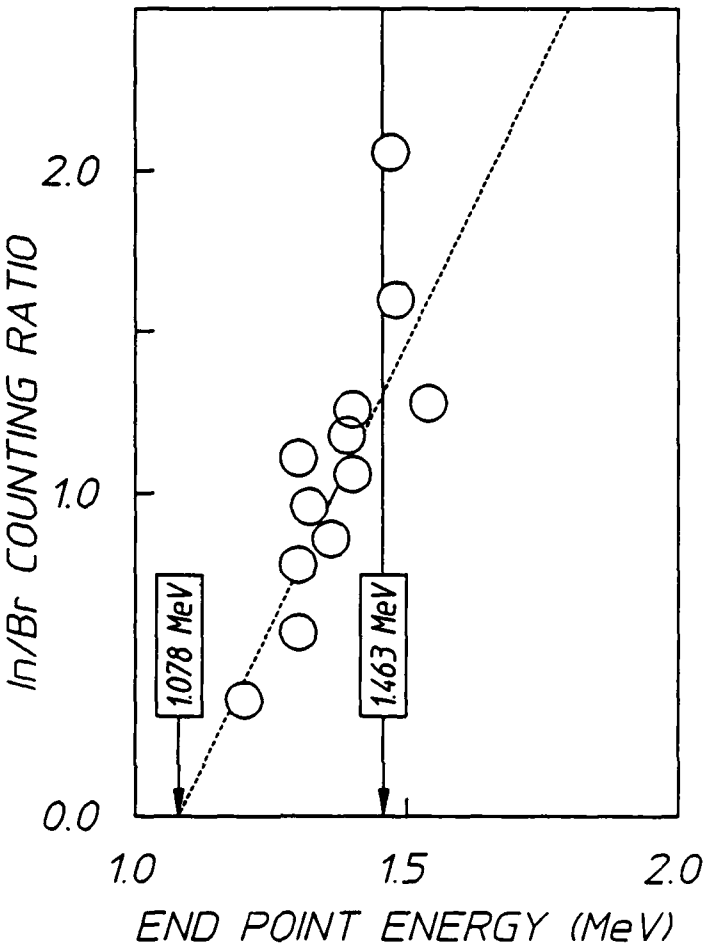

Figure 21: Ratios of fluorescent photons from ^{115m}In to those from ^{79m}Br, produced by single discharges from PITHON, as corrected for the finite duration of the counting interval and plotted as a function of the end point energies of the electrons producing the bremsstrahlung. The dashed line shows a linear fit to the data intercepting the x-axis at a gateway energy of 1.078 MeV. Excitation energy of the next higher gateway is shown at 1.463 MeV.

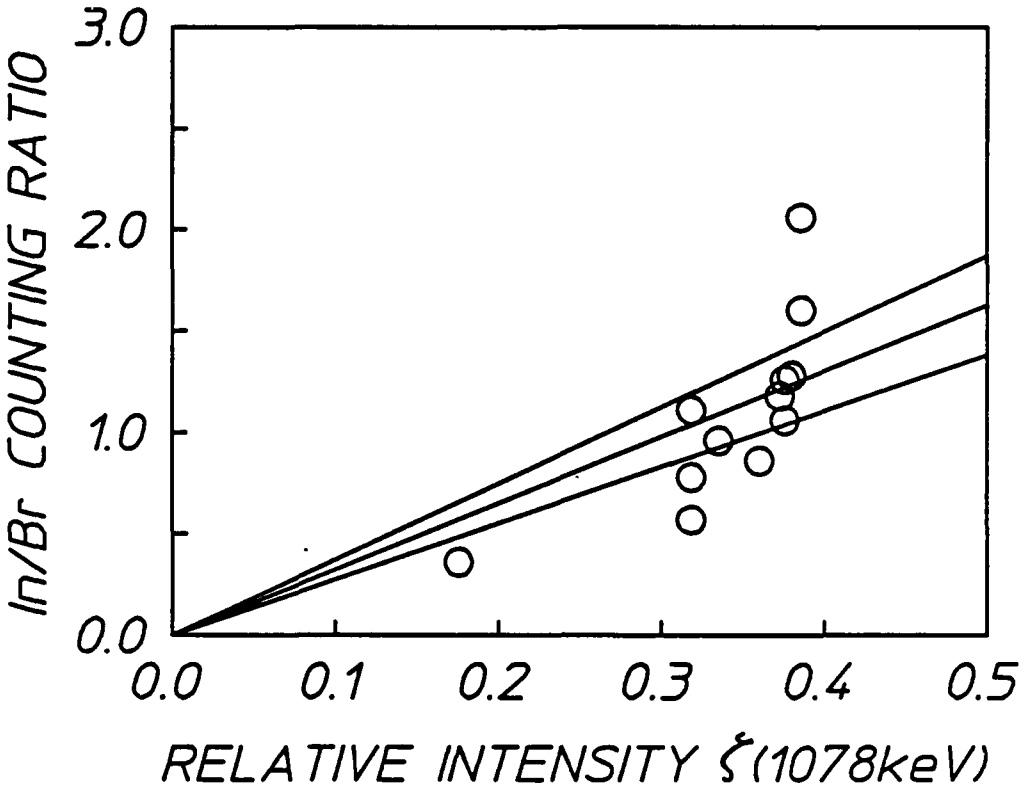

Figure 22: Plot of the ratios of ^{115m}In to ^{79m}Br fluorescence observed as a function of the relative intensity of irradiation at 1078 keV normalized to the intensity at 761 keV. The center line shows the least squares fit including the origin and the outer lines bound uncertainty in such a fit introduced by varying the characterization of the intensities of Fig. 20 over acceptable limits.

From the linear fit to the data of Fig. 22 shown as the center line, Eqs. (16) and (17), and the value of the integrated cross section for ^{79}Br mentioned earlier, we obtain

$$\zeta_{1078}(\text{In}) = (17.3 \pm 2.5) \times 10^{-32}\ \text{cm}^2 \quad . \qquad (18)$$

The uncertainty was obtained from application of the same analyses to the outer lines in Fig. 22 reasonably bounding the scatter from the least squares fit to the data. The lines actually shown were obtained by determining the extent to which data points of Fig. 22 would be displaced horizontally if the corresponding abscissae were varied by the maximum extent of the uncertainty in the value of $\zeta(1078)$ arising from the nature of the calibration and the interpolations being employed.[8]

The statistical scatter in the data is within the bounds established by the uncertainty in intensity.

Finally, substituting Eq. (18) into Eq. (17) and solving for the integrated cross section give for the 1078 keV transition in ^{115}In,

$$\pi b_a b_o \sigma_o \Gamma/2 = (18.7 \pm 2.7) \times 10^{-29} \text{ cm}^2 \text{ keV} \quad . \qquad (19)$$

This is the value we report in Table IV.

Conclusions

The detailed characterization of the spectrum emitted by the intense source of pulsed bremsstrahlung described earlier[8] has been found to be sufficient to describe the quantitative yield of the reaction ^{115}In$(\gamma,\gamma')^{115m}$In, for the value of integrated cross section given by Eq. (5).[44] Table IV shows that value to agree with some of the prior measurements. In this work there was no need to invoke any nonresonant reaction channels of the type sometimes used[24] in the description of this reaction.

In addition to providing further evidence against the occurrence of nonresonant reactions in ^{115}In, the results of this work have important implications for the calibration of intense sources of pulsed continua. By providing a means for storing a sample of the illuminating intensity at a single well-defined energy of 1078 keV for subsequent measurement at a later, quieter time, a sample of ^{115}In can readily complement the information supplied[5,8] by ^{79}Br about the intensity at 761 keV. Moreover, both together can be used to identify the component of excitation contributed by the higher energy lines of ^{77}Se so that the remainder can be used to characterize the intensities at lower energies.[8]

Finally, it seems this technique of using single pulses of intense continua to measure integrated cross sections for the production of measurable populations of isomers can provide data of use in astrophysical modeling. Cross sections at energies as low as 1 MeV are quite large for such elements as Se, Br and In and might provide viable photonuclear channels for the production of enough isomeric population to be important in cosmic nucleosynthesis. It seems that the experiments of this type give evidence that it is possible to advance the precision for the characterization of (γ,γ') reactions toward that enjoyed by other types of particle reactions at comparable energies.

ACTIVATION OF ^{111m}Cd BY SINGLE PULSES OF INTENSE BREMSSTRAHLUNG

The lack of convergence of past measurements of (γ,γ') reactions is probably even worse for the case of ^{111}Cd than for ^{115}In. For example, the most recent three measurements[41,45,46] of the integrated cross sections for the reaction $^{111}Cd(\gamma,\gamma')^{111m}Cd$ were conducted in 1979, 1982 and 1987 with results of 35, 5.8, and 14, respectively, in the usual units of 10^{-29} cm^2 keV. Probable errors were quoted as varying only from 7 to 14%, and yet, no two of the measurements were even within a factor of two of each other.

The ^{111m}Cd isomer at 396 keV has a 48.6 minute half-life and is readily detected by observing the 150.6 keV and 245.4 keV gammas radiated in the cascade from the isomer. Experimentally this is an almost ideal vehicle for the study of (γ,γ') reactions, since the lifetime of the isomer is long enough to collect a substantial dose from a variety of excitation sources during the activation cycle and short enough to count with reasonable signal-to-background ratio afterward. Experiments appear to have been carefully executed, and the drastic disagreement in the results has been attributed[45] to the controversial[46] proposal that some mechanism of nonresonant nuclear absorption dominates the excitation step. However, the data that support this intriguing proposal[45] and the data that seem to refute[46] it agree only in indicating that the (γ,γ') reaction producing ^{111m}Cd is not well understood.[39-41,45-48]

The relevant part of the energy level diagram[49] of ^{111}Cd is shown in Fig. 23. All of the adopted levels[49] between 1000 and 1500 keV are shown together with the gamma transitions that have been observed[10] in reactions other than (γ,γ'). Additional transitions to the 1190 and 1330 keV levels have been inferred[39,47] from (γ,γ') studies, but those reports depend upon the validity of arguments which are weakened by the controversy. Moreover, even the existence of the 1330 keV level might reasonably be questioned, since it is based upon a single report[50] of a reaction not dependent upon the interpretations of (γ,γ') data.

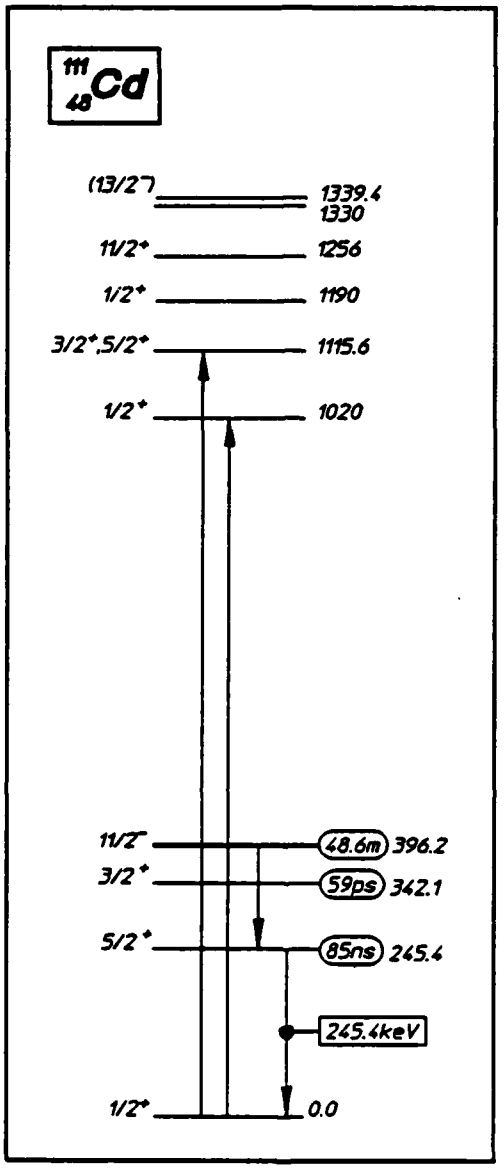

Figure 23: Energy level diagram of the excited states of ^{111}Cd between 1000 and 1500 keV which may be important in the production of the 48.6 m isomer. Also shown are all excited states below 400 keV. Half-lives of the states are shown to the right of each state and known[10] gamma transitions are shown by the arrows. Populations of the 48.6 m isomer are most conveniently detected by the 245.4 keV fluorescent transition as indicated.

For levels in Fig. 23 which might be excited by photons with energies in the range 1000 to 1500 keV, there are a number of possible cascades to the $11/2^-$ isomer through levels below 1000 keV which are not shown. However, no particular path has been proposed.

In the previous chapter we reported a reexamination of the reaction $^{115}In(\gamma,\gamma')^{115m}In$ with the same pulsed bremsstrahlung source used for the reconciliation of the absorption cross sections to ^{79m}Br and ^{77m}Se. Results for ^{115}In were found to be consistent with that reconciliation. Moreover, the quantitative value for the integrated cross section we reported was in good agreement with the other value reported most recently as the result of excitation with a radioactive source.[25] Reported in this chapter is an extension of this technique to the reaction $^{111}Cd(\gamma,\gamma')^{111m}Cd$. We find an integrated cross section of $(9.8 \pm 2.5) \times 10^{-29}$ cm^2 keV for reaction through a gateway level near 1200 keV.

Methods and Apparatus

Unlike our previous study of ^{115}In from which this present work has been extended, none of the elementary nuclear properties of Eq. (2b) entering into the computation of the integrated cross section were known for ^{111}Cd. Although it is uniformly assumed[39-41,45-49] that the dominant gateway level lies at 1330 keV, this is not strongly supported by prior data. Early experiments[11,39,47,51] using bremsstrahlung from accelerators with variable end point energies indicated that the reaction turns on between 1200 and 1400 keV. However, the apparent sharpness seen in some early data at 1330 keV is strongly affected by the logarithmic presentation of a linear threshold and the sensitivity of the instrumentation to low levels of activation. In more recent experiments using ^{60}Co sources, the high level of activation produced and the proximity of the 1330 keV level of ^{111}Cd to the strong 1332 keV line of ^{60}Co made it attractive to identify the (γ,γ') reaction as occurring through the 1330 keV level of undetermined symmetry. Since the experiments reported here were conducted with an accelerator producing a known[8] bremsstrahlung spectrum, it was decided to try to determine experimentally the energy of the gateway needed, as well as the integrated cross section.

In previous chapters, it was shown that the uncertainty in the absolute value of the geometric coefficient coupling the source of pump radiation to the absorbing target could be eliminated by normalizing both the pump fluence and the fluorescence counts to some standard material having a monochromatic excitation spectrum. The reaction $^{79}Br(\gamma,\gamma')^{79m}Br$ was found to be an ideal standard, having an integrated cross section of 6.2×10^{-29} cm^2 keV and a convenient radioactivity in the isomer. Following the formalism reported earlier[8] in Eq. (16), the number of ^{111m}Cd nuclei, S(Cd), which could be excited through a single gateway state at an energy E by a flash of intense bremsstrahlung can be conveniently expressed as a ratio,

$$\frac{S(Cd)}{S(Br)} = \frac{N(Cd)}{N(Br)} \frac{\xi_E(Cd)}{\xi_{761}(Br)} \zeta(E) \quad , \qquad (20)$$

where S(x) and N(x) are the number of nuclei produced and the number of target nuclei of material x, respectively, $\zeta(E)$ is the ratio of pumping intensity at the gateway energy E in keV to the intensity at 761 keV; and the $\xi_E(x)$ are the combinations of nuclear parameters of Eq (17) involved in the excitation. Still more convenient for analysis is the weighted activation ratio R obtained by multiplying Eq. (20) by the ratio of the number of target nuclei,

$$R = \frac{N(Br)S(Cd)}{N(Cd)S(Br)} = \frac{\xi_E(Cd)}{\xi_{761}(Br)} \zeta(E) \quad . \qquad (21)$$

The source of excitation in these experiments[8] was the bremsstrahlung produced by the PITHON nuclear simulator at Physics International as had been used in the In experiment. The typical end point energy of the electrons producing the bremsstrahlung was 1.3 MeV with small shot-to-shot variance. For these particular experiments, the nominal firing parameters were deliberately perturbed so that successive irradiations could be obtained with end point energies varying from 1.3 to 1.54 MeV.

Intensities at the target were determined by measuring the nuclear activation of the ^{79}Br component of a sample of LiBr containing isotopes in natural abundance. This calibrating target was run in a pneumatic transfer system which enabled the population of ^{79m}Br produced by a single irradiation to be subsequently counted at a quiet location

removed from the source. Activation lost during the 1.0 s transit time could be readily corrected during analysis.

The ^{111}Cd sample under study occurred in natural isotopic abundance in a thin Cd foil taped to a fiduciary mark near the pneumatic system. Since the ^{111m}Cd had a substantially longer half-life than the calibrating Br, it could be manually detached after exposure and transferred to the spectrometer, which consisted of an intrinsic Germanium detector with associated electronics. In typical cases a counting time of one hour gave better than 5% statistical accuracy in the area of the ^{111m}Cd peak. In the course of this experimental series, six shots were obtained for sufficiently high end point energies to yield statistically significant numbers of fluorescent isomeric activity.

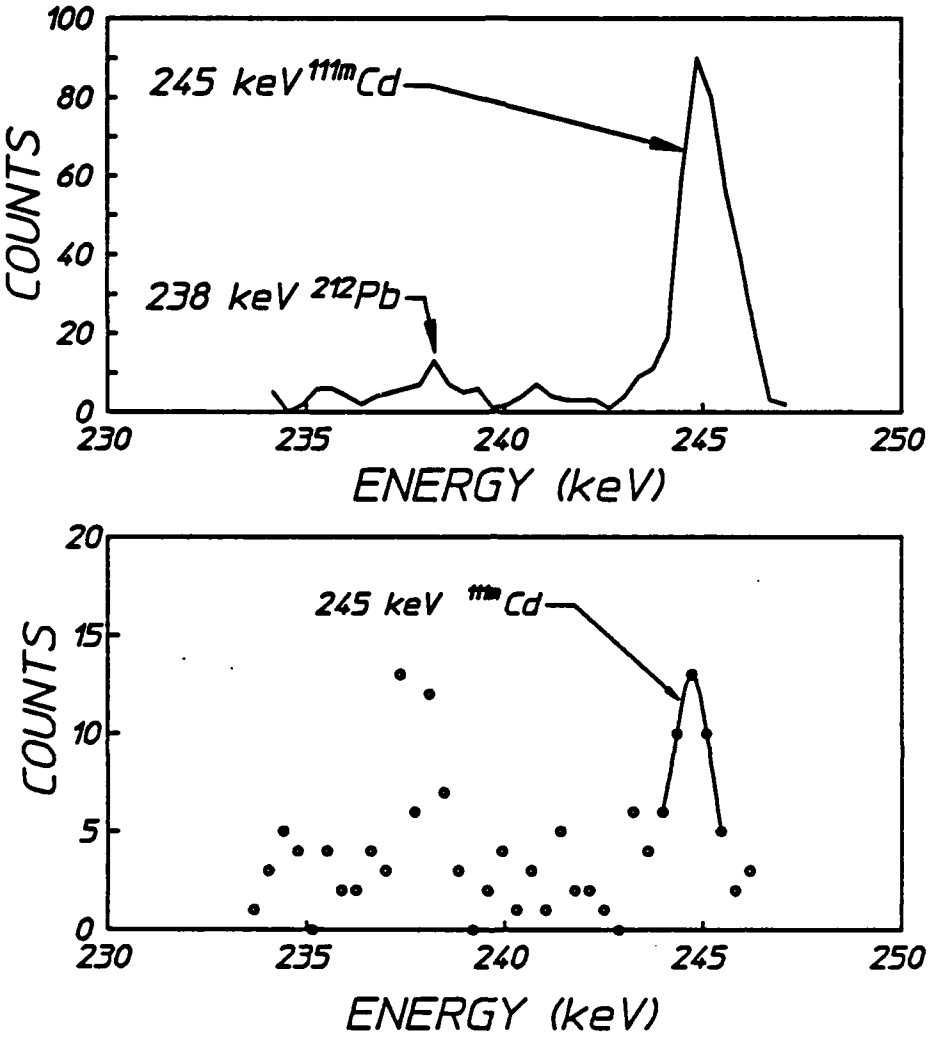

Figure 24: Spectra showing the 245 keV line from the decay of ^{111m}Cd. The spectra were obtained from an 8.02 gm, natural Cd foil sample. The small peak near 238 keV is due to the decay of naturally occurring ^{212}Pb in the counting environment.
(a) Fluorescence from ^{111m}Cd following irradiation with a single bremsstrahlung pulse having an end point energy of 1.4 MeV. Counting time was 3600 sec.
(b) Fluorescence following excitation with an end point of 1.3 MeV. Counting time was 2700 sec.

To confirm that the fluorescence being detected resulted only from decay of the ^{111m}Cd activity, the spectra from irradiated foils were first examined for traces of interference from the 238 keV line from ^{212}Pb in the counting environment. The clear separation of the 238 keV line from the 245 keV line obtained from ^{111m}Cd following irradiation

with a 1.4 MeV end point bremsstrahlung pulse is shown in Fig. 24(a). At an end point energy of 1.3 MeV, where the spectral intensity at the 1330 level in ^{111m}Cd should be negligible, the 245 keV line is weak but clearly observable, as shown in Fig. 24(b).

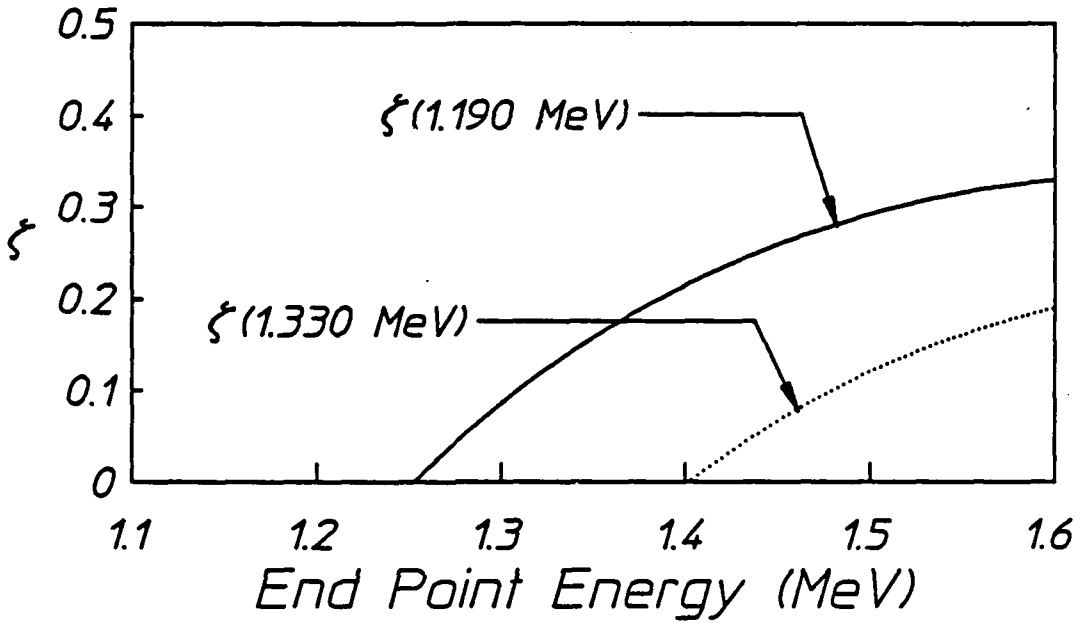

Figure 25: Plots showing the ratio of the spectral density at energy E normalized to the spectral density at the 761 keV gateway of ^{79m}Br for varying end point energies. The solid and dotted lines show the ratio for energies E = 1.190 and E = 1.330 MeV.

In order to determine an experimental value of the ξ_E(Cd) by fitting Eq. (21) to measurements of the fluorescence yields from the sample and from the LiBr calibrator, the relative bremsstrahlung intensity ζ(E) emitted at E must be known. For these experiments, these data were obtained by numerically fitting theoretical computations of bremsstrahlung spectra. As in the In experiment confidence was established by examining quantitatively the number of fluorescent nuclei produced by successive irradiations of samples of ^{79}Br and ^{77}Se at a variety of end point energies. The relative bremsstrahlung intensity emitted at a particular energy was found to be a strong function of the end point energy of the accelerator; two examples are shown in Fig. 25.

Results

Because of a small physical displacement of the ^{111}Cd sample from the mixed $^{79}Br/^{77}Se$ target providing calibration, the observed number of fluorescent photons counted had to be corrected for the different source intensities. This was done by mounting thermoluminescent diodes (TLD's) at both positions and then comparing the total dose recorded at the different points for each shot. The number of photons from ^{111m}Cd was scaled by the value of relative dose received at the ^{111}Cd and at the calibrating positions.

The cadmium sample was optically thin at both the 150 keV and the 245 keV fluorescence energies, requiring relatively small factors of 1.645 and 1.222 for the self-absorption correction. Data were corrected for fluorescence and detector efficiencies, as well as for variations in measurement time. Good agreement was found between corrected counts due to each of the fluorescence lines, and their weighted average was taken for each exposure. The resulting values of the weighted activation ratio R from Eq. (21) are shown in Fig. 26.

The linear form of the dependence of the relative yield of fluorescence from the cadmium isomers seen in Fig. 26 between 1.1 and 1.6 MeV is a strong indication of the dominance of a single channel of excitation through a gateway level lying at an energy given by the value of the x-intercept. From the data of Fig. 26, it is seen that the intercept lies near 1200 keV in agreement with the known state at 1190 keV. Also shown in Fig. 26 is the energy of the next higher gateway state not excluded by an unacceptable J^{π}, the poorly characterized level at 1330 keV. It is interesting to observe that for end point energies above this value there seems to be no clear tendency of the data to depart from the simple linear fit because of the availability of this additional gateway. A greater number of measurements at successively higher end point energies would be needed to confirm this indication that the 1330 keV level has no particular role in the excitation of ^{111m}Cd.

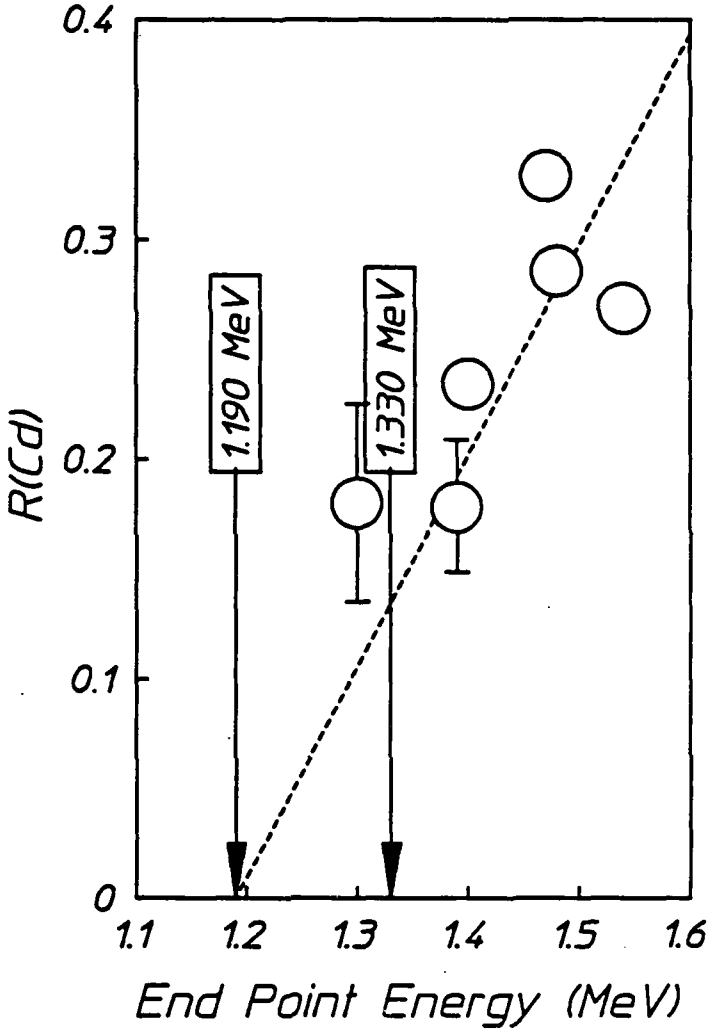

Figure 26: Ratios of isomeric fractions produced in ^{111m}Cd to those in ^{79m}Br, as corrected for the finite duration of the counting interval and plotted as a function of the end point energy of the bremsstrahlung. The dashed line shows a linear fit to the data intercepting the x-axis at a gateway energy of 1.19 MeV. Excitation energy of the next higher gateway is shown at 1.33 MeV. In this figure and in Fig. 27, the error bars for the two least precise points have been shown. The statistical errors for the other points are commensurate with the plotting symbols in the figures.

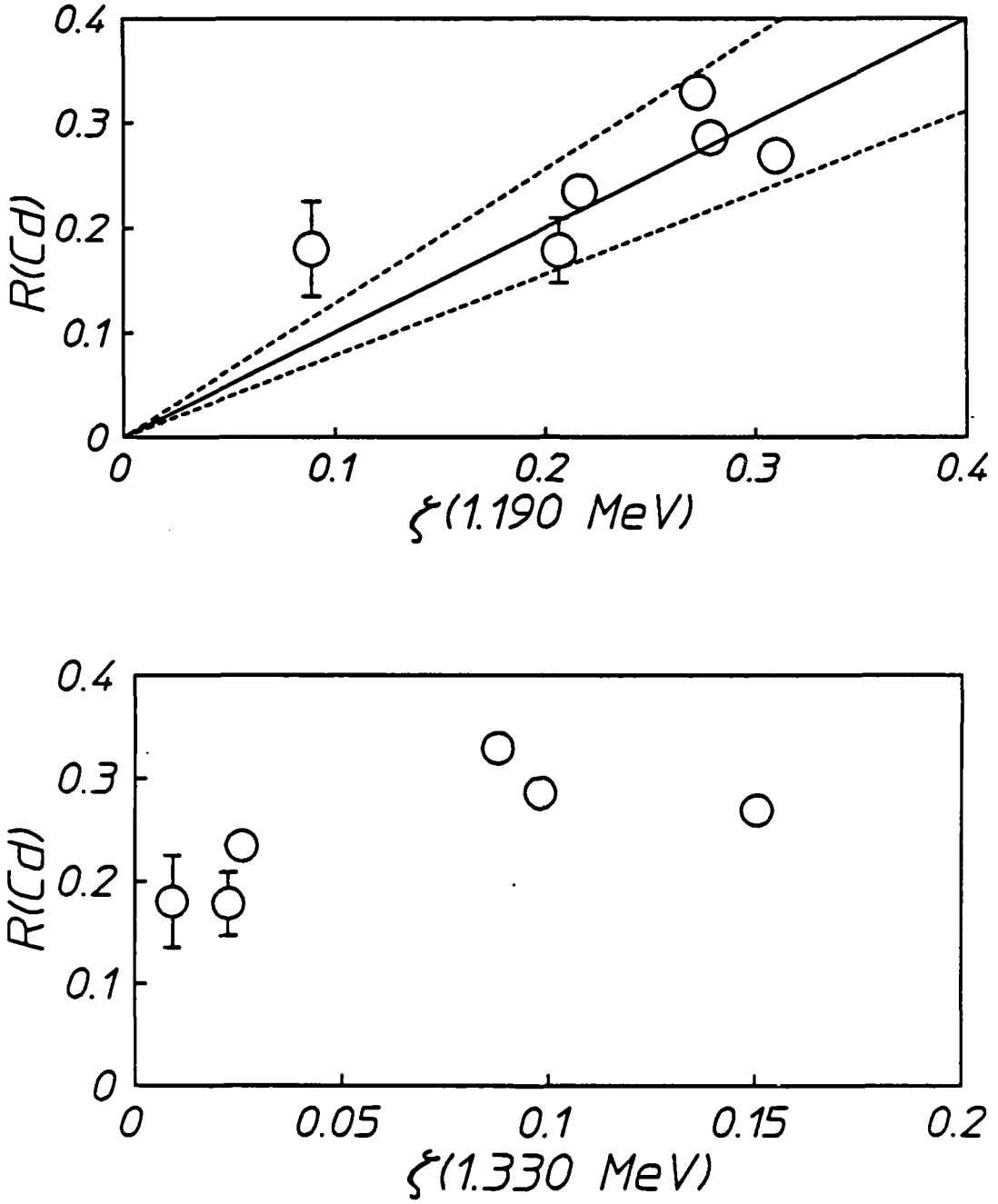

Figure 27: Plots of the weighted activation ratio R(Cd) as a function of the spectral intensity at energy E normalized to the intensity at the 761 keV gateway in ^{79m}Br.
(a) Plot for E = 1190 keV. The heavy line shows the least squares fit through the origin, and the dashed lines bound the uncertainty in such a fit.
(b) Plot for E = 1330 keV, showing the absence of a reasonable fit that would include the origin.

Once most of the data are established as being consistent with the model of excitation through a single level at 1190 keV, Eq. (21) provides a means of determining the absolute cross section for the excitation. In Fig. 27(a) data for the measured values on the left side of Eq. (21) are plotted as functions of the relative intensities $\zeta(1190)$ appearing on the right. As can be seen from Eq. (21), the best slope around which the data of Fig. 27(a) scatter would represent our experimental determination of the product of the first two terms on the right of Eq. (21). For comparison, the same approach is repeated in Fig. 27(b) to show the difficulty in attempting to force the interpretation that the principal gateway level is the state at 1330 keV. In Fig. 27(b) the weighted activation ratios are plotted as functions of $\zeta(1330)$. It is difficult to consider these data as approximating a linear dependence of R upon ζ, and particularly one which extrapolates to the origin as required by Eq. (21).

From the linear fit to the data of Fig. 27(a) shown as the heavy line, Eqs. (17) and (21), and the value of the integrated cross section for ^{79}Br mentioned earlier, we obtain

$$\xi_{1190}(\mathrm{Cd}) = (8.2 \pm 2.1) \times 10^{-32}\ \mathrm{cm}^2 \quad . \qquad (22)$$

The uncertainty was obtained from application of the same analyses to the dashed lines in Fig. 27(a) reasonably bounding the scatter from the least squares fit to the data. The statistical scatter in the data is within the bounds established by the uncertainty in intensity.

Finally, substituting Eq. (22) into Eq. (17) and solving for the integrated cross section give for the 1190 keV transition in ^{111}Cd,

$$\pi b_a b_o \sigma_o \Gamma/2 = (9.8 \pm 2.5) \times 10^{-29}\ \mathrm{cm}^2\ \mathrm{keV} \quad . \qquad (23)$$

This is the value we report in Table V.

Table V

Summary of integrated cross sections reported for the reaction $^{111}Cd(\gamma,\gamma')^{111m}Cd$ through a level near 1200 keV.

Cross Section $\pi b_a b_o \sigma_o \Gamma/2$ ($\times 10^{-29}$ cm^2 keV)	Reference
8 (+4,-0.5)	Cauchois, Heno and Boivin (Ref. 47)
6 ± 2	Boivin, Cauchois and Heno (Ref. 39)
15 ± 3	Yoshihara (Ref. 48)
10.2 ± 2.6	Lakosi, Csuros, and Veres (Ref. 40)
35 ± 4	Watanabe and Mukoyama (Ref. 41)
5.8 ± 0.8	Krcmar et. al. (Ref. 45)
14 ± 1	Bikit et. al. (Ref. 46)
9.8 ± 2.5	This work

Conclusions

The detailed characterization of the spectrum emitted by this intense source of pulsed bremsstrahlung has been found to be sufficient to describe the quantitative yield of the reaction $^{111}Cd(\gamma,\gamma')^{111m}Cd$, for the value of the integrated cross section given by Eq. (23). Table V shows that value to fall within the interval over which the prior measurements have scattered. In this work there was no need to invoke any nonresonant reaction channels of the type sometimes used[45] in the description of this reaction.

In addition to providing further evidence against the occurrence of nonresonant reactions in ^{111}Cd, the results of this work have important implications for the calibration of intense sources of pulsed continua. By providing a photoactivation channel with a well-defined gateway at 1190 keV, a sample of ^{111}Cd can readily complement the information supplied[5,8] by ^{79}Br about the intensity at 761 keV and by ^{115}In at 1078

keV.[7] Moreover, the results of this work may indicate why previous work gave such disparate results, no matter how carefully done. The most recent experiments[45,46] with ^{60}Co sources were strongly model dependent. In those efforts, the irradiating intensity and its dependence upon experimental variables were assumed to be a result of Compton scattering from the ^{60}Co line at 1332 keV to the absorption energy at 1330 keV. From Fig. 26 it can be seen that the actual excitation energy is nearer 1200 keV. In the ^{60}Co experiments, the intensities at the real gateway must have differed drastically from what had been calculated because of the substantial differences in energies assumed for the gateway.

PHOTOACTIVATION OF INDIUM AND CADMIUM INTO ISOMERIC STATES PUMPED BY BREMSSTRAHLUNG RADIATION FROM A MEDICAL LINEAR ACCELERATOR

Because electromagnetic transitions tend to occur with small changes of angular momenta, (γ,γ') reactions have the potential of offering insights into nuclear structure that could be rather unique. Although the literature on such reactions spans nearly 50 years, experimental results are disappointing when measured against the levels of precision routinely achieved with other types of processes at low energies. The cross sections for (γ,γ') reactions are often small in cases where the product is required to have a lifetime convenient for detection, and so intense sources or accelerators must be used. In turn, these are poorly characterized; and it has been argued that the cause of the general lack of agreement in the results reported for (γ,γ') reactions has been the deviation of the pump spectrum from expectations.

Only this year has technology been able to support the direct measurement[5,8] of the spectrum of a pulsed source of bremsstrahlung sufficiently intense in the 0.5 - 1.5 MeV range to insure a product yield large enough for accurate characterization of the (γ,γ') reactions being excited. As just described in the preceding chapters, it was found that both[7] $^{115}In(\gamma,\gamma')^{115m}In$ and[9] $^{111}Cd(\gamma,\gamma')^{111m}Cd$ occurred through the resonant excitation of a state near 1 MeV broadened by its relatively short lifetime as would have been reasonably expected but has been recently disputed.[24,45] The sharp onset we found for the (γ,γ') reaction with increasing energy of the γ relegated to less than 3% any contributions from nonresonant channels that are sometimes considered domi-

nant.[24,45,52] Thus it can be reasonably concluded that the results of the studies of the (γ,γ') reactions in ^{115}In and ^{111}Cd were able to convey information about the particular gateway state in each system, namely that it was reasonably well-connected by radiative transitions to both initial and final states of the reaction.

The integrated cross sections for excitation of the isomers such as those of ^{115}In and ^{111}Cd are usually expressed as $\pi b_a b_o \sigma_o \Gamma/2$, as described in Eq. (2b). Cross sections we found for the archetype cases of ^{115}In and ^{111}Cd were of the order of 10 in the conventional units of 10^{-29} cm^2 keV. Such values for excitation through a gateway near 1 MeV are characteristic of products of branching ratios $b_a b_o$ somewhat degraded from the optimal value of 0.25. One transition is primarily responsible for the favorable width of the gateway; and the other is parasitic, contributing lesser additional width. Whether this is simply coincidental for these two cases or the result of a general principle is not known.

Very early data[11,51] indicated that yields from (γ,γ') reactions increased as higher energy gateway states were accessed. Evidence was accumulated[11,51] in the form of increases in the slopes of curves showing product yields as functions of the end point energies of the bremsstrahlung used to pump the reactions, but the changes were not dramatic. Morever, the more recent insistences[24,45] that nonresonant channels dominated such excitations cast some doubt on the appropriate interpretation of that early data.

Systematic studies[17] have shown that collective octupole oscillations of the nuclear core can unhinder E1 transitions, making very short lived states available for (γ,γ') reactions excited from ground states at energies between 1 and 2 MeV. However, the literature[18] suggests that the branching from such a collective state would almost entirely favor the initial transition so that a diminishing product, $b_a b_o$, would largely offset the greatly increased width Γ in expressions for the integrated cross section for a (γ,γ') reaction excited through such a collective state. Such an expectation is supported by the early data mentioned above.

Since the density of states is considerably elevated at energies of 1 to 2 MeV above the ground state, an alternate hypothesis is attractive. A strong octupole or other oscillation of the core might serve to

mix enough single particle states so that radiative branches to several different lower levels might become comparable. In this case a very large integrated cross section of (γ,γ') reactions producing isomers from ground state nuclei might be found to be only slightly dependent upon the detailed single particle assignments of neighboring nuclei. Just such an effect is reported in this chapter. Integrated cross sections of the order of 10,000 in units of 10^{-29} cm^2 keV are described for the excitation of isomers of ^{111}Cd, ^{113}In and ^{115}In through resonant gateways pumped by bremsstrahlung from a linear accelerator producing most of its intensity near 2 MeV.

Experimental Procedure

Figure 28 shows the energy level diagram for the three nuclei of interest in these experiments, ^{111}Cd, ^{113}In and ^{115}In, together with the lifetimes of the isomers and the transitions convenient for detection. Excited states of the ^{111}Cd result primarily from promotion of the odd neutron, while those of the In isotopes arise from the odd proton. The two indiums differ only by a pair of neutrons, implying that their energy levels and angular momenta assignments should be very similar, while those of the cadmium are quite different, as seen in Fig. 28.

In these experiments, foils were used containing natural isotopic abundances of 12.8, 4.3 and 95.7%, respectively, for the ^{111}Cd, ^{113}In and ^{115}In isotopes. Two complex target assemblies including thin rectangular samples of indium and cadmium were exposed to the output of a Varian Clinac 1800 linear accelerator at the Department of Radiology of the University of Texas Southwestern Medical Center. This linear accelerator has an end point energy of 6 MeV.

The indium sample was irradiated for 121 minutes, and the cadmium sample for 240 minutes. The foils were removed to the counting facility at the Center for Quantum Electronics at the University of Texas at Dallas, where the decay of the isomeric products of the (γ,γ') reactions were measured with an HPGe spectrometer system. Only the results from indium and cadmium will be considered in this chapter, although other isomers were produced in additional foils in the target package. Figures 29 and 30 show the measured counting rates as a function of time. By experimentally measuring the decay of the count rate, the decay constant of the observed peaks was determined in order to verify the identity of the peaks.

Figure 28: (Opposite) Energy level diagrams of the excited states of ^{111}Cd, ^{113}In and ^{115}In important in the production of populations of the isomers. Half-lives of the states are shown to the right of each, and sequences of (γ,γ') reactions leading to the isomer are shown by the arrows. Dashed γ' transitions occur either directly or by cascading through levels not shown. The greater width of the new gateway state formed in this work is implied by the rectangle at the higher energies of each system.

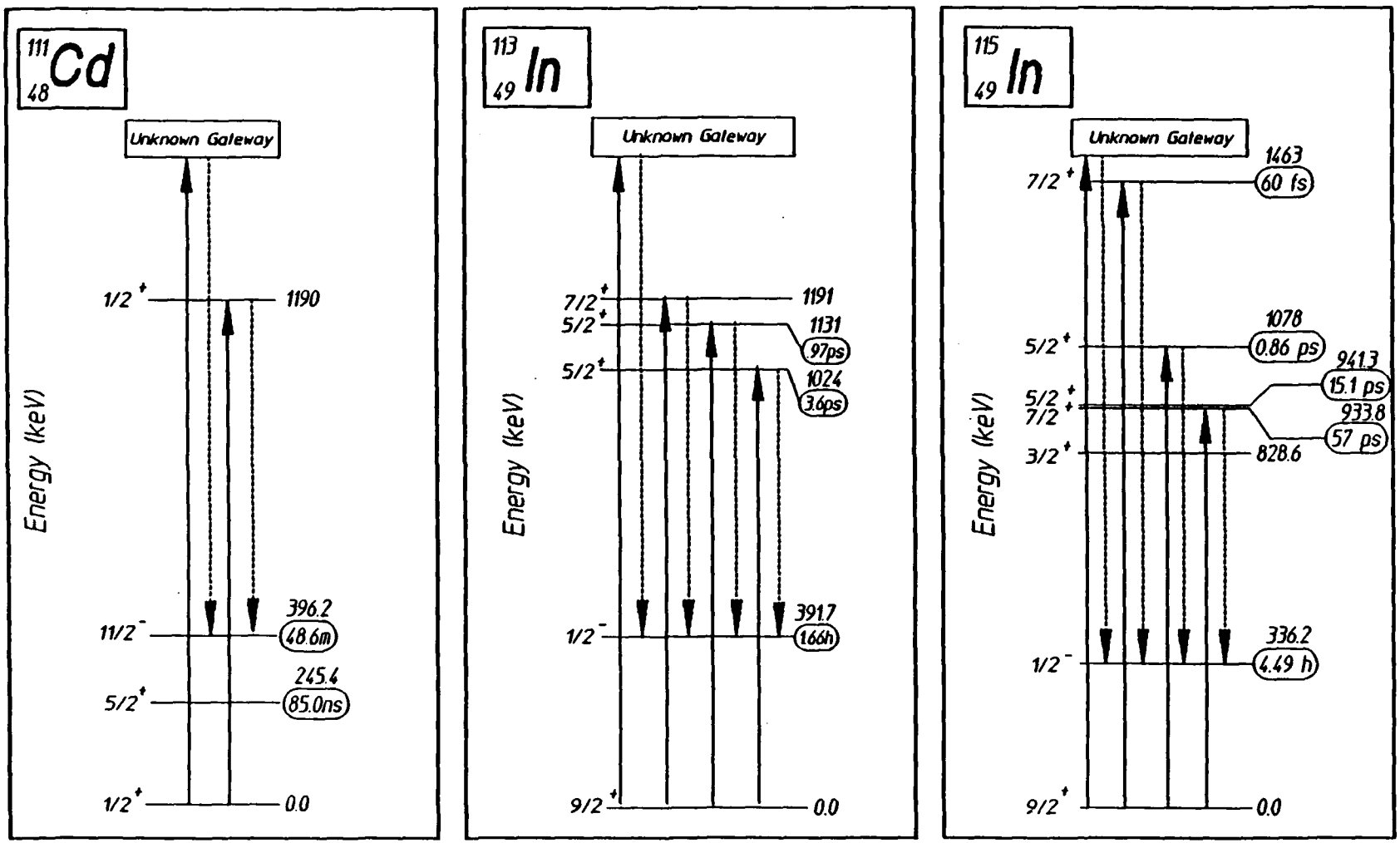
111 48 Cd
Unknown Gateway
Energy (keV)
1/2+
1190
11/2-
396.2
48.6m
5/2+
245.4
85.0ns
1/2+
0.0
113 49 In
Unknown Gateway
Energy (keV)
7/2+
1191
5/2+
1131
97ps
5/2+
1024
3.6ps
1/2-
391.7
1.66h
9/2+
0.0
115 49 In
Unknown Gateway
Energy (keV)
7/2+
1463
60 fs
5/2+
1078
0.86 ps
5/2+
941.3
15.1 ps
7/2+
933.8
57 ps
3/2+
828.6
1/2-
336.2
4.49 h
9/2+
0.0

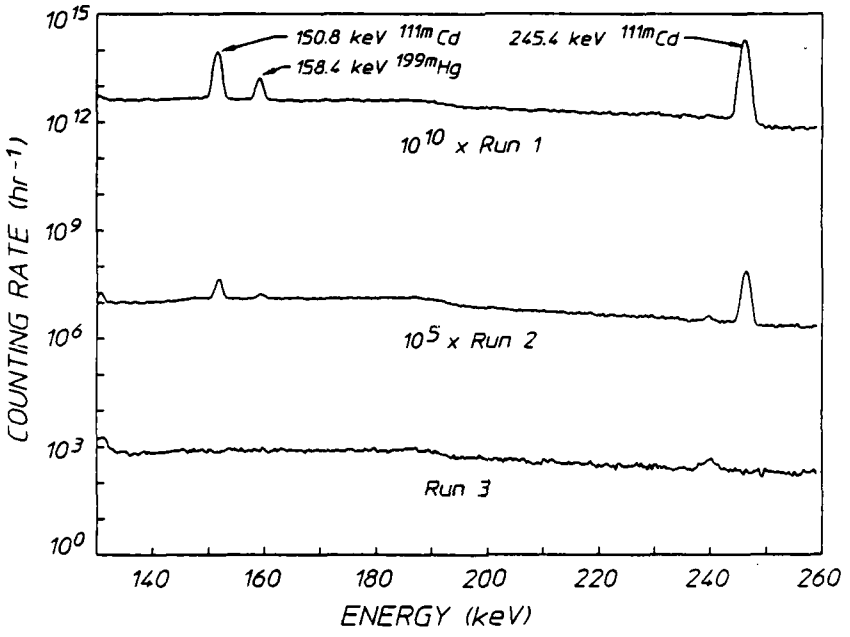

Figure 29: Three sequential spectra from an intrinsic Ge detector emphasizing the lower range of energies shown. The elapsed time from the end of the irradiation to the start of each of the counting intervals of 123, 600, and 600 m was 75, 203, and 1331 m for Runs 1, 2 and 3, respectively. Data have been offset vertically for clarity.

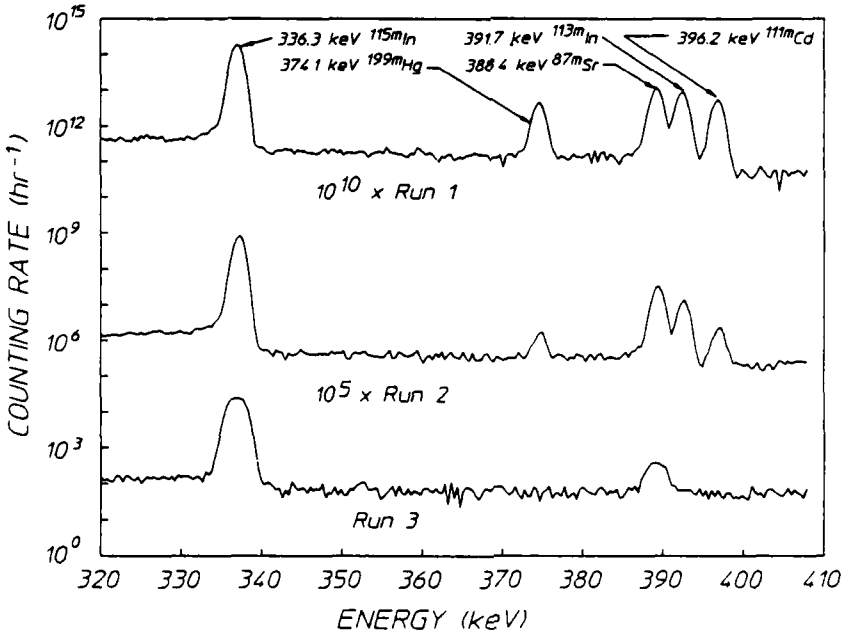

Figure 30: Continuation of the spectra of Fig. 2 to the higher energy range shown.

During the irradiation of a target which is thin in comparison to the mean free path of a pump photon, at time t the total number of metastables formed of a given isotope, $N_m(t)$, is given by

$$N_m(t) = N_o \tau \left[\Sigma_i (\sigma\Phi)_i\right] \left[1 - \exp(-t/\tau)\right] \qquad (24)$$

where

N_o = the total number of target nuclei,

$\tau = (\tau_{1/2}/\ln 2)$ = the natural lifetime, and

$(\sigma\Phi)_i = (\pi b_a b_o \sigma_o \Gamma/2)_i \, \Phi(E_i)$ = the product of the effective cross section for the excitation and subsequent decay to the isomer of the i^{th} gateway state located at the energy E_i and the flux of photons with energy E_i. The summation is carried out over the gateway states below the end point energy of the bremsstrahlung spectrum.

After the samples have been irradiated for a time T and removed from the irradiation source, the total number of counts accumulated in the interval from T_1 to T_2 is given by

$$\Delta C = K \, N_m(T) \exp(-T_1/\tau) \left[1 - \exp\{-(T_2-T_1)/\tau\}\right] \quad , \qquad (25)$$

where T_1 is the time elapsed from the end of the irradiation to the beginning of the counting interval, and K is the net detection efficiency factor. By measuring the accumulated counts in a given time interval and correcting for detector efficiencies, branching ratios, and self absorption, $N_m(T)$ may be determined. If the photon spectrum is known, the effective integrated cross section may be extracted.

The shape of the expected output spectrum of the linear accelerator as calculated by Monte Carlo methods[53] is shown in Fig. 31. The function describing the probability per unit energy for the emission of a photon, F(E), is normalized such that the integral under the curve is unity. In usage it must be multiplied by the total photon flux density of the linear accelerator which was 1.74×10^{12} photons/cm^2 min for the indium exposure and 1.54×10^{12} photons/cm^2 min for the cadmium exposure. The spectrum has been shown to be quite uniform over the field of exposure used in the irradiation, becoming somewhat harder near the beam centerline.[54]

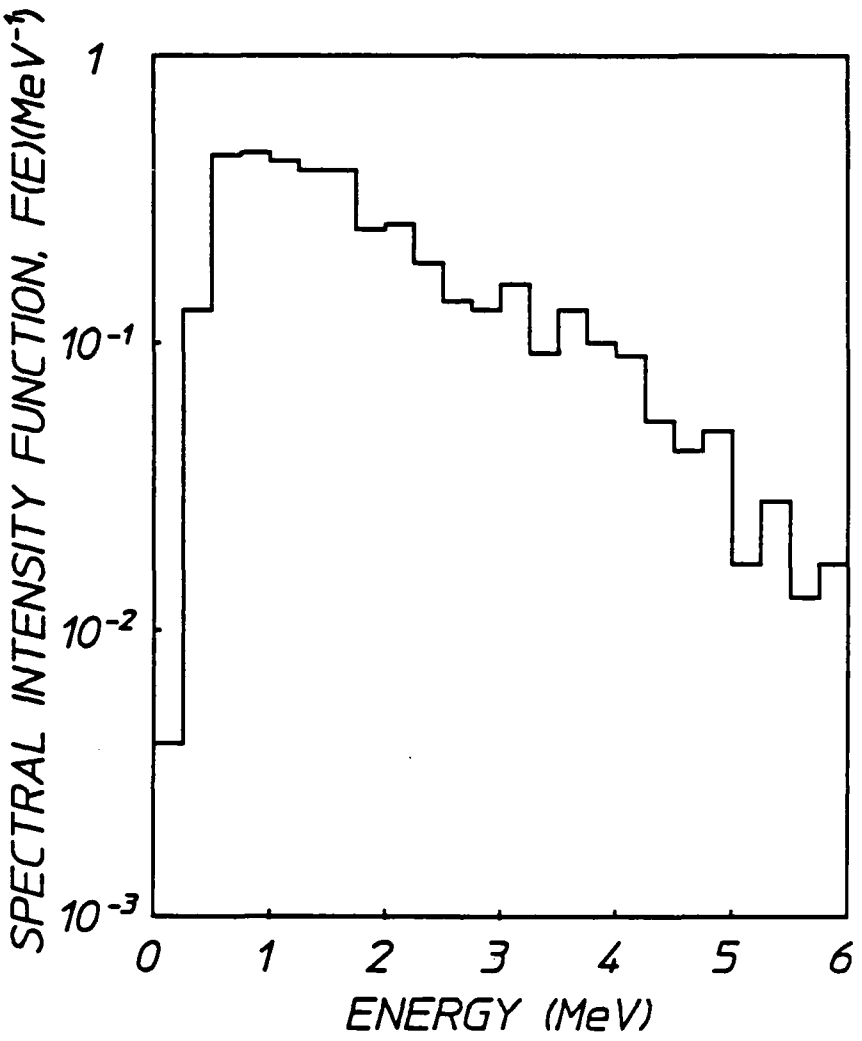

Figure 31: Relative spectral intensities of the bremsstrahlung used for irradiation in these experiments normalized so that the integral under the curve is unity.

Results

The total numbers of metastables formed, $N_m(T)$, are listed below:

$$N_m(121 \text{ min}) = 2.86 \times 10^7 \text{ for } ^{115}\text{In} \quad (26a)$$

$$N_m(121 \text{ min}) = 4.61 \times 10^5 \text{ for } ^{113}\text{In} \quad (26b)$$

$$N_m(240 \text{ min}) = 8.24 \times 10^6 \text{ for } ^{111}\text{Cd} \quad (26c)$$

The 2.2 g indium foil contained 1.10×10^{22} nuclei of ^{115}In and 4.60×10^{20} nuclei of ^{113}In. The isotope ^{115}In has a known gateway state[7] at 1078 keV for which

$$(\pi b_a b_o \sigma_o \Gamma/2) = 20 \times 10^{-29} \text{ cm}^2 \text{ keV} \quad . \quad (27)$$

The contribution of the absorption at the relatively narrow gateway at 941 keV is negligible compared to that at 1078 keV.

The isotope ^{113}In has gateways at 1024, 1131, and 1191 keV for which $(\pi b_a b_o \sigma_o \Gamma/2)$ is computed[10] to be 2.62, 10.2, and 0.044 in units of 10^{-29} cm^2 keV respectively. These cross sections are estimates based on Breit-Wigner cross sections and measured lifetimes taken from the Nuclear Data Sheets. Figure 31 shows that the flux is nearly constant at 7.5×10^8 photons/cm^2 min keV in this region so that the three gateways may be combined into a single gateway for which

$$(\pi b_a b_o \sigma_o \Gamma/2) = 12.9 \times 10^{-29} \text{ cm}^2 \text{ keV} \quad . \quad (28)$$

The isotope ^{111}Cd has been found to have a gateway state[5] at 1191 keV for which the effective cross section is given by

$$(\pi b_a b_o \sigma_o \Gamma/2) = 9.8 \times 10^{-29} \text{ cm}^2 \text{ keV} \quad . \quad (29)$$

The summation in Eq. (24) may be decomposed into a contribution for the known gateway(s) below 1.3 MeV plus another term $(\sigma\Phi)_x$ representing an unknown gateway state above 1.3 MeV, that is,

$$(N_m(T)/N_o\tau) = [(\sigma\Phi)_{known} + (\sigma\Phi)_x] [1 - e^{(-T/\tau)}] \quad . \quad (30)$$

When the known parameters of ^{115}In are substituted into Eq. (28), the ($\sigma\Phi$) products are found to be

$$(\sigma\Phi)_{known} = 1.5 \times 10^{-19} \text{ min}^{-1} \quad , \tag{31}$$

which is negligible compared to the contribution to the summation from the unknown gateway state(s) obtained by substituting the results of Eq. (26a) into Eq. (24) and solving for $(\sigma\Phi)_x$, namely

$$(\sigma\Phi)_x = 2.48 \times 10^{-17} \text{ min}^{-1} \quad . \tag{32}$$

The activations due to the known gateway state comprise less than 1% of the total number of activations. If the assumed spectrum of the linear accelerator is that shown in Fig. 31 represented by

$$\Phi(E) = \Phi_o F(E) \quad , \tag{33}$$

the effective cross section $\sigma = (\pi b_a b_o \sigma_o \Gamma/2)$ may be found as a function of the energy of the assumed gateway state,

$$(\pi b_a b_o \sigma_o \Gamma/2) = 1.43 \times 10^{-26}/F(E) \text{ cm}^2 \text{ keV} \quad . \tag{34}$$

This function is plotted in Fig. 32 for ^{115}In. A study[7] of the photoactivation of ^{115}In utilizing a variable end point x-ray source indicated that the assumed gateway state must lie at least as high as 1.4 MeV. Inspection of the energy level diagrams and angular momenta assignments[7] suggests that a second significant gateway state is expected to lie at 1.418 MeV and that this may be the gateway being excited by the linear accelerator, but such an identification is speculative at this time.

For ^{113}In, the ($\sigma\Phi$) products are found to be

$$(\sigma\Phi)_{known} = 7.63 \times 10^{-20} \text{ min}^{-1} \quad , \tag{35}$$

which again is insignificant compared to the contribution of the unknown gateway state(s),

$$(\sigma\Phi)_x = 1.22 \times 10^{-17} \text{ min}^{-1} \quad . \tag{36}$$

The energy levels and angular momenta assignments below 1.5 MeV imply that the additional gateway state(s) must lie above 1.5 MeV.[10] With the assumption of the single combined gateway state for ^{113}In, the effective

cross section of the gateway state above 1.5 MeV as a function of gateway energy is given by

$$(\pi b_a b_o \sigma_o \Gamma/2) = 6.99 \times 10^{-27}/F(E) \text{ cm}^2 \text{ keV} \quad , \qquad (37)$$

which may be found in Fig. 33. Below 1.9 MeV possible gateway levels occur at 1.510 and 1.631 MeV.[55]

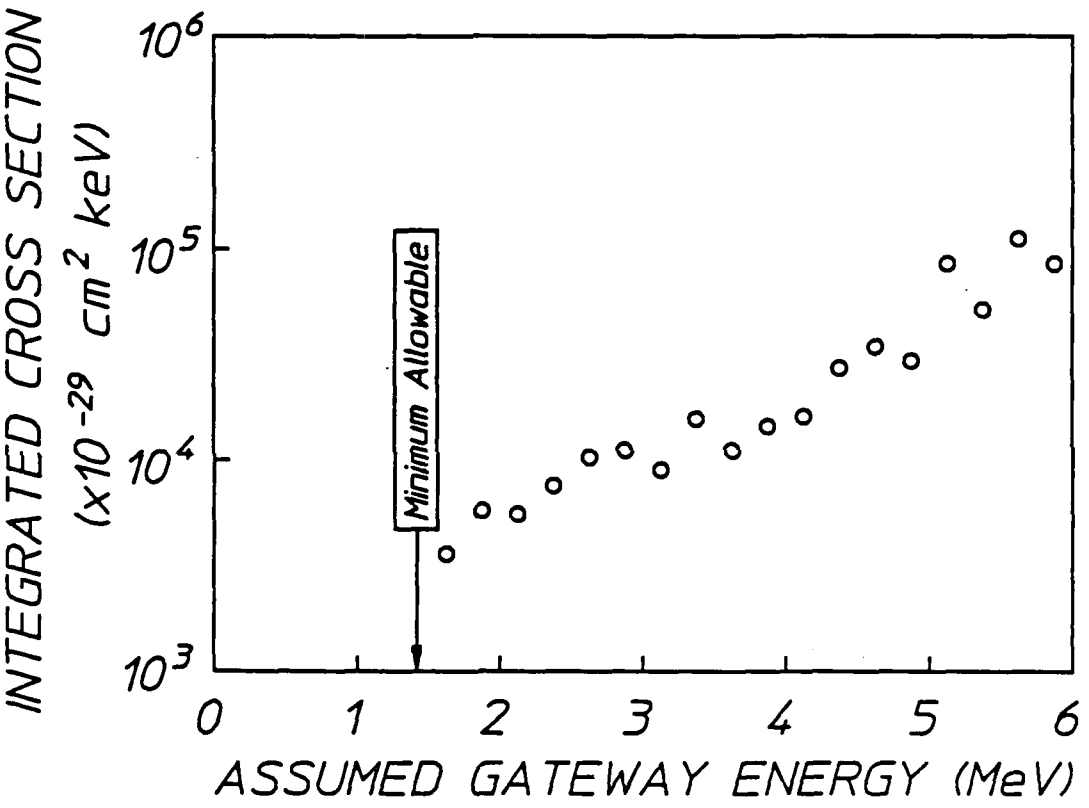

Figure 32: The integrated cross section for the photoactivation of ^{115}In through a single, unknown gateway state above 1.5 MeV as a function of the energy at which it could be assumed to lie.

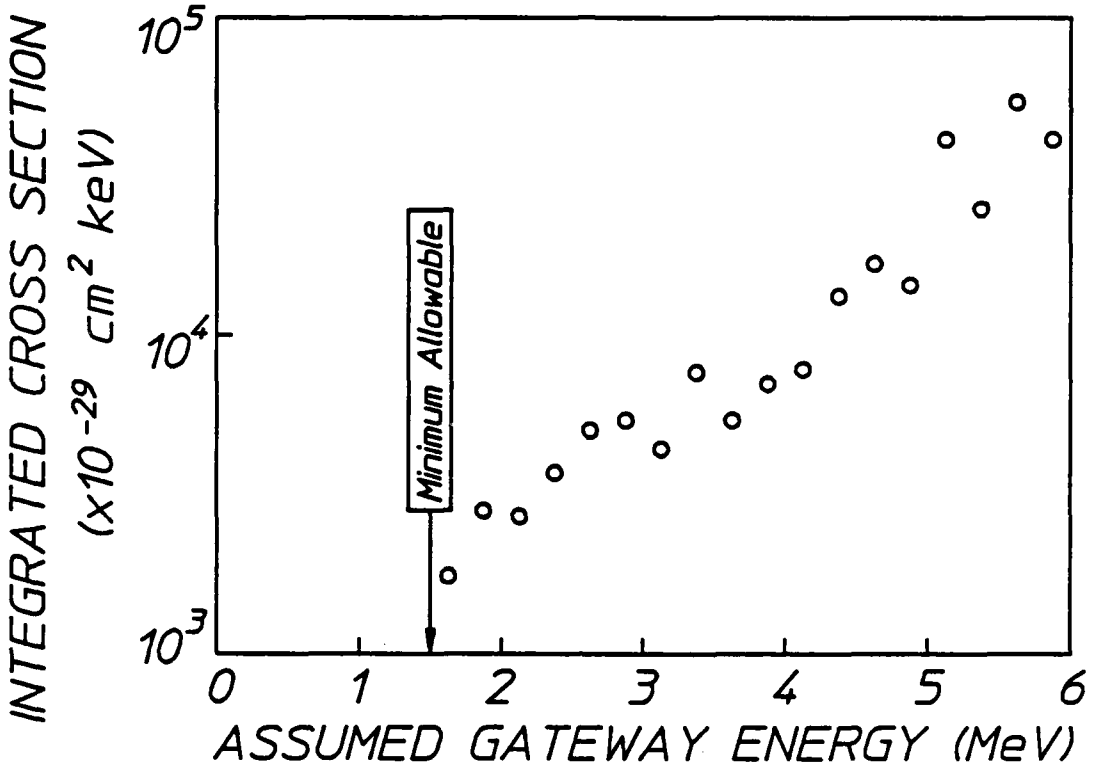

Figure 33: The integrated cross section for photoactivation through a single, unknown gateway state above 1.5 MeV as a function of the assumed gateway energy. This curve approximated the results obtained for the activation of both ^{113}In and ^{111}Cd to within the plotted size of the data points.

The 16.3 g cadmium sample contained 1.12×10^{22} nuclei of ^{111}Cd. The $(\sigma\Phi)$ products are found to be

$$(\sigma\Phi)_{known} = 6.49 \times 10^{-20} \text{ min}^{-1} \quad , \tag{38}$$

and

$$(\sigma\Phi)_{x} = 1.08 \times 10^{-17} \text{ min}^{-1} \quad . \tag{39}$$

The effective cross section of the assumed gateway state as a function of gateway energy is expressed by

$$(\pi b_a b_o \sigma_o \Gamma/2) = 7.01 \times 10^{-27}/F(E) \text{ cm}^2 \text{ keV} \quad , \tag{40}$$

which would plot to be indistinguishable from the curve derived for ^{113}In shown in Fig. 33. The minimum energy of the unknown gateway state is again considered to be about 1.4 MeV.

Conclusions

From Figs. 32 and 33 it can be seen that integrated cross sections for the excitation of isomers of indium and cadmium reach 10^{-25} cm^2 keV for (γ,γ') reactions proceeding through channels open to the bremsstrahlung from a 6 MeV linear accelerator. This is three orders of magnitude greater than values characteristic of excitation with photons of energy below 1.4 MeV. Qualitatively such an increase is of the magnitude expected to result from a change of gateway states with picosecond lifetimes to the femtosecond lifetimes characteristic of E1 transitions at these energies, unhindered by the occurrence of collective octupole vibrations. The similarity of results for nuclei with both similar and dissimilar single particle structures supports the identification of this strong channel for (γ,γ') reactions with some type of core property varying only slowly among neighboring nuclei. In such a case, however, there would need to be a mixing of several single particle states so the decay of the gateway state could occur into several different cascades with comparable probabilities.

DEPOPULATION OF THE ISOMERIC STATE $^{180}Ta^{m}$ BY THE REACTION $^{180}Ta^{m}(\gamma,\gamma')^{180}Ta$

The isotope $^{180}Ta^{m}$ carries a dual distinction. It is the rarest stable isotope occurring in nature[13] and it is the only naturally occurring isomer.[14] It is the only one of the 29 candidates for a gamma-ray laser that is available in milligram quantities. The actual ground state of ^{180}Ta is 1^{+} with a half-life of 8.1 h while the tantalum nucleus of mass 180 occurring with 0.012% abundance is the 9^{-} isomer, $^{180}Ta^{m}$. It has an adopted excitation energy of 75.3 keV and half-life in excess of 1.2×10^{15} years.[14]

The stellar s-process[56,57] for nucleosynthesis has steadily gained favor for the production of $^{180}Ta^{m}$ and the role of the most critical intermediary, $^{180}Hf^{m}$, has been well established.[14,58] However, the viability of this cosmic mechanism rests upon the absence of any reactive channel $^{180}Ta^{m}(\gamma,\gamma')^{180}Ta$ which could destroy the isomeric population in the photon bath present in the stellar interior at the time of creation. Prior experiments[52,59] have failed to show such a channel having any gateway for excitation below 1332 keV, but the rarity of the target material limited the sensitivity of those measurements. Reported here is the measurement of a very large cross section for the photonuclear deexcitation of $^{180}Ta^{m}$ through a gateway level at an energy $E \geq 1.4$ MeV. This definitive observation of such a strong radiative coupling between isomeric and ground states of ^{180}Ta may affect explanations for the natural occurrence of $^{180}Ta^{m}$.

The energy level diagram of ^{180}Ta and its daughters is shown in Fig. 34, together with a schematic representation of the individual steps in the excitation and detection of the $^{180}Ta^{m}(\gamma,\gamma')^{180}Ta$ reaction. As can be seen in Fig. 34, the principal means for the detection of the ^{180}Ta ground state lies in observing the K_{α} lines of its daughter, ^{180}Hf, following the decay by electron capture of the parent ^{180}Ta. The efficiency for the emission of K_{α} photons relative to the number of ^{180}Ta decays is about[60] 57%.

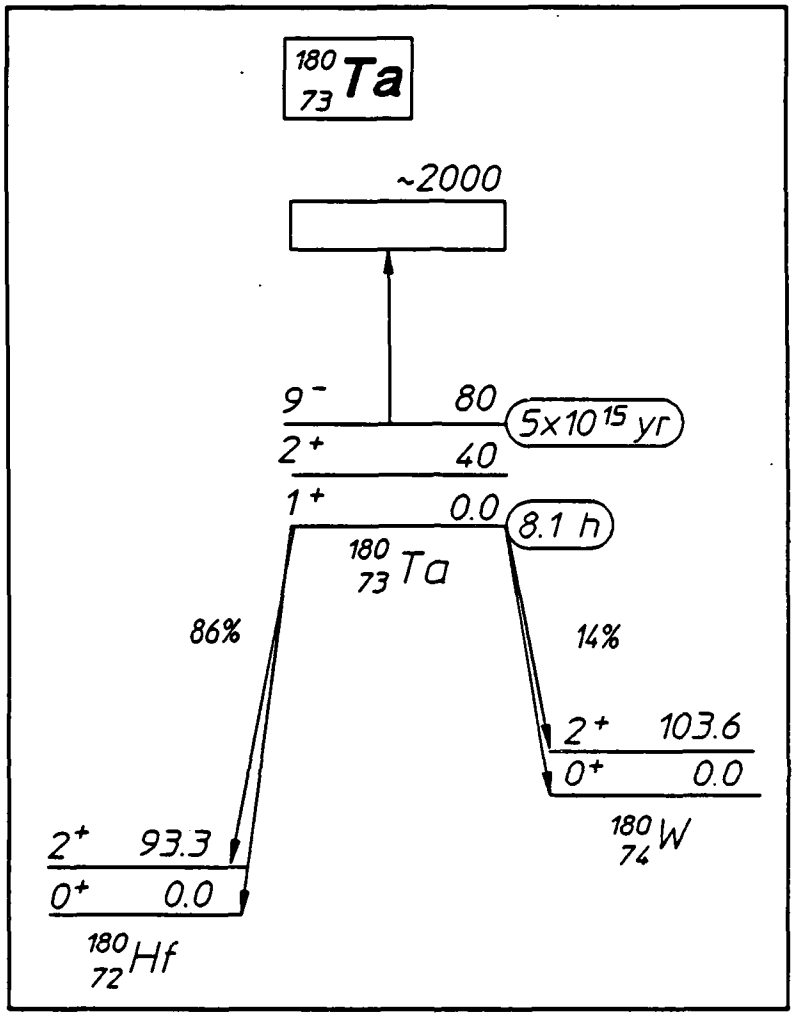

Figure 34: Schematic energy level diagram of ^{180}Ta and its daughters. Half-lives are shown in ovals to the right of the ground and isomeric levels. Energies are in keV. The initial transition of the (γ,γ') reaction is shown by the arrow pointing upward to the broad state represented by the rectangle. Cascade through the levels of ^{180}Ta is not known, but leads finally to the ground state. Electron capture to the left and beta decay to the right are indicated by the diagonal downward arrows. The final debris from pumping down the isomer is found principally in the K_α fluorescence from the ^{180}Hf characterized by the 8.1 hour lifetime of its ^{180}Ta parent.

Two targets were used in these experiments. One consisted of a disk 5 cm in diameter of tantalum in natural isotopic abundance. It contained about 0.5 mg of $^{180}Ta^{m}$ in the surface layer of thickness equal to the mean distance for escape of a 55 keV x-ray photon. The second target was enriched to contain 1.3 mg of $^{180}Ta^{m}$ in 24.7 mg of ^{181}Ta. Deposited as a dusting of oxide near the center of the surface of a 5 cm disk of Al and overcoated with a 0.25 mm layer of Kapton, this second sample was believed[61] free from self-absorption of the x-rays from the daughter Hf.

The samples were exposed to bremsstrahlung radiation from the Varian Clinac 1800 linear accelerator (LINAC) operated with an end-point energy of 6 MeV that was used in the experiments with In and Cd. This device has been well characterized,[53,54] and its output dose rate has been calibrated with an accuracy of ± 3%. After irradiation, the samples were counted with an N-type, HPGe spectrometer having a beryllium entrance window. Conventional techniques were used to calibrate the counting system with isotopic standards.

Figure 35 shows the spectra of the enriched target before and after 4 hours irradiation. The spectrum from the other target was entirely similar with the Hf signal reduced by the ratio of the masses of the $^{180}Ta^{m}$ and the background increased by the appearance of K-lines of Ta excited in the large mass of diluent ^{181}Ta by the decay of natural activity in the counting shield.

Figure 36 shows the dependence upon time of the counting rate observed in the Hf(K_{α}) peaks after irradiation. Data points are plotted at the particular times at which the instantaneous counting rate equals the average counting rate measured over the finite time interval shown. The figure shows the close agreement of the measured rates to the decay expected for a half-life assumed to be 8.1 hours.

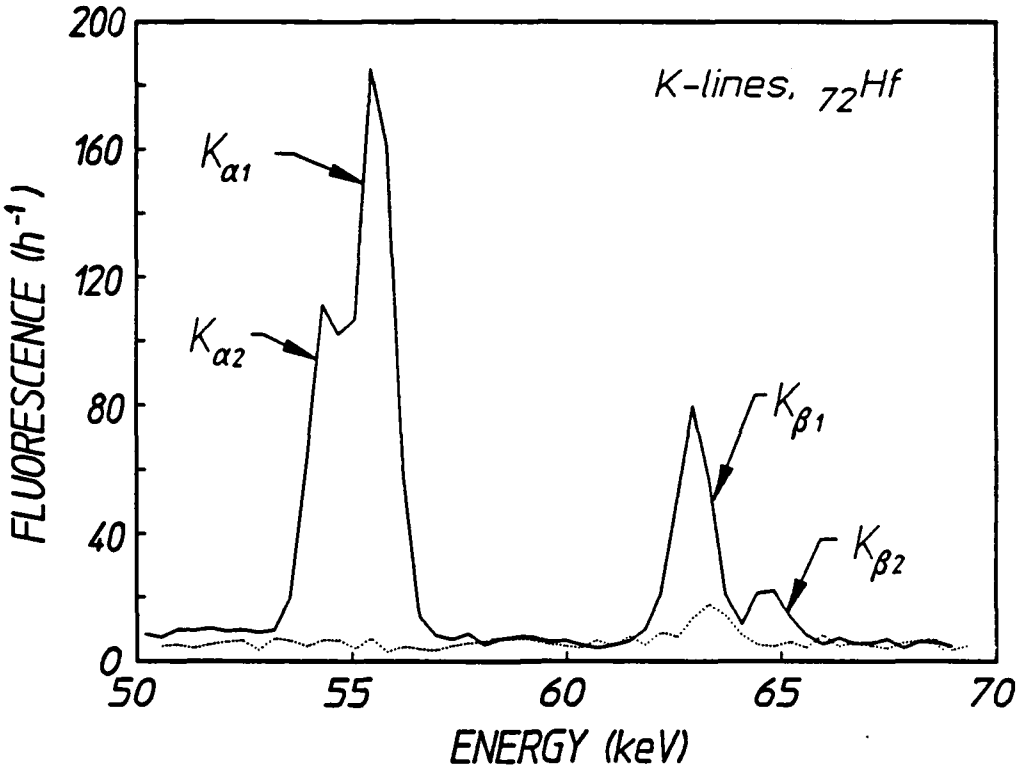

Figure 35: Dotted and solid curves show, respectively, the spectra obtained before and after dumping some of the isomeric $^{180}Ta^{m}$ contained in a target sample enriched to 5%. An HPGe detector was used to obtain the dotted spectrum before irradiation. The feature at 63 keV is from traces of natural activity in the counting shield. The solid curve shows activity resulting from the transmutation of the pumped ^{180}Ta measured in the same sample and counting system after irradiation. The prominent additions are the K_{α} and K_{β} hafnium x-ray lines resulting from electron capture in the ^{180}Ta.

The spectrum of the bremsstrahlung pumping the fluorescence seen in Fig. 35 was taken from the literature[53] and normalized to the total dose measured in this experiment. In this way the time integrated spectral intensity producing the fluorescence was found to be constant[62] to within a factor of two over the range 1-5 MeV at a value of 2×10^{14} keV/keV/cm^2. The number of counts observed in the Hf K_{α} lines were corrected for finite irradiation and counting times, the absolute counting efficiency of the spectrometer, and the 57% emission intensity from the parent ^{180}Ta to obtain the number of nuclei pumped to the ground state. Assuming self-absorption in the enriched target to be negligible, the integrated cross section for the deexcitation of the isomer can

be readily calculated if the reaction is assumed to occur through a gateway state narrow in comparison to the range of energies spanned by the irradiation. A value of $\sigma\Gamma = 4.8 \times 10^{-25}$ cm^2 keV is obtained for the integrated cross section if the gateway energy is arbitrarily assumed to be near the lowest value consistent with prior[52] negative results, 2.0 MeV. Even larger cross sections would result from the assumption that the gateway lies at higher energies where the pumping flux is decreased or from from inclusion of an exact self-absorption correction. Once the gateway energy is fixed, experimental error in the integrated cross section is bounded on the lower side by a total uncertainty of 15% contributed by the calibrations of source and detector and on the upper side by a factor of two arising from the possible loss of signal because of self-absorption of the Hf x-rays.

The results of this work show a radiative connection between the isomer $^{180}Ta^m$ and the ^{180}Ta ground state of remarkable strength. Comparative values for the deexcitation of other isomers are not available as it appears this is the first such measurement. However, the inverse process for the excitation of isomers by (γ,γ') reactions typically proceed[11,39,63] with integrated cross sections at least two orders of magnitude smaller. The value reported here for the reaction $^{180}Ta^m(\gamma,\gamma')^{180}Ta$ is inexplicably large and may have several consequences. If the gateway level through which it proceeds is not sufficiently above the thermal energies expected to characterize the s-process of nucleosynthesis, current models of the stellar production of the nuclei of $^{180}Ta^m$ will be severely affected.

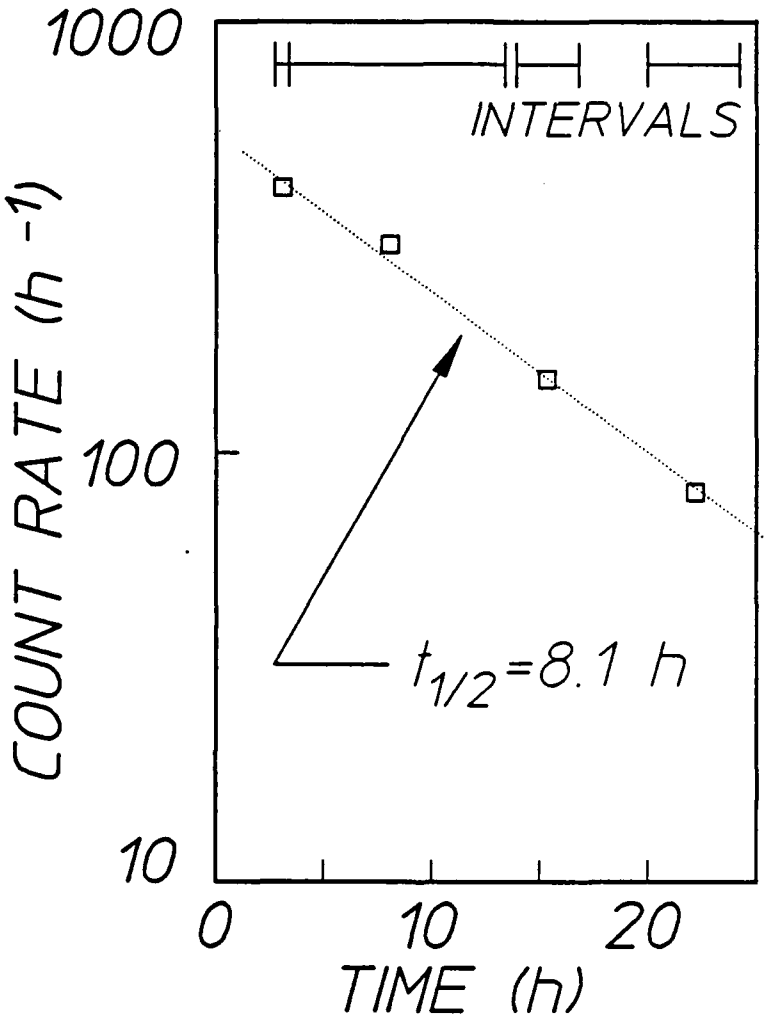

Figure 36: Plot of the counting rates measured for the Hf(K_α) fluorescence from the target fabricated from natural tantalum as functions of the time elapsed from the end of the irradiation. The vertical dimensions of the data points are consistent with 1σ deviations of the measured number of counts accumulated during the finite counting intervals shown at the top of the graph. The dotted line shows the rate expected for a half-life of 8.1 hours.

The greatest significance of this experiment in pumping $^{180}Ta^{m}$ bears on the feasibility of a gamma-ray laser. There is a threefold significance to this demonstrationof the efficiency for pumping isomers with x-rays.

1) The first real isomer to be tested for a gamma-ray laser was successfully pumped down with an astonishingly large cross section of 80,000 on a scale where 10 describes a fully allowed process.

2) The nuclear analog to the ruby laser is a fully viable scheme for a gamma-ray laser, and $^{180}Ta^{m}$ narrowly misses being an acceptable candidate. It performed about 10^{4} times better than would have been expected theoretically.

3) These results with a seemingly unattractive candidate indicate the probabilities should be raised for full success of one of the other 28 materials.

RADIATIVE COUPLING TO THE ISOMERIC STATE $^{123}Te^{m}$

The first observation[15] of a (γ,γ') reaction leading to the deexcitation of an isomeric population revealed an unexpected large cross section for the process as just discussed. The reaction $^{180}Ta^{m}(\gamma,\gamma')^{180}Ta$ was found to proceed through a partial width of 0.5 eV when pumped with the bremsstrahlung from a medical linear accelerator (linac). This is an enormous value which exceeds anything previously reported for (γ,γ') reactions[11,39,63] by two to three orders of magnitude. Such a high probability for deexcitation had been least expected for this isomer because of the unlikely change of $\Delta J = 8$ between $^{180}Ta^{m}$ and its ground state. For this reason it had been considered one of the poorest of the 29 candidates for a gamma-ray laser.

The extremely large size of the integrated cross section for the deexcitation of $^{180}Ta^{m}$ of 4.8×10^{-22} cm^2 eV allowed us to perform those experiments with as little as one milligram of $^{180}Ta^{m}$. Unfortunately, even milligram sized samples are not available for any of the remaining 28 candidates so the general applicability of the lessons taught by the tantalum experiment cannot be directly examined. However, $^{123}Te^{m}$ is one of the few candidates for which indications can be found by less direct means. It has both a radioactive signature sufficiently distinctive to permit its unequivocal detection and a stable ground state from which to fabricate a target. In this case the ground state ^{123}Te is a rare, but naturally occurring radioactive isotope with 0.91% natural abundance and a half-life of 1.3×10^{13} years. Thus, instead of deexciting the isomeric state to the ground state, the inverse reaction can be studied.

In fact, experimental difficulties remain because of the combination of the low natural abundance of ^{123}Te in the ground state and a long half-life of 119.7 days for the emission of the fluorescence. Before there was any reason to expect that such negative factors could be compensated by a great width to the process, there was little motivation to try to examine the reaction $^{123}Te(\gamma,\gamma')^{123}Te^{m}$ and it was not reported in the previous general survey.[64] In the experiments described here it was found that a large width did compensate the other difficulties and substantial amounts of fluorescence were observed.

The energy level diagram of ^{123}Te is shown in Fig. 37, together with a schematic representation of the individual steps in the excitation and detection of the $^{123}Te(\gamma,\gamma')^{123}Te^{m}$ reaction. As can be seen in Fig. 37,

detection of the isomer depends on observing the 159 keV line from the lowest lying excited state in ^{123}Te, which is populated by the decay of $^{123}Te^{m}$ through an M4 transition. The efficiency for the emission of 159 keV photons relative to the number of $^{123}Te^{m}$ decays is about[60] 84%.

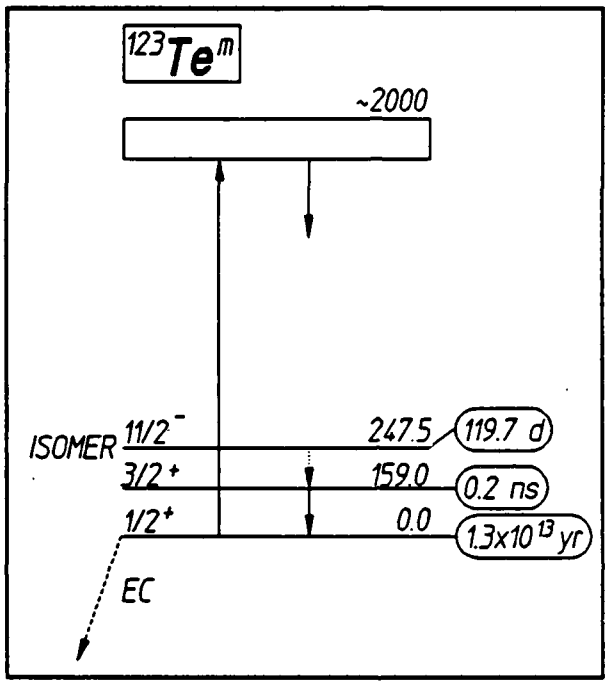

Figure 37: Schematic energy level diagram of ^{123}Te. Half-lives are shown in ovals to the right of the levels, and energies are in keV. The pump band is shown by the arrow pointing upward to the broad state represented by the rectangle. The cascade from this gateway is not known, but leads finally to the isomeric state. The resulting population of the laser candidate $^{123}Te^{m}$ is detected by the 159 KeV fluorescence with a 119.7 day half-life.

The target used in these experiments was a planchet of elemental tellurium in natural abundance. It was 5.2 cm in diameter and 0.47 cm thick. The sample consisted of 32.4 g of tellurium, containing 0.294 g of ^{123}Te in its ground state.

The sample was exposed to bremsstrahlung radiation from the same Varian Clinac 1800 linear accelerator (linac) operated in the In, Cd,

and $^{180}Ta^{m}$ experiments with an end-point energy of 6 MeV. This device has been well characterized,[53,54] and its output dose rate is maintained in calibration with an accuracy of ± 3%. The accumulated dose at 2 MeV near the peak of the spectrum was 5.6×10^{10} photons/cm^2/keV delivered in a sequence of pulses each having a peak intensity of about 4 W/cm^2 at the sample. After irradiation, the sample was counted with an N-type, HPGe spectrometer having a beryllium entrance window. Conventional techniques were used to calibrate the counting system with isotopic standards.

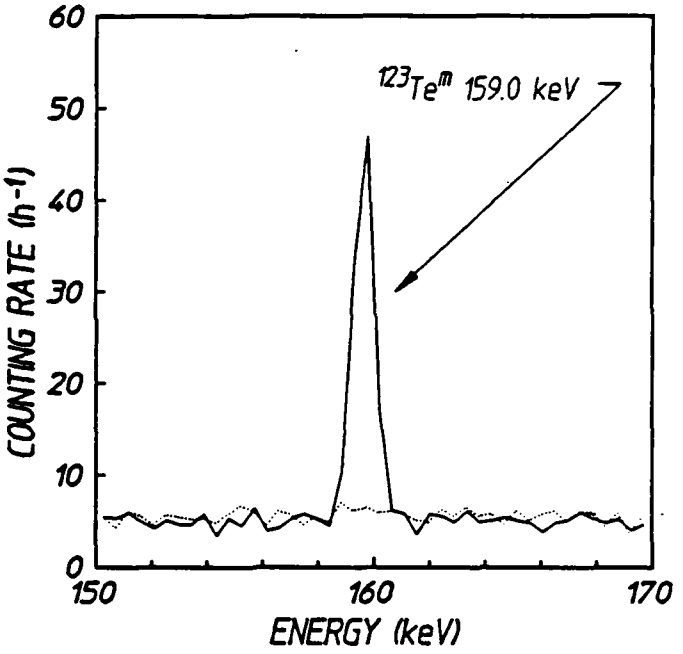

Figure 38: Dotted and solid curves show, respectively, the spectra obtained before and after pumping some of the 294 mg of ^{123}Te to the isomeric $^{123}Te^{m}$.

Figure 38 shows the spectra of the target before and after 4.0 hours irradiation. Figure 39 shows the dependence upon time of the counting rate observed in the 159 keV peak after irradiation. Data points are plotted to have a size comparable to the 1σ statistical error in the number of counts accumulated during the measurement periods. The figure shows the close agreement of the measured rates to the decay expected for a half-life assumed to be 119.7 days.

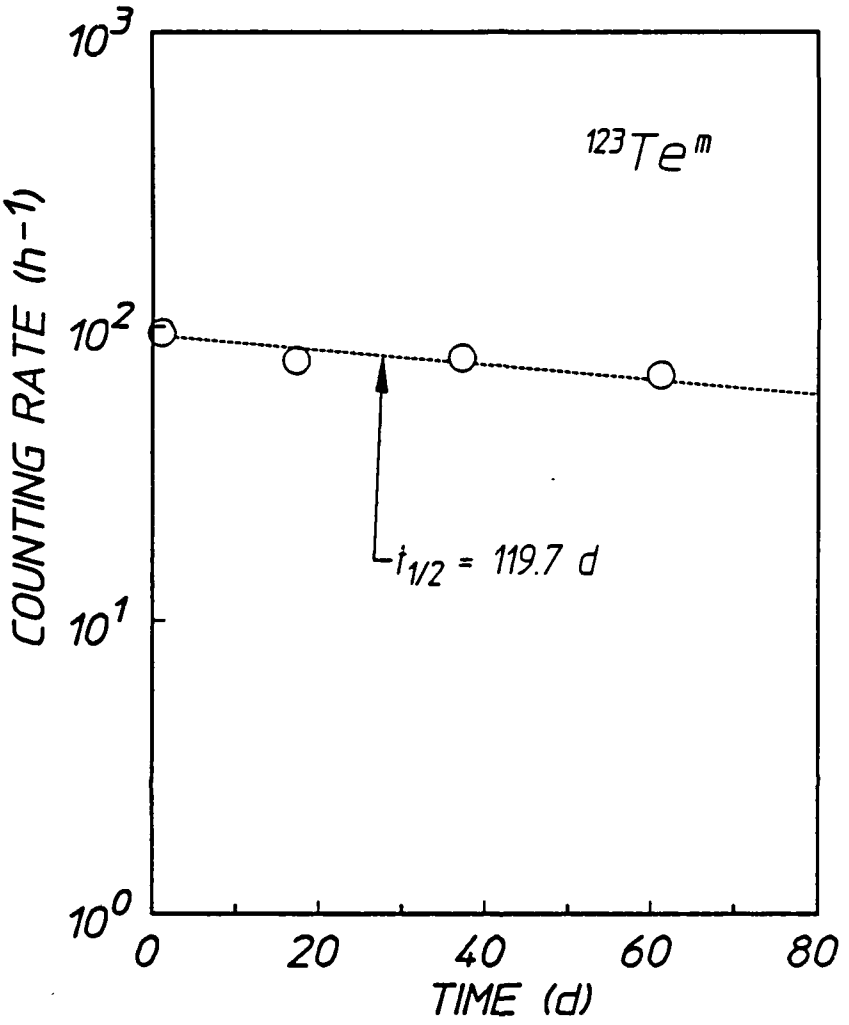

Figure 39: Plot of the time decay of the activity of the $^{123}Te^m$ produced in the target by irradiation with x-rays. The size of the plotted points is comparable to a 1 σ deviation, and the slope indicates the expected 119.7 day half-life.

The spectrum of the bremsstrahlung pumping the fluorescence seen in Fig. 31 was taken from the literature[53] and was normalized to the total dose measured in this experiment. In this way the time integrated spectral intensity producing the fluorescence was found to vary no more than a factor of two over the range 1-5 MeV, being approximately 1.0 * 10^{14} keV/(keV cm^2). The number of counts observed in the 159 keV line was corrected for finite irradiation and counting times. The total number of excitations was then calculated based on the 84% emission

intensity of the 159 keV line from ^{123}Te, the calculated 59% probability for unmodified escape of the photon from the sample, and the calibrated absolute peak efficiency for the detector. From such data the integrated cross section for the deexcitation of the isomer can be readily calculated if the reaction is assumed to occur through a gateway state narrow in comparison to the range of energies spanned by the irradiation. A value of $\sigma\Gamma = 1.0 \times 10^{-25}$ cm^2 keV is obtained for the integrated cross section if the gateway energy is arbitrarily assumed to be near the lowest value consistent with prior[15] negative results, 2.0 MeV. Even larger cross sections would result from the assumption that the gateway lies at higher energies where the pumping flux is decreased. Once the gateway energy is fixed, experimental error in the integrated cross section is bounded by a total uncertainty of 15% contributed by the calibrations of source and detector.

As in the case of the deexcitation of $^{180}Ta^m$, the cross section for the excitation of $^{123}Te^m$ is an enormous value. Moreover, the straightforward path of analyses shown schematically in Fig. 40 leads to rather astonishing conclusions.

Along the path of analysis of Fig. 40, assumptions are shown in ovals and derived results in rectangles. The most conservative results continue to be obtained by supposing the energy of the gateway band to which absorption first occurs to lie around 2 MeV. As shown in Fig. 40, this assumption together with the measured number of decays of $^{123}Te^m$ gives the value being reported for the integrated cross section, $(\pi b_a b_o \Gamma \sigma_o/2)$.

To obtain the partial width in the third row of Fig. 40 requires the Breit-Wigner cross section given in Eq. (4).

The value of α_p is essentially zero for a 2 MeV transition which is highly allowed; and even were it not, σ_o would be reduced further and the partial width would become even larger. Nothing is known about the spin of the gateway state, but it is most reasonable to expect it to lie between that for the initial and final states. In that case $I_e > I_g$, since the process is starting on the $1/2^+$ state. From Eq. (4) it can be seen that the assumption $I_e = 3/2$ results in a possible underestimation of σ_o but not by more than 50%.[66] As shown in Fig. 40, the partial width for pumping the isomer down to the ground state becomes,

$$b_a b_o \Gamma = 0.05 \text{ eV} \quad . \tag{41}$$

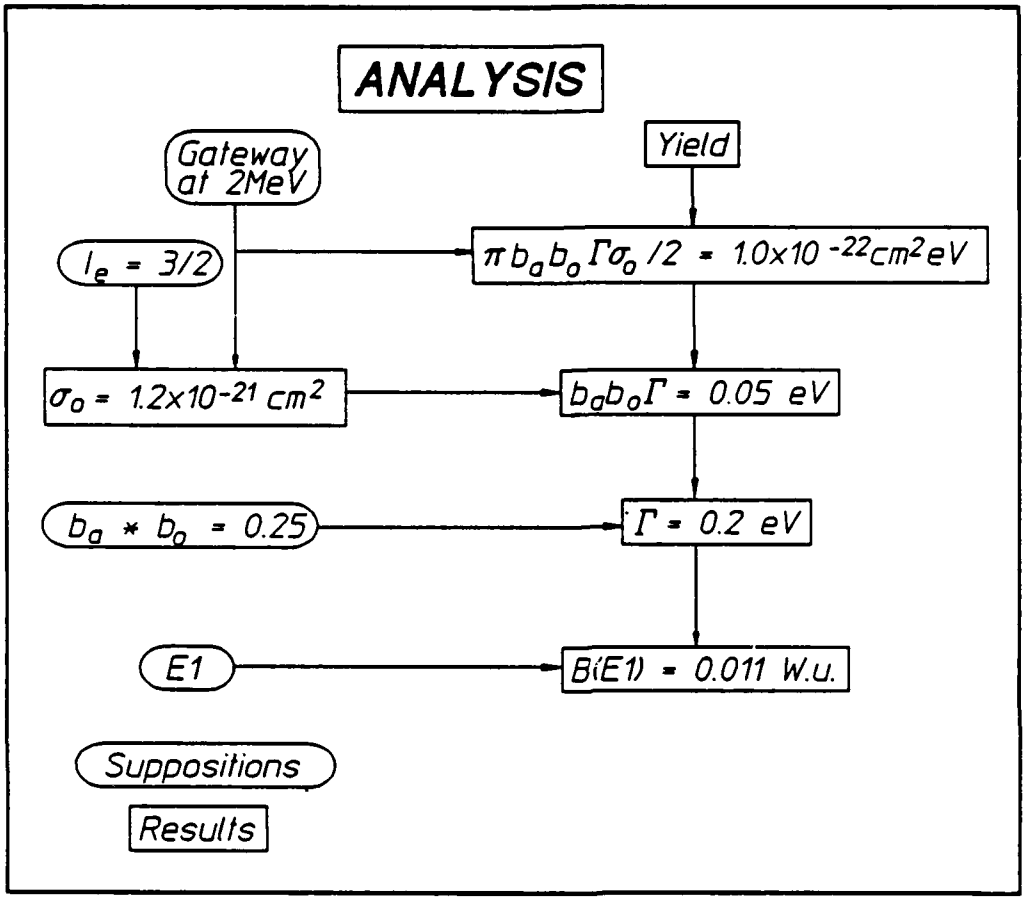

Figure 40: Flow chart showing the interrelation of assumptions and conclusions reached in the analysis of the tellurium data.

If this product is further analyzed as representing the width of a single state coupled to the ground state toward the isomer as shown in Fig. 37, it must be concluded that the width of the gateway state is at least 0.2 eV, as shown in Fig. 40. From the uncertainty principle, it follows that

$$t_{1/2}(\text{gateway}) = 2.2 \text{ fs} \quad . \qquad (42)$$

To be consistent with the assumption $b_a \times b_o = 0.25$ it must be concluded that the total width of 0.2 eV for the funneling level is

contributed equally by two transitions, each of 0.1 eV width. As shown in Fig. 37, one must connect to the ground and one to some other level with angular momentum more nearly comparable to that of the isomer. Transition strengths are often measured in Weisskopf units (W.u.) since 1.0 W.u. is the maximum possible for the transition of a single nucleon for a given multipolarity.[16] Converted into those units the transition probability B(M) for one of the component steps of 0.1 eV width would become,

$$B(E1) = 0.0058 \text{ W.u.} \quad , \tag{43}$$

and

$$B(M1) = 0.6 \text{ W.u.} \quad , \tag{44}$$

respectively, depending upon whether the multipolarity M were E1 or M1.

Again, these are enormous strengths, being almost without precedent. The expected[17] value for an electric dipole transition lies in the range 5×10^{-7} to 6×10^{-5} W.u. for heavy nuclei and fewer than ten are known[17,18] to approach 0.1 W.u. at these energies. For those exceptional cases, the width of the upper level is entirely due to the contribution from a single transition. Prior to the results with $^{180}Ta^{m}$ there were no cases known where two transitions of such strength added comparable components of width to the same upper state.

The situation is little changed if the transitions are assumed to be mediated by the magnetic dipole, M1 operator. Generally not as hindered as E1 transitions,[17] M1 strengths approach 0.1 W.u. in many cases. However, the scale of the W.u. for an M1 transition is smaller in physical units of width; so our measured widths correspond to a much larger number of W.u., thus presenting the equivalent problem. Fewer than ten M1 transitions are known[17] to have B(M1) > 1.0 W.u. and none are paired to share a common level.

While the width of the transfer process is difficult to interpret in the context of a single funneling state in a single particle model, a puzzle of comparable complexity is found in the efficiency with which ΔJ is transferred. As in the case of $^{180}Ta^{m}$, it is an interesting speculation that at certain energies of excitation collective oscillations of the core nucleons could break some of the symmetries upon which rest the identification of the pure single particle states. If single particle

states of differing angular momenta were mixed in this way, the possibility for transferring larger amounts of ΔJ with greater partial widths might be enhanced.

Whatever the cause, the significance of these results is clear. Two of the poorest examples of the 29 candidates for gamma-ray materials were found to have very strong radiative connections between ground and isomeric states. The partial width for creating the $^{123}Te^{m}$ isomer corresponds to 0.05 eV, an enormous value, and the inverse could easily approach the 0.5 eV measured for the dumping of $^{180}Ta^{m}$, since pumping down in energy should be more favorable than pumping up. It appears that both $^{180}Ta^{m}$ and $^{123}Te^{m}$ narrowly missed being acceptable candidates. They performed about 10^4 and at least 10^3 times better than would have been expected theoretically. These results with seemingly unattractive candidates indicate the probabilities should be raised for full success of one of the other 27 materials.

LARGE CHANGES OF ANGULAR MOMENTA PUMPED BY BREMSSTRAHLUNG IN SELECTED NUCLEI

A renaissance in the study of (γ,γ') reactions has been launched by the availability of medical linear accelerators (linacs) which can serve as intense and stable bremsstrahlung sources with particularly well-characterized spectra.[53,54] The total doses which they can deposit in reasonable working periods have made possible the examination of (γ,γ') reactions involving rare materials for which target masses are limited to milligrams. In this way, the first (γ,γ') reaction leading to the deexcitation of an isomeric sample was studied,[15] with rather unexpected results. Requiring an unlikely change of $\Delta J = 8$, this isomer $^{180}Ta^m$ was dumped through a partial width of at least 0.5 eV, an enormous value exceeding anything previously reported for (γ,γ') reactions at comparable energies by two to three orders of magnitude. Rather similar results[67] were found for reactions producing isomers in a few cases. Integrated cross sections of the order of 10,000 in the units of 10^{-29} cm^2 keV were found for the excitation of isomers of ^{111}Cd, ^{113}In, and ^{115}In, and for excitation of the laser candidate $^{123}Te^m$, through resonant gateways pumped by bremsstrahlung from the same linear accelerator producing most of its intensity near 2 MeV.

Reported here is the extension of these studies to the excitation of very long-lived isomers having half-lives varying from hours to weeks. Again pumping with the linac having its end point energy at 6 MeV, the (γ,γ') reactions had to proceed through channels providing for changes of angular momentum ranging from $\Delta J = 4$ to 6. Five nuclides were examined: ^{87}Sr, ^{117}Sn, ^{135}Ba, ^{195}Pt, and ^{199}Hg. Integrated cross sections were found to range from 1,000 to 20,000 in the usual units of 10^{-29} cm^2 keV, the facility for excitation showing no correlation with ΔJ. The largest occurred for $^{195}Pt(\gamma,\gamma')^{195}Pt^m$ which requires $\Delta J = 6$ to excite a 4 day isomer. While the energies of the responsible gateways cannot yet be determined, the pervasiveness of such large partial widths for the exchange of substantial amounts of angular momentum was unexpected at any energies below the thresholds for (γ,n) reactions.

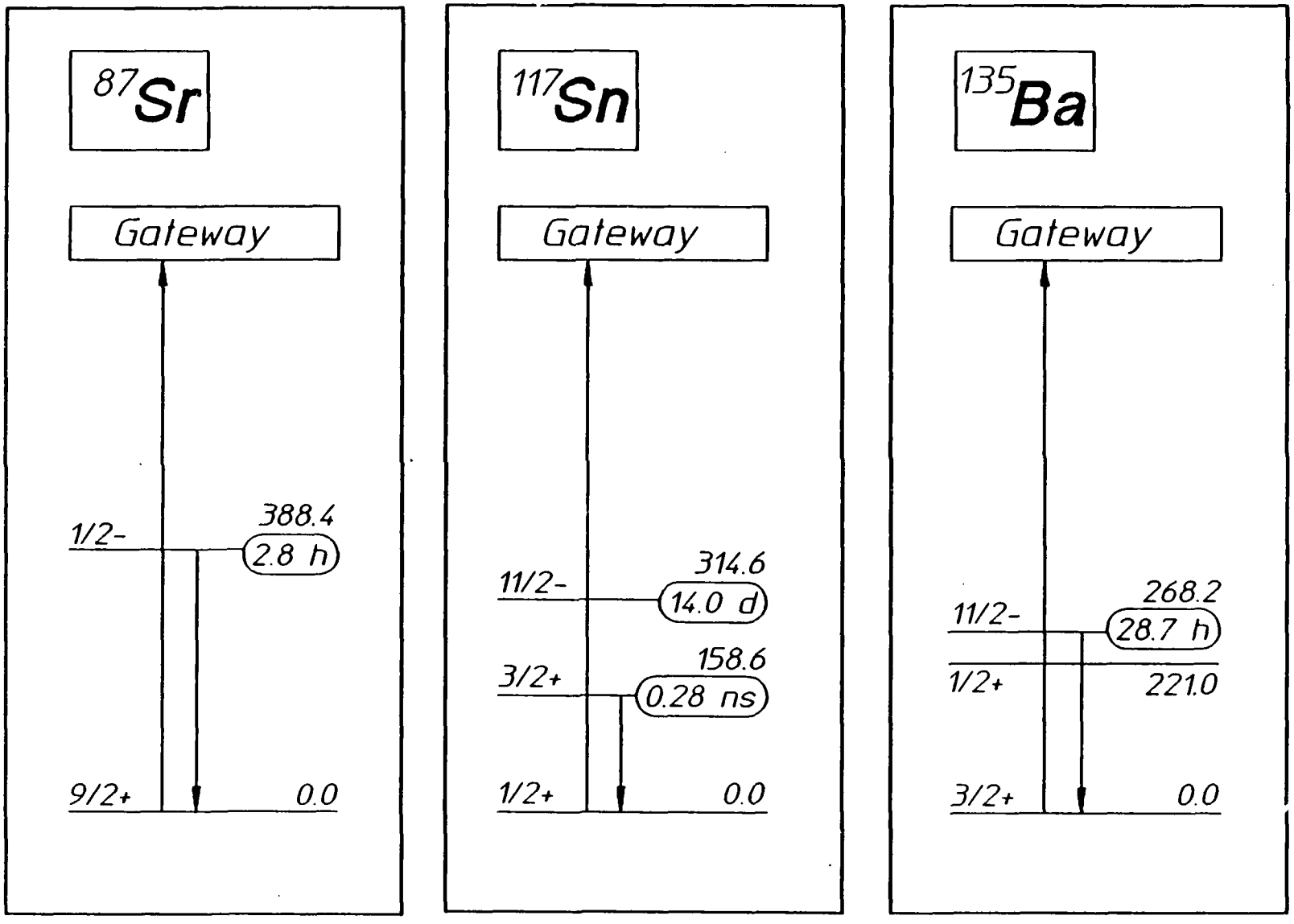
87Sr
Gateway
388.4
1/2-
2.8 h
9/2+
0.0
117Sn
Gateway
314.6
11/2-
14.0 d
158.6
3/2+
0.28 ns
1/2+
0.0
135Ba
Gateway
268.2
11/2-
28.7 h
1/2+
221.0
3/2+
0.0

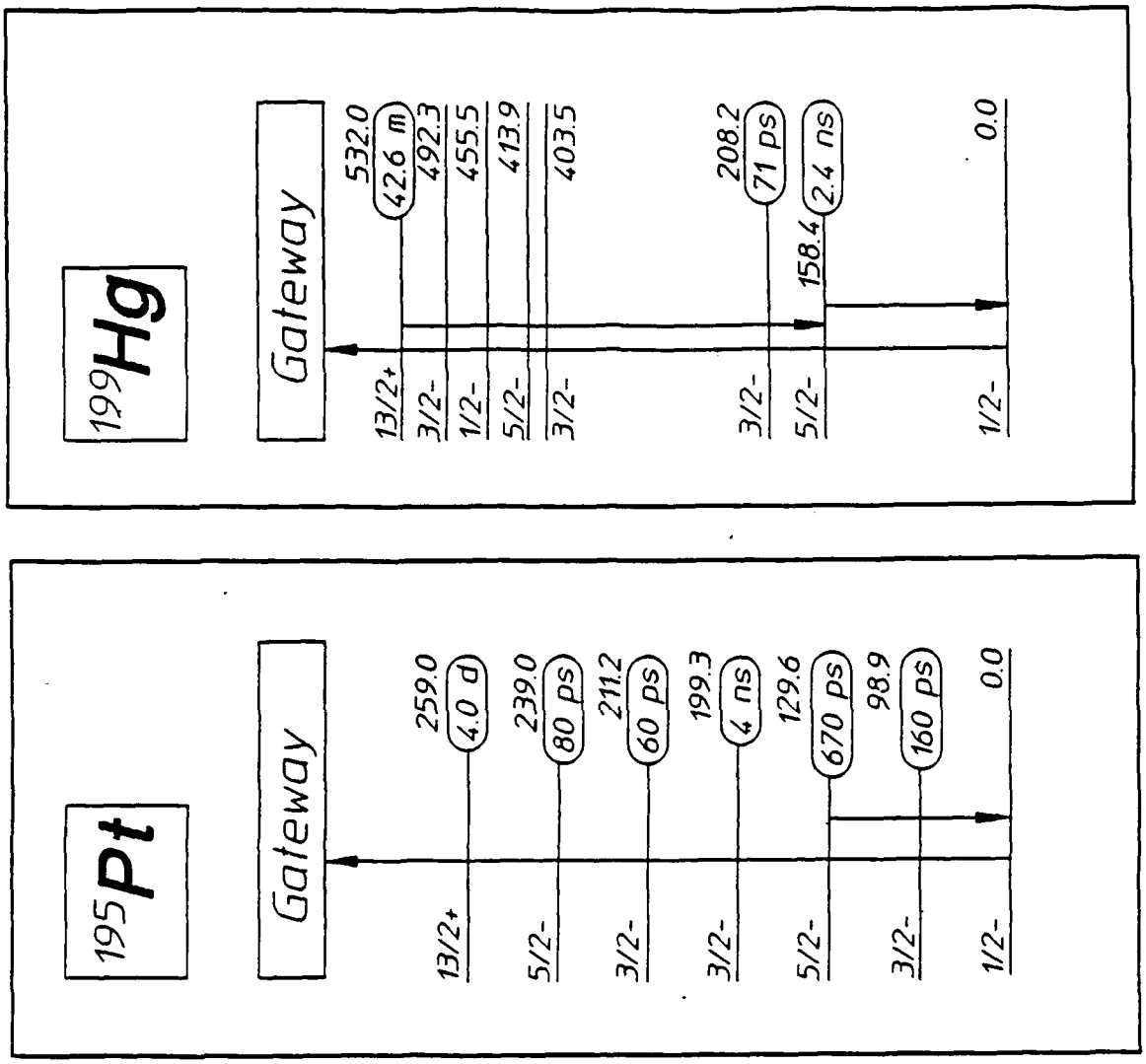

Figure 41: Energy level diagrams of the excited states important to the production and detection of the isomers of the nuclei shown. Half-lives of the states are shown to the right of each, together with their energies in keV. Downward arrows locate transitions used in the detection of populations of the isomers produced by the absorption transitions indicated by the upward arrows. The locations of the gateways through which the (γ,γ') reactions proceed are not to scale, and the details of the cascades downward to the isomers are unknown.
a), b) and c) (opposite from left): Transitions important to the study of (γ,γ') reactions producing the isomers $^{87}Sr^{m}$, $^{117}Sn^{m}$, and $^{135}Ba^{m}$.
d) and e) (from left): Transitions important to the study of (γ,γ') reactions producing the isomers of $^{195}Pt^{m}$ and $^{199}Hg^{m}$. For the latter, two possible transitions are shown for the detection of the isomer.

Experimental Procedures

The relevant energy levels for the five nuclei of interest in these experiments are shown in Fig. 41. They were present in targets fabricated from materials containing natural isotopic abundances. In some cases they were thick enough that self-absorption of the output transition necessitated a correction of significant magnitude. The samples of elemental Pt and Sr were in plate form. The other samples were powders held in flat, cylindrical polyethylene vials. All samples were counted at the endcap window of a 10% relative efficiency, n-type Ge detector. Target parameters are summarized in Table VI, together with the corrections for self-absorption computed from the counting geometry, sample composition, and sample density. As shown in Fig. 41, two fluorescent transitions occurred with sufficient probabilities from the $^{199}Hg^{m}$ state to support measurement of the integrated cross section for the $^{199}Hg(\gamma,\gamma')^{199}Hg^{m}$ reaction. Having different energies, they encountered different levels of self-absorption and served to confirm the procedures for correction.

Table VI

Summary of target parameters for the nuclides used in these experiments. The transparency factor listed in the rightmost column is the computed fraction of the emitted counts able to reach the spectrometer in the particular geometry employed.

Nuclides	Form	Abundance (%)	Sample Mass (g)	Half-life (days)	Fluorescence (keV)	Transparency
^{87}Sr	SrF_2	7.0	13.4	0.117	388.4	0.954
^{117}Sn	Sn	7.7	4.35	13.6	158.6	0.911
^{135}Ba	BaF_2	6.6	8.65	1.20	268.3	0.94
^{195}Pt	Pt	33.8	31.1	4.02	129.8	0.06
^{199}Hg	Hg_2Cl_2	16.9	24.0	0.030	374.1 158.5	0.837 0.41

Targets were exposed for times on the order of four hours to the output of a Varian Clinac 1800 linear accelerator at the Department of Radiology of the University of Texas Southwestern Medical Center at Dallas. This linear accelerator was operated with an end point energy of 6 MeV.

After irradiation, targets were removed to the counting facility of the Center for Quantum Electronics of the University of Texas at Dallas, where the decays of the isomeric products of the (γ,γ') reactions were measured with the Ge spectrometer system. Typical spectra are shown in Figs. 42a - 42e.

Confirmation that the fluorescence peaks were the signatures of the decays of the respective isomers was obtained by examining the decays of the counting rates as functions of the time elapsed from the cessation of the irradiation. These decay curves are shown in Fig. 43a - 43e, together with lines recording the expectations based upon literature values of the half-lives. Fluctuations expected at the 1σ level correspond roughly to the sizes of the plotted points with one exception in which the 1σ error bars are explicitly shown. For each of the five nuclides studied, both spectral and temporal content of the fluorescence conformed to the unequivocal signatures of the five isomers expected.

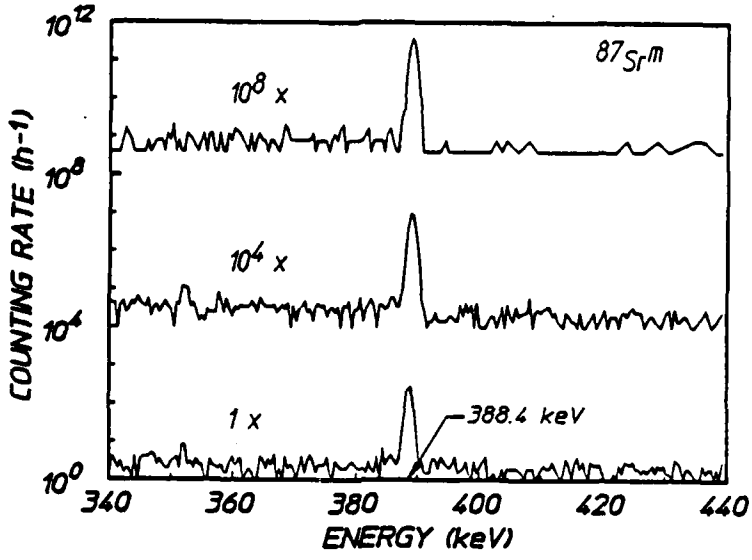
10^{12}
10^{8}
10^{4}
10^{0}
COUNTING RATE (h-1)
87_{Sr^m}
10^{8} x
10^{4} x
1 x
388.4 keV
340
360
380
400
420
440
ENERGY (keV)

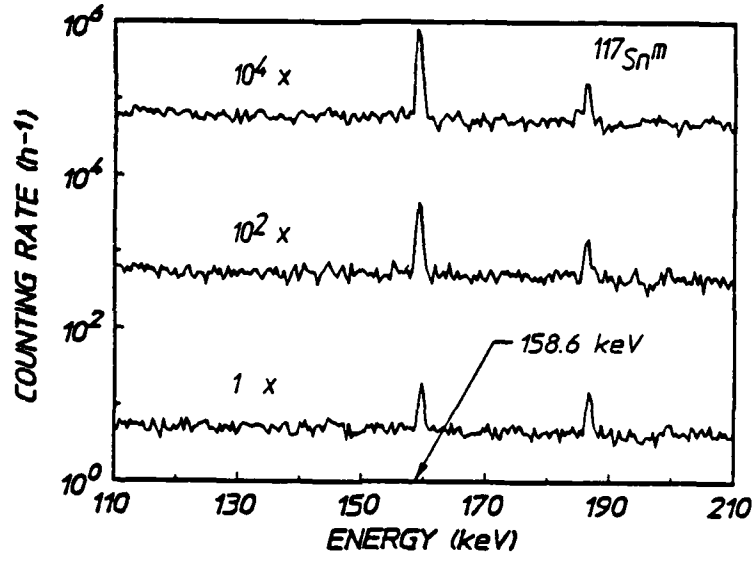
10^{6}
10^{4}
10^{2}
10^{0}
COUNTING RATE (h-1)
117_{Sn^m}
10^{4} x
10^{2} x
1 x
158.6 keV
110
130
150
170
190
210
ENERGY (keV)

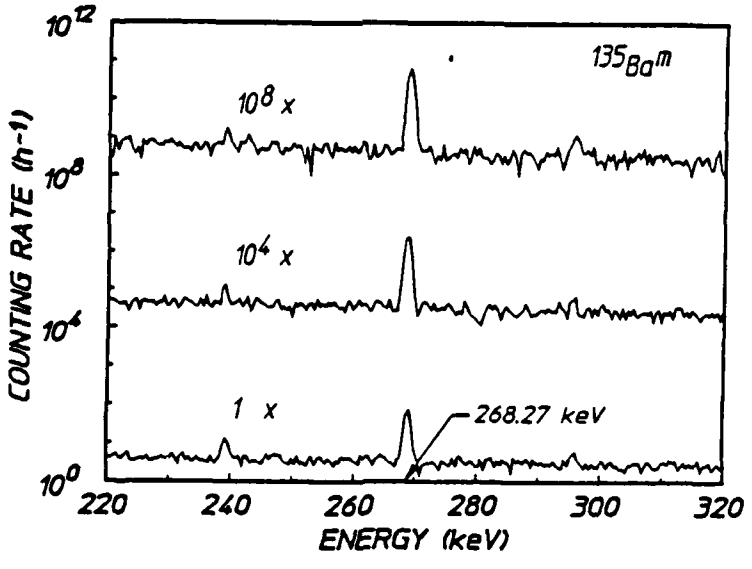
10^{12}
10^{8}
10^{4}
10^{0}
COUNTING RATE (h-1)
135_{Ba^m}
10^{8} x
10^{4} x
1 x
268.27 keV
220
240
260
280
300
320
ENERGY (keV)

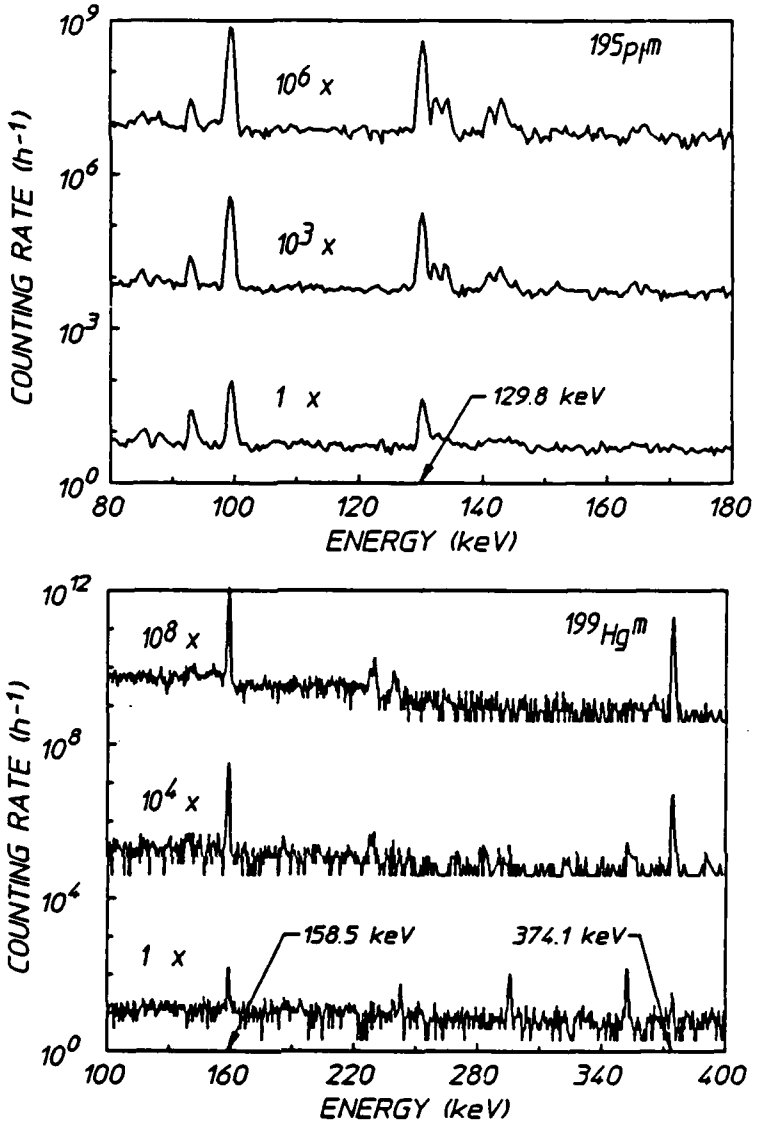

Figure 42: Successive spectra of the fluorescences detected with an intrinsic Ge detector emphasizing the ranges of energies shown. Transitions shown in Figs. 41a - 41e for the detection of the isomers are identified by the arrows. In each figure successive spectra have been offset vertically by the amounts shown, with the one taken directly after irradiation at the top. The times elapsed from the ends of irradiation to the start of the counting intervals are as follows:
a) (opposite top) ^{87}Sr; 1.42, 5.77, and 10.87 h for durations of 15, 120, and 120 min, respectively.
b) (opposite center) ^{117}Sn; 3.17, 13.96, and 38.1 days for durations of 600 min each. The peak at higher energies is from the natural background.
c) (opposite bottom) ^{135}Ba; 5.20, 37.8, and 87.6 h for durations of 120, 300, and 402.8 min, respectively. The spurious peak at lower energies is from the natural background.
d) (top) ^{195}Pt; 0.59, 4.99, and 12.96 days for durations of 300, 600, and 600 min, respectively. The transition at 98.9 keV is also part of the cascade from the isomer $^{195}Pt^m$, originating on the lowest excited state in Fig. 1d. Structures at even lower energies are part of the background.

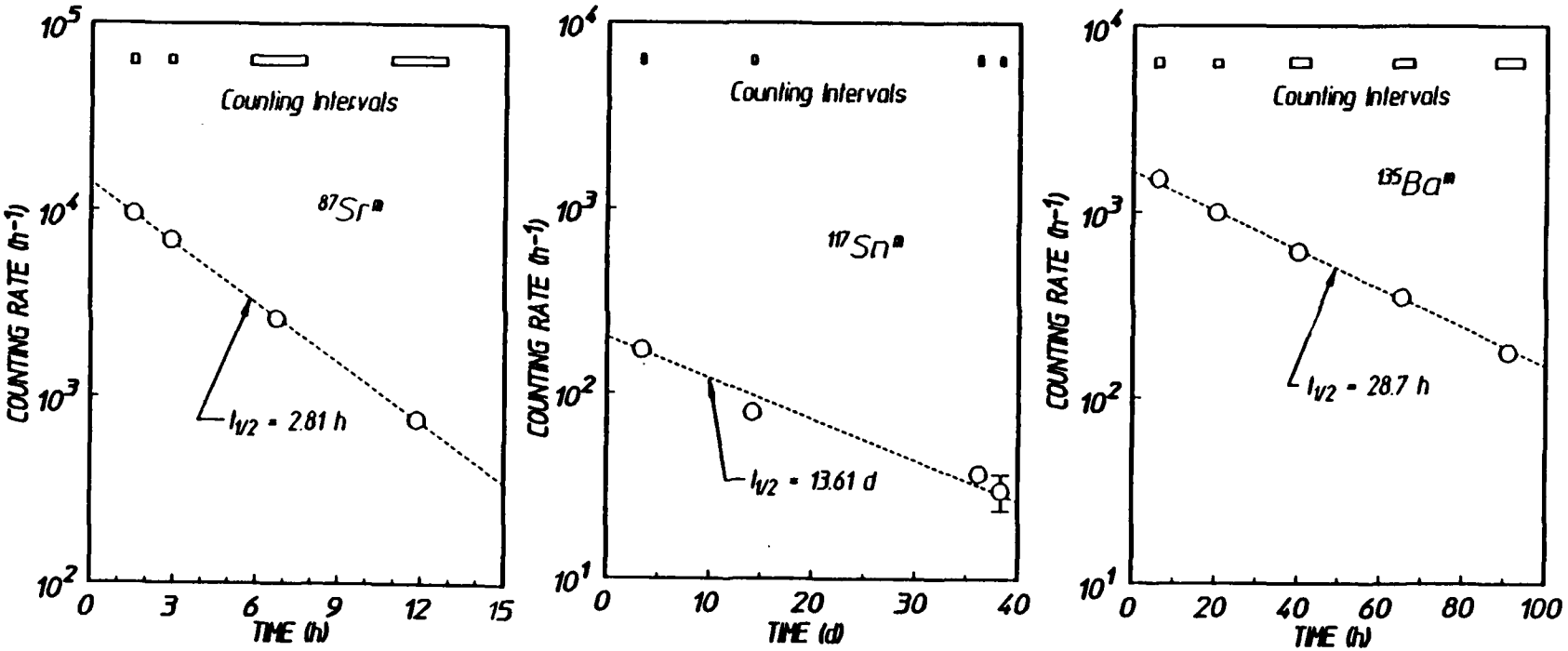
Counting Intervals
$^{87}Sr^{m}$
$t_{1/2}$ = 2.81 h
COUNTING RATE (h^{-1})
TIME (h)
Counting Intervals
$^{117}Sn^{m}$
$t_{1/2}$ = 13.61 d
COUNTING RATE (h^{-1})
TIME (d)
Counting Intervals
$^{135}Ba^{m}$
$t_{1/2}$ = 28.7 h
COUNTING RATE (h^{-1})
TIME (h)

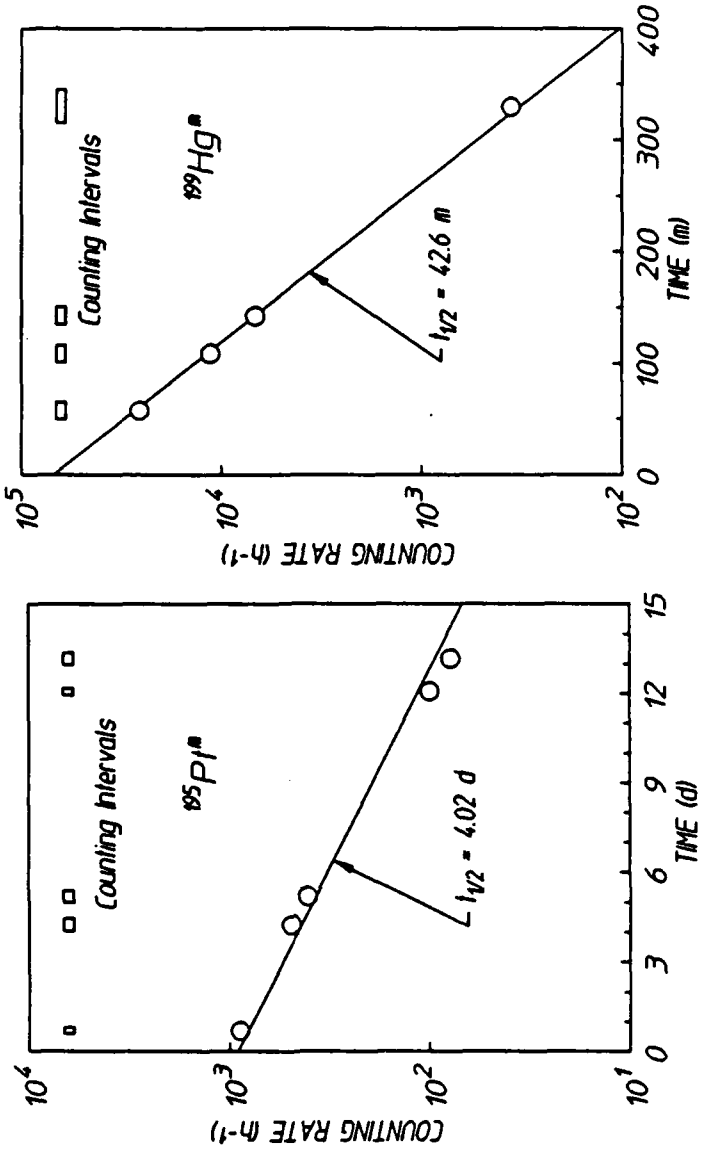

Figure 43: Plots of the counting rates measured in the peaks of the lines identified in Figs. 42a - 42e as functions of time elapsed from the end of the irradiation. Except where error bars are explicitly shown, the vertical dimensions of the data points are consistent with 1σ deviations of the measured numbers of counts accumulated during the finite counting intervals shown at the tops of the graphs. The dotted lines show the rates expected for the literature values of the half-lives.
a), b), and c) (opposite, top to bottom) Decays of the fluorescences from $^{87}Sr^{m}$, $^{117}Sn^{m}$, and $^{135}Br^{m}$.
d) and e) (top and center) Decays of the fluorescences from $^{195}Pt^{m}$ and $^{199}Hg^{m}$.

Results

From the numbers of counts in the fluorescence spectra of Figs. 42a - 42e, the numbers of activations in the samples were obtained by well-established procedures. The efficiency of the spectrometer was determined with calibrated sources and was found to conform closely to nominal specifications. Self-absorption corrections were taken from Table I, and fluorescence efficiencies from the literature.[60] At this stage of analysis, the numbers of activations in ^{199}Hg indicated by the two different transitions agreed to within 2%, thus verifying the procedure for calculating the self-absorption corrections.

The rates of activations of the samples, dN/dt, were obtained by dividing the observed numbers of activations by the irradiation times after correcting for finite counting and irradiation times. Literature values of the half-lives were used in making these corrections.[10]

From Eq. (2a) the excitation rate is,

$$\frac{dN}{dt} = N_o \sum_i (\pi \Gamma_x \sigma_o / 2)_i \, \phi_i \quad , \tag{45}$$

where the parameters in parentheses comprise the integrated cross section for pumping the (γ,γ') reaction through the i-th gateway, ϕ_i is the photon flux at the energy needed to excite that gateway, and N_o is the number of target nuclei. The combination, Γ_x

$$\Gamma_x = b_a b_o \Gamma \quad , \tag{46}$$

is the partial width for excitation with parameter being defined as for Eq. (2b).

In our experiment, the spectrum of irradiation, $\phi_i(E)$, cannot yet be varied in a controlled manner so that the sum of Eq. (45) cannot be decomposed from the experimental measurements of dN/dt into components from each of the contributing bands. An interesting alternative is to extract the effective cross section $\sigma(E)$ which would be necessary to produce the observed activation through a single gateway,

$$\sigma(E) = \frac{dN/dt}{N_o \phi(E)} \quad . \tag{47}$$

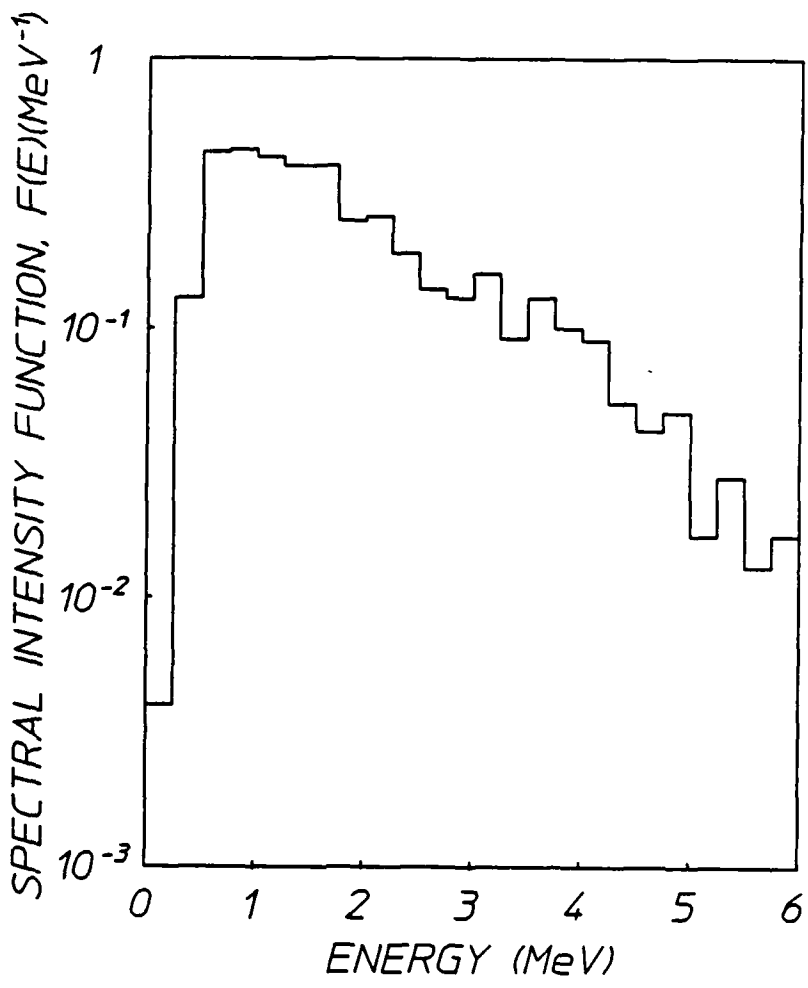

Figure 44: Relative spectral intensities of the bremsstrahlung used for irradiation in these experiments normalized so that the integral under the curve is unity.

The spectral distribution from the Clinac 1800 medical linac is considered to be well-known[53,54] and is normalized by a measurement of the total dose delivered during the irradiation. The expected distribution is reproduced from Fig. 31 in Fig. 44 shown here for convenience. From the $\phi(E)$ determined in this way, the effective, integrated cross section can be determined from the measured activation rate as shown in Eq. (47). The $\sigma(E)$ is a function of the energy E at which the effective gateway is assumed to lie. Results for the five isotopes examined in these experiments are shown in Figs. 45a - 45e. In each case the possible values of energies for the gateways are limited at the lower end by prior reports of much smaller cross sections for (γ,γ') reactions known to occur through gateways lying between 1 and 1.5 MeV.

Conclusions

From Figs. 45a - 45e it can be seen that the integrated cross sections for the excitations of isomers proceeding through channels open to the bremsstrahlung from a 6 MeV medical linear accelerator for these five species reach values exceeding almost all previous results by two to three orders of magnitude. However, most earlier work was conducted with sources having end point energies lying below 3 MeV so it might be initially supposed that these larger cross sections describe channels open near the threshold for (γ,n) reactions where state density is high. However, a troubling aspect is the large change of angular momentum spanned by these reactions and the lack of correlation of reaction probabilities with minimal changes in J.

The reproducibility of the experiment is demonstrated in Fig. 46, which reports the absolute level of agreement between experimental series conducted three months apart after complete disassembly and reintegration of the apparatus. Figure 47 presents a summary of the results of this work which suggests some groupings of the magnitudes of these cross sections. In the lowest group, values are reasonably continuous with prior work.[11]

The most indicative point of comparison is found in Fig. 45a reporting the cross sections for the reaction $^{87}Sr(\gamma,\gamma')^{87}Sr^{m}$. There is plotted the largest value previously reported[11] for such a reaction, that of 280 - 580 ($\times 10^{-29}$ cm^2 keV) for the gateway at 2.66 MeV. The discrepancy between that value and our work is not greater than what was

usually found between successive measurements at those times.[68] However, since our results are greater, an alternative explanation which relies on a complete agreement with the prior work demands the opening of additional gateways at higher energies.

The pervasiveness found for the unexpectedly large values for integrated cross sections for the transfers of such large amounts of angular momenta suggests some type of core property varying only slowly with increasing nuclear size. In such a case, however, there would seem to be the need for a mixing of several single particle states so the decay of the gateway state could occur into several different cascades with comparable probabilities. In any case, the integrated cross sections found in this experiment correspond to remarkably large partial widths. Derived values are summarized in Table VII. Such widths are characteristic of relatively unhindered E1 transitions and motivate further investigation of their occurrence.

Table VII

Summary of the partial widths for the (γ,γ') reactions producing the isomers of the species shown. Values were obtained from the integrated cross sections by assuming the gateway energies lay at 2 MeV, near the bremsstrahlung maximum, and that statistical weights were the same in the ground and gateway states, so that $\sigma_o = 6.1 \times 10^{-22}$ cm^2.

Nuclide	$\pi\sigma_o(b_a b_o \Gamma)/2$ at 2 MeV ($\times 10^{-29}$ cm^2 keV)	Partial width (meV)
^{87}Sr	1,000	10
^{117}Sn	1,030	11
^{135}Ba	6,900	72
^{195}Pt	22,900	240
^{199}Hg	1,740	18

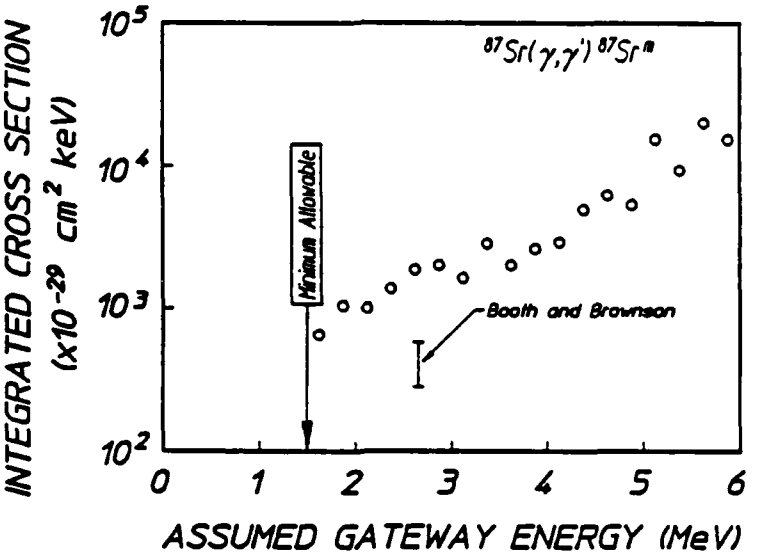
$^{87}Sr(\gamma,\gamma')^{87}Sr^{m}$
Minimum Allowable
Booth and Brownson
INTEGRATED CROSS SECTION
(x10^{-29} cm^2 keV)
ASSUMED GATEWAY ENERGY (MeV)

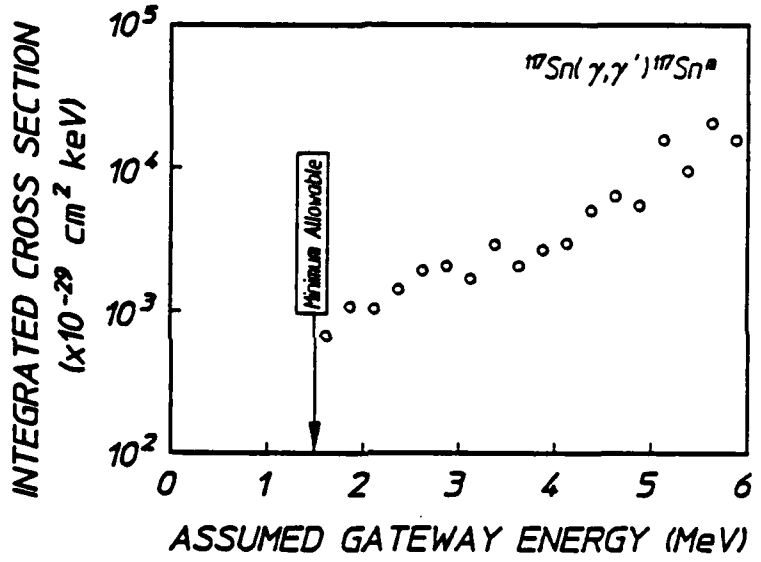
$^{117}Sn(\gamma,\gamma')^{117}Sn^{m}$
Minimum Allowable
INTEGRATED CROSS SECTION
(x10^{-29} cm^2 keV)
ASSUMED GATEWAY ENERGY (MeV)

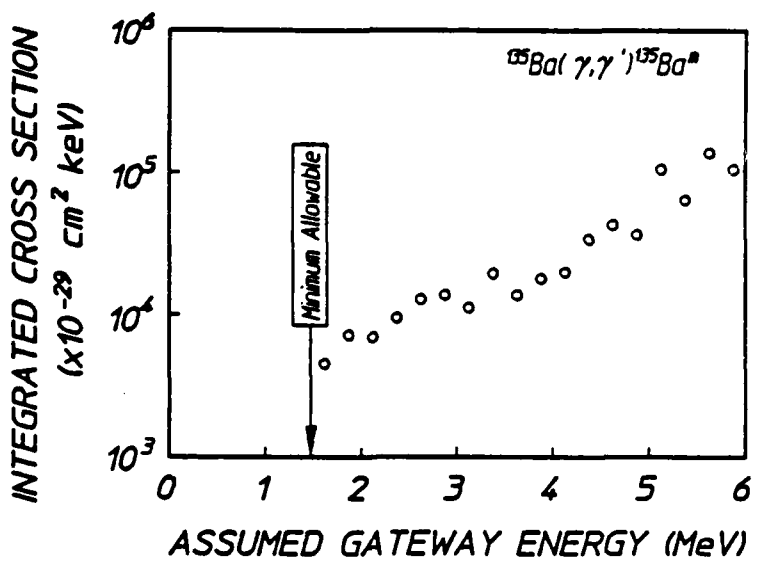
$^{135}Ba(\gamma,\gamma')^{135}Ba^{m}$
Minimum Allowable
INTEGRATED CROSS SECTION
(x10^{-29} cm^2 keV)
ASSUMED GATEWAY ENERGY (MeV)

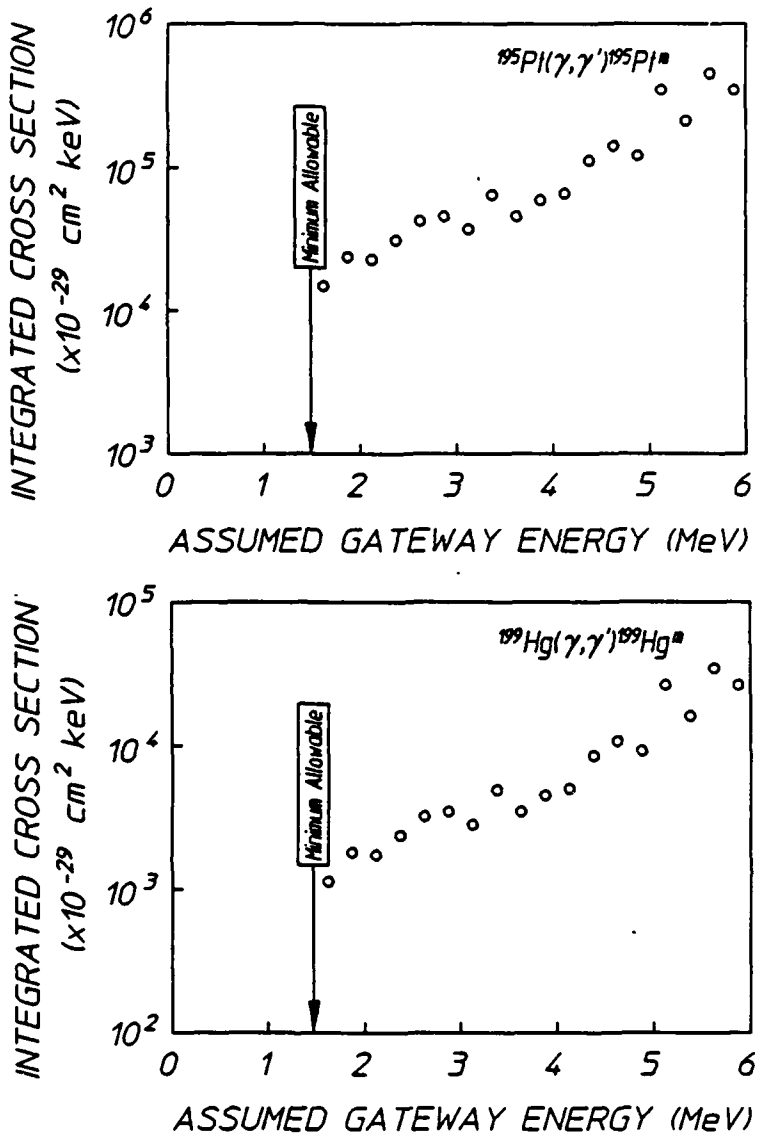

Figure 45: The integrated cross sections for the (γ,γ') reactions shown on each panel through single, unknown gateway states as functions of the energies at which they could be assumed to lie. Literature values preclude the possibilities that these gateways could lie at energies below the minima shown.
a) (opposite top) Reaction of ^{87}Sr together with a previous measurement from Ref. 11.
b) and c) (opposite center and bottom) Reactions of ^{117}Sn and ^{135}Ba.
d) and e) (top and center) Reactions of ^{195}Pt and ^{199}Hg.

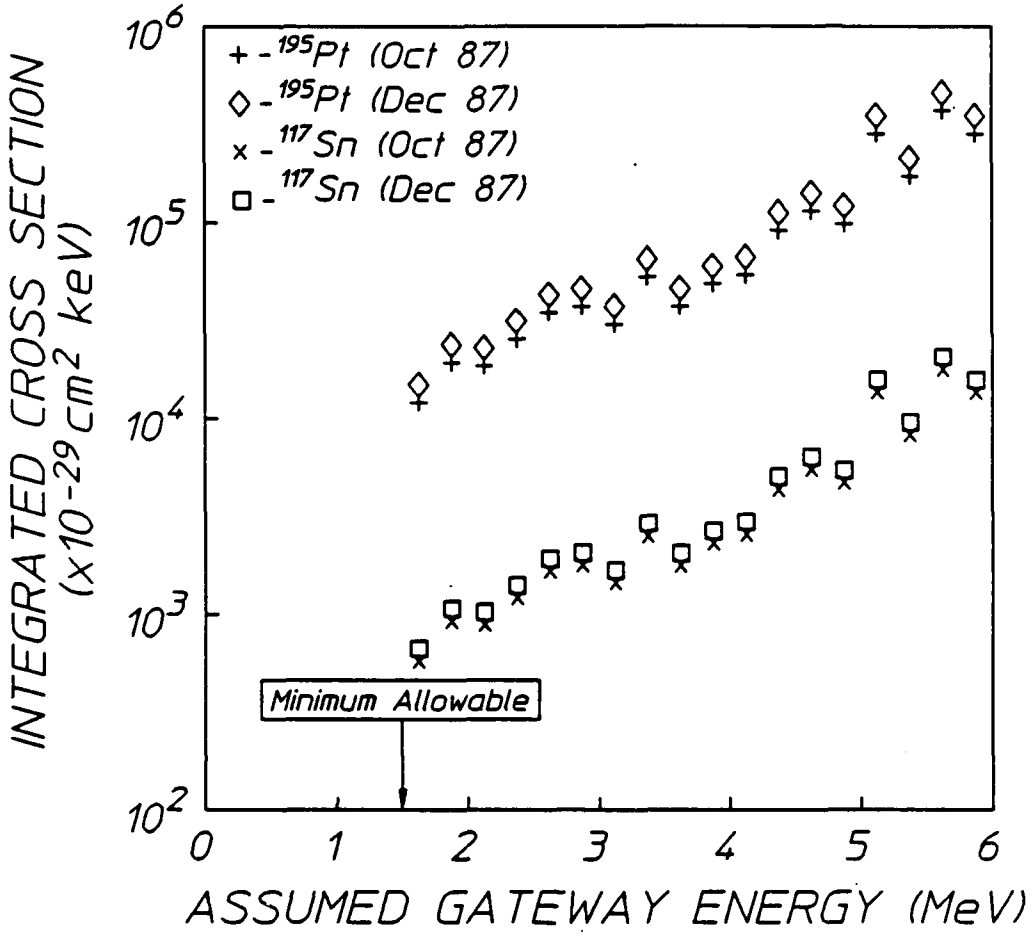

Figure 46: The integrated cross section for the (γ,γ') reactions producing the isomers $^{195}Pt^{m}$ and $^{117}Sn^{m}$ through single, unknown gateway states as functions of the energies at which they could be assumed to lie. Data from two separate experimental series are shown to illustrate long-term reproducibility.

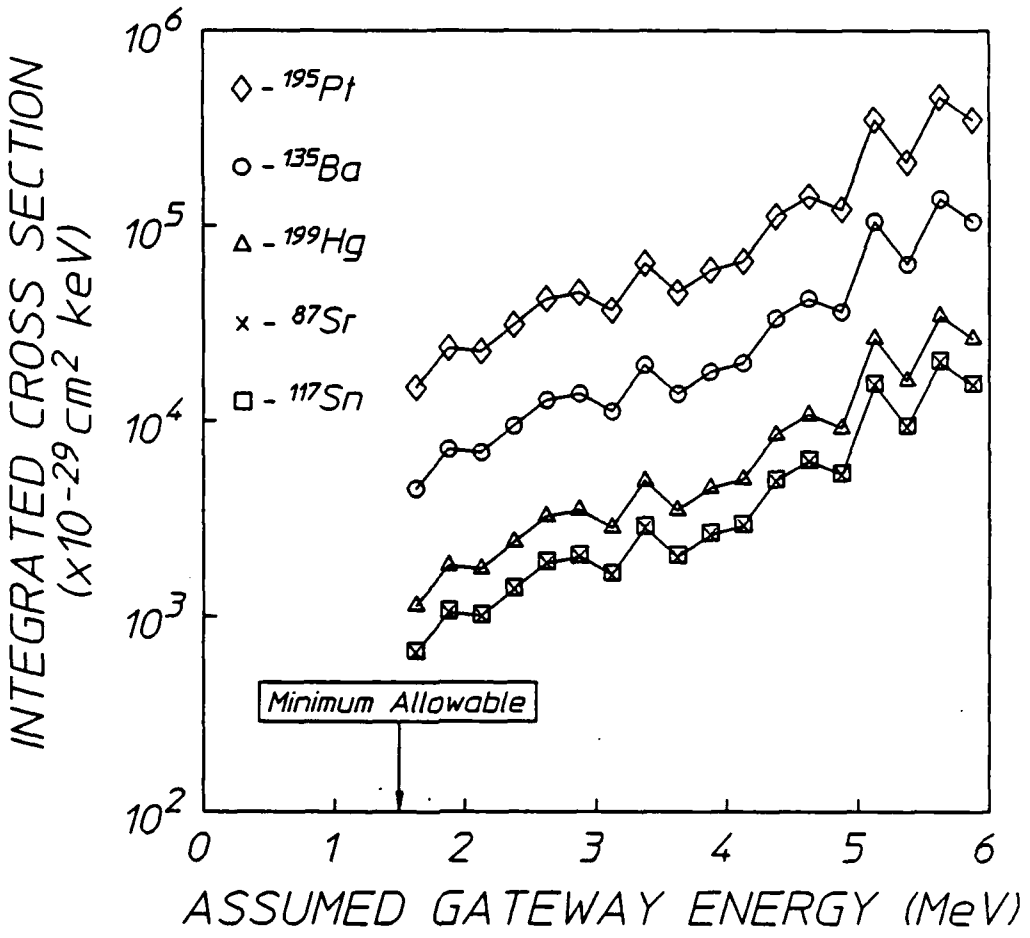

Figure 47: Summary of the integrated cross sections for the (γ,γ') reactions producing the isomers of the species shown, plotted as functions of the energies at which a single gateway state could be assumed for each.

PHOTOACTIVATION OF SHORT-LIVED ISOMERS WITH BREMSSTRAHLUNG RADIATION FROM A MEDICAL LINEAR ACCELERATOR

Reported here is the extension of the studies of the excitation and deexcitation of long-lived isomers with the bremsstrahlung from a 6 MeV linac. This work was concerned with excitation of short-lived isomers having half-lives varying from 2.3 to 153 seconds. Pumped with the same linac as used with the longer-lived isomers, these (γ,γ') reactions proceeded through channels providing for changes of angular momentum ranging from $\Delta J = 3$ to 5. Eight isomers were successfully activated and studied in this work: ^{167}Er, ^{79}Br, ^{191}Ir, ^{183}W, ^{197}Au, ^{89}Y, ^{77}Se, and ^{137}Ba. In addition, silver was photoactivated, but the limited resolution of our NaI(Ti) spectrometer was inadequate to separate the contributions of ^{107}Ag ($T_{1/2}$ = 44.2 s, E = 93.2 keV) and ^{109}Ag ($T_{1/2}$ = 39.6 s, E = 88.0 keV). Six other isomers, ^{207}Pb, ^{90}Zr, ^{177}Hf, ^{178}Hf, ^{176}Yb, and ^{190}Os, exhibited no measurable activation.

Because of the short half-lives a pneumatic system was needed to transfer the samples from the site of the irradiation to the counting system. Since the activation saturated after a few half-lives for the isomeric population, irradiation times were short and only (γ,γ') reactions proceeding through highly allowed channels could be studied. Nevertheless, integrated cross sections were generally found to be as large for the short-lived isomers as had been found for the longer-lived ones, ranging from 2000 to 100,000 in the usual units of 10^{-29} cm^2 keV. In contrast to the previous work with the long-lived isomers, these studies showed some roughly inverse correlation of cross section with the magnitude of ΔJ that had to be spanned between ground state and isomer. While the energies of the responsible gateways still cannot be determined, the pervasiveness of such large partial widths for the exchange of substantial amounts of angular momentum remains surprising for any energies below the thresholds for (γ,n) reactions.

Experimental Procedures

The relevant energy levels for the ten nuclei of interest in these experiments are shown in Fig. 48. With two exceptions, they were present in targets fabricated from materials containing natural isotopic abundances in the form of either powders held in cylindrical poly-

ethylene vials or in metallic foils. In some cases the samples were sufficiently thick that self-absorption of the output transition necessitated a correction of significant magnitude. The samples of ^{167}Er and ^{77}Se were isotopically enriched materials.

Targets were exposed for times on the order of a few minutes to the output of the Varian Clinac 1800 linear accelerator at the Department of Radiology of the University of Texas Southwestern Medical Center at Dallas. This linear accelerator was operated with an end point energy of 6 MeV. After irradiation, the samples were transferred to a counting system with the same pneumatic arrangement described in previous reports of experiments conducted on e-beam sources of bremsstrahlung.[19] The transit time was logged and all samples were counted in a well-type NaI(Tl) crystal spectrometer.

Target parameters are summarized in Table VIII, together with the corrections for self-absorption computed from the counting geometry, sample composition, and sample density. The validity of the self-absorption calculation was verified by comparing cross-section results obtained for idential materials using samples that presented different geometrical conditions.

TABLE VIII

LINAC Short-lived Isomer Study
Sample Parameters for Nuclides in LINAC Study

Nuclide	Abundance (%)	Chemical Form	Sample Mass (g)	Half-life (s)	Exposure Time (s)	Count Time (s)	Principal Fluorescence (keV)	Fluorescence Intensity (%)	Transparency
^{167}Er	91.54	Er_2O_3	9.00	2.28	25	5	207.79	41.70	0.579
^{79}Br	50.69	LiBr	12.83	4.86	50	10	207.20	75.80	0.842
^{193}Ir	37.30	Ir	3.97	4.94	50	10	129.43	25.70	0.0793
^{182}W	14.30	W	20.75	5.15	50	10	107.93	18.40	< 0.0584
^{197}Au	100.00	Au		7.80	80	20	279.11	73.00	0.399 - 0.092
^{89}Y	100.00	YF_3	10.23	16.06	160	32	909.15	99.14	0.945
^{77}Se	96.38	Se	3.38	17.45	150	40	161.92	52.40	0.837
^{109}Ag	44.16	Ag	53.05	39.60	400	80	88.03	3.60	
^{107}Ag	51.84	Ag	53.05	44.30	400	80	93.15	4.67	
^{127}Ba	11.74	BaF_2	7.40	153.00	599	300	661.66	90.10	0.953

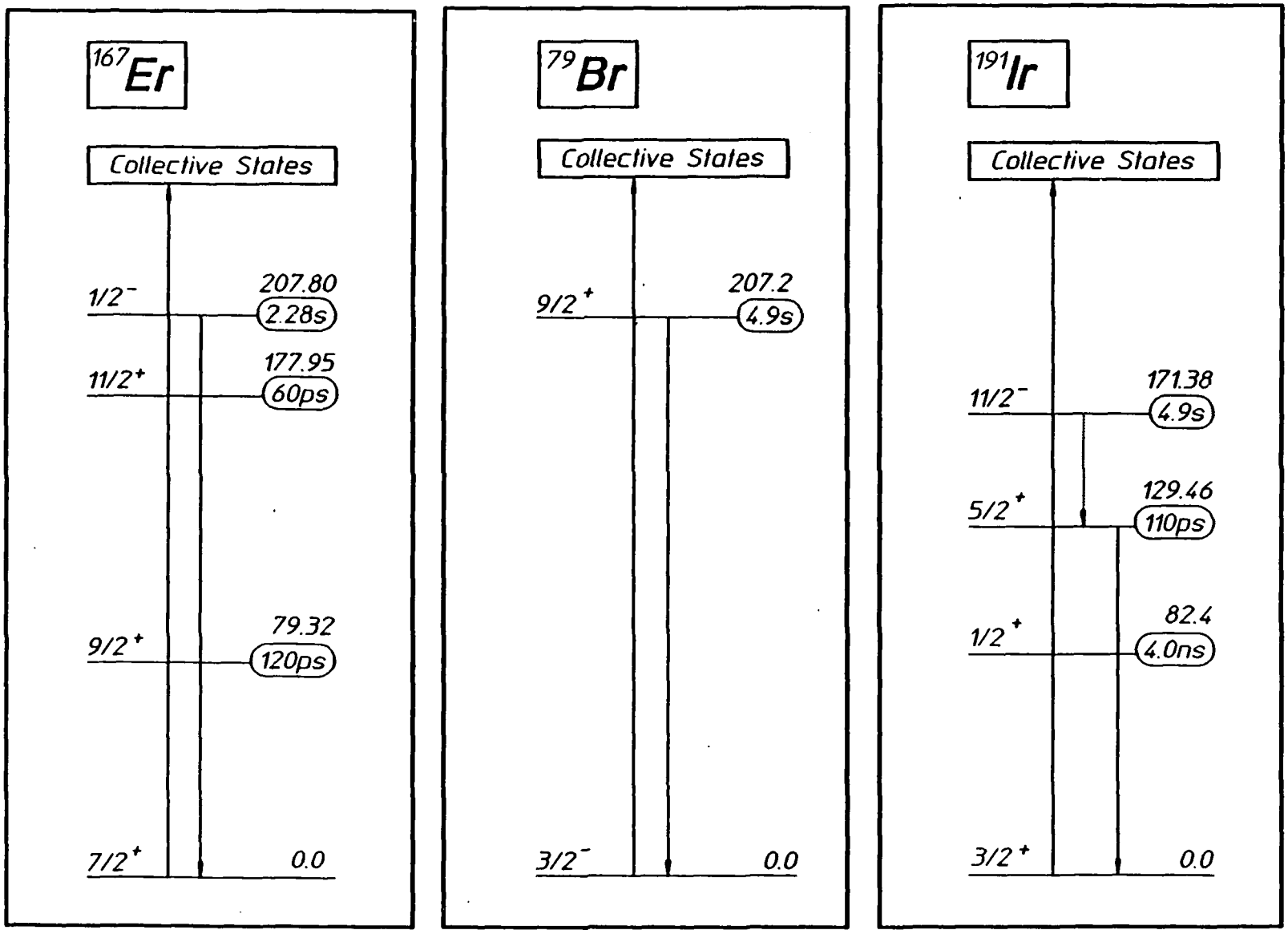
167Er
Collective States
1/2⁻
207.80
2.28s
11/2⁺
177.95
60ps
9/2⁺
79.32
120ps
7/2⁺
0.0
79Br
Collective States
9/2⁺
207.2
4.9s
3/2⁻
0.0
191Ir
Collective States
11/2⁻
171.38
4.9s
5/2⁺
129.46
110ps
1/2⁺
82.4
4.0ns
3/2⁺
0.0

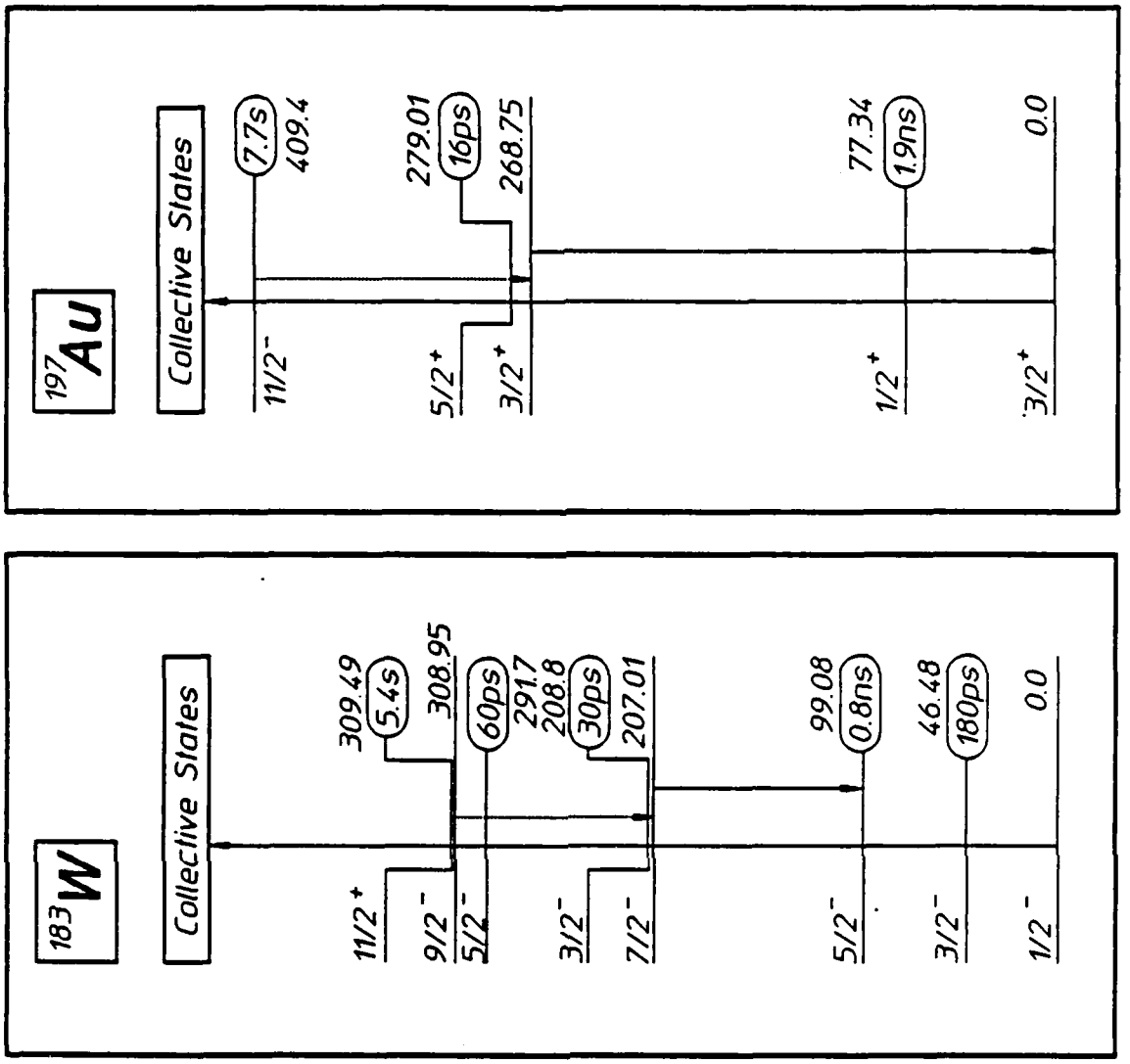

Figure 48: Energy level diagrams of the excited states important to the production and detection of the isomers of the nuclei shown. Half-lives of the states are shown to the right of each, together with their energies in keV. Downward arrows locate transitions used in the detection of populations of the isomers produced by the absorption transitions indicated by the upward arrows. The locations of the gateways through which the (γ,γ') reactions proceed are not to scale, and the details of the cascades downward to the isomers are unknown. Shown by dotted arrows are components of cascades from the product isomers useful in feeding the transitions used for detection. a), b) and c) (opposite from left): Transitions important to the study of (γ,γ') reactions producing the isomers $^{167}Er^{m}$, $^{79}Br^{m}$, and $^{191}Ir^{m}$. d), and e) (from left): Transitions important to the study of (γ,γ') reactions producing the isomers $^{183}W^{m}$, and $^{197}Au^{m}$.

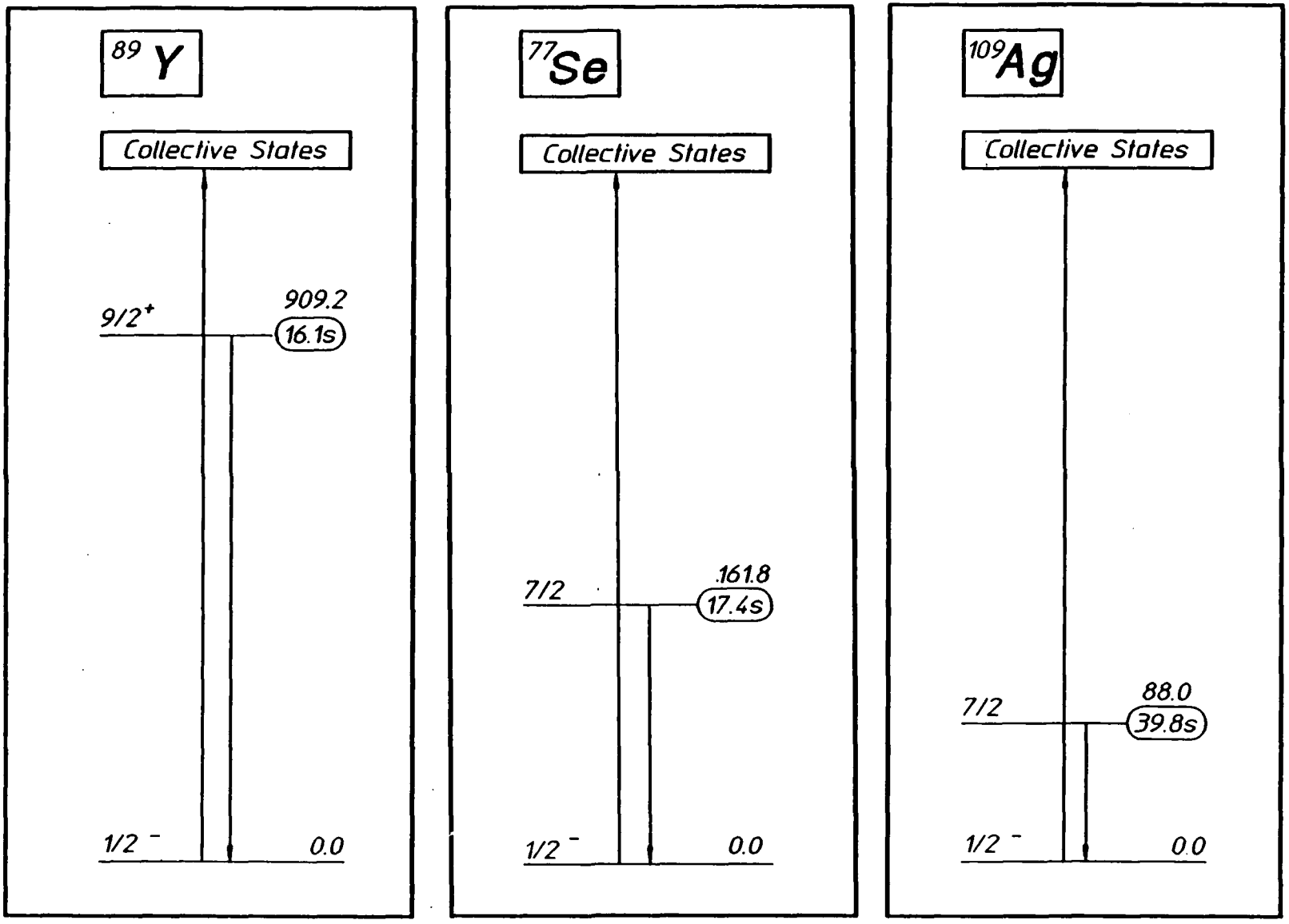
89 Y
Collective States
9/2+
909.2
16.1s
1/2 -
0.0
77Se
Collective States
7/2
161.8
17.4s
1/2 -
0.0
109Ag
Collective States
7/2
88.0
39.8s
1/2 -
0.0

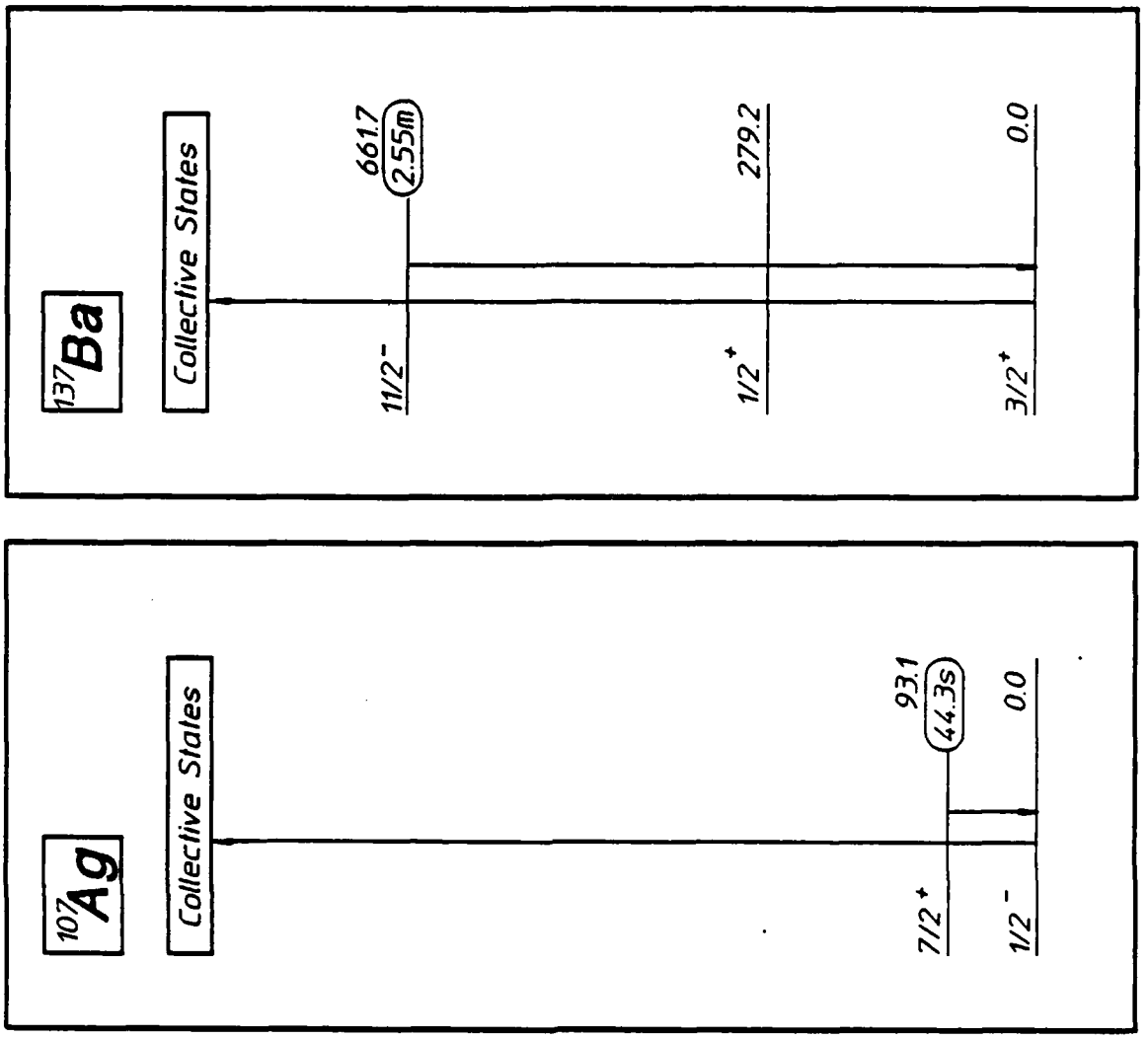

Figure 48: (continued) Energy level diagrams of the excited states important to the production and detection of the isomers of the nuclei shown. Half-lives of the states are shown to the right of each, together with their energies in keV. Downward arrows locate transitions used in the detection of populations of the isomers produced by the absorption transitions indicated by the upward arrows. The locations of the gateways through which the (γ,γ') reactions proceed are not to scale, and the details of the cascades downward to the isomers are unknown. Shown by dotted arrows are components of cascades from the product isomers useful in feeding the transitions used for detection. f), g), and h) (opposite from left): Transitions important to the study of (γ,γ') reactions producing the isomers $^{89}Y^{m}$, $^{77}Se^{m}$, and $^{109}Ag^{m}$. i) and j), (from left): Transitions important to the study of (γ,γ') reactions producing the isomers $^{107}Ag^{m}$ and $^{137}Ba^{m}$.

Typical nuclear fluorescence spectra from the isomers excited in this work by the irradiations are shown in Figs. 49a - 49i. The low resolution of the NaI(Tl) system necessitated a greater level of concern over the identity of the various prominent features in the spectra than would have been necessary had the data been taken with an HPGe spectrometer. Confirmation that the fluorescence peaks were the signatures of the respective isomers was obtained by examining the decays of the counting rates as functions of the times elapsed from the cessation of the irradiation. These decay data are shown in Fig. 50a - 50i, together with curves reflecting expectations based upon literature values of the half-lives. For each of the ten nuclides studied, both spectral and temporal content of the fluorescence were consistent with the expected signatures.

Results

From the numbers of counts in the fluorescence spectra of Figs. 49a - 49i, the numbers of activations in the samples were obtained by well-established procedures. The efficiency of the spectrometer was determined with calibrated sources and was found to conform to nominal specifications. The self-absorption corrections used in these calculations are listed as transparencies in Table VIII. Fluorescence intensities were taken from the literature.[60]

The rates of activations of the samples, dN/dt, were obtained by dividing the observed numbers of activations by the irradiation times after correcting for finite counting and irradiation times. Literature values of the half-lives were used in making these corrections.[10] Procedures for obtaining the integrated cross sections from such data were described in Eqs. (45) - (47) in the preceeding chapter.

Results for the eight isotopes characterised in these experiments are shown in Figs. 51a - 51h. In each case the possible values of energies for the gateways are limited at the lower end by prior reports of much smaller cross sections for (γ,γ') reactions known to occur through gateways lying between 1 and 1.5 MeV.

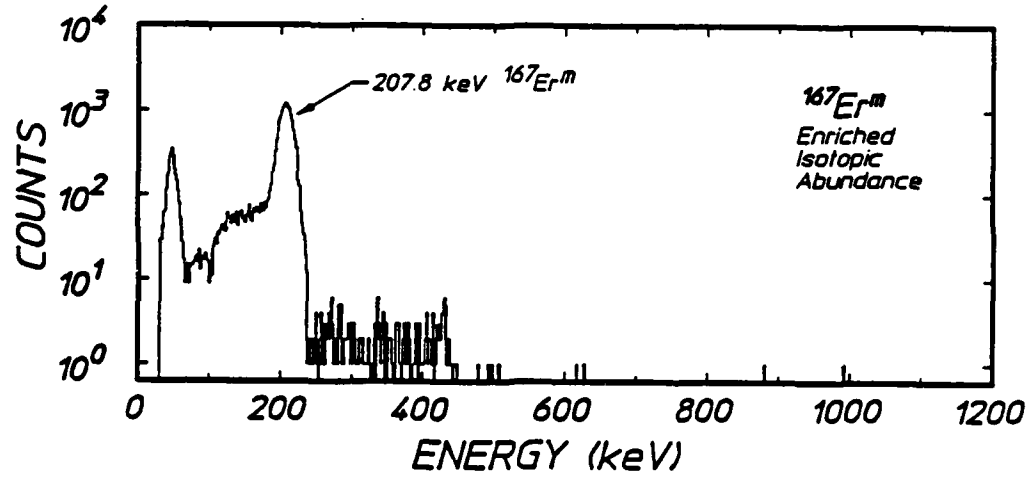
COUNTS
10^4
10^3
10^2
10^1
10^0
207.8 keV $^{167}Er^m$
$^{167}Er^m$
Enriched
Isotopic
Abundance
0
200
400
600
800
1000
1200
ENERGY (keV)

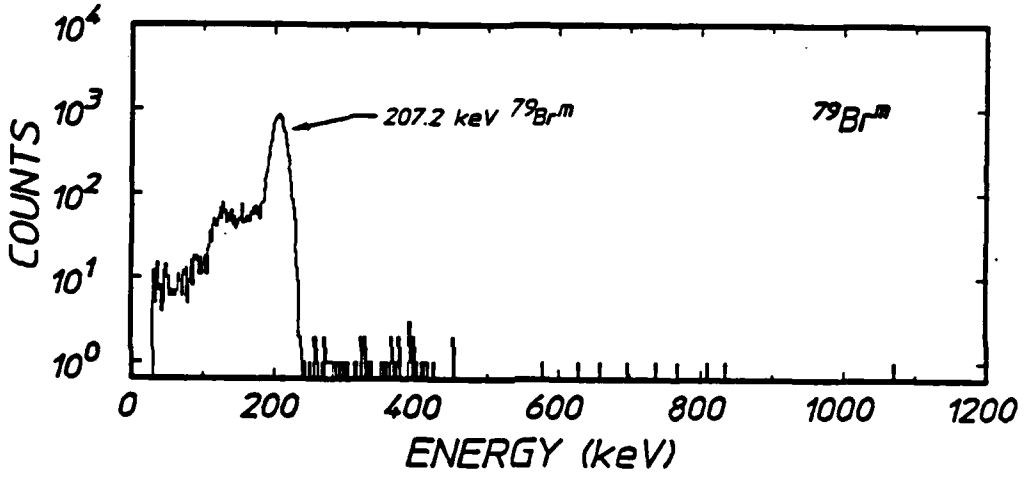
COUNTS
10^4
10^3
10^2
10^1
10^0
207.2 keV $^{79}Br^m$
$^{79}Br^m$
0
200
400
600
800
1000
1200
ENERGY (keV)

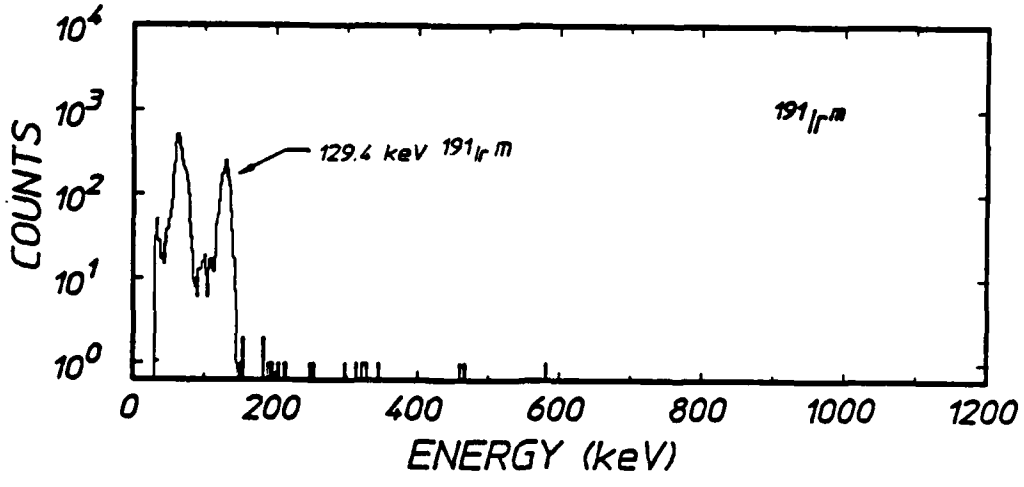
COUNTS
10^4
10^3
10^2
10^1
10^0
129.4 keV $^{191}Ir^m$
$^{191}Ir^m$
0
200
400
600
800
1000
1200
ENERGY (keV)

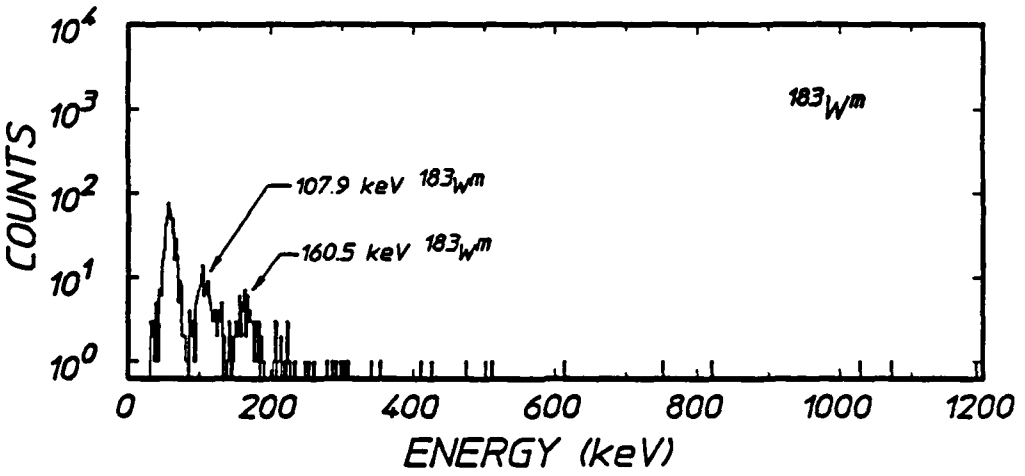
COUNTS
10^4
10^3
10^2
10^1
10^0
$^{183}W^m$
107.9 keV $^{183}W^m$
160.5 keV $^{183}W^m$
0
200
400
600
800
1000
1200
ENERGY (keV)

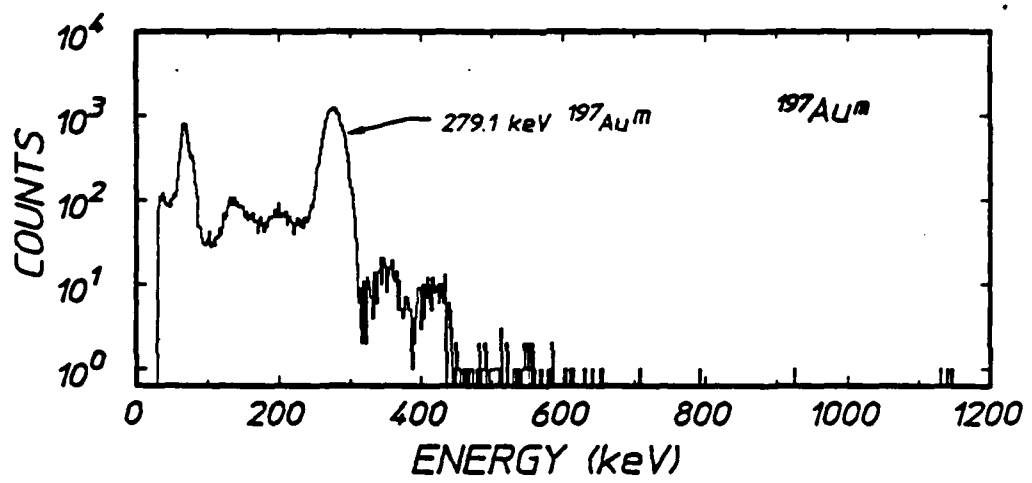
COUNTS
10^4
10^3
10^2
10^1
10^0
279.1 keV $^{197}Au^m$
$^{197}Au^m$
0
200
400
600
800
1000
1200
ENERGY (keV)

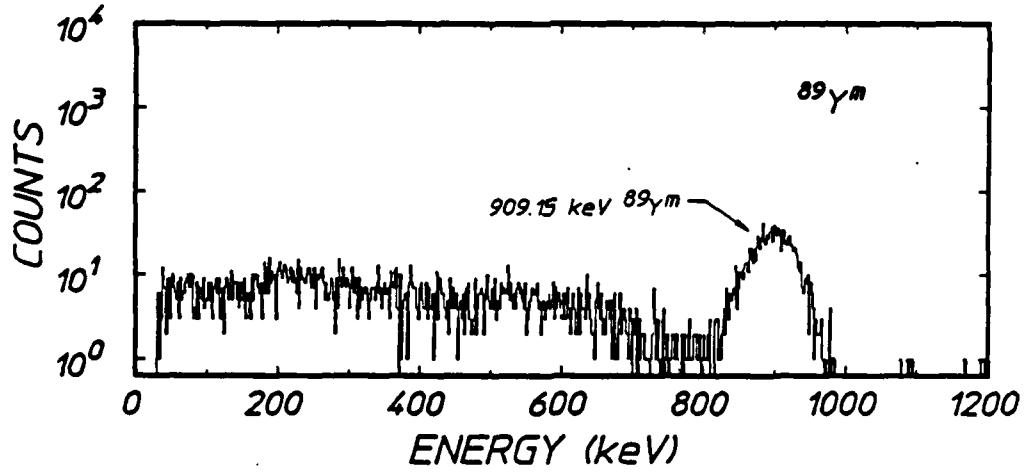
COUNTS
10^4
10^3
10^2
10^1
10^0
$^{89}Y^m$
909.15 keV $^{89}Y^m$
0
200
400
600
800
1000
1200
ENERGY (keV)

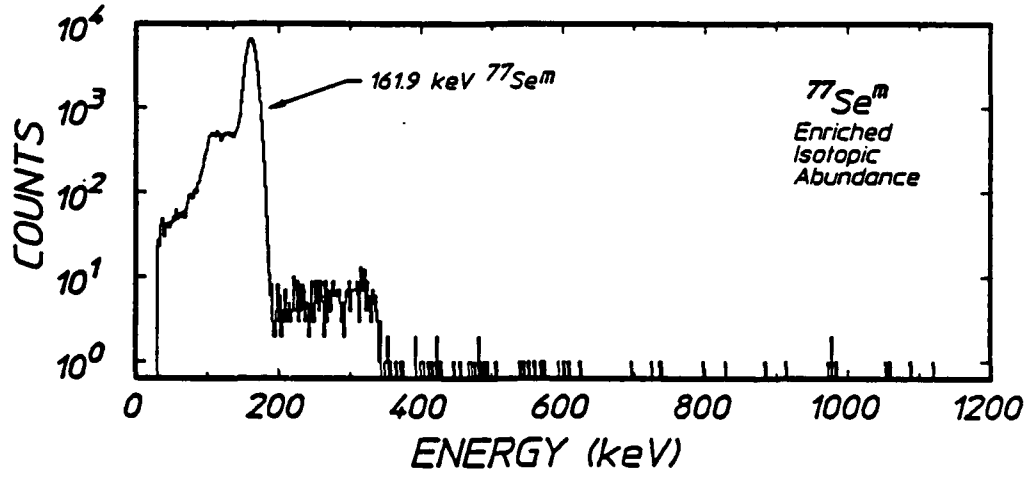
161.9 keV 77Sem
77Sem
Enriched
Isotopic
Abundance
COUNTS
ENERGY (keV)

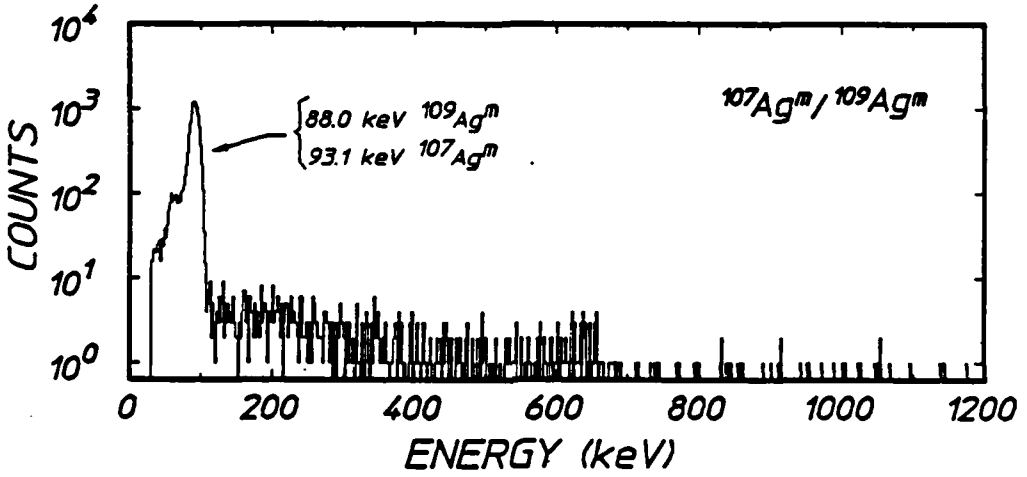
88.0 keV 109Agm
93.1 keV 107Agm
107Agm / 109Agm
COUNTS
ENERGY (keV)

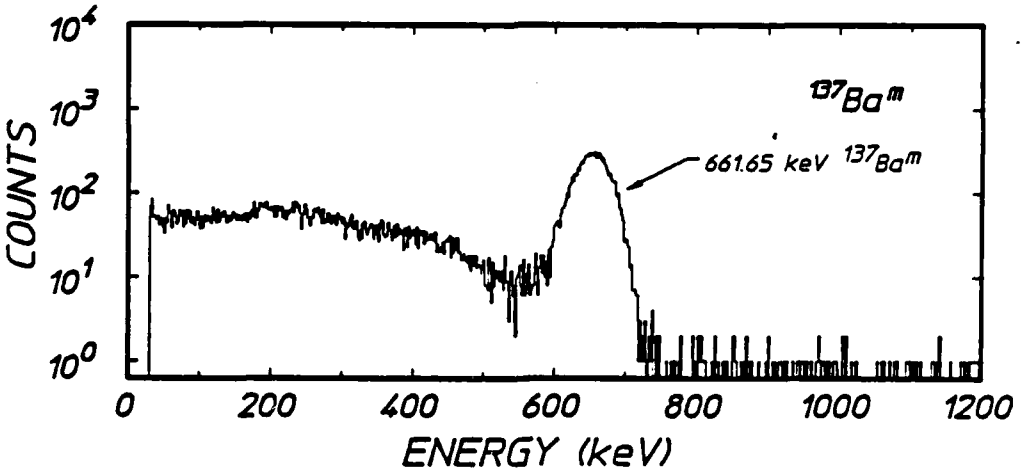
137Bam
661.65 keV 137Bam
COUNTS
ENERGY (keV)

Figure 49: Characteristic energy spectra for isomeric decays obtained in this work with a 7.6 cm × 7.6 cm diameter NaI(Tl) detector having a 5.1 cm × 2.5 cm diameter well. Transitions shown in Figs. 48a - 48i for the detection of the isomers are identified by the arrows. Counting times are given in Table VIII and the times elapsed between irradiation and counting are as follows:
a), b) and c) (third preceding page) ^{167}Er, ^{79}Br, *and* ^{191}Ir: *Delays of 2.06, 2.06, and 1.77 sec.*
d), e) and f) (second preceding page) ^{183}W, ^{197}Au, *and* ^{89}Y: *Delays of 2.31, 1.63, and 2.00 sec.*
g), h) and i) (preceding page) ^{77}Se, $^{107}Ag/^{109}Ag$, *and* ^{137}Ba: *Delays of 2.00, 3.04, and 1.84 sec.*

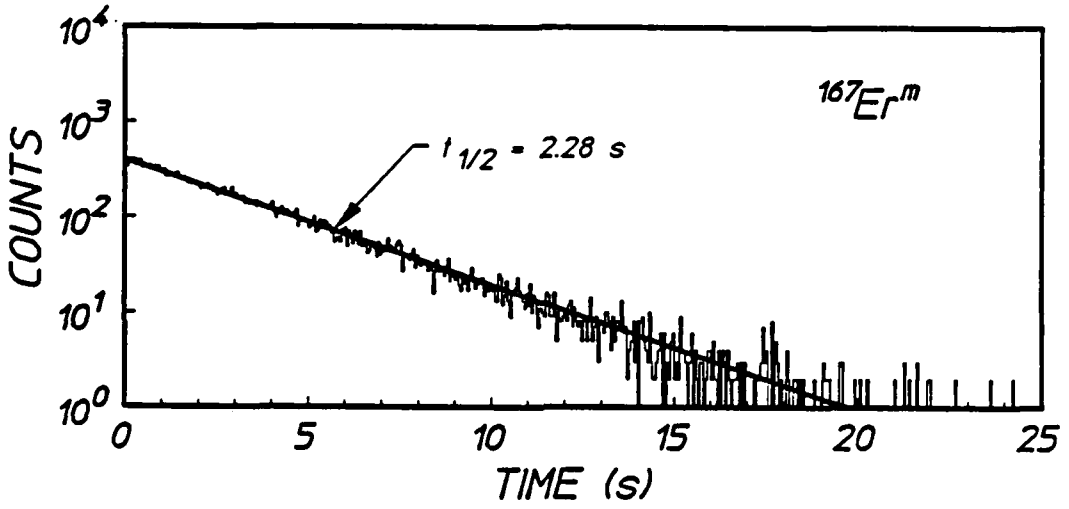
$^{167}Er^{m}$
$t_{1/2}$ = 2.28 s
COUNTS
TIME (s)

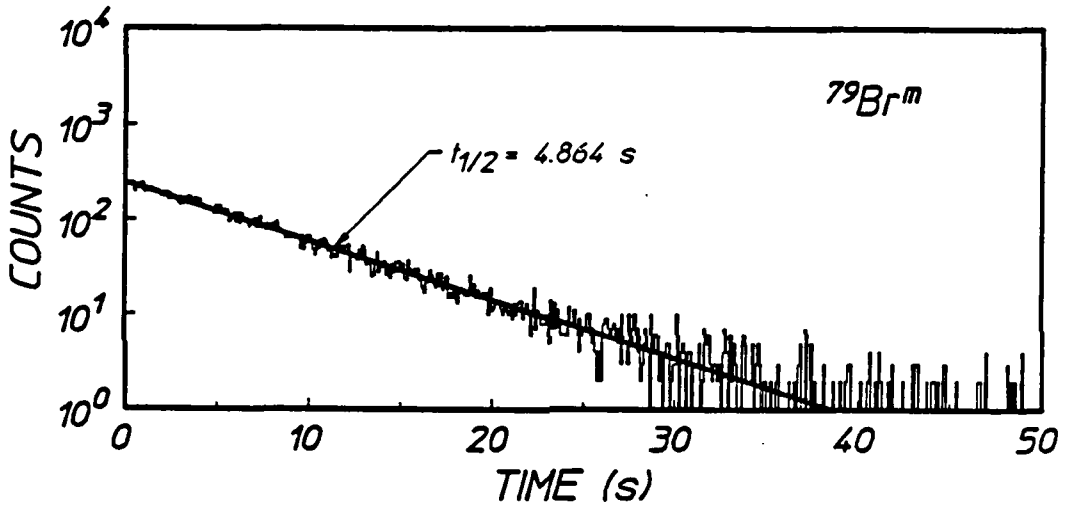
$^{79}Br^{m}$
$t_{1/2}$ = 4.864 s
COUNTS
TIME (s)

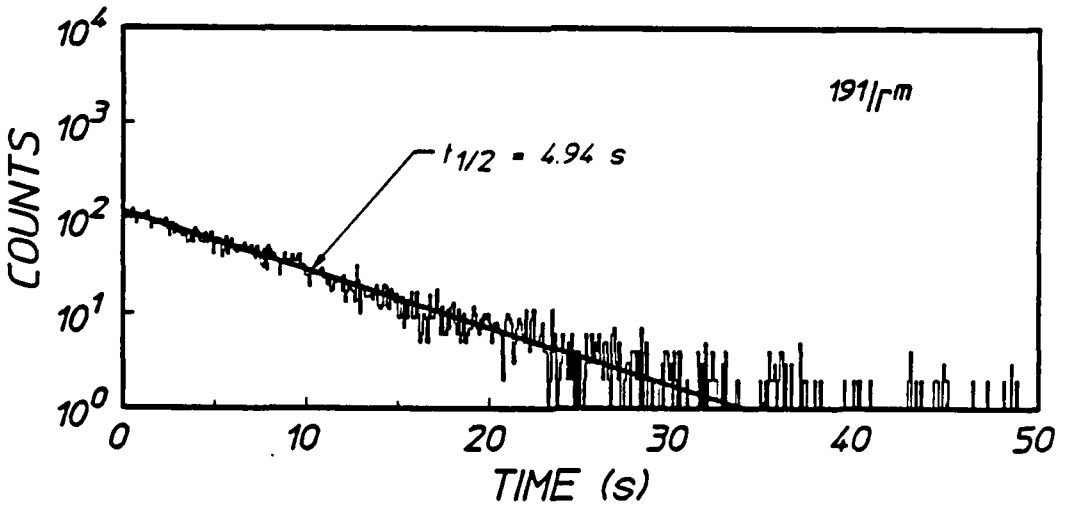
$^{191}Ir^{m}$
$t_{1/2}$ = 4.94 s
COUNTS
TIME (s)

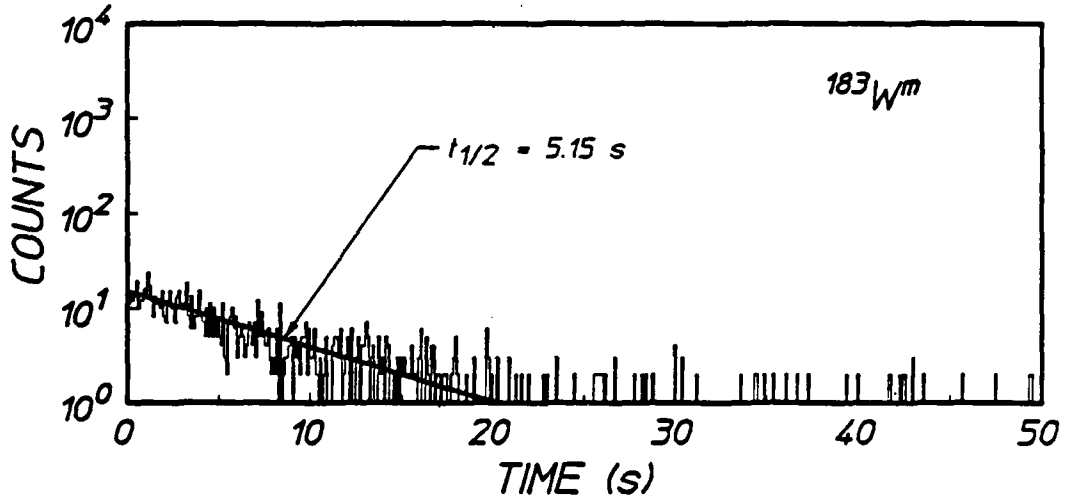
10^4
10^3
10^2
10^1
10^0
COUNTS
$^{183}W^m$
$t_{1/2}$ = 5.15 s
0
10
20
30
40
50
TIME (s)

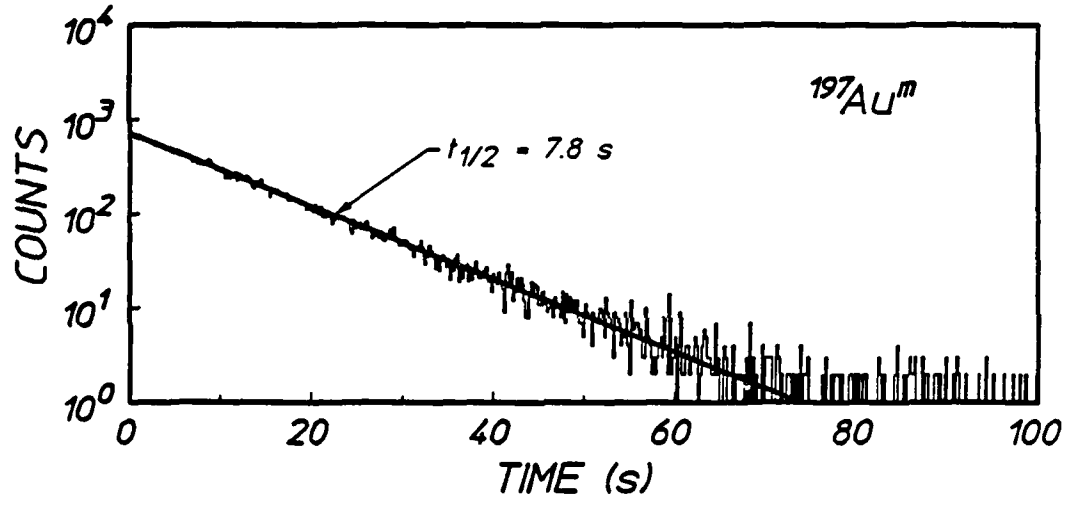
10^4
10^3
10^2
10^1
10^0
COUNTS
$^{197}Au^m$
$t_{1/2}$ = 7.8 s
0
20
40
60
80
100
TIME (s)

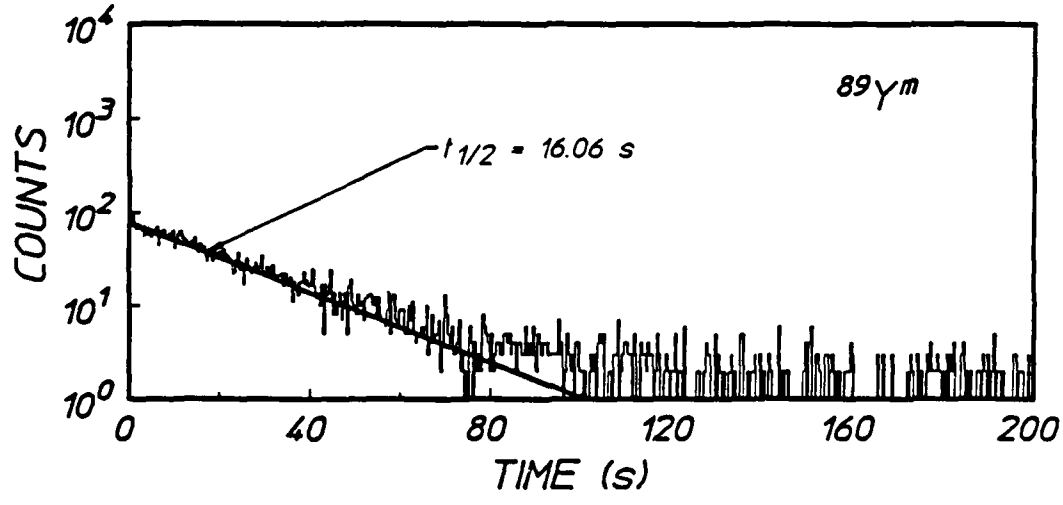
10^4
10^3
10^2
10^1
10^0
COUNTS
$^{89}Y^m$
$t_{1/2}$ = 16.06 s
0
40
80
120
160
200
TIME (s)

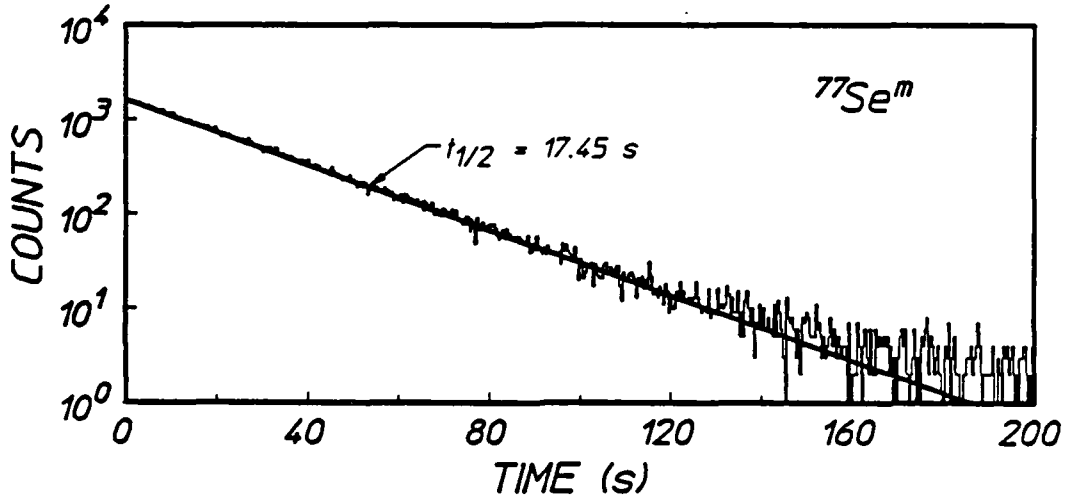
$^{77}Se^{m}$
$t_{1/2}$ = 17.45 s
COUNTS
TIME (s)

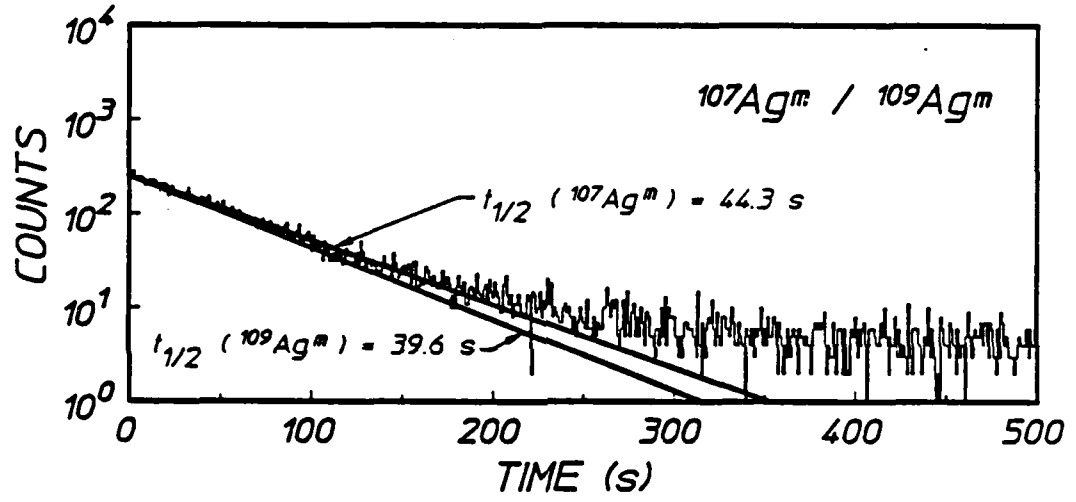
$^{107}Ag^{m}$ / $^{109}Ag^{m}$
$t_{1/2}$ ($^{107}Ag^{m}$) = 44.3 s
$t_{1/2}$ ($^{109}Ag^{m}$) = 39.6 s
COUNTS
TIME (s)

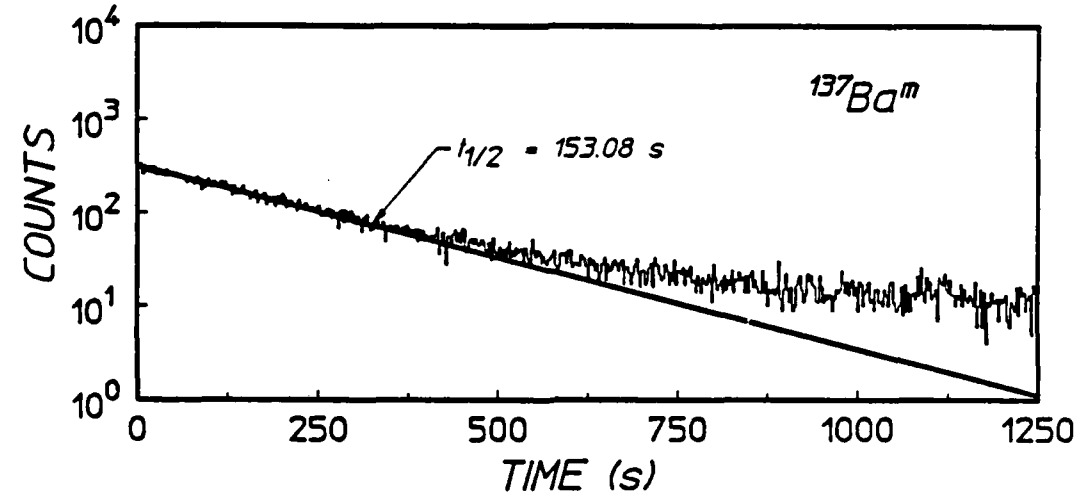
$^{137}Ba^{m}$
$t_{1/2}$ = 153.08 s
COUNTS
TIME (s)

Figure 50: Plots of the total counting rate as a function of time elapsed from the start of counting for the isomers studied in this work. Plots are presented as total counts observed in successive dwell intervals of the multichannel scaler. All events above a chosen lower level discriminator are recorded. The dotted lines show the decay curves expected from the literature values of the half-lives.
a), b), and c) (third preceding page) Fluorescence decay curves for $^{167}Er^{m}$, $^{79}Br^{m}$, and $^{191}Ir^{m}$. Dwell times are 0.05, 0.1, and 0.1 seconds per channel.
d), e), and f) (Second preceding page) Fluorescence decay curves for $^{183}W^{m}$, $^{197}Au^{m}$, and $^{89}Y^{m}$. Dwell times are 0.1, 0.2, and 0.4 seconds per channel.
g), h), and i) (preceding page) Fluorescence decay curves for $^{77}Se^{m}$, $^{107}Ag^{m}/^{109}Ag^{m}$, and $^{137}Ba^{m}$. Dwell times are 0.4, 1.0, and 2.5 seconds per channel. The presence of photoactivated $^{135}Ba^{m}$ ($T_{1/2}$ = 28.7h) is indicated by the elevated background at long times.

Conclusions

From Figs. 51a - 51h it can be seen that the integrated cross sections for isomeric excitation in these eight species through channels open to 6 MeV bremsstrahlung reach values exceeding almost all previous results by two to three orders of magnitude, continuing the trend found in the excitation of the longer-lived isomers. However, most earlier work was conducted with sources having end point energies lying below 3 MeV so it might be initially supposed that these larger cross sections describe channels open near the threshold for (γ,n) reactions where state density is high. A troubling aspect is the large change of angular momentum spanned by these reactions and the lack of any strong correlation of reaction probabilities with minimal changes in J. Figure 52 presents a summary of the results of this work which suggests some groupings of the magnitudes of these cross sections.

The pervasiveness of the unexpectedly large values of integrated cross sections for the transfers of such large amounts of angular momenta continues to suggest some type of core property varying only slowly with increasing nuclear size. In such a case, however, there would seem to be the need for a mixing of several single particle states so the decay of the gateway state could occur into several different cascades with comparable probabilities. In any case, the integrated cross sections found in this experiment correspond to remarkably large partial widths. Derived values are summarized in Table IX. Such widths are characteristic of relatively unhindered E1 transitions and motivate further investigation of their occurrence.

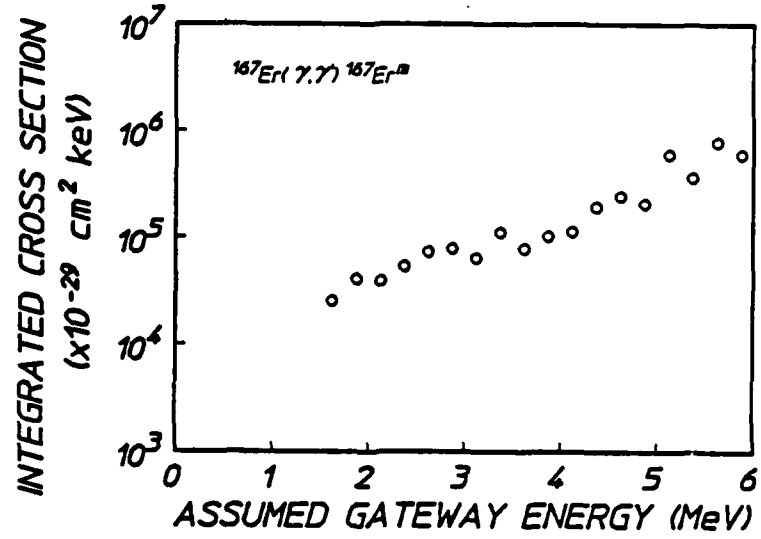
INTEGRATED CROSS SECTION
(x10⁻²⁹ cm² keV)
¹⁶⁷Er(γ,γ')¹⁶⁷Er^m
10⁷
10⁶
10⁵
10⁴
10³
0 1 2 3 4 5 6
ASSUMED GATEWAY ENERGY (MeV)

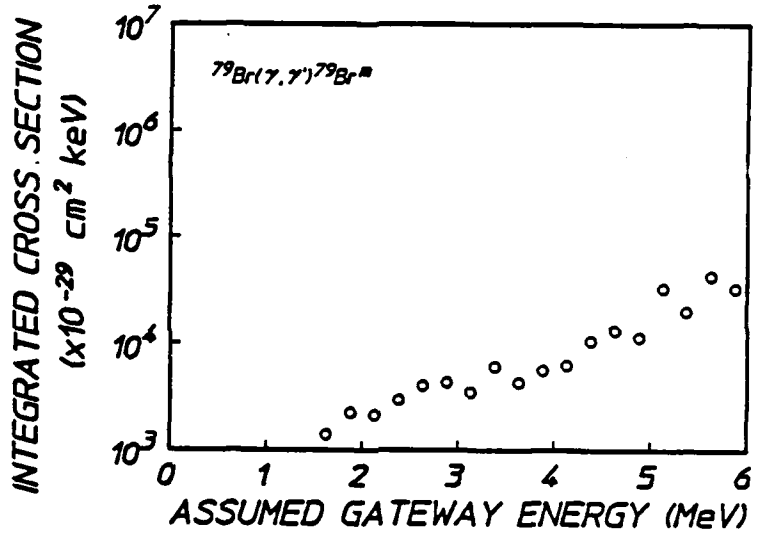
INTEGRATED CROSS SECTION
(x10⁻²⁹ cm² keV)
⁷⁹Br(γ,γ')⁷⁹Br^m
10⁷
10⁶
10⁵
10⁴
10³
0 1 2 3 4 5 6
ASSUMED GATEWAY ENERGY (MeV)

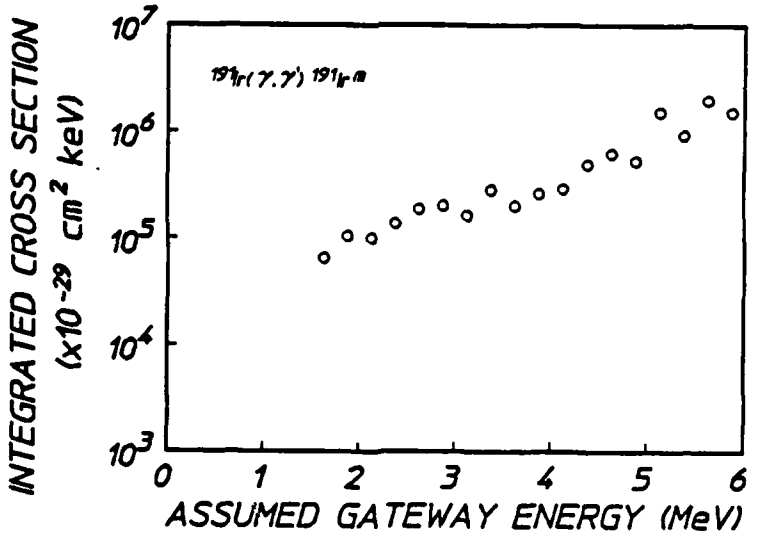
INTEGRATED CROSS SECTION
(x10⁻²⁹ cm² keV)
¹⁹¹Ir(γ,γ')¹⁹¹Ir^m
10⁷
10⁶
10⁵
10⁴
10³
0 1 2 3 4 5 6
ASSUMED GATEWAY ENERGY (MeV)

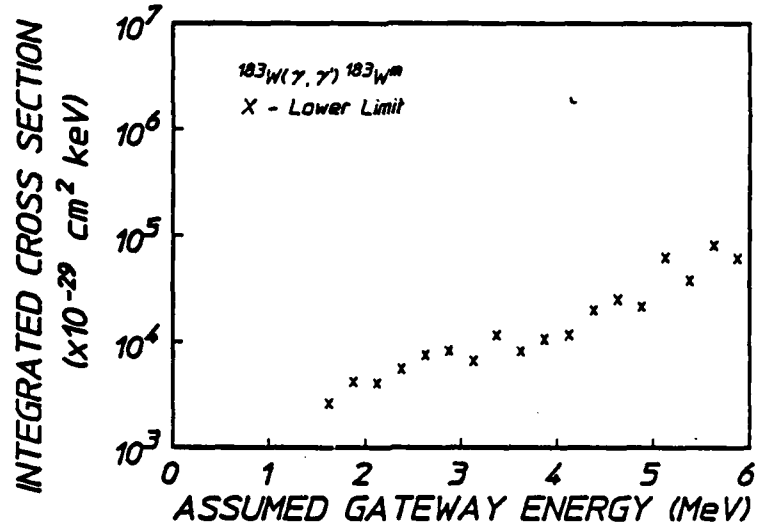
INTEGRATED CROSS SECTION
(x10^-29 cm^2 keV)
183W(γ,γ')183Wm
X - Lower Limit
ASSUMED GATEWAY ENERGY (MeV)

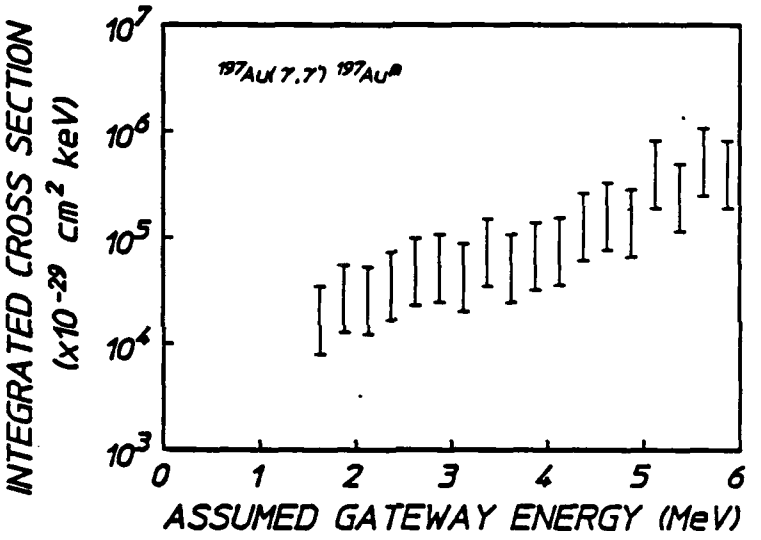
INTEGRATED CROSS SECTION
(x10^-29 cm^2 keV)
197Au(γ,γ')197Aum
ASSUMED GATEWAY ENERGY (MeV)

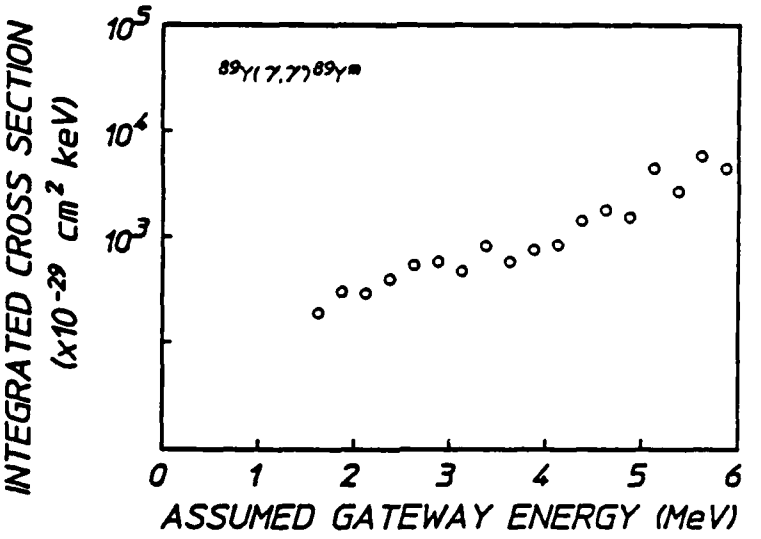
INTEGRATED CROSS SECTION
(x10^-29 cm^2 keV)
89Y(γ,γ')89Ym
ASSUMED GATEWAY ENERGY (MeV)

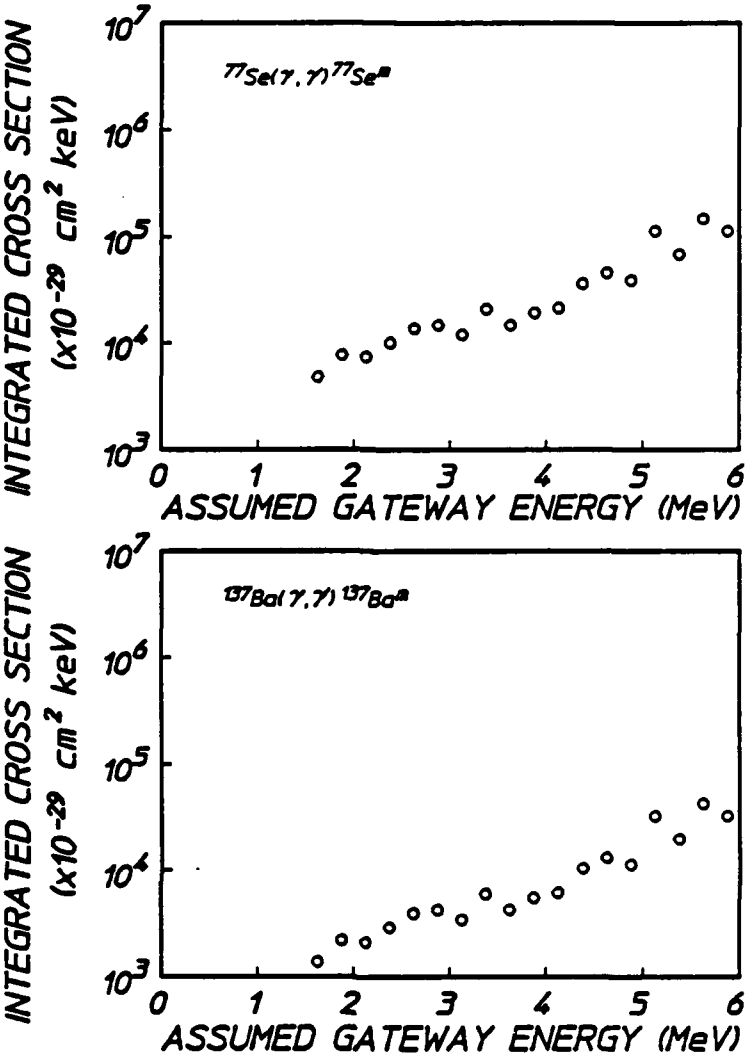

Figure 51: The circles plot integrated cross sections for the (γ,γ') reactions shown on each panel through single, unknown gateway states as functions of the energies at which they could be assumed to lie. Literature values preclude the possibilities that these gateways could lie at energies below the minima shown. As shown in two cases, ^{183}W and ^{197}Au uncertainties in the computations of target transparencies introduced probable errors which were larger than the plotted sizes of the symbols.
a), b) and c) (second preceding page) Reactions of ^{167}Er, ^{79}Br, and ^{191}Ir.
d), e) and f) (preceding page) Reactions of ^{183}W, ^{197}Au, and ^{89}Y.
g) and h) (above) Reactions of ^{77}Se and ^{137}Ba.

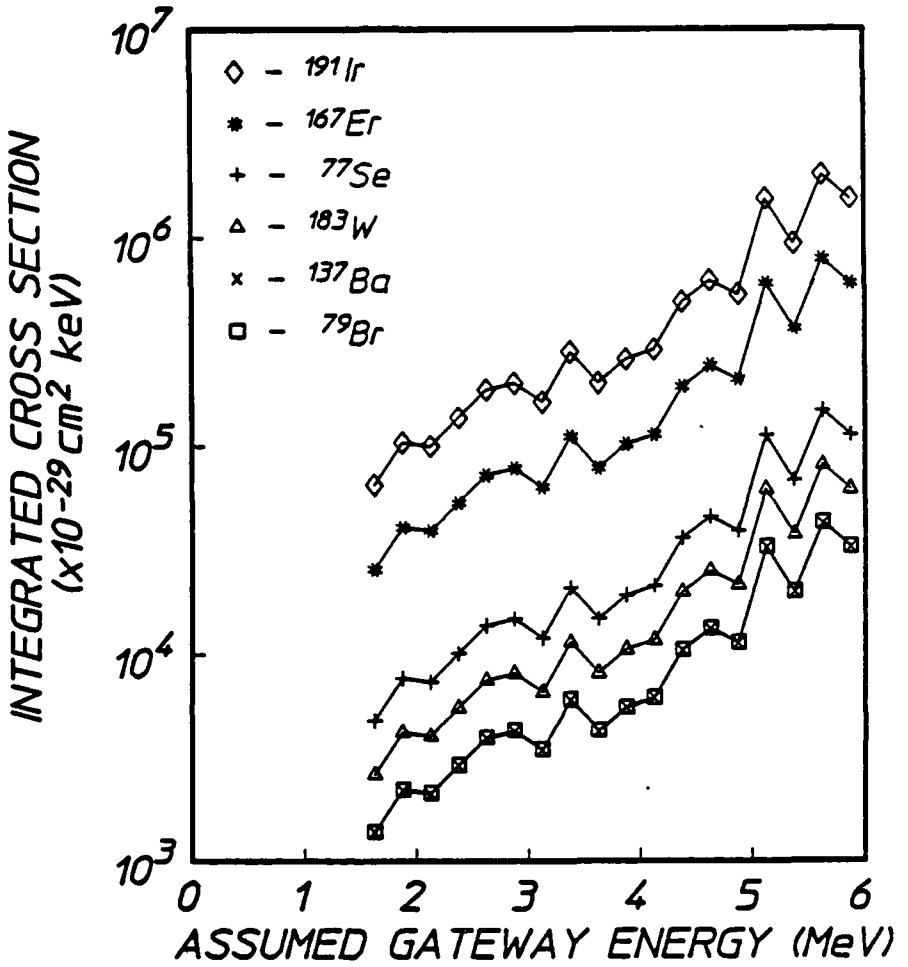

Figure 52: Summary of the integrated cross sections for the (γ,γ') reactions producing the isomers of the species shown, plotted as functions of the energies at which a single gateway state could be assumed for each. For simplicity the range of values possible for ^{197}Au were not shown and the data for ^{183}W must be considered to be lower limits.

Table IX

Summary of the partial widths for the (γ,γ') reactions producing the isomers of the species shown. Values were obtained from the integrated cross sections by assuming the gateway energies lay at 2 MeV, near the bremsstrahlung maximum, and that statistical weights were the same in the ground and gateway states, so that $\sigma_o = 6.1 \times 10^{-22}$ cm^2.

Nuclide	$\pi\sigma_o(b_a b_o \Gamma)/2$ at 2 MeV ($\times 10^{-29}$ cm^2 keV)	Partial width (meV)
^{167}Er	36,000	380
^{79}Br	2,000	21
^{191}Ir	91,000	950
^{183}W	> 3,700	> 38
^{197}Au	11,000 - 49,000	110 - 510
^{89}Y	270	2.8
^{77}Se	6,700	70
^{137}Ba	2,000	21

OPPORTUNITIES FOR THE CALIBRATION OF THE DNA/AURORA ACCELERATOR

Recently, we have reported[5,8] how effectively our technique of X-Ray Activation of Nuclei (XAN) can be used to calibrate the spectral intensities found in a single pulse of intense bremsstrahlung. Essential to determining the pump intensities used in schemes for exciting a gamma-ray laser,[2] XAN has also been validated as a means of calibrating nuclear simulators having end point energies $E_m < 1.5$ MeV.

As currently implemented, three isotopes, ^{77}Se, ^{79}Br, and ^{115}In, are used to sample narrow spectral slices of the fluence illuminating a target. Information is stored as isomeric excitations to be "read out" later. With three isotopes, XAN accommodates measurements at three photon energies, 433, 761, and 1078 keV. The spectrum from the DNA/PITHON accelerator was calibrated[8] with this system and found to conform closely to expectations.

The key to the development of that technique was the use of a large number of shots to activate test samples in order to resolve experimentally the level of self-consistency among values of basic nuclear parameters in the current database.[10] Five of six critical parameters for these three isotopes were found to be consistent and the sixth was repaired. Lest this give a false sense of security in the use of the existing database for the extension of this technique to a greater range of energies, it must be recognized that these three materials were chosen because it appeared <u>a priori</u> that they were the ones most precisely characterized for $E_m < 1.5$ MeV by the study of particle reactions reported in the literature. The resulting score of 83% for consistency should be considered representative of only the very best group of test nuclei. Fortunately, the level of consistency was this high, or XAN could not have been validated in a practical number of test shots.

The next logical step would be to add more isotopes to the calibration target in order to improve both range and resolution of the photon energies covered, and a number of candidates suggest themselves. During the same series of experiments on the PITHON nuclear simulator during which self-consistency of the basic three was demonstrated, 29 other isotopes were irradiated in a survey mode. Four, ^{167}Er, ^{179}Hf, ^{191}Ir, and ^{197}Au, were found to be particularly promising and others were certainly

interesting. The opportunity for using those four to add four more energies below 1.5 MeV to the list for which XAN is applicable was discussed[65] in a previous quarterly report. Unfortunately, of the ten nuclear parameters of importance, *at least five accepted values were found to be drastically erroneous*. An error rate in excess of 50% for this part of the nuclear database, coupled with the lack of foreknowledge of which of the materials should have borne greatest scrutiny, resulted in insufficient data to extract the self-consistent parameters needed for the application of XAN at four additional points.

At higher energies 1.5 MeV < E_M < 6 MeV the situation becomes even more complex.[67] Not only is the accepted database[10] flawed severely, but even basic concepts break down.[69] Most recent experiments[67,69] with the bremsstrahlung from a medical linear accelerator (LINAC) have shown the importance of a new class of giant gateways providing a path for selective excitation of delayed fluorescence about 1000 times greater than anything found earlier.[67] Moreover, conservation principles tending to limit such activations to states requiring that only small changes of angular momentum be imparted together with the x-ray energy seem no longer to apply[69] at the higher end points.

With the discovery of these giant gateway states for sampling bremsstrahlung fluences above 1.5 MeV, there is a clear motivation to attempt to determine the relevant nuclear parameters and energies, E_i, so that the XAN procedure for calibrating impulsive sources can be extended to the range of photon energies 2 - 6 MeV. Reported here are the results of a series of ranging shots into a target package irradiated by DNA/AURORA. The objective was to determine whether the case could be made for the potential utility of the XAN method for the calibration of the spectral intensity emitted from such a source. Two issues were examined. The first was to determine to what extent the DNA/AURORA could be cross calibrated to the LINAC in terms of relative fluorescence yield from a single target material. The second was to survey a selected group of materials to determine whether they evidenced any individually distinctive dependence of fluorescence efficiency upon bremsstrahlung end point.

Experimental Detail

The relevant energy levels for the six nuclei of interest in these preliminary experiments are shown in Fig. 53a - 53f. They were present in targets fabricated from materials occurring in natural isotopic abundance. Since two were isotopes of indium, there were only five target materials irradiated.

For the resolution of the first experimental issue the indium target was used in the form of a thin foil. It was hung on a test stand 31.5 cm from the plane bounding the outermost projections of the window assemblies of the four triaxial output lines of DNA/AURORA. After irradiation the target was dismounted and dispatched to our counting facility at the Center for Quantum Electronics in Dallas. There, the fluorescence was measured at the endcap window of a 10% relative efficiency, n-type Ge detector. In this geometry some correction had to be made for the reabsorption of the output fluorescence shown in Fig. 53 in the target material. Computations indicated that 95% of the fluorescent photons escaped this self-absorption.

The activation induced by the reaction $^{113}In(\gamma,\gamma')^{113}In^{m}$ shown in Fig. 53d was so intense that usable levels of fluorescence were still found in the 1.7 hr isomer of the 4.3% natural fraction of the 7.6 g foil after the 6 hour and 16 minute transit to the counting facility in Dallas.

For the comparative studies, targets of BaF_2, Hg_2Cl_2, and SrF_2 were fabricated from powders, Cd and In from solid pellets, held in cylindrical polyethylene vials. These were hung at the position of the indium foil, and were irradiated perpendicular to the axes of the vials. After irradiation they were dismounted and carried to a locally positioned NaI(Tl) spectrometer. The entire target package was backed with an array of thermoluminescent diodes (TLD's) which were used to determine the morphology of the radiation pattern.

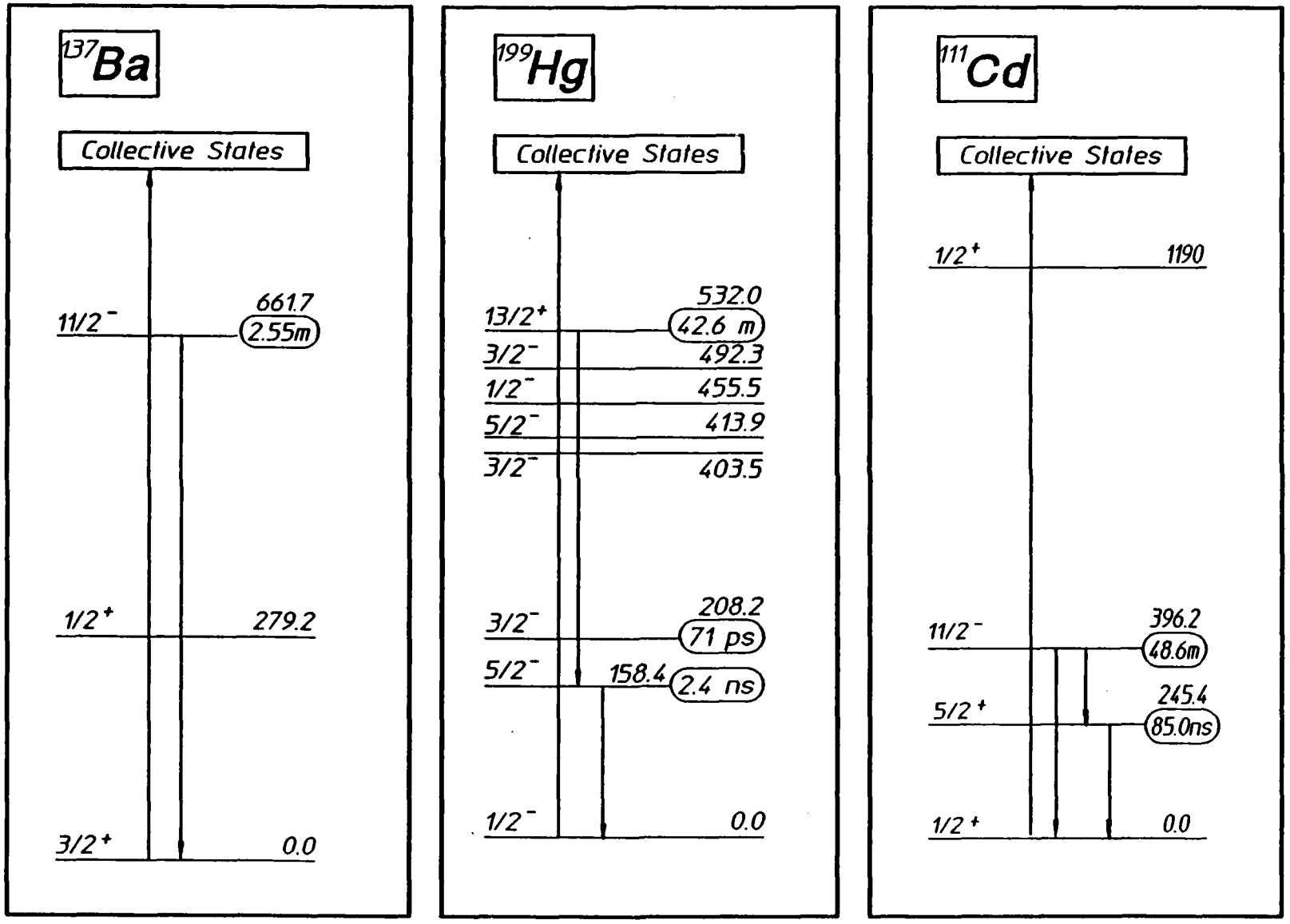
137Ba
Collective States
661.7
11/2⁻
2.55m
1/2⁺
279.2
3/2⁺
0.0
199Hg
Collective States
532.0
13/2⁺
42.6 m
3/2⁻
492.3
1/2⁻
455.5
5/2⁻
413.9
3/2⁻
403.5
208.2
3/2⁻
71 ps
5/2⁻
158.4
2.4 ns
1/2⁻
0.0
111Cd
Collective States
1/2⁺
1190
396.2
11/2⁻
48.6m
245.4
5/2⁺
85.0ns
1/2⁺
0.0

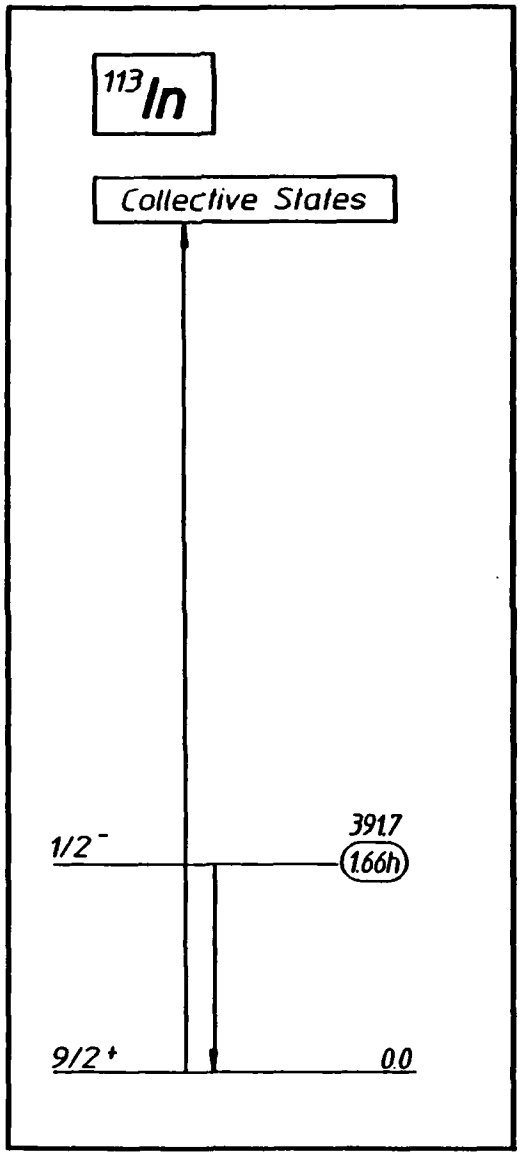
^{113}In
Collective States
391.7
1/2⁻
1.66h
9/2⁺
0.0

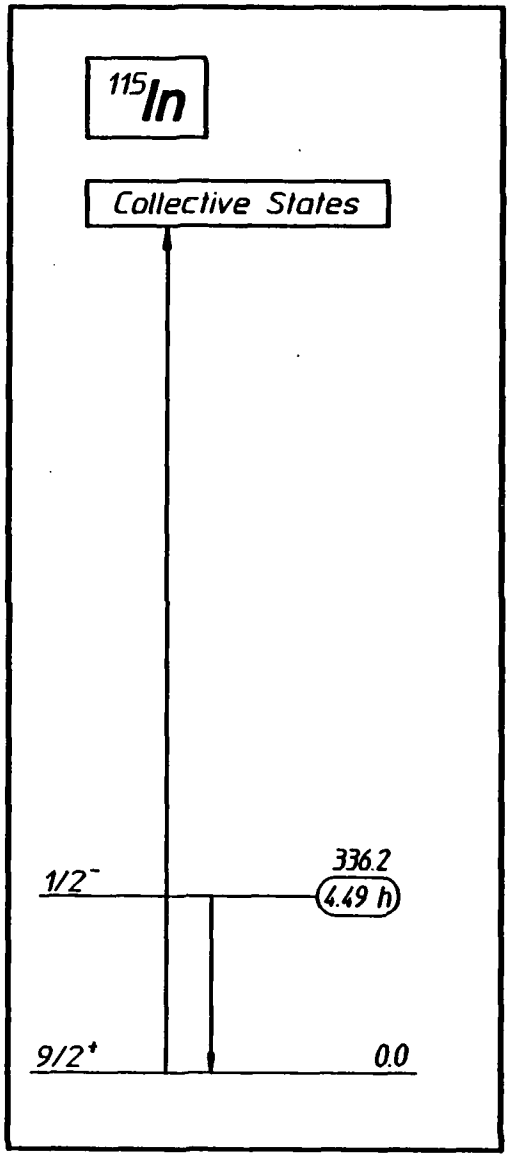
^{115}In
Collective States
336.2
1/2⁻
4.49 h
9/2⁺
0.0

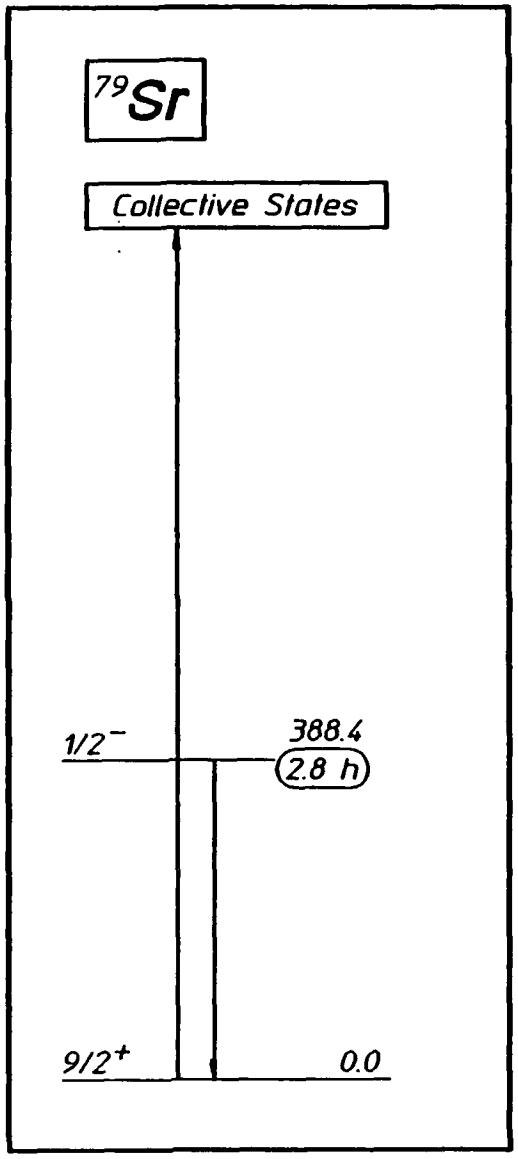
^{79}Sr
Collective States
388.4
1/2⁻
2.8 h
9/2⁺
0.0

Figure 53: Energy level diagrams of the excited states important to the production and detection of the isomers of the nuclei shown. Half-lives of the states are shown to the right of each, together with their energies in keV. Downward arrows locate transitions used in the detection of populations of the isomers produced by the absorption transitions indicated by the upward arrows. The locations of the gateways through which the (γ,γ') reactions proceed are not to scale, and the details of the cascades downward to the isomers are unknown.
a), b), and c) (second preceeding page, from left): Transitions important to the study of (γ,γ') reactions producing the isomers $^{137}Ba^{m}$, $^{199}Hg^{m}$, and $^{111}Cd^{m}$.
d), e), and f) (preceeding page, from left): Transitions important to the study of (γ,γ') reactions producing the isomers $^{113}In^{m}$, $^{115}In^{m}$, and $^{87}Sr^{m}$.

Results–Cross Calibration Studies

From the number of counts in the fluorescence peaks corresponding to the transitions of Figs. 53d and 53e, the numbers of activations in the indium foil sample were obtained by well-established procedures. The efficiency of the spectrometer was determined with calibrated sources and was found to conform closely to nominal specifications. Self-absorption corrections were calculated as discussed and fluorescence efficiencies were taken from the literature.[60] The actual numbers of activations of the samples, S, were obtained by correcting for finite counting and irradiation times. Literature values of the half-lives were used in making these corrections.[10]

The spectral fluence can be obtained if it is assumed that one channel at energy E_1 dominates the excitation so that the basic Eqs. (2a) and (2b) can be inverted,

$$\frac{\phi(E_1)}{A} = \frac{SE_1}{N}\,(\pi b_a b_o \sigma_o \Gamma/2)^{-1}_1 \quad . \qquad (48)$$

As mentioned earlier the term in parentheses is the integrated cross section for the excitation of the fluorescence. Values reported as a result of the linac experiments[70] are shown in Fig. 54 as functions of the energies E_1 at which the pump intensity was being sampled.

Using the data of Fig. 54 in Eq. (48) together with the actual numbers of activations of ^{115}In and ^{113}In gives the values of spectral fluence shown in Fig. 55. Data shown there define the locii of the single measurement of intensity which would result *if the precise energy, E_1, of the dominant gateway were known.*

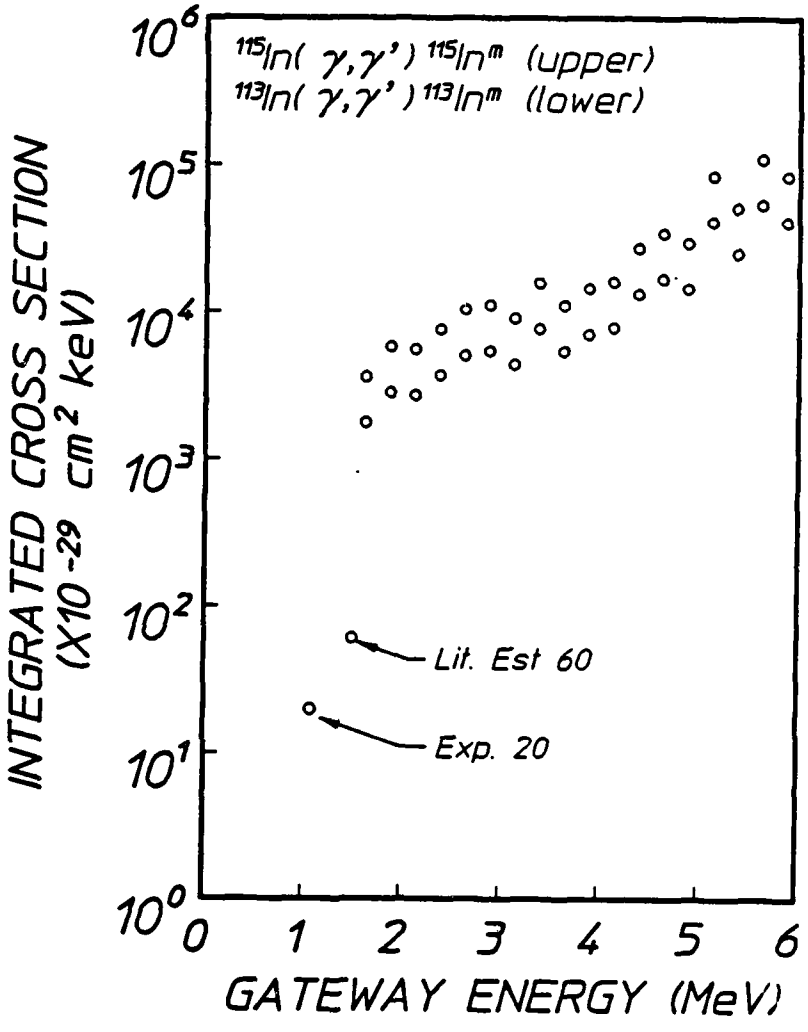

Figure 54: The integrated cross sections reported for the photoactivation of selected nuclei through individual, unknown gateway states as functions of the energies at which they could be assumed to lie. The lower family of points approximated the results obtained for the activation of ^{113}In to within the plotted sizes of the data while the upper characterizes the excitation of ^{115}In. Shown at the successively lower energies are the two points taken from Refs. 11 and 7, respectively.

For comparison, the spectrum indicated by dosimetry is shown in Fig. 55 by the solid line. It was obtained by scaling the results of a theoretical computation of the spectrum[71] to the dose measured with the TLD's. The dose is defined as the energy absorbed per unit mass of target and is computed from the expression,

$$D = \sum_i \left(\frac{\mu_a}{\rho}\right)_i E_i \left.\frac{d\varphi}{dE}\right|_i \Delta E_i \quad , \tag{49}$$

where

$\left(\frac{\mu_a}{\rho}\right)_i$ - mass energy absorption coefficient[72] for bremsstrahlung at E_i in units of cm^2/g,

E_i - photon energy,

$\left.\frac{d\varphi}{dE}\right|_i$ - spectral flux, derivative with respect to photon energy of the photon fluence; in units of photons/keV/cm^2,

ΔE_i - size of the mesh of energies over which the previous variable is reported.

It is the quantity,

$$G(E_i) = gE_i \left.\frac{d\varphi}{dE}\right|_i \quad , \tag{50}$$

that is reported[72] as a result of computations of the bremsstrahlung. In this expression g is a constant normalizing the intensities to the total measured output. In actual practice it is determined from measurements of the dose at the position of the target being irradiated. Dividing Eq. (50) by g and substituting into Eq. (49) and solving for g gives,

$$g = \frac{1}{D} \sum_i \left(\frac{\mu_a}{\rho}\right)_i G(E_i)\Delta E_i \quad . \tag{51}$$

Finally substituting back into Eq. (50) and solving for $Ed\varphi/dE$,

$$E_i \left.\frac{d\varphi}{dE}\right|_i = DG(E_i) \left[\sum_i \left(\frac{\mu_a}{\rho}\right)_i G(E_i)\Delta E_i\right]^{-1} \quad , \tag{52}$$

which is the quantity for which measurements are reported in Fig. 55.

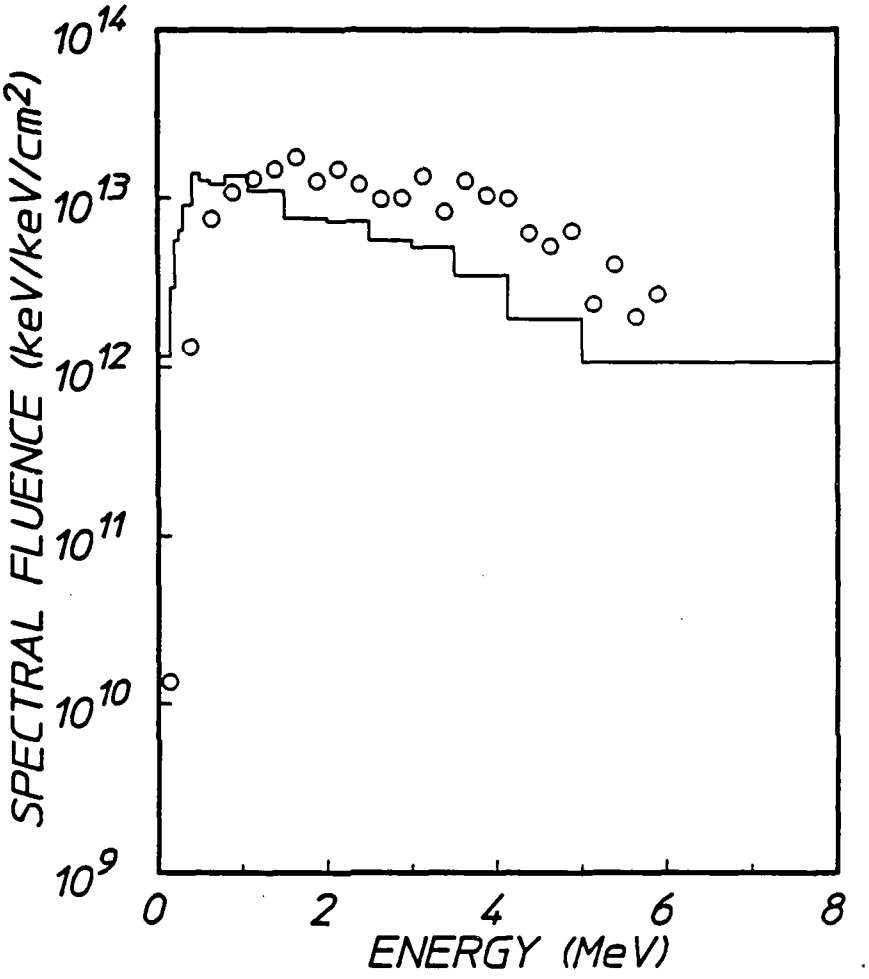

Figure 55: Data points record the locii of the spectral intensity of DNA/AURORA measured at one energy by nuclear activation calibrated in the linac in comparison with the computed spectrum normalized by a dosimeter measurement. The computed spectrum is represented by the solid line. The energy to which the activation procedure is most sensitive is not known but locii record possible values and corresponding intensitites. The bremsstrahlung was produced by DNA/AURORA charged to 90 KV at the Marx input.

Values of G(Ei) were available[72] for charging voltages of 90 kV and 110 kV. Plotted by the solid line in Fig. 55 is the spectral fluence calculated from Eq. (52) for the $G(E_i)$ reported for 90 kV. It is particularly interesting that the functional form of that $G(E_i)$ closely

resembles the spectrum[53] from the 6 MeV linac and the resulting spectral fluence is in rough agreement with the measurements obtained with the indium absorbers.

Results-Target Survey

Since the end point energy of the bremsstrahlung from DNA/AURORA was close to the threshold value for neutron evaporation from (γ,n) reactions, it was necessary to examine the fluorescence spectra from the materials being considered as calibrators for the 2 - 6 MeV range of energies. These spectra are shown in Figs. 56a - 56e. Dominant structures are marked and all correspond to the signatures of the respective (γ,γ') reactions.

The end point energy of the bremsstrahlung could be varied over a limited range at DNA/AURORA by changing the primary charge voltage on the Marx bank while adjusting the spark gaps, correspondingly. If the end point at first lay below the energy of excitation of the first of the giant gateways, relatively little excitation would be expected. Then as it were increased, the activation should "turn-on" when the gateway energy was reached. To search for such evidence of a distinctive gateway characteristic of each target material, fluorescence photons in the peaks of the spectra of Fig. 56a - 56e were counted as functions of the charging voltage of the Marx generator.

Data were corrected to obtain relative numbers of activations by compensating for the delay in the start of the counting period and for its finite duration. An onset of excitation through a gateway is more readily observed if the relative numbers of activations are scaled by the input dose of irradiation measured by the TLD's at the position of the target. In this way the increase in activation simply associated with the greater dose emitted by the accelerator at higher charging voltages is less able to mask the increases resulting from the opening of a new channel for absorption in the nuclei. Shown in Figs. 57a - 57e are the resulting values of the activation per unit dose normalized to the activation at 110 kV, as functions of the charging voltage on the Marx. Due to insufficiently complete transit time information, the ^{137}Ba data could not be reduced to this form.

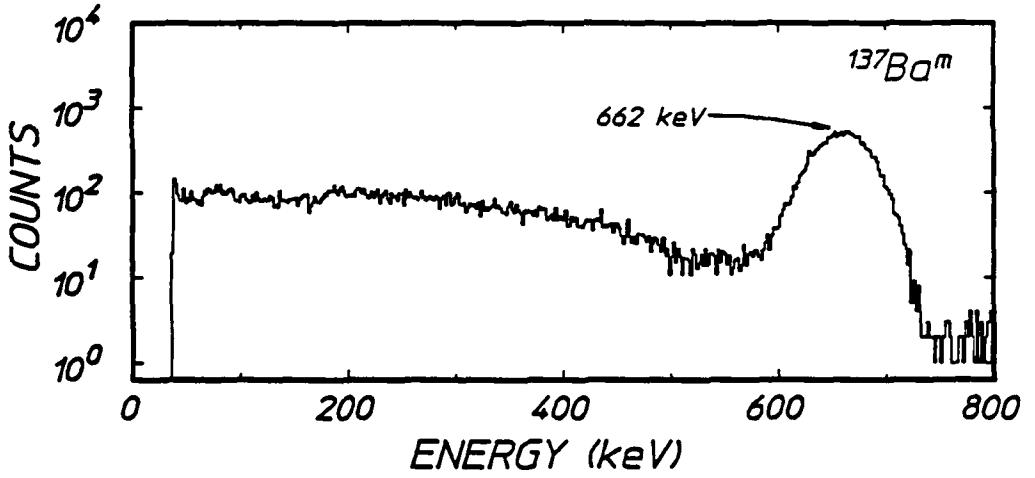
10^4
10^3
10^2
10^1
10^0
COUNTS
$^{137}Ba^m$
662 keV
0
200
400
600
800
ENERGY (keV)

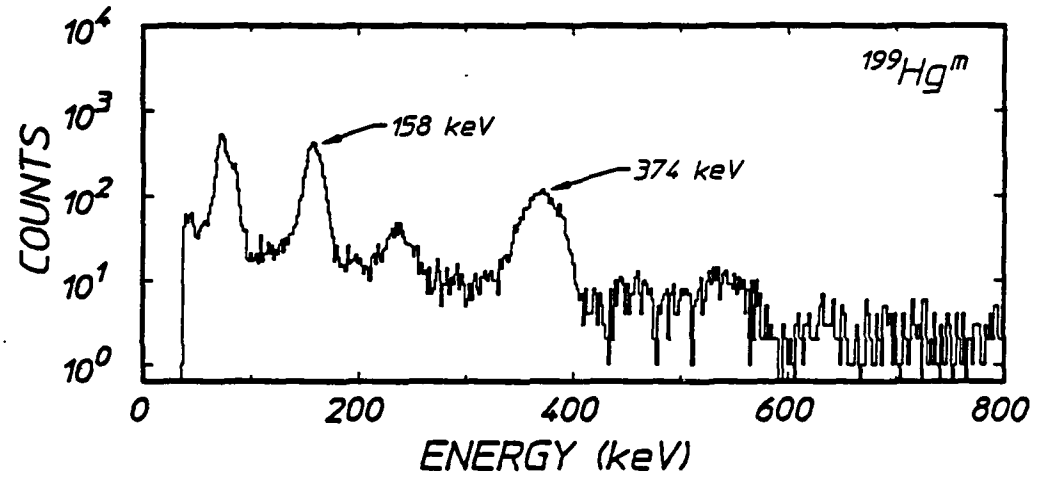
10^4
10^3
10^2
10^1
10^0
COUNTS
$^{199}Hg^m$
158 keV
374 keV
0
200
400
600
800
ENERGY (keV)

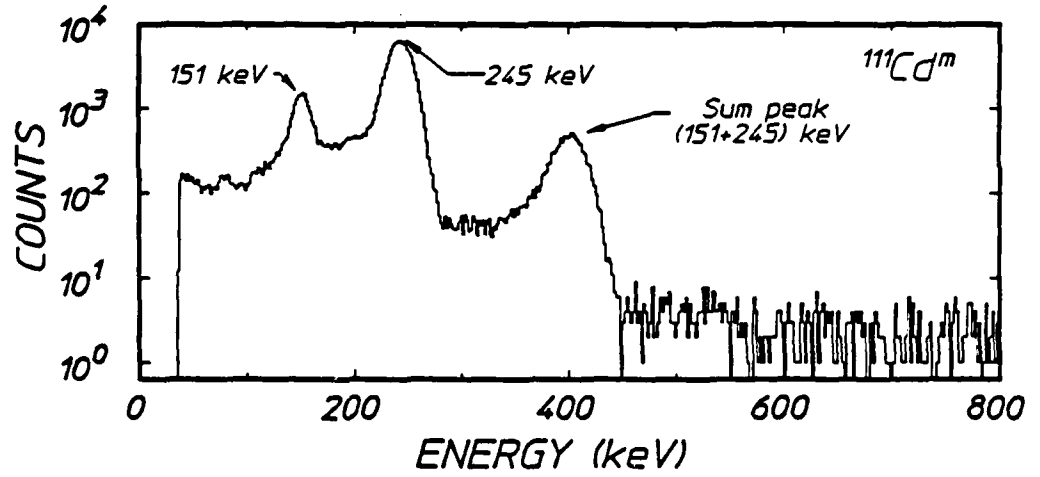
10^4
10^3
10^2
10^1
10^0
COUNTS
$^{111}Cd^m$
151 keV
245 keV
Sum peak
(151+245) keV
0
200
400
600
800
ENERGY (keV)

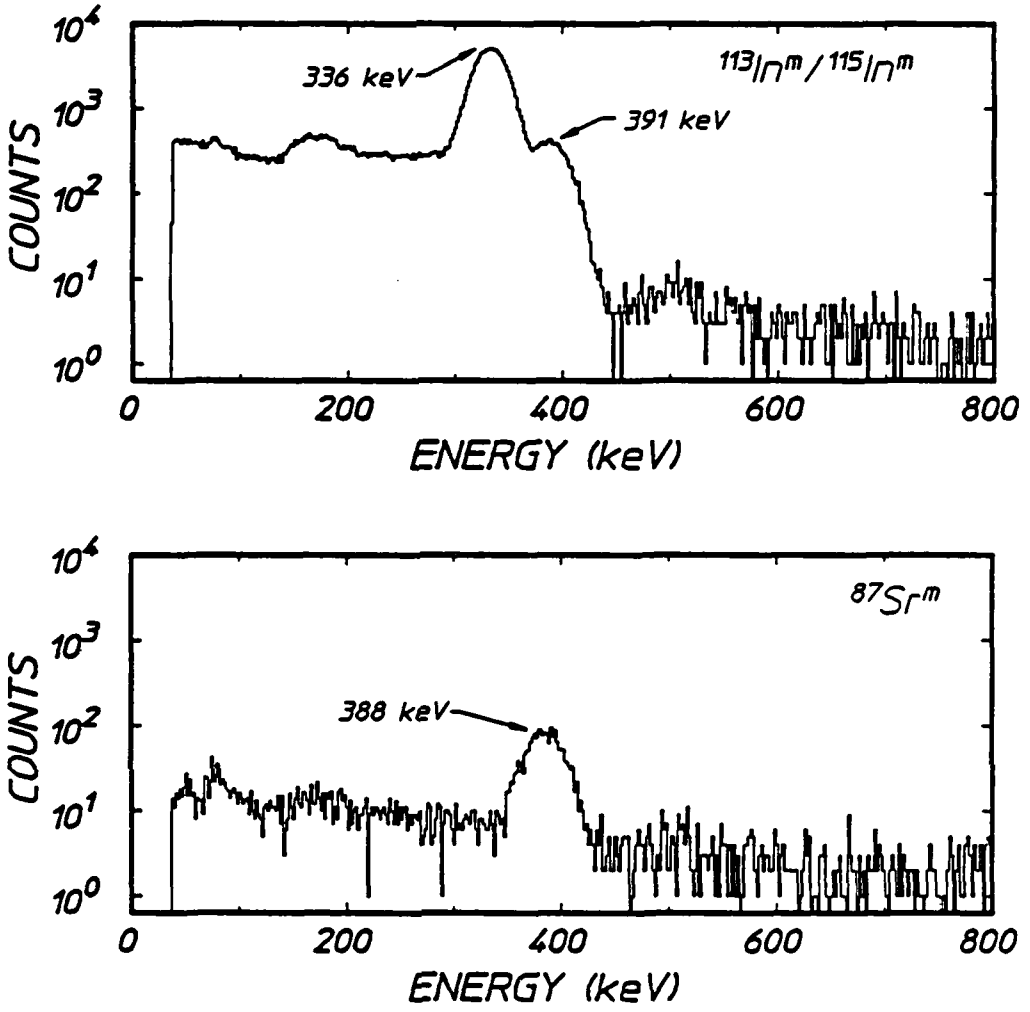

Figure 56: Spectra of the fluorescence detected with an NaI(Tl) detector over the range of energies shown. Transitions shown in Figs. 53a-53f for the detection of the isomers are identified by the arrows. All samples were counted for 600 s. The elapsed times from irradiation to the start of counting are as follows:
a), b), and c) (preceding page): ^{137}Ba, ^{199}Hg, and ^{111}Cd: Transit times were 6 m, 63 m, and 27 m.
d) and e) (above): $^{113}In/^{115}In$ and ^{87}Sr: Transit times were 45 m and 82 m.

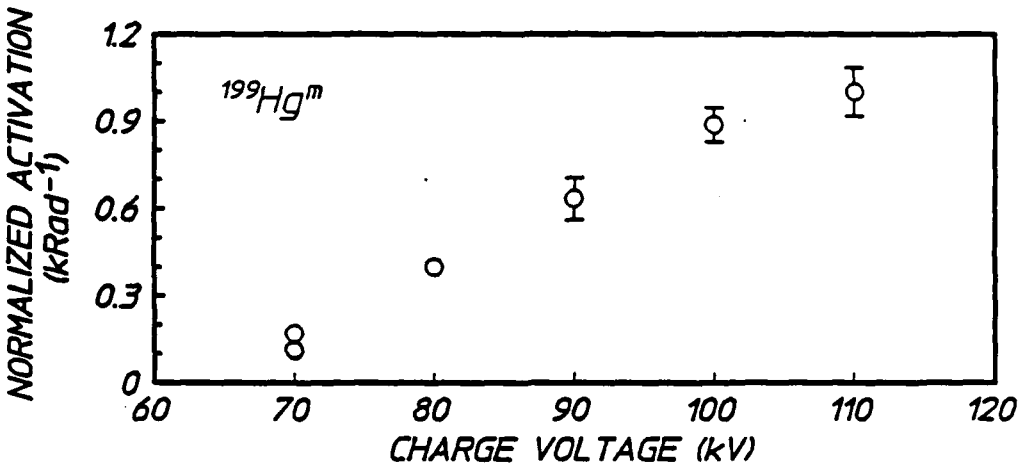
NORMALIZED ACTIVATION (kRad⁻¹)
199Hgm
1.2
0.9
0.6
0.3
0
60
70
80
90
100
110
120
CHARGE VOLTAGE (kV)

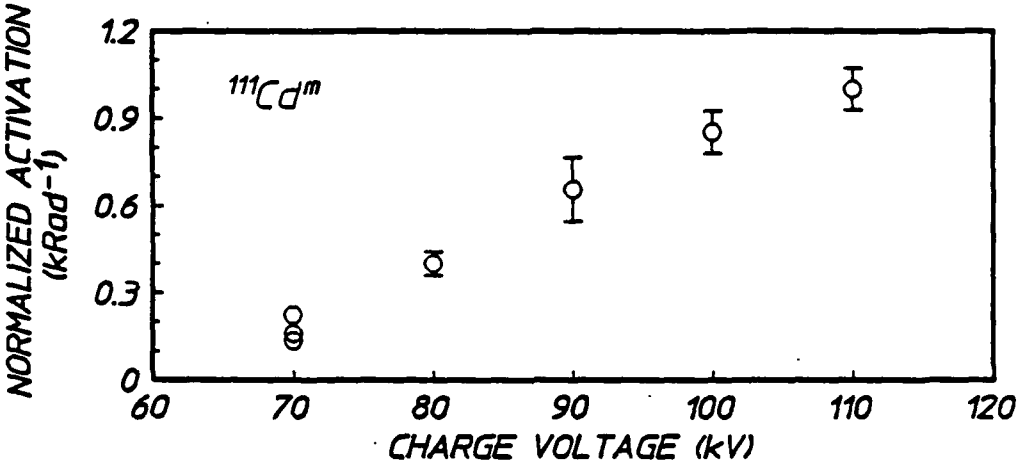
NORMALIZED ACTIVATION (kRad⁻¹)
111Cdm
1.2
0.9
0.6
0.3
0
60
70
80
90
100
110
120
CHARGE VOLTAGE (kV)

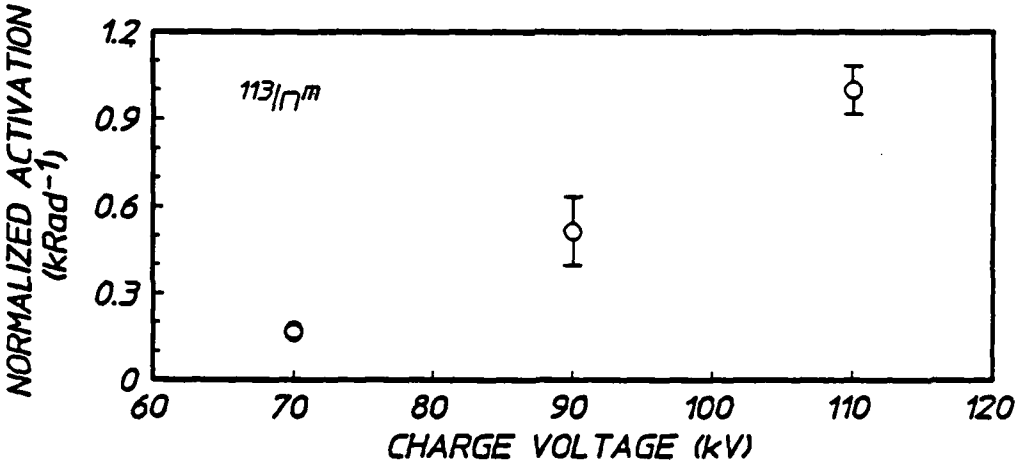
NORMALIZED ACTIVATION (kRad⁻¹)
113Inm
1.2
0.9
0.6
0.3
0
60
70
80
90
100
110
120
CHARGE VOLTAGE (kV)

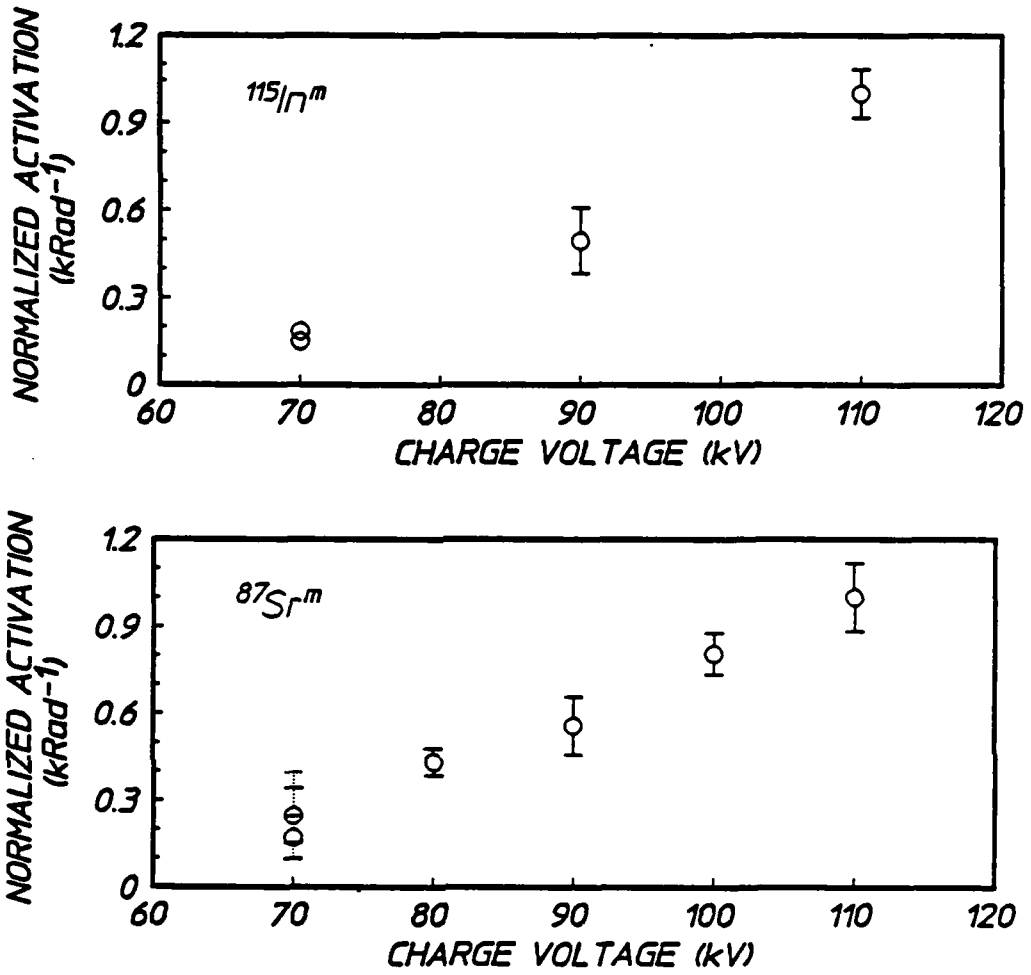

Figure 57: Isomeric activation per kilorad of dose normalized to the activation at 110 kV, as a function of the DNA/AURORA charging voltage for the following nuclei:
a), b), and c) (preceding page): $^{199}Hg^{m}$, $^{111}Cd^{m}$, and $^{113}In^{m}$:
d) and e) (above): $^{115}In^{m}$ and $^{87}Sr^{m}$.
Where no error bars are shown, the error is commensurate with the symbol size. For $^{87}Sr^{m}$, the dashed error bar indicates the largest extent of the error associated with the cluster of points.

Conclusions

The general agreement between the calculated and measured values of spectral fluence from DNA/AURORA shown in Fig. 55 are both surprisingly good and disturbingly inconsistent. Since the dominant gateway energies of the ^{115}In and ^{113}In components of the target are not known, deviations between theory and experiment of less than an order of magnitude are most heartening. This is the first and most overriding conclusion.

Finer details are troublesome. Not having access to a variable energy LINAC, the calibrating values of the integrated cross sections for indium activation had been obtained earlier by fitting calculations of LINAC spectra to dosimeter measurements for comparison to measured yields of fluorescence. Rather surprisingly the calculated spectra for the 6 MeV LINAC were extremely close to those for DNA/AURORA charged to 90 kV. Because of that, it would have seemed unlikely that the activations were proceeding through gateways at different energies, one being preferred in the LINAC case and the other in AURORA. As a consequence, it would seem that the differences seen in Fig. 55 should have accrued only from variances in counting accuracy and dosimeter calibrations and thus, should have been far smaller. The most attractive speculation is that in fact, gateways were accessed at different energies because one or the other of the two sources had a tail of higher energies more intense than computed. Such a possibility emphasizes the need for more definitive calibration of the sampling targets.

The survey data pursuant to the second objective is interesting in that evidence for individual gateways may be appearing at the lower charging voltages. Mercury seems to show a sharper onset between 70 and 80 kV than does cadmium. If better data confirms this trend it will indicate that the dominant gateway lies at higher energies in ^{111}Cd than in ^{199}Hg. In the latter case the onset would have occurred at even lower charging voltages than tested here and the sharp part of the increase in fluorescence would have passed before 70 kV were reached.

The present data is of such a cursory nature that only speculations can be supported about detailed mechanisms. What is clear is that there is a strong case for the efficacy of calibrating such a large accelerator as DNA/AURORA with the nuclear activation technique we proved at lower x-ray energies. Success would be certain if a variable energy

LINAC were available to first determine the gateway energies of the sampling targets. Without such a device, the present results suggest that a repetition of the "bootstrap" process which succeeded at lower energies has a reasonable chance of succeeding at these higher energies.

A FREQUENCY MODULATION SPECTROMETER FOR MOSSBAUER STUDIES

Introduction

There is a more complex path toward the realization of a gamma-ray laser that holds the promise of great practical efficiency. Based upon the concept of "coherent pumping" which we introduced[2] in 1982, it depends upon the existence from one of the candidate isomers of a transition resonant with some intense source of coherent radiation such as a laser. Just as in the case of the priority scheme for pumping isomers with x-rays, coherent pumping represents another nuclear analog to a familiar laser process, upconversion.

To find the resonant levels needed to mount the upconversion process at the nuclear level requires the conduct of spectroscopic measurements of nuclear energies with an optical level of precision and tuning range. Such measurements have not been made before, and it seemed reasonable to consider that if the problem is analogous to one on the optical scale; then perhaps so is the solution. Both this and the next chapter report advances in the technology with which nuclear analogs of high resolution optical spectroscopy can be pursued.

As early as 1960 it had been noted that radiofrequency (Rf) sidebands to the hyperfine structure of ^{57}Fe could be observed with a Mössbauer spectrometer.[73] The six lines (Parent Transitions) in a normal absorption spectrum of ^{57}Fe in iron (Fig. 58a) are accompanied by additional absorption peaks (Rf sidebands) when the absorber is subjected to an Rf field (Fig. 58b). In 1960 Ruby and Bolef reported the observation of Rf sidebands in iron produced by mounting a ^{57}Co Mössbauer gamma ray source on an ultrasonic transducer driven at MHz frequencies.[73] It should be noted that the Rf transducer was used in addition to a long period oscillator which provided the energy range for the Mössbauer spectrum by introducing controlled Doppler shifts. In 1968 Perlow reported the generation of Rf sidebands in iron directly, by subjecting the gamma-ray source to Rf field without the involvement of any external ultrasonic source.[74] In that same year Heiman, Pfeiffer and Walker reported observing Rf sidebands in iron as a result of subjecting the iron foil absorber to an Rf field.[75] Finally, in 1976

Chien and Walker presented a method for producing Rf sidebands in a nonferromagnetic stainless steel absorber with an Rf field, by using nickel as a ferromagnetic non-absorbing driver.[76] In all cases, the Rf sidebands appeared at integral multiples of the frequency of the applied Rf (Fig. 59). Figure 59 shows Rf sidebands produced in a stainless-steel foil driven by a nickel foil immersed in Rf fields of different frequencies. The frequency dependence of these Rf sidebands can be utilized to make a high resolution adaptation of Mössbauer spectroscopy which is freed from many of the mechanical constraints tending to limit conventional devices.

In 1967, Bolef and Mishory reported the development of a spectrometer which was based upon Rf sidebands induced in a Mössbauer source with an Rf electromechanical transducer (an X-cut quartz crystal).[77] As the frequency of the applied Rf was changed, the energies of the sideband gamma ray emissions changed. This phenomenon enabled Bolef and Mishory to obtain an absorption spectrum as a function of the frequency of the applied rf. In 1985 DePaolo, Wagal and Collins reported success in developing a spectroscopic technique using Rf sidebands induced in a ferromagnetic absorber by an Rf field.[78] Modulating the absorber has numerous advantages over modulating the source. It is easier and safer to work with a stable isotope, and it is also easier to interpret a spectrum from a single line source, as opposed to a Zeeman split source or a source with Rf sidebands. Therefore, we have improved the technique for a modulated gamma-ray absorption cross section spectroscopy which we call Nuclear Frequency Modulation Spectroscopy (NFMS).

The technique reported by DePaolo, Wagal and Collins was slow and laborious, with data collection times on the order of months for tens of data points. We can now report[79] the automation of this technique, with resulting data collection times of two days for 1024 data points and a signal to noise ratio of 8:1 for a signal that represents a relative absorption of 3%. This chapter describes the NFMS apparatus, describes the interface to an Apple computer which automates NFMS data collection, and presents some typical NFMS data.

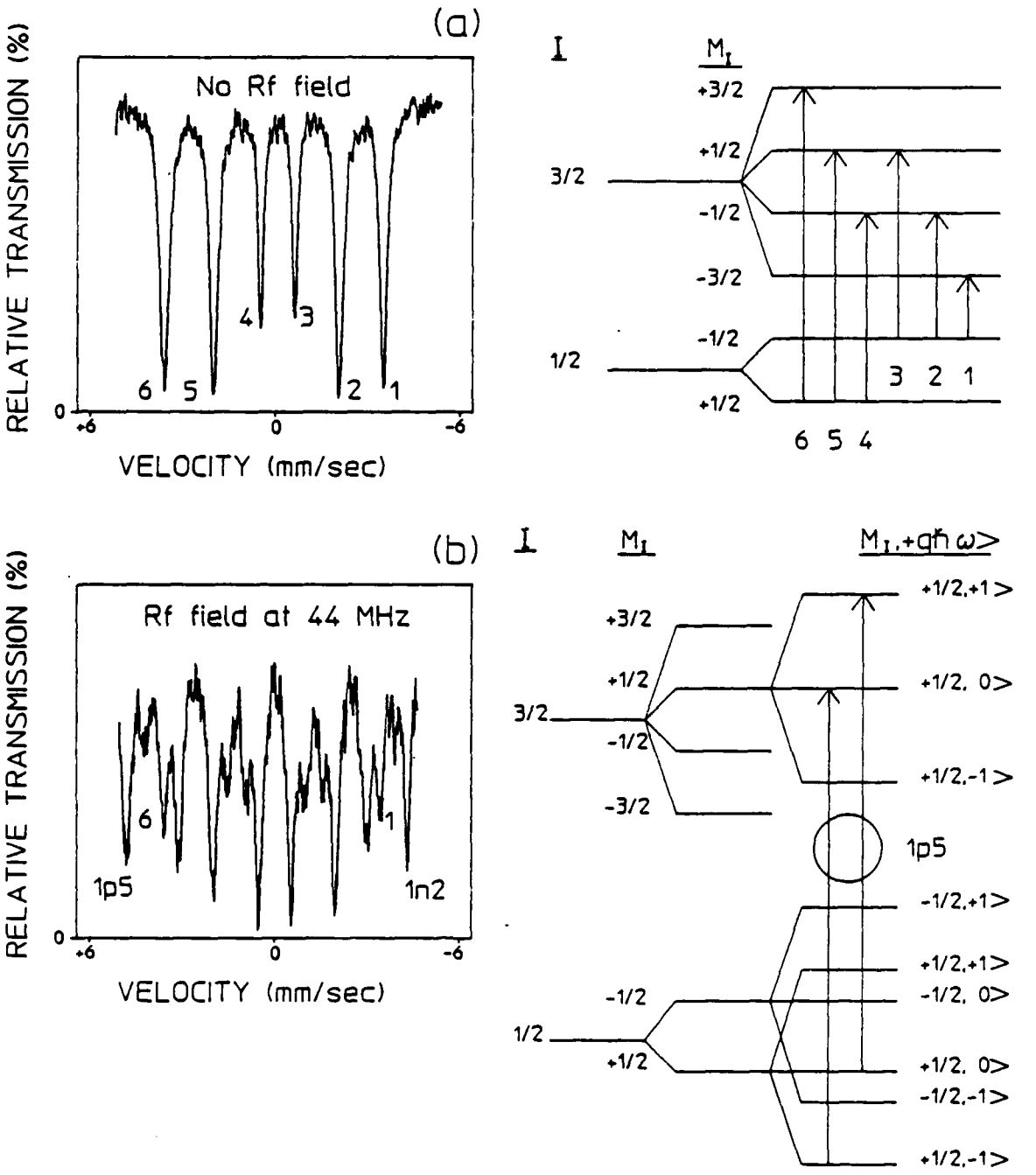

Figure 58: Mössbauer absorption spectra and energy level diagrams for ^{57}Fe in iron, a) with no Rf field at the absorber, and b) with a 4 Oersted Rf field applied to the absorber at a frequency of 44 MHz, showing the effect of the Rf field.

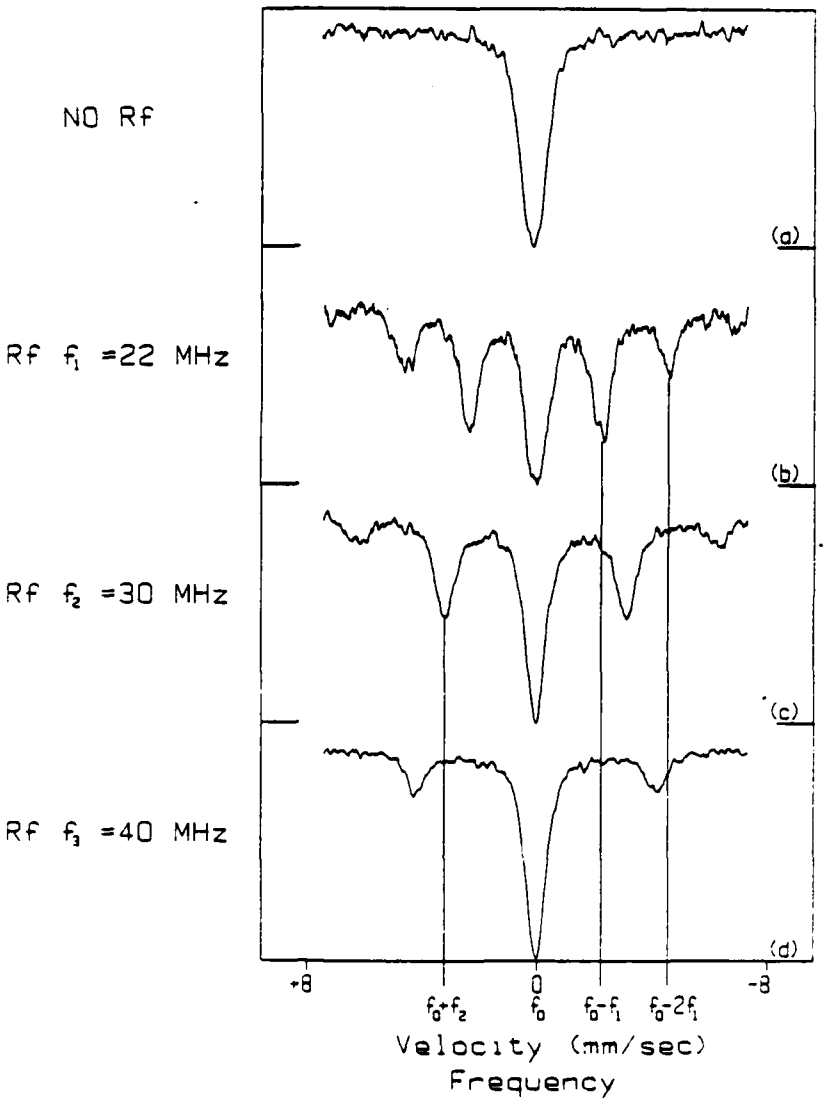

Figure 59: Mössbauer absorption spectra of ^{57}Fe in 310-stainless steel driven by a nickel foil, showing the effect of an Rf field applied to the absorber-nonabsorber sandwich at frequencies of b) 22 MHz, c) 30 MHz, and d) 40 MHz in comparison to a) a no Rf spectra. It can be seen from the figure that sidebands appear at integral multiples of the frequency of the Rf field.

Spectrometer Design

The NFMS is a modification of a conventional Mössbauer spectrometer comprised of the equipment in the dotted box in the schematic of Fig. 60. A Kr gas filled proportional counter (ASA PC-KR-1) biased with 1.8 kV from a Bertran Associates model 303 DC voltage supply was used as our gamma-ray detector. The signal from the detector was amplified by an ASA CSP-400A preamp and ASA LA-200 amplifier. The amplified signal was then fed into an ASA LG-200 linear gate which produced 1 μsec TTL pulses for counting.

A 10 mCi ^{57}Co Mössbauer source in a Pd matrix was mounted on an ASA K-4 linear motor capable of operating at a constant velocity or with constant acceleration. A stable means of doppler shifting the energy of the emitted gamma ray is needed, therefore an ASA S-700 motor controller is used to produce the voltage waveforms which drive the linear motor. The constant acceleration voltage waveform is derived from a 5 Hz square wave which must be provided by the multi-channel scalar (MCS). If the motor is driven at a constant velocity, then the motor controller gates off data to the MCS while the motor is rewinding.

The key to NFMS is the presence of the Rf field at the absorber, for which a very stable Rf signal generator and amplifier are needed. A Wavetek 3510 signal generator, with a frequency range of 1 MHz to 1GHz, and a 100 Hz resolution with a 500 Hz/(10 min) stability, was used. The Rf amplifier was an ENI 550L 50 watt linear amplifier with a range of 1.5-400 MHz. There were two basic circuits used to generate the Rf field at the absorber. One was a series LC circuit in parallel with an impedance matching capacitor (Fig. 60). This series-resonant tank circuit was designed to have either a low Q when used in a narrowband NFMS, or a high Q when used to obtain a Mössbauer spectrum in the presence of a single frequency Rf field. It should be noted that narrowband in these instances refers to a 12 Mhz or less bandwidth. The other circuit, used in the wideband NFMS, simply incorporated an inductor in series with an impedance matching non-inductive load. The absorber was then mounted in the induction coil of the appropriate circuit and subjected to field intensities on the order of 1-5 Oersteds.

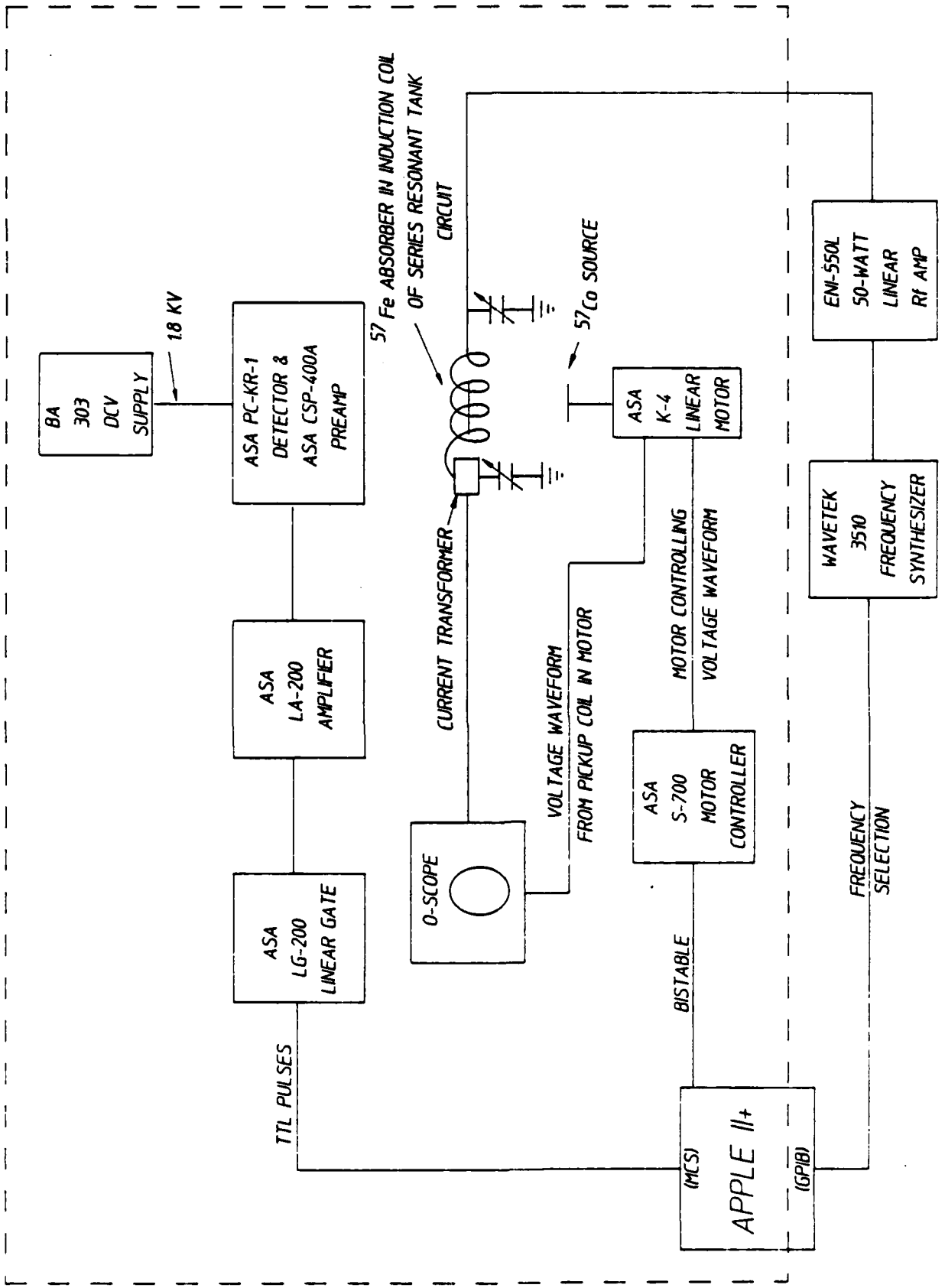

Figure 60: This schematic shows the NFMS, while the portion of the apparatus which is in the dotted box can be used as a conventional Mössbauer spectrometer.

In order to monitor the field intensity in the coil, a Pearson 2877 current transformer was used to measure the current flowing into the induction coil. This transformer outputs 1 V/Amp with a usable range of 300 Hz to 200 MHz and an insertion impedance of 0.02 Ohms. In order to monitor the velocity of the motor, there is a pickup coil mounted in the linear motor. The output from this pickup is used to stabilize the driving voltage waveform, but it can also be monitored on an oscilloscope. The velocity of the motor was established by correlating the pickup coil voltages to the positions of the peaks in the 6 line spectrum of ^{57}Fe. Currently work is underway building an interface to an Apple II+ from an ASA LC-9A laser interferometer. This interface will enable the computer to display real time velocity information as well as track any drifting.

The heart of the NFMS, however, is the MCS/GPIB interface (Fig. 61). It enables an Apple II+ computer to be used for data acquisition and real time data display with either the conventional Mössbauer spectrometer (constant acceleration mode), or with the NFMS (constant velocity mode with GPIB interface to signal generator). The MCS is a card designed around two VIA's, or Versatile Interface Adapters (6522's). The GPIB, or IEEE-488 General Purpose Interface Bus (9914), is a commercially available interface card available for the Apple computer. The GPIB is necessary only for scanning frequencies of the signal generator. Therefore, the GPIB is not needed if one intends to use only the Mössbauer spectrometer.

The central components of the MCS are the two 6522's, the multiplexing logic, and a 12-bit counter. Each 6522 is a 40 pin chip which has a 16-bit counter with a 16-bit latch, a 16-bit counter with an 8-bit latch, two 8-bit parallel ports, and a serial port. The counter with the full latch can be set to count down in a free running mode and generate interrupts. In other words, the 6522 can be set to generate evenly spaced interrupts so that the Apple's CPU need not be wasted keeping track of time. The counter with the half latch can be set to count negative logic pulses at one of the pins of the 6522. The multiplexing logic is an assortment of gates which channel the pulses to be counted to one of the 6522's while channeling the Apple's data bus to the other 6522. When an interrupt is generated, the pulses to be counted are gated to the other 6522 while the Apple's data bus is then channeled to the first 6522. As a result, the time it takes the Apple's CPU to add a count to the proper channel is not dead time for the MCS.

The twelve bit counter, actually three 4-bit counters, is needed to count 512 interrupts. This counting produces the 5 Hz square wave which is used by the motor controller to generate a constant acceleration voltage waveform for the linear motor. Therefore, the time between interrupts, hence the dwell time per channel, must be 195 μsec for a 1024 data point Mössbauer spectrum. The NFMS, on the other hand, does not require an accelerating source. Therefore, when using the MCS in an NFMS the dwell time can be user selected. The optimum dwell time minimizes the total dead time, which arises from the time needed to allow the Rf signal to stabilize each time the frequency is changed, without compromising the stability of the signal.

Use of this hardware as an NFMS or a Mössbauer spectrometer is determined by the software. Written in 6502 assembly language, the software for the two spectrometers is similar in principle but different in particulars. In both spectrometers the MCS transfers data to the Apple on an interrupt basis. Both programs consist of four basic routines: an initialization routine, a display routine, a keyboard interpreting routine, and an interrupt routine. The initialization routine uses the multiplexing logic on the MCS card to address each of the 6522's and set the appropriate registers. The display routine has two options. The data can be displayed graphically at different resolutions, or counts can be displayed as counts per channel and total counts per sweep. The graphics data display uses table look up and two graphics screens to provide a real time data display. The initialization routine generates a table in memory which stores the address for a given vertical coordinate on the screen in a memory location which is correlated to the value of the vertical coordinate. The value of the horizontal coordinate is correlated to the memory address of the channel to be displayed. As the display routine scans through memory at the data, the data value and the channel value are used to address indirectly the appropriate graphics screen coordinate through this table. Therefore, by using table lookup, all of the mathematical operations necessary to obtain the appropriate screen addresses (including a division by seven) are performed only once. While one graphics screen is displayed, the other is cleared and plotted with the current data. The updated screen is then activated and the first screen is cleared and replotted, and so on. The keyboard interpreting routine allows one to change the display, change the resolution of the graphics display, or stop the spectrometer and store the data on a disk, all with single key

Figure 61: This block diagram shows the basic components of the interface to the Apple II+ computer. This interface enables the computer to be used for automatic NFMS data acquisition, or it can enable one computer, with two cards, to control and collect data from up to two Mössbauer spectrometers.

codes. A table of these key codes is displayed at the bottom of the counts display screen, the default display. Finally, the interrupt routine collects the count from the currently accessible 6522 and stores it in the appropriate three byte location. The display and keyboard routines for the two spectrometers are identical, but the initialization and interrupt routines for the two spectrometers are necessarily very different.

In the Mössbauer spectrometer, the initialization routine must enable the MCS card to generate interrupts at 195 μsec intervals. Next, the interrupt routine must be capable of pushing all values in the CPU's registers to the stack, accessing the count from the appropriate 6522 and adding it to the appropriate memory locations, and then reloading the CPU's registers with their initial values, all in less than 195 μsec, with enough time left over to update the display between interrupts. This feat was best accomplished by using four separate interrupt routines. Since the spectrometer has 1024 channels, the data is stored in twelve 256-byte pages for three bytes per channel. Each interrupt routine addresses a channel comprising three bytes through the sum of base addresses plus a counter value. Upon completion, each routine stores the address of the next interrupt routine in the interrupt vector. The fourth routine stores the address for the first routine in the interrupt vector and increments the addressing counter. The result is an interrupt routine that lasts 50-60 μsec from interrupt to return, depending on the number of bytes which must be incremented. As a result, one Apple II+ computer can easily handle two Mössbauer spectrometers with a real time data display for each.

In the NFMS, the initialization routine enables the MCS card to generate interrupts at 1/20 of a second intervals. This routine also initializes the signal generator through the GPIB. The interrupt routine must then translate the number of interrupts generated into an elapsed time and compare this time to the selected dwell time. In addition, this interrupt routine must perform all of the functions of the Mössbauer spectrometer interrupt routine. After the elapsed dwell time, the interrupt routine must step the frequency of the signal generator and change the address (channel) for data storage. When the frequency of the signal generator is changed, and for a time thereafter, the data to the MCS must be gated off and the timing stopped until the signal is stabilized. In the NFMS the speed of the interrupt routine is no longer a major concern due to the significant increase in the time

between interrupts and the fact that the data is gated off while the interrupt routine is delaying for the signal generator. Unfortunately, however, the time required to change the frequency is unavoidable dead time. Yet the total dead time in a run can be minimized by selecting a sufficiently long dwell time which does not allow the signal to drift significantly.

Data and Discussion

Figures 58 and 59 show data collected with our Mössbauer spectrometer and processed with a 5 point running average. These figures show Rf sidebands in an iron foil absorber, and the frequency dependence of the Rf sideband energies in a stainless steel foil absorber. All NFMS spectra to be shown were obtained from a 1.5 cm x 0.85 cm x 2.5 μm iron foil absorber enriched with 95% ^{57}Fe. This foil is the same absorber which gave us the spectra in Fig. 58. All spectra shown were obtained from an absorption geometry, using a ^{57}Co source in a Pd matrix. All NFMS spectra have been processed with a five point running average.

The first set of NFMS data concentrates on the first order sidebands from the 1 and 6 parent transitions (Fig. 62). The nomenclature for identifying the Rf sidebands is as follows. The first digit corresponds to the order of the sideband. Rf sidebands of the j'th order from a given parent transition are found at the sum and difference frequencies of the static field, or Zeeman splitting, and j times the frequency of the applied Rf field. The letter after the first digit, either an "n" or a "p", indicates whether the sideband is a negative or positive sideband respectively. A negative sideband appears at an energy lower than the energy of the parent transition, while a positive sideband is at a higher energy. The last digit identifies the parent transition of the sideband. There are six allowed transitions for ^{57}Fe in a metallic iron foil, of which the lowest energy transition is identified as parent transition one and the highest energy transition is identified as six. The energy difference between parent transitions one and six is 123 MHz, therefore, at 61.5 MHz the 1n6 and 1p1 sidebands should overlap at the transition center of the spectrum. If the gamma ray source is stationary, then the energy of the gamma rays emitted differ from the energy of the transition center of the absorber by the isomer shift. Therefore, a stationary source should provide an NFM spectrum of the 1n6 and 1p1 sidebands displaced from 61.5 MHz by plus

and minus the isomer shift respectively (Fig. 62a). The source used was in a Pd lattice, which has an isomer shift of -0.185 mm/sec relative to metallic iron. If the source is then given a constant velocity, the ln6 and lp1 sidebands should be displaced from 61.5 MHz by plus and minus (isomer shift - velocity) respectively (Fig. 62b-g). The sign convention is to define a velocity as negative when the source and absorber are moving away from each other. Note that the Rf sideband ln5, which appears in Fig. 62, should be separated from ln6 by 25.9 MHz, the excited state splitting frequency in metallic iron.

The second set of NFM spectra (Fig. 63a-c) were obtained at a lower frequency range. Higher order sidebands add together at these lower frequencies and present significant cross sections. These particular spectra are comprised of 24 different sidebands, if one takes into account sidebands out to the fifth order. Following the spectra are computer generated simulations (Fig. 64a-c). The model, a simple algorithm, shows remarkable agreement with the data. The frequency at which a sideband will appear is

$$F_{j,ord}(MHz) = [vel-(P_j+iso)]*K/ord \quad , \tag{53}$$

where P_j is the position of the j'th parent transition in mm/sec, vel is the velocity of the source in mm/sec, iso is the isomeric shift between the source and absorber, ord is the order of the sideband, and K is a conversion factor = 11.6 MHz/(mm/sec) for the 14.4 keV gamma ray being detected. The linewidth of the sideband in the NFM spectrum is

$$\Gamma_{j,ord} = (\Gamma_{pj}+\Gamma_g)/ord \quad , \tag{54}$$

where Γ_{pj} is the linewidth of the sideband's parent transition and Γ_g is the linewidth of the 14.4 keV gamma ray emitted by the source. The apparent linewidth's dependence on sideband order can be understood by realizing that an n'th order sideband will be displaced by n frequency units while a first order sideband is displaced by one frequency unit. Since we were concerned only with the relative amplitudes of a sideband within a given NFM spectrum the amplitude of a sideband in a spectrum was assumed to be

$$A_{j,ord} = A_{pj}/ord \quad , \tag{55}$$

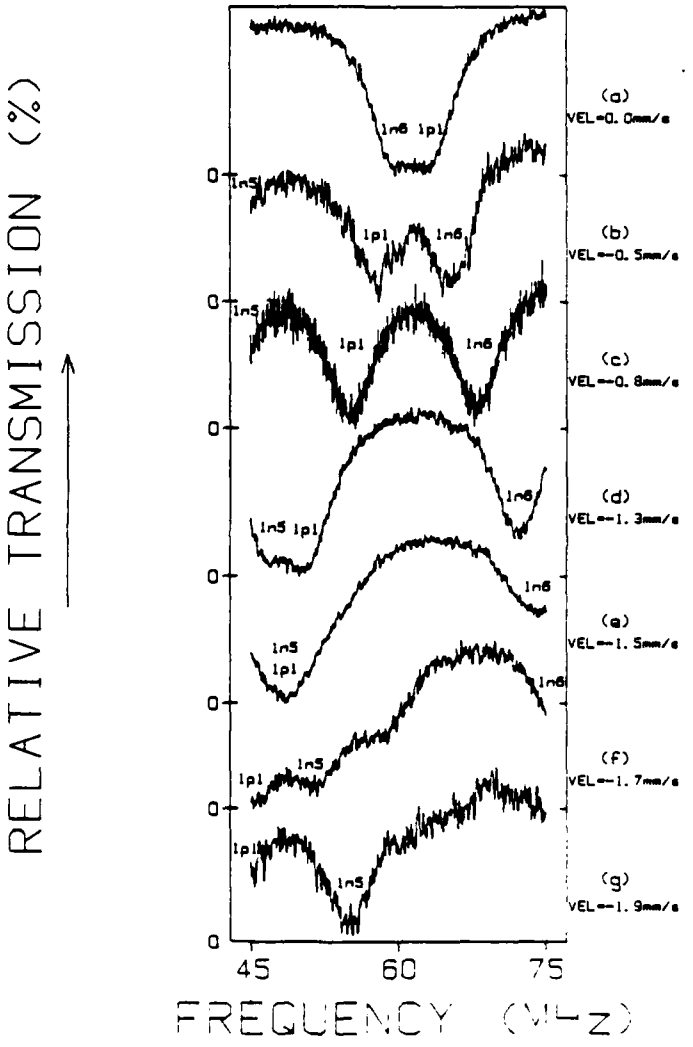

Figure 62: Typical NFMS data showing first order sidebands from the highest and lowest energy transitions of ^{57}Fe in iron, 1n6 and 1p1 respectively, a) in the vicinity of the transition center of this Zeeman split absorber. An "n" in the sideband label indicates that the sideband is at a lower energy than its parent transition, whereas a "p" indicates that the sideband is at a higher energy. As the velocity of the source is decreased b)-g), the energy of the probing radiation is decreased, and as a result the sideband from the lower energy transition, 1p1, appears at lower frequencies. The sidebands from the higher energy transitions, 1n5 and 1n6, appear separated by the excited state splitting frequency of ^{57}Fe in iron, 26 MHz.

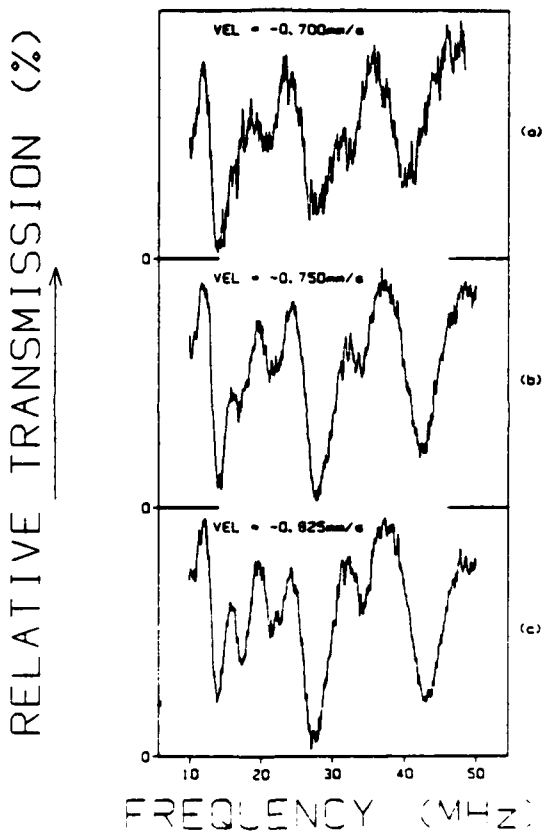

Figure 63: NFMS data obtained at lower frequencies has an appearance which belies the underlying complexity of the spectra. Sidebands add together to produce composite sidebands which have amplitudes, widths, and lineshapes with a high degree of dependence upon the energy of the probing radition. As a result, a small change in the source velocity can lead to a significant change in the appearance of a spectrum.

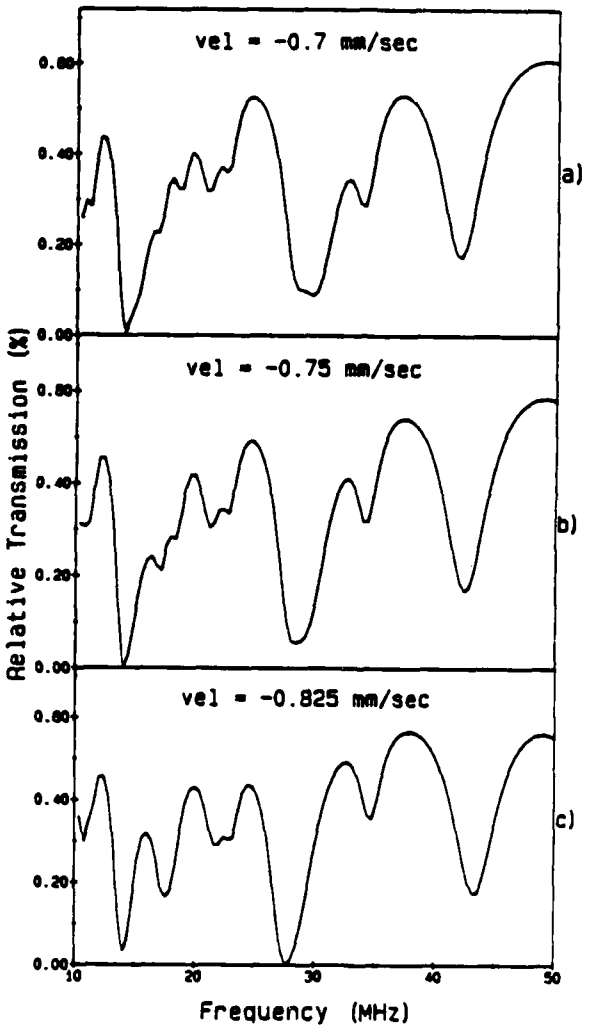

Figure 64: Computer generated simulations of the NFM spectra in Fig. 63 obtained from equations (53-55). Each simulation is composed of 24 different sidebands.

where A_{pj} is the amplitude of the sideband's parent transition. By using this equation we have assumed that our spectra were not exhibiting the saturation effects discussed in Ref. 78. This assumption was a convenient mechanism for introducing a sideband amplitude dependence on the relative amplitudes of the parents. For the iron foil used, the relative amplitudes of the parents were taken as 2:2:1:1:2:2 (Fig. 58a). The NFMS is a tool for directly measuring Rf sideband position, width, and amplitude. This model shows that the NFMS is a powerful means of indirectly measuring isomeric shifts and the positions and relative amplitudes of the parent transitions.

The NFMS apparatus is versatile. This apparatus is a conventional Mössbauer spectrometer with or without an Rf field, as well as an Rf sideband spectrometer. A conventional Mössbauer spectrometer is not capable of measuring Rf sidebands when they overlap a parent transition, and resonances have been predicted for certain such overlappings. The NFMS enables one to observe the behavior of Rf sidebands in the vicinity of a parent transition, with high enough resolution to discern any fine structure in the sideband which might result from such resonances, because in NFMS the parent transition appears only as a baseline due to its lack of any frequency dependence. With the NFMS it is also possible to observe directly the effect of the Rf field intensity on sideband position, amplitude, and width. It should also be noted that the MCS described in this paper may also be used in a spectrometer similar to the type described by Bolef and Mishory in Ref. 77.

COMMENT ON MOSSBAUER SIDEBANDS FROM A SINGLE PARENT LINE

Foils composed of alternating layers of ferromagnetic and nonmagnetic materials immersed in magnetic fields oscillating at radiofrequencies display sidebands on Mössbauer transitions from the nuclei contained in the nonmagnetic regions. Attributed by Chien and Walker[76] [Phys. Rev. B13, 1876 (1976)] to the transfer into the nonmagnetic layer of acoustic phonons excited by magnetostriction in the ferromagnetic layers, this accepted cause of such effects is challenged by new data resulting from a reexamination and extension of that classic experiment.

The paper of Chien and Walker[76] was of such critical importance that it warrants comment over a decade later. Generally perceived as reporting an unarguable proof of a certain basic proposition, it has now been found to have rested upon a demonstrably false assumption. A reexamination of the original experiment shows it to have been so flawed that any conclusions drawn from it must now be considered unproven.

The point of inception had been the original proposal of Mitin[80,81] that Mössbauer transitions could be excited as part of a multiphoton process in nuclei immersed in intense radiofrequency (rf) fields. In those cases the Mössbauer spectrum was expected to show additional sum and difference frequency lines displaced from the normal lines by integral multiples of the perturbing frequency. In appearance such multiphoton spectra are expected to resemble the transmission spectra which Ruby and Bolef[73] obtained by imposing periodic Doppler shifts of purely mechanical origin upon the Mössbauer source. This unfortunate similarity in appearance between phenomena arising from such different origins provided the basis for years of critical controversy seemingly resolved by the work of Chien and Walker.[76] The purpose of this comment is to report new data from a repetition and extension of the Chien and Walker experiment that shows their conclusions to be unjustified. Without the force of conviction conveyed by their work, the controversy must be reopened to further investigation.

The earliest experiment in radiofrequency sideband production, reported by Perlow[74] in 1968, focused upon the components of the 14.4 keV transition in ^{57}Fe. Several ^{57}Co sources diffused into ferromagnetic hosts were immersed into intense magnetic fields oscillating at radiofrequencies. Those results were explained[74] as the magnetodynamic modulation of the hyperfine fields and generally conformed to the Mitin

hypothesis for multiphoton transitions. Two of the three groups who initially documented this phenomena favored the magnetodynamic explanation which required no mechanical action[74,82,83] while the other group began to develop an alternative based entirely upon magnetostriction.[75,84] Most of the actual experiments had used ferromagnetic hosts to enhance the applied magnetic fields, and such materials are almost invariably magnetostrictive. In the model finally synthesized, periodic Doppler shifts were assumed to be driven by acoustic phonons which were excited by magnetostriction along the greatest dimensions of the material and scattered onto the axis connecting source and absorber. To be effective, this mechanism required the sample to have a large acoustic Q so that displacements of the active nuclei could build to significant values.

Despite the accretion over the years of a large body of phenomenology presumed to describe rf sidebands on Mössbauer transitions, the magnetostrictive-acoustic theory never quantitatively predicted the amplitudes of the sidebands as functions of either applied power or frequency. However, the magnetodynamic models of that time fared no better, and attention turned to "proving" a magnetostrictive origin by distressing the alternative explanations.[85] The obvious difficulty with proving a theory by distressing the alternatives is that those other explanations may not have reached comparable levels of maturation. The magnetodynamic models of the late 60's were relatively easy to destroy.[85] However, the recent successes of ferromagnetodynamics[86,87] show the early models[74] of sideband formation to have been inspired, but inadequate approximations. These models simply did not embody the level of sophistication necessary to describe the complex switching behavior of magnetization in ferromagnetic foils subjected to various combinations of static and oscillating fields in those geometries employed.

More recent experiments[88,89] have shown that the applications of such oscillating magnetic fields to Mössbauer nuclei embedded in nonmagnetic hosts do produce radiofrequency sidebands by directly modulating the phases of the nuclear states involved in the transitions. However, amplitudes were rather small in those experiments because the driving forces depended only upon the value of applied field, $\mu_o H$. In 1984, we extended such approaches further by deriving the phase modulation of a nuclear state in a magnetic material.[90] In this case driving forces were proportional to the magnetization $\mu_o M$ and effects were found to be large.[78,90,91] It appears that many prior results attributed

exclusively to acoustic effects driven by magnetostriction could have also benefited from an unrecognized contribution from direct phase modulations of the nuclear states involved.

From a current perspective it is the experiment reported by Chien and Walker[76] that forms the bulwark of the magnetostrictive-acoustic explanation of Mössbauer sidebands. In that experiment an absorbing foil composed of ferromagnetic and nonmagnetic layers was used to study transport of the causitive agent from the ferromagnetic layer into the nonmagnetic region where the sidebands were produced upon Mössbauer transitions of embedded ^{57}Fe nuclei. Very clear evidence showed that the cause did arise in the ferromagnetic Ni layers, producing sidebands in the nonmagnetic stainless steel layers. The most ready explanation at that time was a transport of phonons from one layer to the next with a high acoustic Q. Those experiments were repeated in the work reported here, but with extensions which contradict the classic interpretation of Chien and Walker.[76]

Although not unique for all sidebands in a spectrum,[76] the idea of a modulation index m as a measure of the strength of the development of the sidebands offers practical convenience for descriptions. For a magnetostrictive origin,[76]

$$m = x_0/\lambda \quad , \tag{56}$$

where x_0 is the amplitude of the periodic displacement of the nuclei and λ= 0.137 A for the 14.4 keV line of ^{57}Fe. In the corresponding magnetodynamic model,[90]

$$m = bH \quad , \tag{57}$$

where H is the applied magnetic field and b provides proportionality between M_s, the saturation magnization of the medium, and H. For relatively small m, the ratio of the magnitude of the first order sidebands to the intensity in the original parent line is proportional to m^2, which in turn is proportional to P, the applied radiofrequency power.

One of the most compelling results presented by Chien and Walker[76] was a demonstration supposed to show the enhancement of m^2 afforded by tighter acoustic coupling of the layers. They found that electroplating Ni upon a stainless steel foil produced much higher values of m^2 in

absorption experiments than could be obtained by gluing a Ni foil to the stainless foil. They attributed the difference to the obviously poorer acoustic properties of the glue. However, as part of this report we observe that their stainless steel foil was electroplated on both sides with Ni while the epoxied bond was used to join a single Ni foil to one side of the stainless absorber. While the m defined by Eq. (56) for a single foil could not be additive if produced in different magnetostrictive layers, in principle the M_s upon which m depends in Eq. (57) could add coherently. Two sources of m arising from distinctly separate sources could give a resulting modulation of $4m^2$ in a magnetodynamic model. Chien and Walker failed to recognize[76] that even in the magnostrictive model two sources of m generated in the two electroplated layers should give a modulation index of $2m^2$ in the absorber foil. Instead, they attributed the increased sideband intensity developed by the two plated sources in comparison to the one glued source only to the advantage they assumed for a plated contact over a glued interface. They reported no comparison of the effects of gluing or plating the *same number of ferromagnetic layers to the absorber foil*. Reported here is a repetition of the Chien and Walker experiment which showed that the effect of two foils varied from two to four times that produced by a single foil joined in the same fashion, depending upon the static magnetic bias applied.

In our experiment the absorber was a 2.5 μm paramagnetic stainless steel (SS) foil with 90.6% enrichment of ^{57}Fe. For the nonabsorbing ferromagnetic drivers, 2.5 μm Ni foils were used, all of which were cut from a single sheet of polycrystalline Ni. The stainless-steel absorber was sandwiched between two Ni foils and held in rigid contact by mounting the foils between glass cover slides of 100 μm thickness. A conventional Mössbauer spectrometer, modified for rf experiments, Fig. 65, utilized a 25 mCi source in a Rh matrix to obtain the ^{57}Fe absorption spectra. The 14.4 keV gamma rays were detected with a Kr gas filled proportional counter biased with 1.8 kV.

A 25 MHz rf magnetic field was applied by mounting the foils in the cylindrical induction coil of an L-C tank circuit. In obtaining data for a direct comparison between the effect of one Ni driver versus two, the product of the applied rf power P and the electrical Q of the circuit containing the rf induction coil was maintained at constant values. Elementary analysis shows that if PQ is constant the rf current in the coil of such a circuit is also constant and hence the two

absorber arrangements are subjected to applied fields of the same intensity H. The results of the first experiment verified the linearity of the first order sideband amplitudes at 25 MHz for SS with two Ni drivers with PQ products of 75, 150, and 300 W Fig. 66. The spectra are scaled so that the intensity of the central Mössbauer absorption peak of ^{57}Fe in SS is held constant in order to make direct comparisons of the sideband amplitudes.

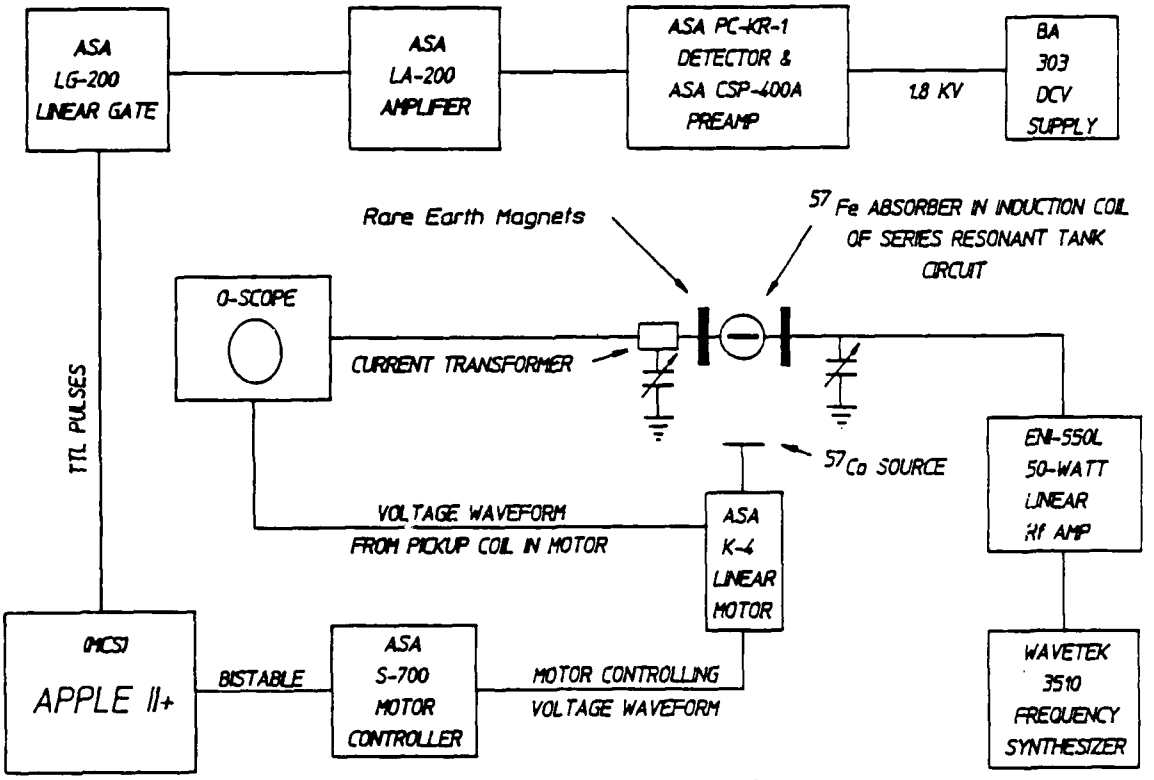

Fig. 65: Schematic drawing of the experimental arrangement used.

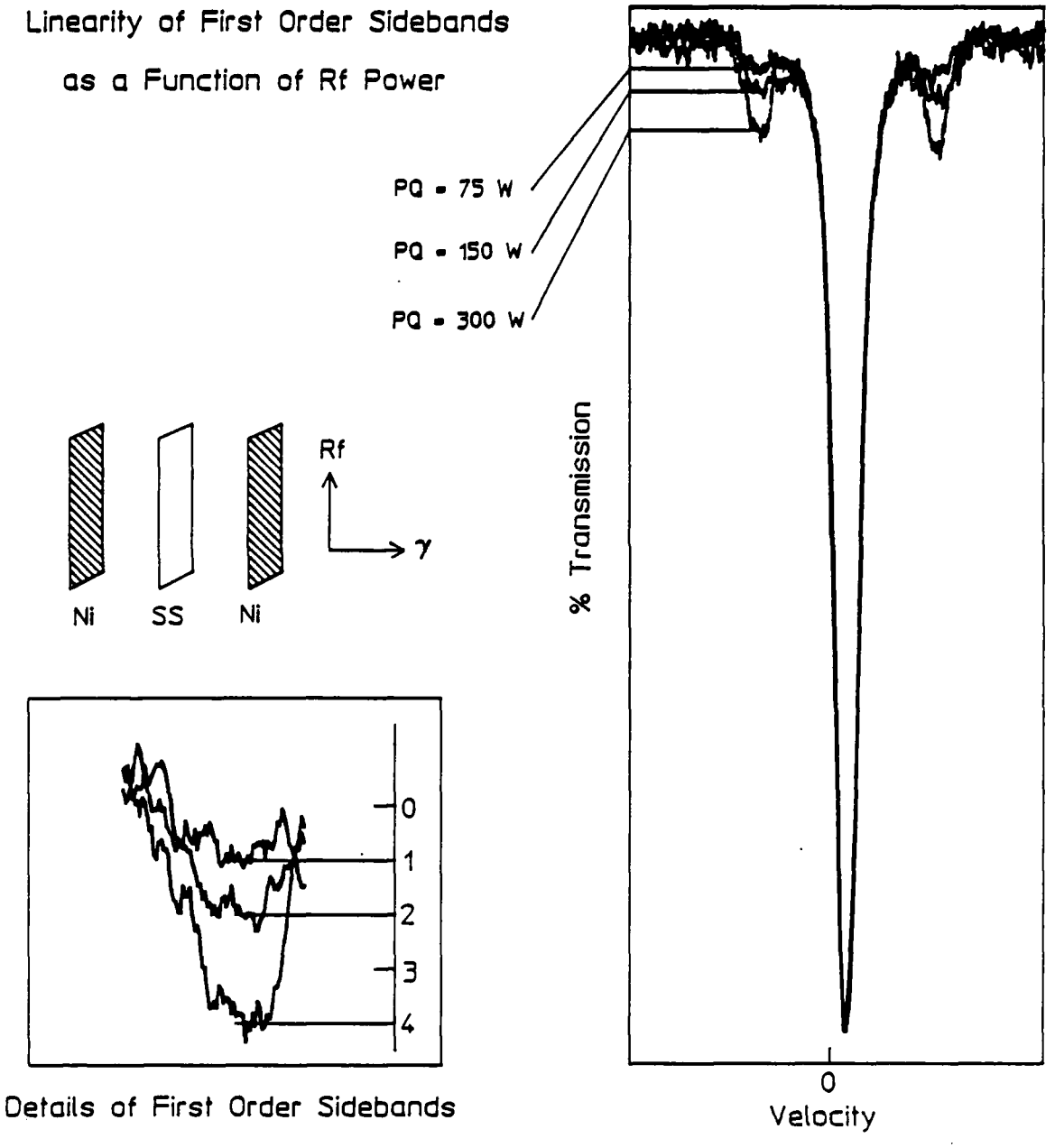

Fig. 66: Experimental verification of the linearity of the first order sidebands at 25 MHz as a function of the applied rf power. The product of the applied rf power, P, and the quality factor, Q, of the circuit are used to insure reproducibility of the rf field strengths.

Having established the linearity of the first order sidebands in the Ni-SS-Ni sandwich, one of the Ni drivers was removed and the experiment was repeated with the same PQ products as before. Figure 67 shows a comparison of the sideband amplitude for two Ni drivers versus one; in this configuration two Ni drivers give twice the effect of one driver foil.

In the next experiment a comparison between the effect of one source of excitation with that from two sources when both were biased with a static magnetic field. Rare earth magnets were placed about the induction coil such that the static magnetic field was mutually orthogonal to the rf magnetic field and the direction of gamma-ray propagation.

The linearity of the sideband amplitudes at 25 MHz as a function of PQ was again established (Fig. 68) to insure that the introduction of the static magnetic field did not introduce any nonlinearities to the system. The scale thus established was used to measure the decrease in the sideband amplitude when one of the sources of excitation was removed from this biased sandwich. As is clearly shown in Fig. 69, the sideband amplitudes obtained with two driver foils are four times the amplitudes obtained with one driver foil. Therefore, with the application of a static B-field, two sources of excitation give four times the effect.

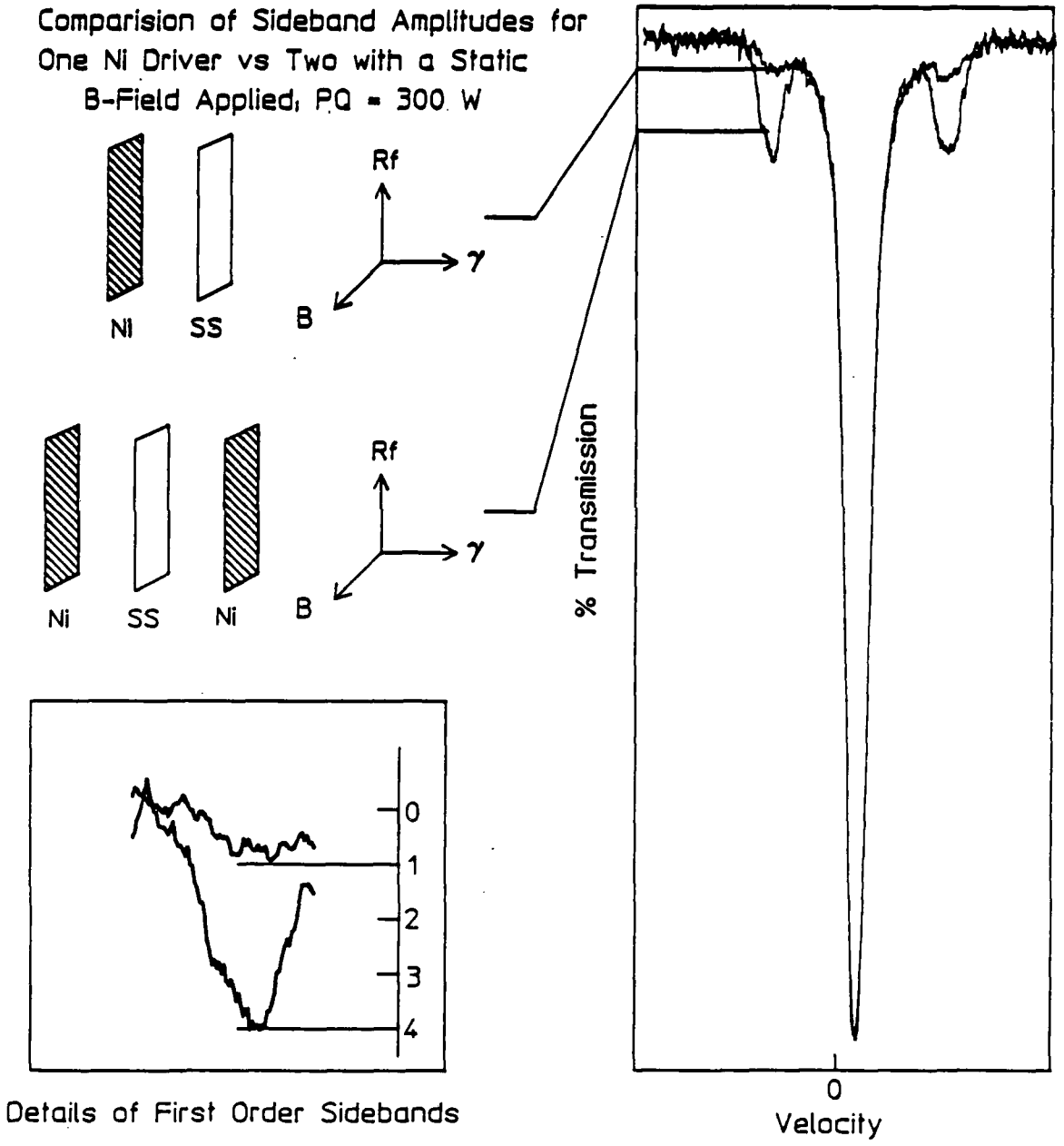

Fig. 67: Comparison of first order sideband amplitudes for one Ni driver foil versus two at 25 MHz with a PQ product of 300 W.

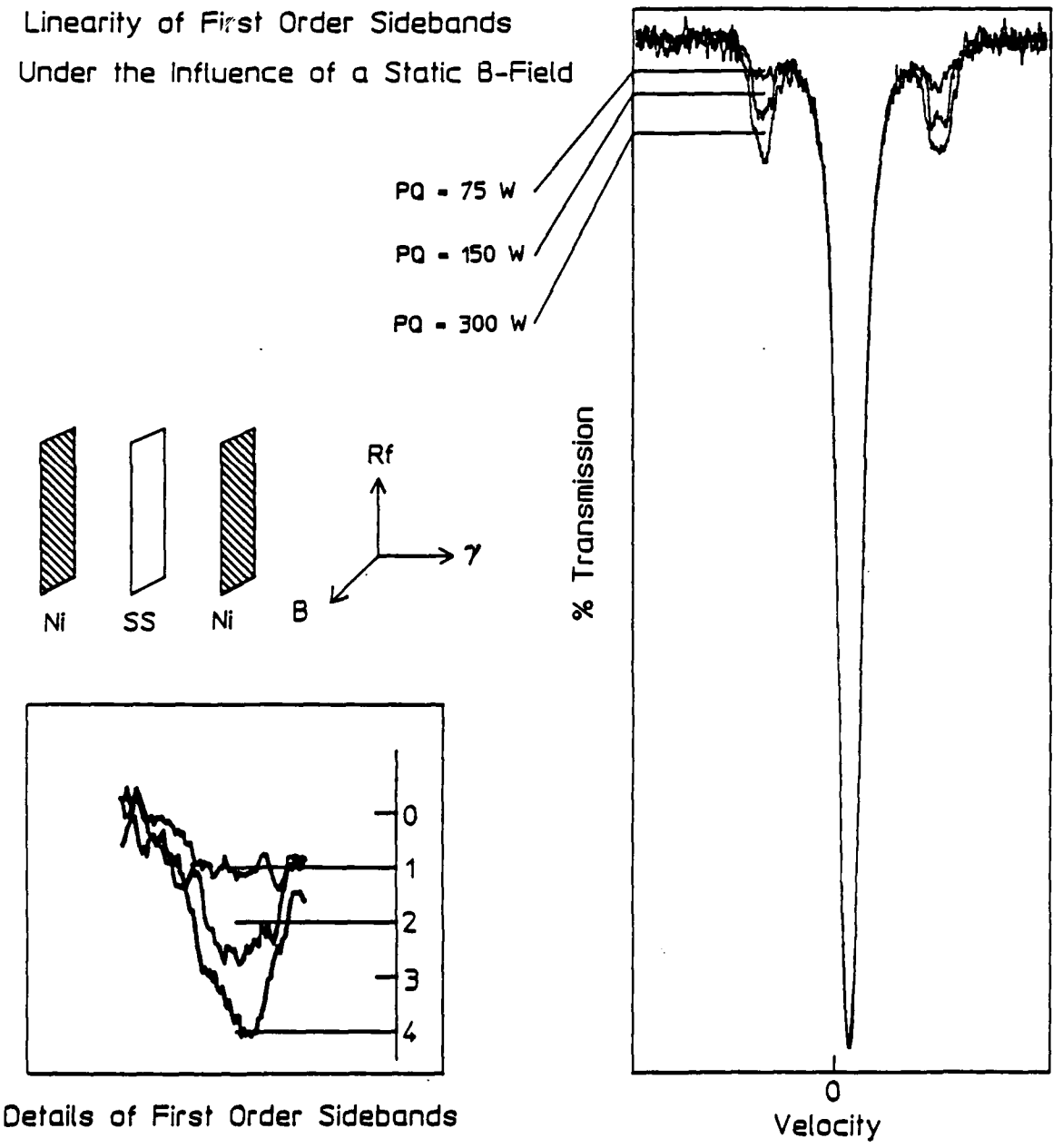

Fig. 68: Establishment of linearity of the first order sidebands at 25 MHz with PQ = 75, 150 and 300 W when the foils are biased with a static B-field.

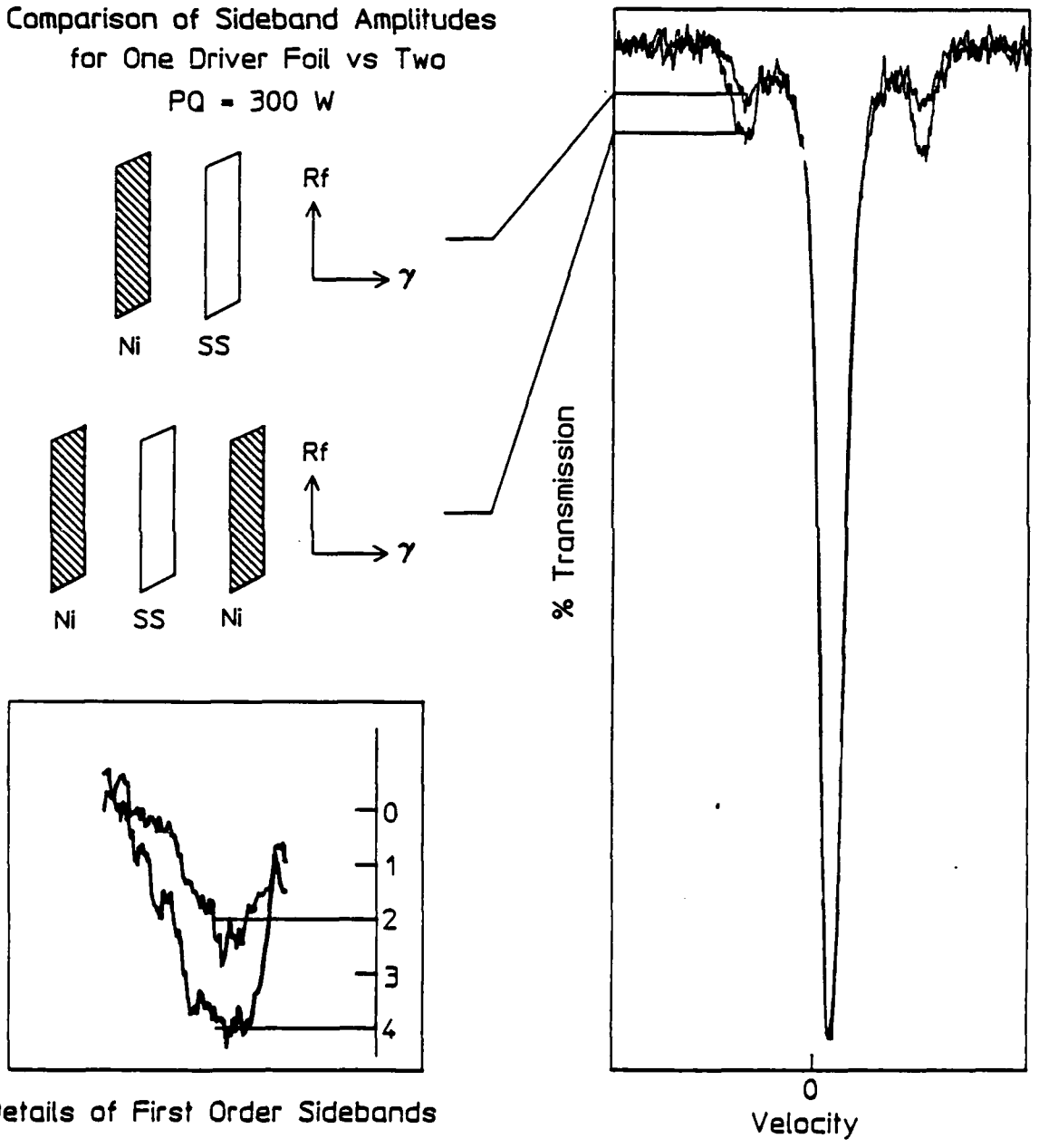

Fig. 69: Comparison of sideband amplitudes for one driver foil versus two when both are biased by a static B-field with PQ = 300 W. Here two foils give four times the effect of one thus giving a modulation index of $4m^2$.

The results of this reexamination of the Chien and Walker experiment support only the first conclusion reached in that original work, namely that the causitive agent of rf sidebands can be produced in a ferromagnetic layer and then transported into a nonmagnetic layer. Their other conclusion is completely refuted by this demonstration because the effects they attributed to the type of coupling between layers most probably resulted from the relative numbers of magnetic and nonmagnetic layers.

These new results go beyond the propositions tested by Chien and Walker[76] and display behaviors completely inconsistent with the traditional magnetostrictive-acoustic origin of Mössbauer sidebands. In experiments such as these, acoustic phonons are the bosons associated with vector fields driven by tensor forces, *not vector forces*. Without invoking stimulated emission, we can conceive of no way in which tensor sources which are physically separated can produce coherent vector fields in a space between them, even if they are temporally synchronized. The stimulated emission of phonons to produce coherent additions of the displacements arising from the different sources would imply the existence of a threshold of power, above which two modulation indices of m would give an effect of $4m^2$ and below which only $2m^2$. No such threshold was suggested by data similar to that of Fig. 69 which was obtained over an adequate range of powers.

In view of the growing number of successes of the model for the direct modulation of the phases of the nuclear states and these new results which question the validity of the conclusions of the Chien and Walker[76] experiment, it would appear that the controversy over the origin of Mössbauer sidebands must be reopened.

CONCLUSIONS

Achieved during this second year of research into the feasibility of a gamma-ray laser were advances which exceeded all reasonable expectations. Giant resonances were discovered to funnel across drastic changes of angular momentum the nuclear populations produced by a broad absorption of x-rays. The rule-of-thumb for the useful absorption of flash x-rays in this nuclear analog to the gamma-ray laser proved a million times too pessimistic. Limiting bandwidths were not microvolts, as expected, but volts.

Culminating this year's work were two major milestones which showed that both of the two poorest of the 29 candidates for a gamma-ray laser possessed the giant resonances for pumping. One, $^{180}Ta^{m}$, is nature's rarest stable element. It was available in the U.S. in the macroscopic amount of 1 mg and part was successfully dumped through an enormous cross section contributed by one of these pumping resonances. The results are now published in the literature and represent the first time in the 50 year history of (γ,γ') reactions that an isomeric population has been dumped. In retrospect it was easy, the technology had just not been assembled before.

Supporting the scientific results have been new technologies developed in the course of this work. The experiences with the x-ray pumping of nuclei have spun-off a nuclear analog of the optical double resonance instrumentation with which the spectra from large impulsive sources of bremsstrahlung can be calibrated for the first time. Described in this report are successes in calibrating the spectral outputs from DNA/PITHON and DNA/AURORA with our methodology. In a different direction the precision and tuning range available to nuclear spectroscopy have been extended through the successes in implementing the nuclear analogs to upconversion.

Generally, our computer codes predicting the feasibility of a gamma-ray laser have been substantiated by these intermediate results reported this year. Surprises when they have arrived, have been extremely favorable. The giant pumping resonances have contributed four to six order of magnitude toward feasibility and prime examples have been found in both of the 29 candidates available for examination. If the pervasiveness of these resonances extends to the good candidates for

a laser, a gamma-ray laser should be feasible, just as described[2] in 1982.

References

1. Both the dressed state (coherent) scheme and the flash x-ray (incoherent) pumping techniques still appear feasible just as we originally proposed in Ref. 2. However, the latter, being simpler, is developing at a more dramatic rate.

2. C. B. Collins, F. W. Lee, D. M. Shemwell, B. D. DePaola, S. Olariu, and I. I. Popescu, J. Appl. Phys. 53, 4645 (1982).

3. C. B. Collins, in Center for Quantum Electronics Report #GRL/8602, University of Texas at Dallas, 1987 (unpublished), pp. 1-28.

4. Center for Quantum Electronics Report #GRL/8701, 1987 (unpublished), pp. 1-10.

5. J. A. Anderson and C. B. Collins, Rev. Sci. Instrum. 58, 2157 (1987).

6. Center for Quantum Electronics Report #GRL/8601, University of Texas at Dallas, 1987 (unpublished), pp. 1-14.

7. C. B. Collins, J. A. Anderson, Y. Paiss, C. D. Eberhard, R. J. Peterson, and W. L. Hodge, Phys. Rev. C (pending).

8. J. A. Anderson and C. B. Collins, Rev. Sci. Instrum. 59, 414 (1988).

9. J. A. Anderson, M. J. Byrd, and C. B. Collins, Phys. Rev. C (pending).

10. Evaluated Nuclear Structure Data File (Brookhaven National Laboratory, Upton, New York, 1986).

11. E. C. Booth and J. Brownson, Nucl. Phys. A98, 529 (1967).

12. J. A. Anderson and C. B. Collins, in Center for Quantum Electronics Report #GRL/8701, University of Texas at Dallas, 1987 (unpublished), pp. 11-34.

13. A. B. W. Cameron, Essays in Nuclear Astrophysics, edited by C. A. Barnes, D. D. Clayton and D. N. Schramm, (Cambridge Univ. Press, Cambridge, 1982), p. 23.

14. E. Browne, Nucl. Data. Sheets 52, 127 (1987).

15. C. B. Collins, C. D. Eberhard, J. W. Glesener, and J. A. Anderson, Phys. Rev. C 37, 2267 (1988).

16. P. J. Brussard and P. W. M. Glaudemans, Shell-Model Applications in Nuclear Spectroscopy, (North-Holland, Amsterdam, 1977), Ch. 10.

17. A. deShalit and H. Feshbach, Theoretical Nuclear Physics Vol. I: Nuclear Structure (J. Wiley, New York, 1974), Ch. 8, Section 11.

18. C. F. Perdrisat, Rev. Mod. Phys. 38, 41 (1966).

19. C. B. Collins, J. M. Carroll, and J. A. Anderson, in Center for Quantum Electronics Report #GRL/8702, University of Texas at Dallas, 1987 (unpublished), pp. 13-44.

20. C. D. Eberhard, J. W. Glesener, Y. Paiss, J. A. Anderson, C. B. Collins, W. L. Hodge, E. C. Scarbrough, and P. P. Antich, in Center for Quantum Electronics Report #GRL/8702, University of Texas at Dallas, 1987 (unpublished), pp. 89-103.

21. B. Pontecorvo and A. Lazard, C. R. Acad. Sci. 208, 99 (1939).

22. G. B. Collins, B. Waldman, E. M. Stubblefield, and M. Goldhaber, Phys. Rev. 55, 507 (1939).

23. K. Yoshihara, Zs. Nemeth, L. Lakosi, I. Pavlicsek, and A. Veres, Phys. Rev. C33, 728 (1986) contains a thorough review.

24. A. Ljubicic, K. Pisk, and B. A. Logan, Phys. Rev. C33, 2238 (1981).

25. K. Yoshihara, Zs. Nemeth, L. Lakosi, I. Pavlicsek, and A. Veres, Phys. Rev. C33, 728 (1986).

26. We recently learned that apparently the first demonstration of the feasibility of the principle of this technique was made in 1971 before tabulations of nuclear parameters had matured to the point of being able to provide adequate practical guidance. See: L. Cohen and E. A. Wolicki, NRL Report 7306 (1971).

27. C. M. Lederer and V. S. Shirley, ed. Table of Isotopes (John Wiley, New York, 1978).

28. The actual values for the fractions of the fluorescent photons unaffected by self-absorption were calculated to be 91 and 88% for ^{79}Br and ^{77}Se, respectively.

29. As seen in Table I, the best values of nuclear parameters differ from those used in Ref. 5. Our earlier reports used data from Ref. 27, while more recently we used Ref. 10, current to 1986.

30. W. Miller, J. W. Motz, and C. Cialella, Phys. Rev. 96, 1344 (1954).

31. J. A. Halbleib and T. W. L. Sanford, Sandia Report SAND83-2572 (1983).

32. Data actually plotted in Figs. 15-17 are ratios of the numbers of detected photons corrected for the finite period of counting, while the analyses of Eqs. (2a) - (14) are written in terms of the ratios of the numbers of active nuclei produced in the target. Slopes obtained from the figures must be multiplied by 1.50, the product of the ratios of corrections for detector and fluorescence efficiencies and for self-absorption in the target before being used in the equations.

33. The scatter of the residues in Fig. 10 does not appear completely random and a trend might be perceived as indicating another gateway opening around 1.2 MeV. It is tempting to identify this with the level at 1186 keV favored in Table II. However, more shots with higher end point energies would be needed to obtain a meaningful assessment of such a possibility.

34. The first, 433 keV, is the average of the energies of the lowest two transitions in ^{77}Se weighted by their respective ξ_i from Eq. (6). Pragmatically this corresponds to an average line at 433 keV having $\xi_{433}(\mathrm{Se}) = 3.9 \times 10^{-32}$.

35. G. Harbottle, Nucleonics 12, 64 (1954).

36. N. Ikeda and K. Yoshihara, Radioisotopes 7, 11 (1958).

37. A. Veres, Int. J. Appl. Radiat. Isot. 14, 123 (1963).

38. B. T. Chertok and E. C. Booth, Nucl. Phys. 66, 230 (1965).

39. M. Boivin, Y. Cauchois, and Y. Heno, Nucl. Phys. A137, 520 (1969).

40. L. Lakosi, M. Csuros, and A. Veres, Nucl. Instrum. and Meth. 114, 13 (1974).

41. Y. Watanabe and T. Mukoyama, Bull. Inst. Chem. Res., Kyoto Univ. 57, 72 (1979).

42. In the units usually employed, the integrated cross section $\pi b_a b_o \sigma_o \Gamma/2$ for the 941 keV level is computed from Ref. 10 to be 0.72 $\times 10^{-29}$ cm^2 keV.

43. Data actually plotted in Figs. 21 and 22 are ratios of the numbers of detected photons corrected for the finite period of counting, while the analyses of Eq. (16) are written in terms of the ratios of the numbers of active nuclei produced in the target. Slopes obtained from the figures must be multiplied by 0.75, the product of the ratios of corrections for detector and fluorescence efficiencies and for self-absorption in the target before being used in the equations.

44. The value of $\pi b_a b_o \sigma_o \Gamma/2$ was determined in this work relative to the calibration value for ^{79}Br taken from the literature and confirmed in recent experiments described in Ref. 8.

45. M. Krcmar, A. Ljubicic, K. Pisk, B. Logan, and M. Vrtar, Phys. Rev. C 25, 2097 (1982).

46. I. Bikit, J. Slivka, I. V. Anicin, L. Marinkov, A. Rudic, and W. D. Hamilton, Phys. Rev. C 35, 1943 (1987).

47. Y. Cauchois, Y. Heno, and M. Boivin, C. R. Acad. Sci. Ser. B 262, 503 (1966).

48. K. Yoshihara, Isot. Radia. Technol. 3, 464 (1960).

49. B. Harmatz, Nuc. Data Sheets 27, 453 (1979).

50. B. Rosner, Phys. Rev. 136, B664 (1964).

51. M. L. Wiedenbeck, Phys. Rev. 67, 92 (1945).

52. E. B. Norman, S. E. Kellogg, T. Bertram, S. Gil, and P. Wong, Astrophys. J. 281, 360 (1984).

53. R. Mohan, C. Chui, and L. Lidofsky, Med. Phys. 12, 595 (1985).

54. N. C. Ikoro, D. A. Johnson, and P. P. Antich, Med. Phys. 14, 93 (1987).

55. J. Lyttkens, K. Nilson, and L. P. Ekström, Nucl. Data Sheets 33, 1 (1981).

56. K. Yokoi and K. Takahashi, Nature, 305, 198 (1983).

57. H. Beer and R. A. Ward, Nature, 291, 308 (1981).

58. E. Runte, W. D. Schmidt-Ott, W. Eschner, I. Rosner, R. Kirchner, O. Klepper, and K. Rykaczewski, Z. Phys. A, 328, 119 (1987).

59. J. Law and F. A. Iddings, J. Radioanalytical Chem., 3, 53 (1969).

60. E. Browne and R. B. Firestone, Table of Radioactive Isotopes, edited by V. S. Shirley, (J. Wiley, New York, 1986) pp. 180-2.

61. Although the grain size of the Ta_2O_5 was small compared to escape lengths for the 55 keV x-ray, close examination of the target subsequent to the experiment indicated that some clumping of the material had occurred. As discussed in the text, this could cause our result to become a lower limit for the integrated cross section.

62. Since the spectral intensity is roughly constant, the flux decreases as E^{-1} toward the end point with a final more rapid drop between 5 and 6 MeV.

63. M. Boivin, Y. Cauchois and Y. Heno, Nucl. Phys. A176, 626 (1971).

64. H. R. Lukins, J. W. Otvos, and C. D. Wagner, Int. J. of Appl. Rad. and Isotopes 11, 30 (1961).

65. C. B. Collins and J. A. Anderson in Center for Quantum Electronics Report #GRL/8701, University of Texas at Dallas, 1987 (unpublished), pp. 35-53.

66. It is unlikely I_e could be greater than 5/2 and still support such a highly allowed transition from the ground state.

67. C. D. Eberhard, J. W. Glesener, Y. Paiss, J. A. Anderson, C. B. Collins, W. L. Hodge, E. C. Scarbrough, and P. P. Antich, Phys. Rev. C (pending).

68. Difficulties in characterizing the source spectra led to wide variations in reported cross sections as reviewed in Refs. 7 and 9.

69. C. B. Collins, J. A. Anderson, C. D. Eberhard, J. F. McCoy, J. J. Carroll, E. C. Scarbrough, and P. P. Antich in Center for Quantum Electronics Report #GRL/8703, University of Texas at Dallas, 1988 (unpublished), pp. 37-56.

70. C. B. Collins in Center for Quantum Electronics Report #GRL/8703, University of Texas at Dallas, 1988 (unpublished), pp. 1-20.

71. K. G. Kerris in Harry Diamond Laboratories Report No. HDL-TM-81-18, Harry Diamond Laboratories, 1981 (unpublished).

72. J. H. Hubbell, Photon Cross Sections, Attenuation Coefficients, and Energy Absorption Coefficients from 10 keV to 100 GeV, NSRDS-NBS-29, (U.S. Gov. Printing Office, Washington, D.C., 1969).

73. S. L. Ruby and D. I. Bolef, Phys. Ref. Lett. 5, 5 (1960).

74. Gilbert J. Perlow, Phys. Rev. 172, 319 (1968).

75. Neil D. Heiman, Loren Pfeiffer, and J. C. Walker, Phys. Rev. Lett. 21, 93 (1968).

76. C. L. Chien and J. C. Walker, Phys. Rev. B 13, 1876 (1976).

77. D. I. Bolef and J. Mishory, App. Phys. Lett. 11, 321 (1967).

78. B. D. DePaolo, S. S. Wagal, and C. B. Collins, J. Opt. Soc. Am. B 2, 541 (1985).

79. P. W. Reittinger, T. W. Sinor, S. S. Wagal, and C. B. Collins, Rev. Sci. Instrum. 59, 362 (1988).

80. A. V. Mitin, Sov. Phys. JETP 25, 1062 (1967).

81. A. V. Mitin, Sov. Phys. Dok. 15, B27 (1971).

82. G. Asti, G. Albanese, and C. Bucci, II Nuovo Cimento 57B, 531 (1968).

83. G. Asti, AB. Albanese, and C. Bucci, Phys. Rev. 184, 260 (1969).

84. N. D. Heiman and J. C. Walker, Phys. Rev. 184, 281 (1969).

85. L. Pfeiffer, N. D. Heiman, and J. C. Walker, Phys. Rev. B 6, 74 (1972).

86. T. H. O'Dell Ferromagnetodynamics (Wiley, New York, 1981), Chap. I.

87. C. W. Chen, Magnetism and Metallurgy of Soft Magnetic Materials (North-Holland, Amsterdam, 1977).

88. P. J. West and E. Matthias, Z. Phys. A 288, 369 (1978).

89. E. Ikonen, P. Helistö, J. Hietanieni, and T. Katila, Phys. Rev. Lett. 60, 643 (1988).

90. C. B. Collins and B. D. DePaola, Optics Lett. 10, 25 (1985).

91. B. D. DePaola and C. B. Collins, J. Opt. Soc. Am. B 1, 812 (1984).